Diss. ETH No. 14944

Terrestrial Water Storage: A Critical Variable for Mid-latitude Climate and Climate Change

A dissertation submitted to the
Swiss Federal Institute of Technology (ETH)
Zurich

for the degree of
Doctor of Natural Science

presented by
Sonia I. Seneviratne
Dipl. Natw. ETH
born 5 June 1974
citizen of Lutry (VD), Switzerland

accepted on the recommendation of
Prof. Dr. C. Schär (ETH, Zurich), examiner
Dr. P. Viterbo (ECMWF, Reading, UK), co-examiner
Prof. Dr. W. Kinzelbach (ETH, Zurich), co-examiner

2003

Cover Pictures:
Satellite images of the confluences of the Illinois, Mississippi, and Missouri Rivers during the 1988 drought (left: July 4, 1988) and the 1993 flood (right: July 18, 1993). Courtesy of the Illinois State Water Survey.

Abstract

Water resources and their future availability represent one of the major issues of the 21st century. With the growing population pressure, the increasing groundwater withdrawals, and the uncertainties linked to climate change, it is likely that some semi-arid regions might suffer from an increased lack of freshwater in the future. Current climate-change scenarios suggest that mid-latitude regions might also be touched by enhanced water scarcity, due to the occurrence of more frequent and longer-lasting summer droughts. This is an issue of major concern, particularly for agricultural areas. Therefore, it is essential to obtain reliable predictions of the future evolution of water resources, and the extent to which terrestrial water storage will be impacted by climate change both globally and regionally.

The role of terrestrial water storage and its main components (soil moisture, groundwater, snow, and land ice) in the water cycle is complex. Soil moisture in particular, through its impact on evapotranspiration, significantly influences the predictability of the climate system, and is known to induce feedbacks on the regional precipitation climate. Current models still have limited skill at accurately reproducing mid-latitude summer climates, probably due to these complex interactions. Due to the lack of soil moisture observations, the employed land-surface parameterizations can only be insufficiently tested and validated, which significantly hampers their improvement. Therefore, climate-change predictions performed with these still imperfect models need to be considered with caution.

The aim of this thesis is to assess the role of the terrestrial part of the water cycle for mid-latitude climate, to explore the sensitivity of terrestrial water storage to greenhouse gas warming, and to utilize atmosphere and runoff data to provide new estimates of large-scale variations in terrestrial water storage. To this end, regional climate simulations are analysed for present and future climate conditions, and atmospheric reanalysis data and conventional streamflow measurements are used for the derivation of the estimates. The core of the thesis consists of two papers presented in chapters 2 and 3. Further results and applications follow in chapter 4, and an additional paper is presented in the appendix.

The first study (chapter 2, Seneviratne et al. 2002) investigates the role of the land-surface processes for mid-latitude climate change, focusing on the predicted risk of enhanced summer droughts in these regions. These scenarios are largely based on General Circulation Model (GCM) simulations using the so-called bucket model, a very simplified parameterization of the land-surface hydrology. In this study, regional climate simulations are run over North America for present and future climatic conditions, using a land-surface scheme of intermediate complexity (BATS), and a simplified version of it, mimicking the behaviour of the bucket model. With BATS, the warmer-climate simulations show little to no enhancement of soil drying. With the bucket-type formulation, however, a positive feedback loop induces an extreme enhancement of soil drying when drought-like condi-

tions are prevalent. The differing sensitivity of the two parameterizations is ascribed to the more realistic response of plants to drought stress in BATS, which limits evaporation to a minimum when soil moisture gets scarce. These results suggest that studies using the bucket model might have overestimated the risk of enhanced drought in the mid latitudes, and call for a more detailed investigation of the role of vegetation in climate change.

The second study (chapter 3, Seneviratne et al. 2003) investigates the feasibility of estimating changes in terrestrial water storage from water-balance calculations, using atmospheric reanalysis data (ERA-40) and traditional streamflow measurements for the period 1987-1996. In this validation study, the methodology is applied to the Mississippi river basin, and the results are compared against a unique set of observations available for the State of Illinois that includes soil moisture, groundwater, and snow measurements. The computed estimates show excellent agreement with the observations in terms of monthly variations. The mean seasonal cycle is well represented and the interannual variability is in general well captured. Though the method has some limitations and can only be applied to continental and sub-continental areas (larger than $\sim 10^5$ km^2), these are very promising results with a range of potential applications.

Chapter 4 derives estimates of terrestrial water-storage variations for river basins in Europe and Northern Asia using the aforementioned methodology, and gives a validation of the simulations of chapter 2 against observed soil moisture in Illinois. The computed estimates for Europe and Northern Asia show a realistic mean seasonal behaviour in most basins. Interestingly, the accuracy of the computed water balances appears to depend both on domain size and on regional terrain and climate characteristics. The validation of the control integrations of the chapter 2 study shows that the simulated soil moisture compares well with the observations, suggesting an overall correct representation of the land-surface processes for the considered region.

Finally, a co-authored paper (Vidale et al. 2003) is presented in the appendix A. It discusses the issue of uncertainty and predictability in simulating current mid-latitude climates with a regional climate model. A comparison is conducted of the uncertainties originating from intrinsic predictability limitations with uncertainties originating from the model formulations. It shows that the latter type of uncertainties is predominant during mid-latitude summer climates, while the colder seasons are generally well represented. An important issue discussed in this study is the compensation of model errors. Some model formulations may produce seemingly correct results for incorrect reasons, for instance by compromising the soundness of the model's water cycle. This is of particular concern when using models tuned for present climate in climate-change simulations.

In summary, this study has investigated various aspects involving terrestrial water storage in mid-latitudes, demonstrating the relevance of an accurate representation of the land-surface processes for the simulation of present and future climate, and presenting a methodology that allows the estimation of large-scale monthly and seasonal variations in terrestrial water storage. Due to the lack of suitable observational networks of terrestrial water storage for most parts of the world, it is anticipated that the so-obtained estimates will help validate and improve current climate models.

Résumé

Les ressources en eau et leur disponibilité future représentent l'un des problèmes majeurs du 21ème siècle. Au vu de la constante croissance démographique, de l'exploitation toujours plus importante de l'eau souterraine, et des possibles conséquences du changement climatique, il est probable que les zones semi-arides souffriront d'un plus grand manque d'eau douce dans le futur. Certains scénarios de changement climatique prédisent de plus que les régions des latitudes moyennes pourraient également être touchées par un manque d'eau accru, dû à l'occurrence de périodes de sécheresses plus fréquentes et de plus longue durée. Une telle éventualité serait préoccupante pour les régions concernées, surtout en zone agricole. Pour cette raison, il est essentiel d'obtenir des prévisions fiables concernant l'évolution future des ressources en eau et la façon dont elles seront influencées par le réchauffement climatique, tant à niveau global que régional.

Le stockage d'eau terrestre et ses principaux composants (humidité du sol, eau souterraine, neige et glaciers) ont un rôle complexe dans le cycle hydrologique. L'humidité du sol en particulier, par son impact sur l'évapotranspiration, influence la prédictibilité du système climatique de manière significative, introduisant des rétroactions importantes avec la précipitation régionale. Les modèles actuels ont encore des difficultés à reproduire les climats des latitude moyennes, dû en part à ces interactions complexes. Par suite du manque de mesures d'eau du sol à moyenne et grande échelle, les schémas de surface ne peuvent pas être testés et validés de manière satisfaisante, ce qui représente une entrave sérieuse à leur développement. Pour cette raison, les scénarios de changement climatique réalisés avec ces modèles encore imparfaits sont à considérer avec circonspection.

Cette thèse a pour but l'évaluation du rôle de la branche terrestre du cycle hydrologique pour le climat des latitudes moyennes, l'examination de la sensitivité du stockage d'eau terrestre au réchauffement climatique, et le calcul de changements mensuels de stockage d'eau terrestre à large échelle au moyen de données hydrologiques usuelles. Pour ce faire, des simulations effectuées avec des modèles climatiques régionaux (RCMs) pour les conditions climatiques actuelles et futures sont analysées, et des données de réanalyse et des mesures de débits fluviaux sont utilisées pour la dérivation des variations mensuelles de stockage d'eau terrestre. La partie centrale de cette thèse est constituée de deux articles présentés dans les chapitres 2 et 3. Des résultats complémentaires sont présentés dans le chapitre 4, et un article additionnel est présenté dans l'annexe.

Le premier article (chapitre 2, Seneviratne et al. 2002) examine le rôle des processus de surface pour le climat futur des latitudes moyennes, se concentrant sur les prévisions concernant le risque augmenté de sécheresse dans ces régions. Ces scénarios se basent pour la plupart sur des simulations conduites avec des modèles de circulation générale (GCMs) utilisant le "bucket model", une paramétrisation très simplifiée de l'hydrologie de surface. Dans cette étude, des simulations régionales pour l'Amérique du Nord sont conduites

pour des conditions climatiques actuelles et futures, en utilisant un schéma de surface de complexité moyenne (BATS) et une version simplifiée du dernier imitant le comportement du "bucket model". Avec BATS, les simulations de climat plus chaud présentent peu ou pas d'augmentation de sécheresse pour la région étudiée. Avec la formulation imitant le "bucket model", par contre, une boucle de rétroaction positive induit une forte augmentation de la perte d'eau du sol en été lorsque les conditions atmosphériques forçant le modèle sont déjà caractéristiques de situation de sécheresse. La différence de sensitivité des deux paramétrisations testées est attribuée à la représentation de processus liés à la végétation dans le modèle BATS, qui limitent l'évapotranspiration à un minimum, lorsque la végétation subit un stress dû au manque d'eau. Ces résultats suggèrent que les précédentes études sur ce sujet utilisant un "bucket model" ont possiblement surestimé le futur risque de sécheresse dans les latitudes moyennes, et soulignent l'importance d'une représentation correcte des processus hydrologiques de surface pour la simulation de changements climatiques futurs.

Le deuxième article (chapitre 3, Seneviratne et al. 2003) examine la possibilité d'estimer des changements mensuels de stockage d'eau terrestre au moyen de bilans hydriques, en utilisant des données de réanalyse (ERA-40) et des mesures usuelles de débits fluviaux pour les années 1987-1996. La méthode est appliquée au bassin du Mississippi, et validée au moyen d'un réseau d'observations hydrologiques unique disponible pour l'Etat d'Illinois comprenant des mesures d'humidité du sol, du niveau de la nappe phréatique, et de la couverture neigeuse. Les valeurs estimatives des variations mensuelles de stockage d'eau présentent une excellente corrélation avec les observations. Le cycle mensuel moyen est bien reproduit et la variation inter-annuelle est en général bien saisie. Bien que la méthode testée ait certaines limitations et ne puisse être appliquée qu'à des régions continentales ou sous-continentales (de taille supérieure à $\sim 10^5$ km^2), ces résultats sont très prometteurs et pourraient être employés dans des applications très diverses.

Le chapitre 4 présente des valeurs estimatives de changements mensuels de stockage d'eau terrestre dérivées avec la méthode sus-mentionnée pour des bassins d'Europe et d'Asie du Nord, et discute la validation des simulations du chapitre 2 avec les observations d'humidité du sol d'Illinois. Le comportement saisonnier moyen des valeurs estimatives calculées pour l'Europe et l'Asie du Nord semble correct pour la plupart des bassins. Un résultat intéressant est que l'exactitude des bilans hydriques effectués paraît dépendre à la fois de la taille et des caractéristiques climatiques régionales des domaines considérés. La validation des simulations du chapitre 2 en Illinois montre que les valeurs d'humidité du sol calculées par le modèle sont très proches des observations, suggérant une représentation correcte des processus de surface pour la région considérée.

Finalement, un article rédigé en tant que co-auteur (Vidale et al. 2003) est présenté dans l'annexe A. Cette étude traite de l'incertitude et de la prédictibilité associées avec la simulation du climat actuel des latitudes moyennes au moyen d'un RCM. Les incertitudes dûes aux limitations intrinsèques de prédictibilité sont comparées aux incertitudes provenant du choix des paramétrisations employées. Il est montré que ce dernier type d'incertitudes prédomine pour la simulation des climats estivaux des latitudes moyennes, tandis que les saisons froides sont généralement bien représentées. Une question importante traitée dans cet article est la possible compensation d'erreurs. Certaines paramétrisations peuvent en effet produire des résultats apparemment corrects, mais pour des raisons erronnées, par exemple dû à une représentation inexacte du cycle

hydrologique. Il s'agit d'un problème important, en particulier lors de l'emploi de modèles ajustés au climat actuel pour le calcul de scénarios du climat futur.

En résumé, cette thèse examine divers aspects concernant le stockage d'eau terrestre dans les latitudes moyennes, démontrant l'importance d'une représentation correcte des processus hydrologiques de surface pour la simulation du climat actuel et futur dans ces régions, et présentant une méthode permettant l'estimation de changements mensuels et saisonniers de stockage d'eau à large échelle. Dû au manque d'observations de stockage d'eau terrestre pour la plupart des régions du globe, les estimations dérivées avec cette méthode devraient permettre de contribuer à la validation et à l'amélioration des modèles climatiques actuels.

Contents

Chapter 1

Introduction

Water resources and their future availability represent one of the major issues of the 21st century. A large proportion of the world's population is already experiencing water stress, and global water demand is expected to continue to rise in the future due to population growth and economic development (SCOWAR 1997, Vörösmarty et al. 2000). In this context, it is critical to obtain reliable predictions of the future evolution of the availability of water resources, and the extent to which terrestrial water storage will be impacted by climate change both globally and regionally.

Various modelling studies have suggested that enhanced greenhouse warming might lead to a more frequent occurrence of droughts in mid-latitude summer (Wetherald and Manabe 1995, 1999; IPCC 2001), an issue of major concern, particularly for agricultural areas. Some of the key studies on this subject, however, have been conducted with General Circulation Models (GCMs) including a very simple representation of the land-surface processes known as the "bucket" model. This land surface parameterization tends to overestimate evaporation over bare ground, and for dry and unstressed conditions over vegetated areas (Viterbo 1996, Henderson-Sellers et al. 1996), a behaviour which could be responsible for some of the simulated summer dryness in the considered climate-change experiments. The simulation of mid-latitude summer climate is very sensitive to soil moisture conditions, and the existence of a positive soil moisture-precipitation feedback has been demonstrated in various studies (e.g. Schär et al. 1999). Hence, initial dry soil moisture anomalies may lead to a large erroneous drying at the end of the summer, due to this recurring feedback. A correct representation of land surface processes is therefore crucial for obtaining reliable predictions of future climate evolution in mid latitudes.

An important issue impeding a better understanding of the mid-latitude hydrological cycle, is the lack of large-scale measurements of terrestrial water storage, and of soil moisture in particular. Modelling initiatives have tried to remediate to this issue (e.g. Dirmeyer et al. 1999), but with little success up to now. Remote sensing holds some promise in this field (e.g. Jackson et al. 1999, Rango 1996), however, there are still major limitations to these techniques. In the case of soil moisture, for example, information can only be obtained for a layer of a few centimeters, and the estimation of soil moisture at lower depths has to be inferred through data assimilation techniques (Calvet and Noilhan 2000). Therefore the development of new methods and techniques to measure and estimate terrestrial water storage is greatly needed. A possible solution is provided by the water-balance method, as described in this thesis (see chapter 3).

The next subsections give a brief overview on some aspects of the role of terrestrial water storage and soil moisture in the climate system. First, the distribution of the Earth's water among its various reservoirs and the global hydrological cycle are briefly presented (Section 1.1). Section 1.2 underlines the importance of the land surface in the climate system, presenting the energy and water balance equations at the surface, discussing some of the main land surface-atmosphere feedbacks, and introducing the different generations of land surface parameterizations used in present models. Finally, the different chapters and the overall aims of this thesis are briefly presented in section 1.3.

1.1 Terrestrial water storage in the global hydrological cycle

The global distribution of the Earth's water among its various reservoirs is presented in Table 1.1. The listed numbers are taken from compilations based on data from the Soviet Literature (e.g. Korzun et al. 1978, Shiklomanov 1993). Note that these values can vary slightly depending on the data source (e.g. Peixoto and Oort 1992).

TABLE 1.1: Water Reserves on Earth.

	Distribution area [10^3 km^2]	Volume [10^3 km^3]	Layer [m]	Percentage of global reserves: Of total water	Percentage of global reserves: Of freshwater
World ocean	361,300	1,338,000	3,700	96.5	-
Groundwater	134,800	23,400	174	1.7	-
Freshwater	134,800	10,530	78	0.76	30.1
Soil moisture	82,000	16.5	0.2	0.001	0.05
Glaciers and permanent snow cover	16,227	24,064	1,463	1.74	68.7
Antarctic	13,980	21,600	1,546	1.56	61.7
Greenland	1,802	2,340	1,298	0.17	6.68
Arctic islands	226	83.5	369	0.006	0.24
Mountainous regions	224	40.6	181	0.003	0.12
Ground ice/permafrost	21,000	300	14	0.022	0.86
Water reserves in lakes	2,058.7	176.4	85.7	0.013	-
Fresh	1,236.4	91	73.6	0.007	0.26
Saline	822.3	85.4	103.8	0.006	-
Swamp water	2,682.6	11.47	4.28	0.0008	0.03
River flow	148,800	2.12	0.014	0.0002	0.006
Biological water	510,000	1.12	0.002	0.0001	0.003
Atmospheric water	510,000	12.9	0.025	0.001	0.04
Total water reserves	510,000	1,385,984	2,718	100	-
Total terrestrial water storage	-	47,972	-	3.46	-
Total freshwater reserves	148,800	35,029	235	2.53	100

Sources: Korzun et al. 1978, Shiklomanov 1993

Terrestrial water storage encompasses the land water storage in all its forms, i.e. soil moisture, groundwater, snow and ice cover, as well as surface water and biomass water. As seen from Table 1.1, it only represents a very small amount of the total water available on Earth (3.46 %), as 96.5 % of the total water reserves (1.39 10^6 km^3) is found in the oceans. Most of the terrestrial water is stored as freshwater, with the exception of some saline groundwater and lakes. Note that most of the freshwater is contained in the glaciers and permanent snow cover of the Antarctic and the Arctic, and is therefore not directly available for human consumption. Freshwater lakes and rivers, which are the main sources of water for human consumption (Mays 1996), contain about 90,000 km^3 of water, i.e. only 0.26 % of the total global freshwater reserves. Soil moisture, for its part, only represents a comparatively extremely small amount of the total water stored on land areas (16.5 10^3 km^3, or a mere 0.03 % of the total terrestrial water storage).

Figure 1.1 presents a schematic diagram of stocks and annual fluxes in the hydrological cycle (Dingman 1993). The values are based on data from Shiklomanov and Sokolov (1983)[1]. According to these data, evaporation over the oceans is about 7 times larger than over land, emphasizing the importance of the mechanisms limiting evapotranspiration on the land surface, compared to the sea surface which evaporates at the potential rate. There is less difference in precipitation, which is only about 4 times larger over the oceans than over land, due to the net atmospheric flux of water from the marine to the terrestrial atmosphere. Over land, there is a corresponding flux of river runoff, which brings an equal amount of freshwater back to the ocean, thus closing the cycle.

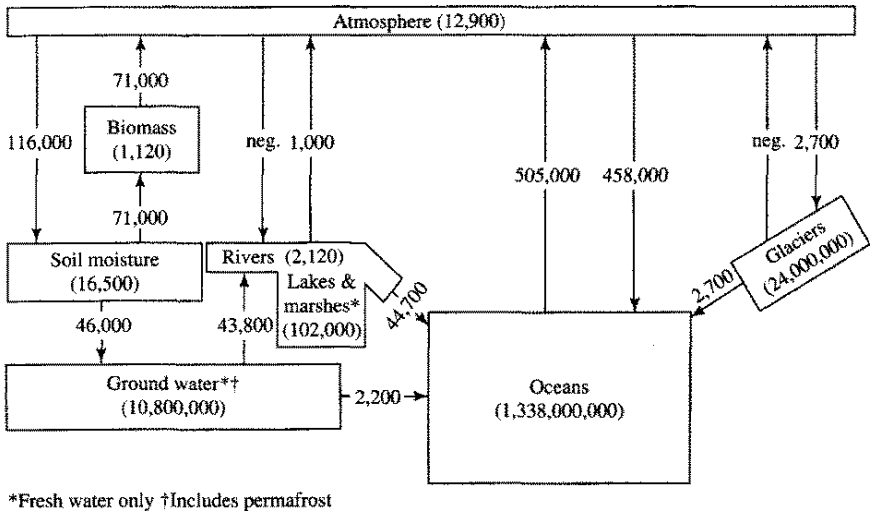

FIG. 1.1: Schematic diagram of stocks [km^3] and annual fluxes [km^{3}yr^{-1}] in the global hydrological cycle (from Dingman 1993, based on data of Shiklomanov and Sokolov 1983).

The ratio of evaporation to precipitation over land amounts to about 2/3, indicating that 1/3 of the total precipitated water is brought through advection of moist air from the

[1]Again these estimates can vary significantly depending on the data sources considered (see also Viterbo 1996). The estimates presented by the National Research Council (1986) and Peixoto and Oort (1992) for instance, suggest a less vigorous hydrological cycle than the values of Shiklomanov and Sokolov (1993, see Fig. 1.1), with 15-30% smaller values of precipitation and evaporation over the ocean, less precipitation over land (–10-20%), and less water exchange between the land and oceans' compartiments (–30%), while evaporation over land is about the same magnitude for the different estimates available.

oceans. This ratio can however vary substantially with location and season, evaporation being higher than precipitation in most mid-latitude continental regions in summer.

From the fluxes and the sizes of the reservoirs, it is possible to compute the mean residence time of water in each of the reservoirs. Based on the data of Figure 1.1, the computed mean residence time of water approximately amounts to 9000 years for the glaciers, 2650 years for the oceans, 250 years for the freshwater of the groundwater storage, 2 years for the surface water (lakes, marshes, and rivers), 52 days for the soil moisture storage, and 8 days for the atmosphere.

1.2 The role of land surface processes in the climate system

The land surface is the lower boundary for approximately 30% of the atmosphere. It exchanges moisture, momentum, and heat with the latter, mostly through turbulent fluxes taking place within the planetary boundary layer (typically the lowest 1000 m). As lower boundaries, oceans and land play different roles in the climate system. While oceans act primarily as a heat reservoir for the atmosphere, the land surface represents a water reservoir for the overlying atmosphere, providing a long-term memory for the rainfall that occurs throughout the year. Because of these differences, the importance of oceans and land for climate varies geographically: In the tropics, sea surface temperatures (SSTs) are the main factor impacting climate, but soil water has a preponderant role in mid-latitudes (Koster et al. 2000).

This section first introduces the equations describing the water and energy balances at the surface, discussing the way in which they are interrelated (section 1.2.a); then some of the main interactions between the land surface and the atmosphere are presented (section 1.2.b); finally, a brief overview on existing land surface parameterizations is given in section 1.2.c.

1.2.a The water and energy balances at the land surface

The water balance within a given area at the land surface is defined as:

$$\frac{\partial S}{\partial t} = P - E - R_s - R_u \quad , \tag{1.1}$$

where S represents the terrestrial water storage, P the precipitation, E the evapotranspiration, R_s the surface runoff, and R_u the subterreanean runoff. The evapotranspiration E encompasses plant transpiration and evaporation from other sources (e.g. bare soil, interception layer, free water surfaces).

The energy balance at the surface is driven by the net radiation at the surface, R_n, which is determined as follows:

$$\begin{aligned} R_n &= SW_{in} - SW_{out} + LW_{in} - LW_{out} \\ &= SW_{in} \cdot (1 - \alpha) + LW_{in} - \epsilon\sigma {T_s}^4 \quad , \end{aligned} \tag{1.2}$$

where SW_{in} and SW_{out} are the incoming and outgoing shortwave radiation, LW_{in} and LW_{out} are the incoming and outgoing longwave radiation, α is the surface albedo, ϵ is surface emissivity ($\cong 1.0$), σ ist the Stefan-Boltzmann constant, and T_s is the land surface temperature (see also Fig. 1.2).

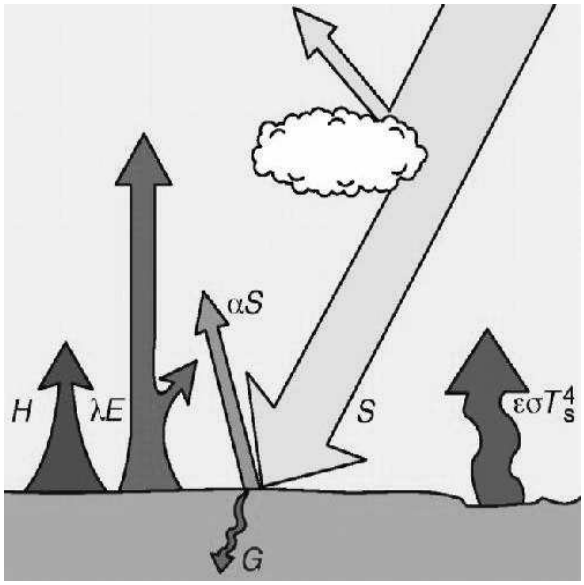

FIG. 1.2: Radiation budget and energy balance at the surface. (From Sellers et al., 1997)

When storage terms in the vegetation are neglected, energy conservation at the interface soil/vegetation/atmosphere implies (e.g. Viterbo 1996):

$$R_n \;=\; SH + LH + G \quad , \tag{1.3}$$

where SH is the sensible heat flux, LH is the latent heat flux, and G is the ground heat flux. In general, G represents only a small fraction (10% or less) of R_n when averaged over a diurnal cycle, but can be an important term in the seasonal energy budget (Sellers et al. 1997). The latent heat flux ($LH = \lambda{\cdot}E$) is directly proportional to evaporation E; λ ($= 2.5{\cdot}10^6$ J kg^{-1}) is the latent heat of vaporization.

The water and energy balance equations (eqs. (1.1) and (1.3)) are thus linked through the evapotranspiration term, which is determined by the soil moisture availability, the local atmospheric conditions, and the surface cover (vegetation, bare soil).

1.2.b Interactions between the land surface and climate

The role of the land surface in the climate system is complex, as it involves a series of processes which are closely interrelated. Terrestrial water storage, and more particularly soil moisture, is an essential element of this system. Its crucial role is due for the most part to its impact on the partitioning between the latent and sensible heat fluxes. A

measure for this partitioning is the Bowen ratio, i.e. the ratio of sensible to latent heat flux ($B = SH/LE$). Under dry conditions, the sensible heat flux tends to clearly exceed the latent heat flux, and B is much larger than 1. For wet conditions, the opposite prevails, and B is much smaller than 1. Both the latent and sensible heat fluxes have important effects on the overlying atmosphere. The sensible heat flux raises the temperature of the overlying air column and forces the development of the boundary layer in the daytime hours. On the other hand, the water vapour released by the latent heat flux moistens the overlying atmosphere and can be lifted by convection or synoptic forcing, forming clouds and precipitation some distance in time and space from its point of release (e.g. Sellers 1992).

A much studied issue has been the impact of land surface processes on precipitation, and the existence of a possible soil moisture-precipitation feedback. Earlier modelling studies gave evidence of such a feedback (e.g. Shukla and Mintz 1982, Rowntree and Bolton 1983), but its detailed mechanisms were not well investigated (see Betts et al. 1996). Recent observational and modelling studies lend support to the hypothesis of a positive soil moisture-precipitation feedback in mid-latitudes (e.g. Betts et al. 1996, Findell and Eltahir 1997, Eltahir 1998, Schär et al. 1999), but do not explain it with classical moisture recycling theories. The investigated feedback appears to rely instead on an indirect mechanism whereby the potential for convective activity is increased in the presence of wet soils, due to the buildup of a comparatively shallow boundary layer (inducing high values of low-level moist entropy), to a lowering of the level of free convection, and to an increase of the net radiative energy flux at the surface (e.g. Schär et al. 1999, Pal and Eltahir 2001). Note that such effects can play a role on time scales of a few days to a few months, and are therefore relevant both for climate modelling and numerical weather forecasting.

Vegetation also plays an important part in land surface-atmosphere interactions, mostly due to its physiological control on transpiration. Plants transpire water as a byproduct of their assimilation of carbon from the atmosphere. When soil moisture gets scarce, water loss by transpiration can be reduced through the closing of the stomata, small apertures in the surface of the leaves where the exchange of water and CO_2 takes place.

Another relevant question in the context of global warming concerns the possible response of vegetation to enhanced CO_2. It is generally assumed that enhanced CO_2 will increase the water-use efficiency of vegetation, since plants will be able to maintain the same intake of CO_2 for photosynthesis, while reducing their water loss by transpiration. This could happen through an enhancement of stomatal resistance in the short term (e.g. Eamus and Jarvis, 1989), or through a down-regulation of photosynthesis in the long term, i.e. a reduction of maximum photosynthesis capacity which is observed in some plants after extended exposure to enhanced CO_2 (e.g. Sellers et al. 1996a). Further possible adaptations of vegetation to enhanced CO_2 include an enhancement of plant growth (e.g. Fajer and Bazzaz 1992), and changes in the root-to-shoot ratio (e.g. Rogers et al. 1996). The extent to which such modifications would impact climate is, at present, still unclear.

A difficult issue for the modelling of plant feedbacks to changes in the surrounding atmosphere is the up-scaling of the measured response from the leaf level to the canopy and community levels, and further to the model resolution level. Indeed, while stomatal response to water stress and CO_2 fertilization is relatively well studied at the leaf level,

the mean response of vegetation on a scale of for instance $\sim 50\,\mathrm{km}$ is very difficult to assess. Moreover, the plant response appears to be often species-specific, and therefore difficult to apply to whole communities

Other important land surface-atmosphere interactions include albedo effects, which feed back on the surface radiation budget. Ice- and snow-albedo feedbacks are for instance essential mechanisms of winter climate. Furthermore, effects combining snow and vegetation cover also appear relevant: The albedo of snow-covered vegetation is for instance much lower for forests than for low vegetation, because the snow does not usually stay on the forest canopy (e.g. Betts et al. 1996); a correct representation of this effect has been shown to significantly improve weather simulations in boreal regions (e.g. Viterbo and Betts 1999b).

Finally, vegetation is also involved in feedbacks occurring on longer time scales such as biogeographical feedbacks involving changes in the vegetation distribution (e.g. Betts et al. 1997, Claussen 2003), or the periodic burning of forests in dry summers (e.g. Betts et al. 1996).

1.2.c Brief survey of existing land surface parameterizations

Land surface parameterizations (LSPs) are submodels used to compute the fluxes of radiation, heat, water vapour, and momentum between the land surface and the lower atmosphere. After Sellers et al. (1997), one can differentiate three stages of complexity in the LSPs currently in use: 1) the so-called "bucket" models, 2) biophysical models, or models of intermediate complexity (e.g. BATS[2], SiB[3]), and 3) physiological models (e.g. SiB2[4]). These three generations of LSPs are briefly presented hereafter. A few concluding remarks are added at the end of this section.

The bucket model

The bucket model (Fig. 1.3) was the first attempt to parameterize surface processes in a general circulation model (GCM). It was implemented by Manabe (1969) based on the concepts of evaporative factor and potential evaporation introduced by Budyko (1956).

It computes evaporation in the following way:

$$\begin{aligned} E &= \beta E_{pot} \\ &= \beta \rho_a \frac{q_{sat}(T_s) - q_r}{r_a} \quad , \end{aligned} \tag{1.4}$$

where E is the actual evaporation, E_{pot} is the potential evaporation, β is the evaporative factor, ρ_a is the density of the air, $q_{sat}(T_s)$ is the saturation water-vapour specific humidity at the temperature of the surface, q_r is the water-vapour specific humidity at the lowest layer of the atmospheric model, and r_a is the aerodynamic resistance between the surface and the lowest layer of the atmosphere. The aerodynamic resistance is defined as

[2]Biosphere-Atmosphere Transfer Scheme, Dickinson (1984)
[3]Simple Biosphere, Sellers et al. (1986)
[4]Simple Biosphere 2, Sellers et al. (1996b)

$r_a = 1/(C_{DE} \cdot U_r)$, where C_{DE} is the aerodynamic transfer coefficient for humidity (generally equal to the aerodynamic transfer coefficient for heat, C_{DH}), and U_r is the wind speed at the reference level. The β factor is a function of the soil moisture content only; it varies linearly between 0 and 1 and is defined as $\beta = \frac{W}{W_k}$, with $0 \leq \beta \leq 1$; W is the actual soil moisture content and W_k is the soil moisture content at which total evaporation is no longer considered to be limited by soil moisture availability. The potential evaporation E_{pot} represents the evaporation that would occur from a free water surface.

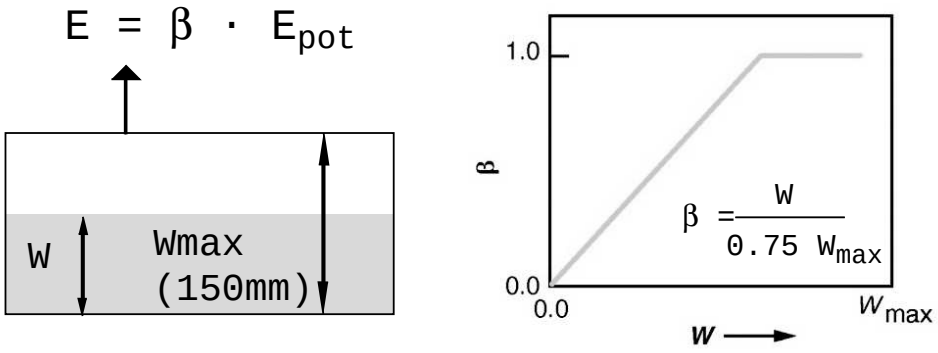

FIG. 1.3: A schematic representation of the bucket model.

The available water capacity of the bucket is generally set to 150 mm independently of the region considered. When the bucket is full, additional water input through precipitation goes into runoff. The albedo and the roughness length are prescribed as global, often uniform, fields (Sellers et al. 1997).

Biophysical models

The second-generation models (e.g. BATS, Dickinson 1984, see also chapter 2) are characterized by an explicit canopy and the accounting of the main physical processes occurring within the vegetation stand and in the soil (Fig. 1.4). This includes evaporation from three distinct sources (potential evaporation from the interception layer, bare soil evaporation, transpiration from the vegetation), leaf and snow drip, infiltration, and percolation. The vegetation cover can make use of deep root-zone water for transpiration, allowing for long-term climate memory. Surface parameters vary geographically, and are specified using look-up tables for the different land cover classes. The most important feature of these models is the biophysical control on evapotranspiration through the stomatal resistance r_s. In the following paragraphs, the computation of transpiration in BATS is described as an example for the models of this level of complexity.

The computation of r_s follows the Jarvis (1976) approach:

$$r_s = r_{smin} R_f S_f M_f V_f \quad , \tag{1.5}$$

where the factors R_f, S_f, M_f, and V_f, give the dependence of r_s on solar radiation (photosynthetically active radiation, PAR), temperature, soil moisture content, and vapour

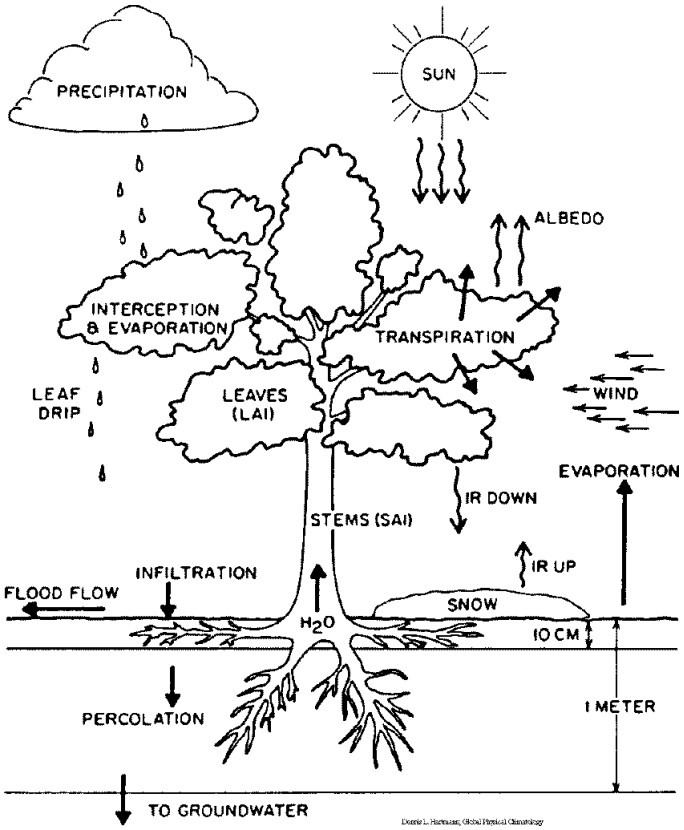

FIG. 1.4: A schematic representation of BATS (from Dickinson 1984).

pressure deficit, respectively. Under stress-free conditions, all four factors are equal to 1 and r_s is equal to the minimum stomatal resistance r_{smin}. An upper limit, r_{smax}, is also specified. The factor M_f depends on the soil moisture content and the leaf potential, and is a measure of root resistance to transpiration. This term is referred to as root resistance in chapter 2.

The resulting transpiration at the leaf level $E_{TR(leaf)}$ is defined as follows:

$$E_{TR(leaf)} = \rho_a \frac{q_{sat}(T_f) - q_{af}}{r_{la} + r_s} \quad , \tag{1.6}$$

where ρ_a is the density of the air, $q_{sat}(T_f)$ is the saturation water-vapour specific humidity at the temperature of the foliage, q_{af} is the water-vapour specific humidity of the air within the canopy, r_{la} is the aerodynamic resistance to moisture and heat transfer through the boundary layer at the foliage surface, and r_s is the stomatal resistance. Note that the term $\rho_a \frac{q_{sat}(T_f) - q_{af}}{r_{la}}$ represents the potential evaporation at the surface of the foliage (i.e. evaporation from the interception storage).

The integrated transpiration for the whole canopy $E_{TR(can)}$ can be represented with the following equation:

$$E_{TR(can)} = \rho_a \frac{q_{sat}(T_f) - q_r}{r_a + r_c} \quad , \tag{1.7}$$

where r_c, the canopy resistance, is the integral mean of the resistance of the individual leaves assumed to act in parallel (Dickinson et al. 1991, Viterbo 1996), and ρ_a, q_r, and r_a are defined in the same way as in (1.4). Thus, the main difference between (1.4) and (1.7) is that, in the case of the bucket model, the moisture limitation term is applied externally to an estimate of the maximum evaporation rate, while in (1.7) the canopy resistance is applied in series with r_a, realistically separating the aerodynamic and surface resistance terms (e.g. Sellers 1996).

Physiological models

These models (e.g. SiB2, Sellers et al. 1996b) explicitly simulate the plant photosynthesis, including nutrients uptake, enzyme kinetics, electron transport, and the light interception by chloroplasts in plant leaves. Leaf conductance g_s $(1/r_s)$ is computed as a function of net CO_2 assimilation (Ball 1988):

$$g_s = m\frac{A_n}{c_s}h_s p + b \quad , \tag{1.8}$$

where m is an empirical coefficient derived from observations, A_n is the net CO_2 assimilation, c_s is the CO_2 concentration at the leaf surface, h_s is the relative humidity at the leaf surface, p is the atmospheric pressure, and b is a minimum value of g_s.

Some of the main advantages of the physiological models compared to the LSPs of the second generation are, first, that they are more realistic biologically, second, that they require fewer empirical parameters, and finally, that they can directly respond to changes in CO_2 in a realistic way, a very important aspect for climate change studies. As mentioned in section 1.2.b, plant response to CO_2 enhancement is diverse and is likely to impact future climate in a significant way.

Concluding remarks

This section has given a brief overview of the LSPs currently available for atmospheric models. As seen above, there have been large improvements in this field in the past few decades, going from the very simple bucket model up to the detailed biophysical and physiological models which are now available. Note that some other important LSP developments are not documented here, such as the inclusion of ecosystem dynamics (e.g. Foley et al. 1996), and the representation of sub-grid scale variability using the so-called "mosaic" approach or statistical-dynamical models (see Chen 2001 for a review).

Despite the availability of more advanced LSPs, the bucket model and variations of it are still used in a few GCMs (e.g. Manabe and Wetherald 1999). It is known, however, to be inadequate for a number reasons (Viterbo 1996): First, it overestimates bare soil evaporation in all regimes; second, it does not include any mechanism reproducing the vegetation control on transpiration and thus overestimates evaporation for dry conditions over vegetated areas; finally, even in the case of unstressed vegetation, it will evaporate at the potential rate (E_{pot}) instead of the maximum transpiration rate allowed by vegetation (minimum, non-zero value of the stomatal resistance). Figure 1.5 from the Project for Intercomparison of Land Parametrization Schemes (PILPS, e.g. Henderson-Sellers et al.

1996) illustrates this last point. It shows a comparison between the investigated LSPs with regards to their partitioning of net radiation in the sensible and latent heat fluxes when forced with observed atmospheric conditions (net radiation, precipitation); the considered site is situated in Cabauw, the Netherlands, and characterized by a permanently saturated deep soil. The observed sensible and latent heat fluxes amount to about 0 Wm^{-2}, and 40 Wm^{-2} respectively. For this site, the bucket model clearly behaves anomalously compared with the other LSPs considered, exhibiting a far too large estimation of latent heat flux compared to sensible heat flux.

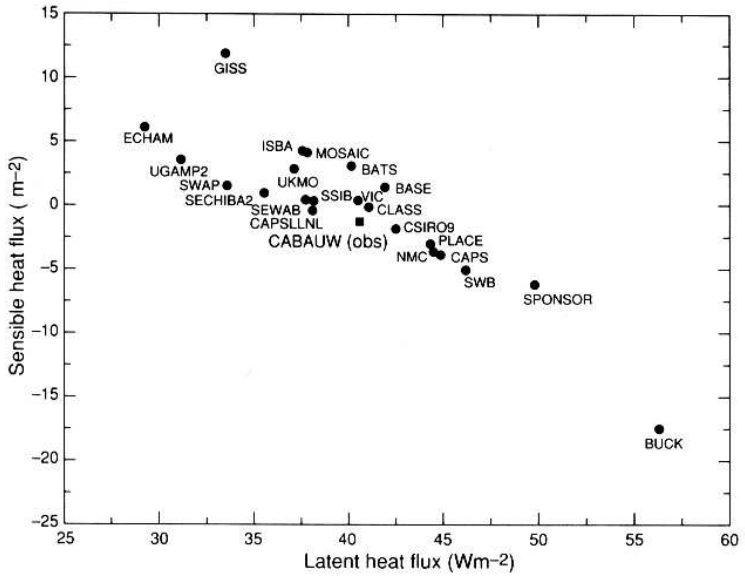

FIG. 1.5: Annually averaged latent and sensible heat fluxes simulated by the PILPS land-surface schemes (dots) and single year's observations from Cabauw, the Netherlands (square). The bucket model is denoted as "BUCK". (Henderson-Sellers et al. 1996).

Though they somewhat better agree with the observations, the other LSPs still show a large spread, and some of them exhibit significant biases. This illustrates the uncertainty still attached to these parameterizations, and the need for further validation and comparison studies such as PILPS.

1.3 Aims and outline of this study

In this thesis, various aspects linked to terrestrial water storage and its role in climate are investigated. The questions addressed are the dependency of simulations of present and warmer climate on the chosen parameterization of the land surface processes, and the possible estimation of monthly variations in terrestrial water storage using water-balance computations based on reanalysis data and observations. The core of the thesis consists of two papers presented in chapters 2 and 3. Further results and applications follow in chapter 4, and an additional paper is presented in the appendix.

The first study (chapter 2, Seneviratne et al. 2002) investigates the role of land-surface processes for mid-latitude climate change, focusing on the risk of enhanced sum-

mer droughts in these regions. As mentioned earlier, these predictions are largely based on GCM simulations using the bucket model as land surface parameterization. In this study, regional climate simulations are run over North America for present and future climatic conditions, using a land-surface scheme of intermediate complexity (BATS), and a simplified version of it, mimicking the behaviour of the bucket model. The chosen set-up allows to investigate thermodynamic changes associated with global warming in comparative isolation. Possible circulation changes, however, are not accounted for. The results suggest that the simulated response of the land surface is very dependent on the land surface scheme employed, and that the risk of enhanced summer dryness in the studied region might be less acute than previously assumed, provided the North American general circulation does not change markedly with global warming.

Recognizing that the deficiencies of current land surface parameterizations are due for the most part to the lack of proper observations of terrestrial water storage, the second study (chapter 3, Seneviratne et al. 2003) investigates the feasibility of estimating changes in terrestrial water storage from water-balance calculations. This method allows to estimate monthly variations in terrestrial water storage using three main variables: the water vapour flux convergence, the atmospheric moisture content, and river runoff. The two first variables are available with high resolution and good accuracy in present reanalysis data, and river runoff is commonly measured in most parts of the world. Results are presented for the Mississippi river basin and validated over Illinois, where measurements of the main components of the terrestrial water storage (soil moisture, groundwater level, and snow cover) are available. The water-balance estimates of the monthly variations in terrestrial water storage show very good agreement with the observations. The mean seasonal cycle is well represented for the studied period and the interannual variability is in general well captured. Though the method has some limitations and can only be applied to large areas (exceeding 10^5 km^2), these are very promising results with a range of potential applications.

Chapter 4 derives estimates of terrestrial water-storage variations for river basins in Europe and Northern Asia using the aforementioned methodology, and gives a validation of the simulations of chapter 2 against observed soil moisture in Illinois. The computed estimates for Europe and Northern Asia show a realistic mean seasonal behaviour in most basins. Interestingly, the accuracy of the computed water balances appears to depend both on domain size and on regional terrain and climate characteristics. The validation of the control integrations of the chapter 2 study shows that the simulated soil moisture compares well with the observed soil moisture, suggesting an overall correct representation of the land-surface processes for the considered region.

Finally, a co-authored paper (Vidale et al. 2003) is presented in the appendix A. It discusses the issue of uncertainty and predictability in simulating current mid-latitude climates with a regional climate model. A comparison is conducted of the uncertainties originating from intrinsic predictability limitations with uncertainties originating from the model formulations. It shows that the latter type of uncertainties is predominant during mid-latitude summer climates, while the colder seasons are well represented. An important issue discussed in this study is the compensation of model errors. Some model formulations may produce seemingly correct results for incorrect reasons, for instance by compromising the soundness of the model's water cycle. This is of particular concern when using models tuned for present climate in climate-change simulations.

Chapter 2

Greenhouse Warming and Mid-latitude Summer Dryness

Summer Dryness in a Warmer Climate: A Process Study with a Regional Climate Model †

Sonia I. Seneviratne[1*], Jeremy S. Pal[2], Elfatih A.B. Eltahir[2], and Christoph Schär[1]

[1]*Atmospheric and Climate Science, ETH Zurich, Switzerland*
[2]*Ralph M. Parsons Laboratory for Hydrodynamics and Water Resources, MIT, Cambridge, USA*

ABSTRACT

Earlier GCM studies have expressed the concern that an enhancement of greenhouse warming might increase the occurrence of summer droughts in mid-latitudes, especially in southern Europe and central North America. This could represent a severe threat for the agriculture of the regions concerned, where summer is the main growing season. These predictions must however be considered as uncertain, since most studies featuring enhanced summer dryness in mid-latitudes use very simple representations of the land-surface processes ("bucket" models), despite their key importance for the issue considered.

The current study uses a regional climate model including a land-surface scheme of intermediate complexity to investigate the sensitivity of the summer climate to enhanced greenhouse warming over the American Midwest. A surrogate climate change scenario is used for the simulation of a warmer climate. The control runs are driven at the lateral boundaries and the sea surface by reanalysis data and observations, respectively. The warmer climate experiments are forced by a modified set of initial and lateral boundary conditions. The modifications consist of a uniform 3 K temperature increase and an attendant increase of specific humidity (unchanged relative humidity). This strategy maintains a similar dynamical forcing in the warmer climate experiments, thus allowing to investigate thermodynamical impacts of climate change in comparative isolation. The atmospheric CO_2 concentration of the sensitivity experiments is set to four times its pre-industrial value. The simulations are conducted from March 15 to October 1st, for 4 years corresponding to drought (1988), normal (1986, 1990) and flood (1993) conditions.

The numerical experiments do on average not present any large enhancement of summer drying under warmer climatic conditions. First, the overall changes in the hydrological cycle (especially evapotranspiration) are of small magnitude despite the strong forcing applied. Second, precipitation increases in spring lead to higher soil water recharge during this season, compensating for the enhanced soil moisture depletion occurring later in the year. Additional simulations replacing the plant control on tranpiration with a bucket-type formulation yield a large enhancement of soil drying in 1988, the drought year. This suggests that vegetation control on transpiration might play an important part in counteracting an enhancement of summer drying when soil water gets limited.

Though further aspects of this issue would need investigating, our results underline the importance of land-surface processes in climate integrations and suggest that the risk of enhanced summer dryness in the studied region might be less acute than previously assumed, provided the North American general circulation does not change markedly with global warming.

†Climate Dynamics (2002), 20: 69-85.

*Corresponding author: Sonia I. Seneviratne, Atmospheric and Climate Science ETH, Winterthurerstr. 190, CH-8057 Zurich, Switzerland. E-mail: sonia.seneviratne@ethz.ch

2.1 Introduction

Earlier numerical studies with general circulation models (GCMs) have expressed the concern that rising concentrations of carbon dioxide and other greenhouse gases might increase the occurrence of summer droughts in mid-latitudes (e.g. Manabe et al. 1981, Wetherald and Manabe 1995, 1999). This could represent a severe threat for the agriculture of the regions concerned, where summer is the main growing season. The regions which might particularly be affected are southern Europe and central North America (e.g. Kattenberg et al. 1996). In this study we focus on the American Midwest, one of the agriculturally most productive areas in the world.

The responsible mechanism was inferred by Wetherald and Manabe (1995; hereafter referred to as WM95). According to their analysis, enhanced greenhouse gas forcing leads to an increase in net surface radiation, which is primarily balanced by latent rather than sensible heat flux in the equatorward side of the mid-latitude rain belt (45°N-60°N). The increase in evapotranspiration accumulates during late spring and summer such as to deplete soil moisture. Towards late summer soil moisture becomes so low that evapotranspiration cannot increase any further, leading to an increase in sensible heat flux and an additional enhancement of surface temperature. Extra precipitation that occurs in winter and spring is unable to correct for this development, as the soil in the control and enhanced-CO_2 experiments is generally close to saturation at this time; this ensures that much of the extra precipitation occurring in the enhanced-CO_2 integrations is not stored in the soil but lost to runoff. Later increases in evapotranspiration can therefore not be counterbalanced.

In agreement with these hypotheses, various GCM studies feature enhanced summer dryness in mid-latitudes under increased atmospheric CO_2 concentrations (e.g. Rind et al. 1990, Kattenberg et al. 1996, Gregory et al. 1997, Cubasch et al. 2001). Transient climate change experiments accounting for future changes in aerosol concentrations yield a somewhat delayed response but qualitatively similar results (Wetherald and Manabe 1999). Accordingly, the enhanced occurrence of summer drought in mid-latitudes, though not confirmed by observations up to now, is generally considered a likely (Cubasch et al. 2001) or very likely (Easterling et al. 2000) future consequence of climate change.

However, the simulation of the summer hydrological cycle over extratropical landmasses is a highly sensitive issue. Even with current atmospheric greenhouse gas concentrations, many models have a mild or even strong summer drying. This problem affects free GCM simulations with prescribed sea surface temperatures (e.g. Wild et al. 1996), regional climate models driven by observed lateral boundary conditions (e.g. Machenhauer et al. 1998), and even weather forecasting models (Betts et al. 1996). Substantial research was devoted to clarify the source of this problem, which proves a difficult task as many model aspects appear relevant (radiation, clouds, convective precipitation, land-surface processes). For the ECHAM3 atmospheric GCM, Wild et al. (1995, 1996) identified excessive solar radiation as one of the key problems, and demonstrated how improving the respective parameterization did largely reduce summer dryness. Another possible source of the summer dryness problem within simulations of the present climate is in the parameterization of convective clouds and their interaction with evapotranspiration. Dry soils can promote a reduction of convective precipitation, and this feedback may further amplify soil moisture loss. The underlying feedback is known to be sensitive to a wide

range of processes, including cloud-radiation interaction (Findell and Eltahir 1997, Schär et al. 1999, Heck et al. 2001).

Finally, as pointed out by Kattenberg et al. (1996), most climate change studies featuring enhanced summer dryness use very simple representations of the land surface ("bucket" models; see Manabe 1969). The bucket model is known to overestimate evaporation over bare ground and for dry conditions over vegetated areas (Viterbo 1996). It does also overestimate daytime evaporation when energy and soil moisture are available (Dickinson and Henderson-Sellers 1988, Henderson-Sellers et al. 1996). These characteristics may exaggerate summer dryness in climate change experiments employing a bucket parameterization of the land-surface hydrology (Gates et al. 1996, Kattenberg et al. 1996). In contrast, Déqué et al. (1998), who use a more sophisticated land-surface parameterization in climate change simulations with a variable resolution GCM, find only little climate change impact upon soil moisture over Europe. It is thus desirable to investigate this issue with models that include realistic representations of short-wave radiation, precipitation and land-surface processes.

Here we use a regional climate model (RCM) with a land-surface scheme of intermediate complexity (the Biosphere-Atmosphere Transfer Scheme BATS, see Dickinson et al. 1993), to investigate this issue over the Midwestern United States. We use the methodology of surrogate climate scenario proposed by Schär et al. (1996) for the simulation of warmer climatic conditions. The procedure is distinct from GCM-based climate change scenarios. The control (CTL) simulations are initialized and driven at their lateral and sea surface boundaries by observations and reanalysis data. The warm climate scenario investigates a hypothetical climate state with enhanced air and surface temperature, unchanged relative humidity and increased CO_2 concentrations. The methodology consists of driving the warm climate experiments (WARM) by a modified set of initial and lateral boundary conditions characterized by a uniform warming of 3 K and an attendent shift in absolute humidity (consistent with unchanged relative humidity). In essence, the driving fields of the WARM and CTL simulations are dynamically identical, but characterized by shifts in temperature and absolute humidity. The two scenarios may therefore be associated with different hydrological cycles within the model domain, while presenting similar synoptic patterns. This methodology is well suited to investigate a complex loop of physical feedback processes, since ambiguities due to different synoptic settings are minimized by design. The simulations are conducted over the contiguous United States for the springs and summers of four years, representing drought (1988), normal (1986, 1990), and flood (1993) conditions.

2.2 Model description

The present experiments are performed with a modified version of the National Center for Atmospheric Research's Regional Climate Model (RegCM); a detailed description of the NCAR RegCM can be found in Giorgi et al. (1993a,b) and Giorgi and Mearns (1999). Here we briefly summarize the main features of the model employed.

RegCM is built upon the NCAR - Pennsylvania State University (NCAR-PSU) Mesoscale Model version 4 (MM4; Anthes et al. 1987). It is a hydrostatic primitive equation model in σ_p vertical coordinates. Here $\sigma_p = (p - p_{top})/(p_s - p_{top})$, where p is pressure, p_{top}

is the pressure specified at the top of the model, and p_s is the prognostic surface pressure. For our experiments, p_{top} is 50 mbar and 14 levels in the vertical are specified.

Large-scale clouds and precipitation are represented using the sub-grid explicit moisture scheme (SUBEX) developed by Pal et al. (2000). Cumulus convection is represented using the Grell parameterization (Grell 1993, Grell et al. 1994) in which the Fritsch-Chappell closure assumption (Fritsch and Chappell 1980) is implemented. The atmospheric radiative transfer computations are performed using the formulation from NCAR's Community Climate Model version 3 (CCM3; Kiehl et al. 1998) with the inclusion of an additional routine accounting for changes in the concentrations of trace gases (E.E. Small, personal communication, 1998). The planetary boundary layer computations are performed using the non-local formulation of Holtslag et al. (1990).

The Biosphere-Atmosphere Transfer Scheme version 1e (BATS1e; Dickinson et al. 1993) is used for the surface physics calculations. BATS describes the exchange of heat, moisture and momentum between the atmosphere and the land surface. It comprises one vegetation canopy layer, three soil layers and one snow layer. The soil layers comprise a 10 cm surface layer, a 1, 1.5 or 2 m root zone (depending on the vegetation type), and a 3 m deep soil layer; all layers start from the surface, i.e. the deep soil layer includes both the root layer and the surface layer, and the root layer includes the surface layer.

Evapotranspiration over land in BATS originates from three sources: bare soil evaporation from the top soil layer, transpiration from the root zone (dry leaves), and potential evaporation from the interception layer (wet leaves). Transpiration (E_{TR}) is by far the largest of the three terms in mid-latitude spring and summer. It is expressed as follows: $E_{TR} = \frac{r_{la}}{r_{la}+r_s} E_{pot}$, where r_{la} is the aerodynamic resistance to moisture and heat transfer through the boundary layer at the foliage surface, r_s is the stomatal resistance, and E_{pot} is the potential evaporation.

The stomatal resistance r_s is the resistance of foliage to water vapor transfer. BATS follows the Jarvis-type approach (Jarvis 1976) for its computation: $r_s = r_{smin} R_f S_f M_f V_f$, where the factors R_f, S_f, M_f and V_f give the dependence of r_s on solar radiation, seasonal temperature evolution, moisture content and vapor pressure deficit, respectively. Under stress-free conditions, all four factors are equal to 1 and r_s is equal to the minimum stomatal resistance r_{smin}. An upper limit, r_{smax}, is also specified.

Transpiration is further limited in BATS by the root resistance to water uptake. A maximum transpiration rate E_{TRmax} is defined using a non-linear function of the soil water content.

A modification used in the present model version is a revised specification of minimum stomatal resistance based on the existing literature. BATS specifies r_{smin} values of 120 s/m for crops, 150 s/m for evergreen broadleef trees, and 200 s/m for all other land cover/vegetation types (including forests and grasslands). These values appear to be too high in view of observations (e.g. Rowntree 1991), results from back-interpolation studies (Dorman and Sellers 1989) or typical modelling applications (e.g. Jacquemin and Noilhan 1990). Here, we use new specifications of r_{smin} of 40 s/m for crops and 80 s/m for all other vegetation types. These values appear to be closer to the aforementioned estimates and observations. The control and sensitivity experiments were conducted for both settings of r_{smin}. The modification shows little impact on the control integrations, except in 1993 where it leads to a better prediction of the Midwest flood, and the impact on the sensitivity experiments is small as well.

2.3 Design of numerical experiments

A summary of the performed experiments can be found in Table 2.1. The control and sensitivity experiments are initialized on March 15 for each of the following years: 1986, 1988, 1990, and 1993. The runs are integrated until October 1st, i.e. for a period of 200 days (6 1/2 months).

The chosen years cover a wide range of historical hydrological situations over the American Midwest. While 1986 and 1990 can be considered "normal" years, 1988 was characterized by the warmest and driest summer experienced in the United States since 1936 (e.g. Ropelewski 1988), and the 1993 summer flooding over the American Midwest was one of the most devastating floods in modern history (e.g. Kunkel et al. 1994). The very different conditions which prevailed during these four years are for instance apparent from the top soil moisture (Fig. 2.1) and precipitation observations (Fig. 2.2).

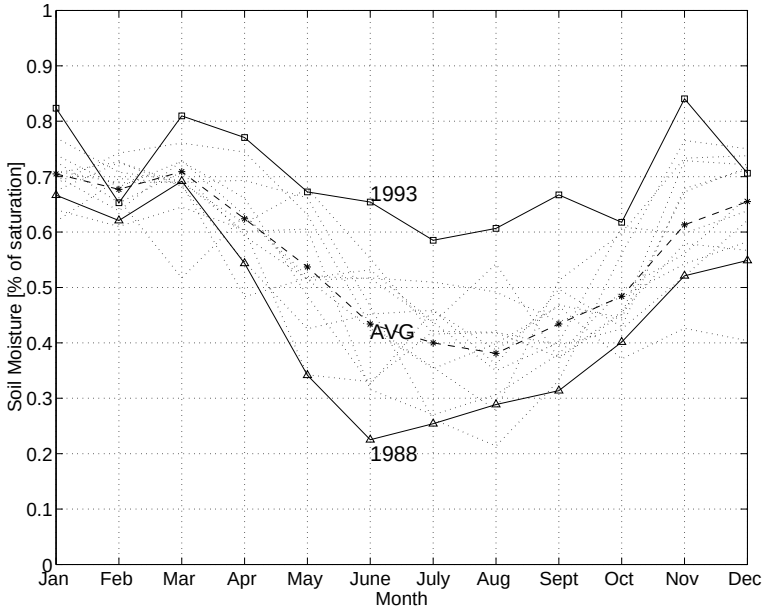

FIG. 2.1: Illinois State Water Survey monthly averaged relative soil moisture content from 0 to 10 cm for 1981 to 1993: 1988 (solid line with triangles); 1993 (solid line with squares); rest of the years (dotted lines); average over all years (dashed line with asterisks). Data from Hollinger and Isard (1994).

The model domain covers all of the contiguous United States and parts of Canada and Mexico (see Fig. 2.3). The grid is defined on a rotated Mercator map projection. The domain is centered at 37.581°N and 95°W, and the origin of the map projection is rotated to 40°N and 95°W. It comprises 129EW×80NS grid points, with a horizontal grid spacing of 55.6 km (approximately half a degree). The region of focus for the analysis is the American Midwest (outlined in Figure 2.3).

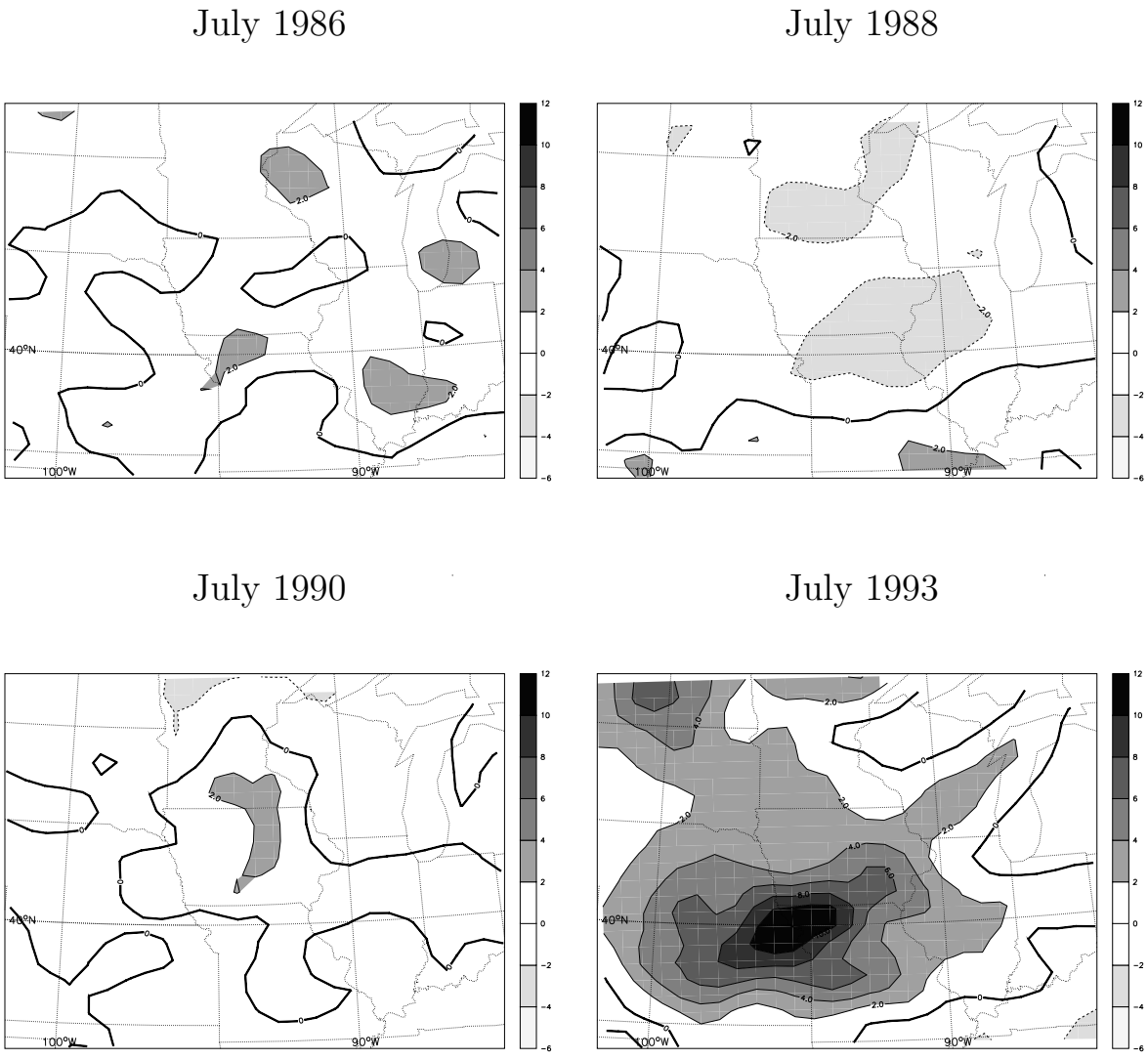

FIG. 2.2: Rainfall anomalies [mm/day] for July 1986, 1988, 1990, and 1993 over the American Midwest as derived from the USHCN data set (Karl et al. 1990) relative to a climatological value based on 16 years of observations (1980-1996). A weak spatial smoothing has been applied for display purposes. Shading occurs above and below anomalies of 2 mm/day.

TABLE 2.1: CTL, WARM, BUCKTRA_CTL, BUCKTRA_WARM, and $NOCO_2$ experiments

Experiments	Initial and Boundary Fields				Atm. CO_2	Transpiration Term
	Air Temp.	Sea Surface Temp.	Rel. Hum.	Other Fields[a]		
CTL86	TA86	SST86	RH86	INBC86	348 ppmv	BATS
CTL88	TA88	SST88	RH88	INBC88	351 ppmv	
CTL90	TA90	SST90	RH90	INBC90	354 ppmv	
CTL93	TA93	SST93	RH93	INBC93	359 ppmv	
WARM86	TA86+3K	SST86+3K	RH86	INBC86	1120 ppmv	BATS
WARM88	TA88+3K	SST88+3K	RH88	INBC88	1120 ppmv	
WARM90	TA90+3K	SST90+3K	RH90	INBC90	1120 ppmv	
WARM93	TA93+3K	SST93+3K	RH93	INBC93	1120 ppmv	
BUCKTRA_CTL86	TA86	SST86	RH86	INBC86	348 ppmv	Bucket-type
BUCKTRA_CTL88	TA88	SST88	RH88	INBC88	351 ppmv	
BUCKTRA_CTL90	TA90	SST90	RH90	INBC90	354 ppmv	
BUCKTRA_CTL93	TA93	SST93	RH93	INBC93	359 ppmv	
BUCKTRA_WARM86	TA86+3K	SST86+3K	RH86	INBC86	1120 ppmv	Bucket-type
BUCKTRA_WARM88	TA88+3K	SST88+3K	RH88	INBC88	1120 ppmv	
BUCKTRA_WARM90	TA90+3K	SST90+3K	RH90	INBC90	1120 ppmv	
BUCKTRA_WARM93	TA93+3K	SST93+3K	RH93	INBC93	1120 ppmv	
$NOCO_2$86	TA86+3K	SST86+3K	RH86	INBC86	348 ppmv	BATS
$NOCO_2$88	TA88+3K	SST88+3K	RH88	INBC88	351 ppmv	
$NOCO_2$90	TA90+3K	SST90+3K	RH90	INBC90	354 ppmv	
$NOCO_2$93	TA93+3K	SST93+3K	RH93	INBC93	359 ppmv	

[a] The other initial and boundary fields (INBC) are the wind components, surface pressure, and soil moisture.

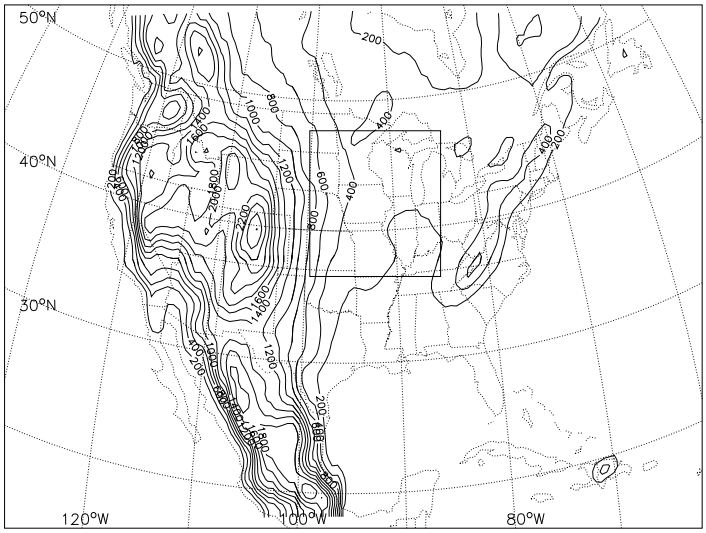

FIG. 2.3: Computational domain and topography [m] used for the numerical simulations. The Midwest analysis region (outlined box) is also indicated (approximately 36°N to 48°N, 99°W to 87°W).

2.3.a *Control experiments*

The control simulations for 1986, 1988, 1990, and 1993 (hereafter CTL86, CTL88, CTL90, and CTL93) are initialized and driven at their sea surface and lateral boundaries by observations and reanalysis data, respectively.

The initial and boundary conditions for wind, temperature, surface pressure, and water vapor are taken from the National Center for Environmental Prediction's (NCEP) reanalysis data. The sea surface temperatures (SST) are taken from the United Kingdom Meteorological Office (UKMO) SST dataset. The soil moisture dataset used to initialize the experiments (hereafter PE01) is described in Pal and Eltahir (2001). It is a merged dataset combining data from the Illinois State Water Survey (Hollinger and Isard 1994), a U.S. derived soil moisture dataset (Huang et al. 1996), and a climatology based on vegetation types. The lateral boundaries are employed using a relaxation technique described in Davies and Turner (1977).

The atmospheric CO_2 concentrations of the control runs are set to the historical value of the respective simulation year; the values for 1986, 1988, 1990, and 1993 range between 350 and 360 ppmv (see Table 2.1).

2.3.b *WARM experiments*

A surrogate climate change scenario following the methodology proposed by Schär et al. (1996) is used for the simulation of a warmer climate. The warm climate simulations for 1986, 1988, 1990, and 1993 (hereafter WARM86, WARM88, WARM90, and WARM93) are driven with the initial and boundary fields of the control runs, modified so that the atmospheric and sea surface temperatures are increased uniformly by 3 K, while the relative humidity remains unchanged (all other initial and boundary fields are identical

for both sets of simulations). This modification results in a substantial increase of the specific humidity (approximately +21% for a temperature increase of +3 K), and retains the system's characteristic dynamic and thermodynamic balances (Schär et al. 1996, Frei et al. 1998).

The atmospheric CO_2 concentration of the WARM simulations is set to four times its pre-industrial value (280 ppmv), i.e. 1120 ppmv. Thus the atmospheric CO_2 concentration of the WARM experiments is equal to about three times the concentration of the control runs (see Table 2.1).

We chose a particularly strong forcing in order to increase the "signal-to-noise ratio" in our experiments. This also allows a better comparison with the experiments of WM95, who use an even larger CO_2 forcing (300 ppmv in the control integrations and 1200 ppmv in the enhanced-CO_2 experiments). Their simulations also display a much larger warming than the temperature forcing applied in the present simulations (about +8 K increase in surface air temperature in global average). This should be kept in mind when comparing the results of these two studies.

The chosen procedure is useful for identifying key mechanisms induced by warmer climatic conditions, but also entails some limitations. In particular, the design of the experiments implies that the control and warmer climate integrations are characterized by similar synoptic climatologies. In reality, one expects that global warming will be associated with possibly significant changes in location and amplitude of the storm tracks (e.g. Cubasch et al. 2001); that may in turn affect the frequency of droughts and floods (e.g. Mo et al. 1997). We should however emphasize that the experiments are only constrained by the initial conditions and at the boundaries; since the model domain is fairly large, the simulations can still develop diverging circulation patterns in the interior. The idealized set-up of the WARM experiments nevertheless implies that they should not be viewed as predictions, but as an investigation of the thermodynamic climate change effects upon the mid-latitude summer climate.

2.3.c BUCKTRA experiments

In order to assess the extent to which the land-surface parameterization is responsible for the sensitivity of the WARM experiments, additional integrations are conducted with a bucket-type formulation of transpiration. These sets of experiments will be referred to as BUCKTRA_CTL and BUCKTRA_WARM (see Table 2.1).

The bucket model (Manabe 1969) computes evaporation as $E = \beta\ E_{pot}$, where β, the "evaporative factor" (Budyko, 1974), is a function of the soil moisture content only and where E_{pot} denotes the potential evaporation. The β factor varies linearly between 0 and 1 and is defined as $\beta = \frac{W}{W_k}$, where W is the actual soil moisture content and W_k is the soil moisture content at which total evaporation is no longer considered to be limited by soil moisture availability. Manabe (1969) uses $W_K = 0.75\ W_{FC}$, where W_{FC} is the field capacity.

In order to simulate a bucket-type behaviour of transpiration in BATS, the following two modifications are performed in the BUCKTRA experiments:

1. In BATS, transpiration (E_{TR}) is defined as: $E_{TR} = \frac{r_{la}}{r_{la}+r_s} E_{pot}$ (see Section 2.2). In the BUCKTRA simulations, the term $\frac{r_{la}}{r_{la}+r_s}$ is replaced by a β evaporative factor

defined in the following manner: $\beta = \frac{W - W_{PWP}}{W_k - W_{PWP}}$, with $0 \leq \beta \leq 1$, where W is the soil moisture content, W_k is 0.75 times the field capacity, and W_{PWP} is the soil moisture content at the plant wilting point.

2. The upper limit for transpiration E_{TRmax}, which represents the impact of root resistance on the plant water uptake (see Section 2.2), is suppressed.

These modifications replace the control imposed by stomatal and root resistances on transpiration by a single factor, depending on the soil moisture content only. Note that the BUCKTRA simulations still include bare soil evaporation and potential evaporation from the interception storage, which are considered of minor importance for the present comparisons. The role of further significant differences between the bucket model and the BATS land-surface scheme, such as the available water capacity or the treatment of runoff and groundwater drainage, are not investigated here, but might also be relevant to the issue.

2.3.d NOCO$_2$ experiments

In order to quantify the relative impact of the local increase in atmospheric CO_2 concentration versus the thermodynamic modifications in the WARM experiments, additional simulations are conducted including the thermodynamic modifications only (warming of air temperature and SST by 3 K with unchanged relative humidity). This set of experiments uses the present-day values of the CO_2 concentrations and will be referred to as NOCO$_2$ (see Table 2.1 for a summary).

2.4 Control integrations

The validation of the control integrations is kept short, since the employed model version has been extensively validated in a similar setup by Pal (2001). In this section we focus therefore on the validation of precipitation against observations from the United States Historical Climate Network data set (USHCN; Karl et al. 1990) and on the comparison of the simulated evolution of evapotranspiration over the state of Illinois with estimates based on observational data (Yeh et al. 1998).

Figure 2.4 shows the temporal evolution of simulated precipitation over the Midwest for the extreme years (1988 and 1993) and the average of the four years. The model is able to capture the interannual variability of precipitation and simulates well the different evolutions observed in the normal and extreme years.

The spatial representation of precipitation over the whole domain is satisfactory as well; for illustration the predicted precipitation for two extreme dry and wet months, June 1988 and July 1993 respectively, are displayed in Figure 2.5. The very low precipitation observed in June 1988 in the Midwestern United States is well captured by the model; there is however an underestimation of precipitation over Texas, Nebraska, and South Dakota during this month. Similarly, the rainfall peak of July 1993 over the Midwest is well captured, although somewhat shifted to the northeast; in the rest of the United States, precipitation is slightly underestimated. From these comparisons, we can conclude that

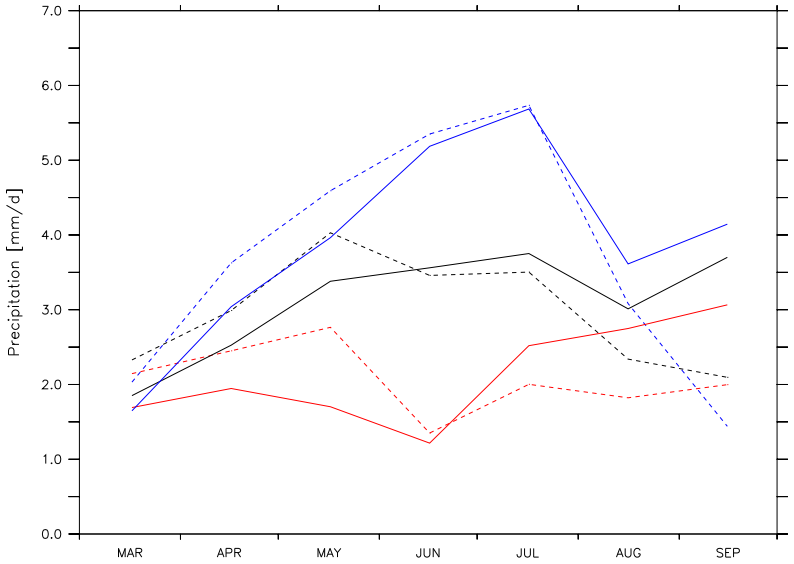

FIG. 2.4: Observed (solid) and CTL (dashed) monthly precipitation [mm/d] over the American Midwest for 1988 (red), 1993 (blue) and the average of the four years: 1986, 1988, 1990, and 1993 (black). Observations are from the USHCN dataset (Karl et al. 1990). The values are spatial averages over the box outlined in Figure 2.3.

the model captures precipitation variations satisfactorily, particularly over the Midwest focus region.

Since the simulation of evapotranspiration is of critical importance for the considered issue, we also compare the simulated evolution of evapotranspiration over the state of Illinois against the soil and atmospheric water balance estimates of Yeh et al. (1998). Figure 2.6 displays the temporal evolutions of the mean evapotranspiration in the CTL integrations over Illinois as well as the monthly evapotranspiration estimates. Though there seems to be an overestimation of evapotranspiration in spring (mostly in 1993, not shown), the simulated evolution of evapotranspiration is on the whole very satisfactory and in qualitative and quantitative agreement with the estimates.

2.5 Results of the sensitivity experiments

Unless otherwise specified, comparisons are made over a focus region centered on the American Midwest (see Figure 2.3). This subdomain extends from about 36°N to 48°N, and 99°W to 87°W. Note that this region is located at lower latitudes than those investigated by WM95 (45°N to 60°N).

2.5.a WARM experiments: Hydrological cycle

The results of the integrations are summarized in Table 2.2 and compared against those of WM95 (Table 2.3). Figure 2.7 presents the mean temporal evolution of precipitation, evapotranspiration, and total runoff over the Midwest subdomain in the CTL and WARM integrations. The magnitude of the observed changes is small compared to the results of WM95. The highest differences in precipitation and evapotranspiration are on the order

(a) Observed Precipitation (b) CTL Precipitation

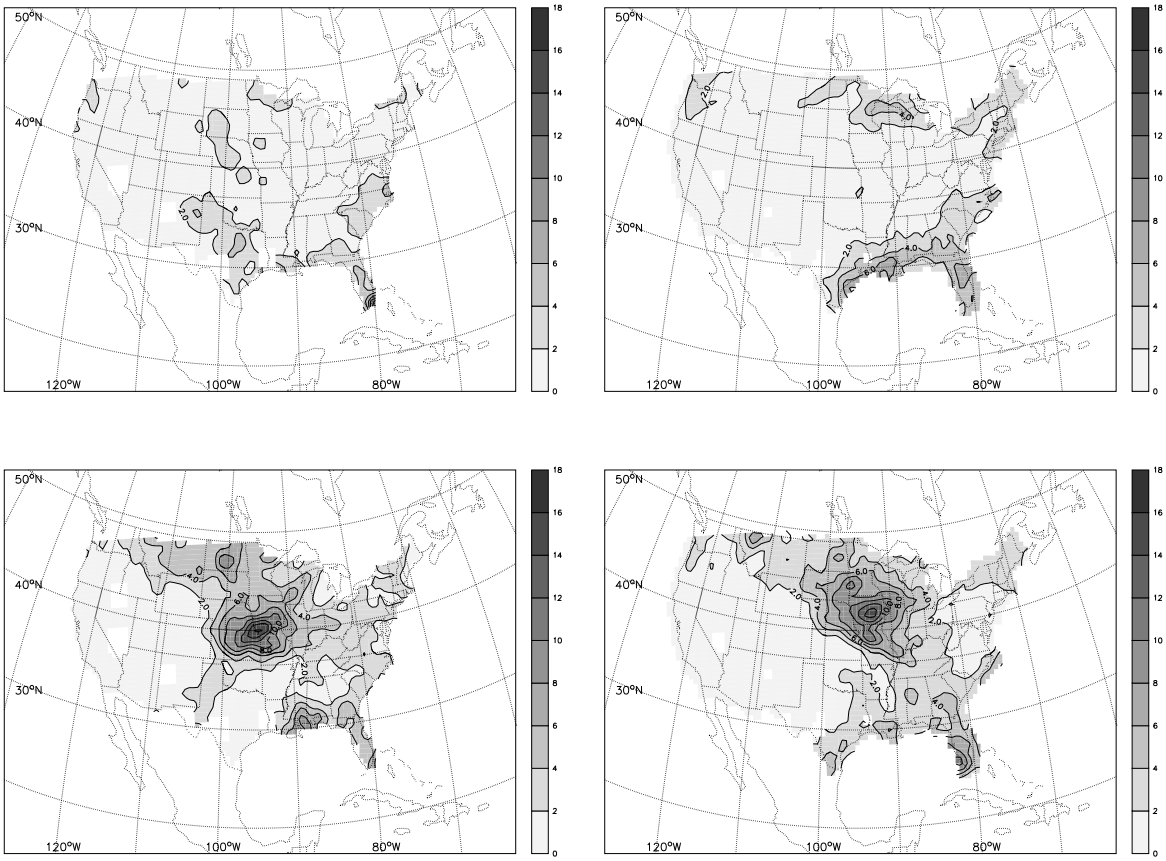

FIG. 2.5: Observed (a) and CTL (b) precipitation [mm/d] over the United States in June 88 (top) and July 93 (bottom). Observations are from the USHCN data set (Karl et al. 1990). Note that the USHCN observations only exist over the United States. A weak spatial smoothing has been applied for display purposes.

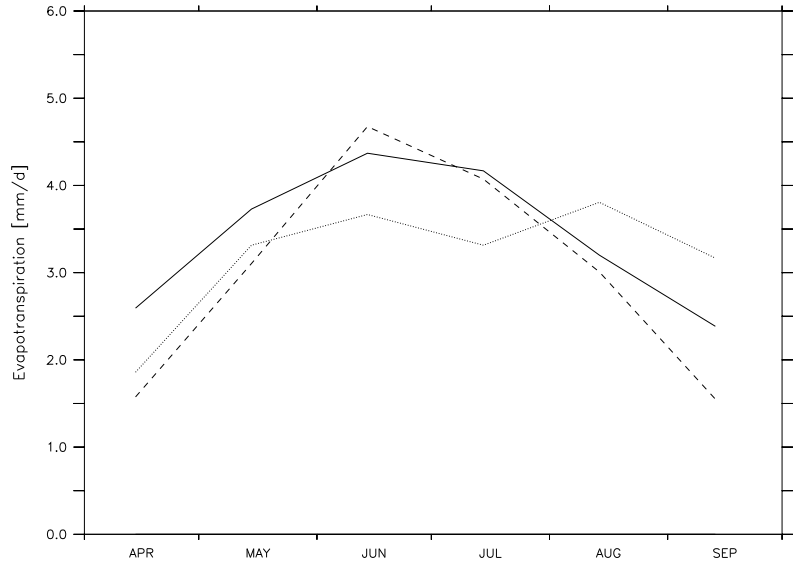

FIG. 2.6: Mean monthly land evapotranspiration in the CTL simulations (solid) averaged over Illinois (coordinates of subdomain: 36°N to 43°N and 93°W to 89°W) compared against atmospheric (dashed) and soil (dotted) water balance estimates based on observational data from 1983 to 1994 (Yeh et al. 1998). All values are in mm/d.

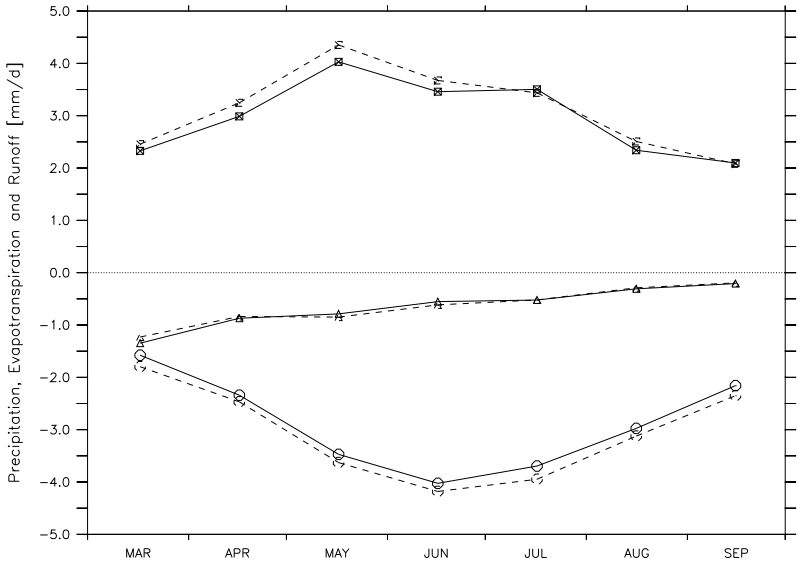

FIG. 2.7: Temporal evolution of precipitation (squares), evapotranspiration (circles), and runoff (triangles) over the Midwest subdomain (outlined in Fig. 2.3) in the CTL (solid) and WARM (dashed) integrations (average over all years). The values are given in mm/day.

TABLE 2.2: Summary of the CTL and WARM experiments: mean of the four years simulated for the months of May, July and September. The values are spatial averages over the Midwest subdomain (outlined in Fig. 2.3). SWI denotes incident shortwave (SW) radiation, SWO outgoing SW, SWN net SW, LWI incident longwave (LW) radiation, LWO outgoing LW, LWN net LW, NR net radiation, LH latent heat flux, SH sensible heat flux, TS surface temperature, and RHA the anemometer relative humidity. Note that evaporation and runoff are negative and that energy fluxes directed downwards are counted positive.

Fields	Units	May			July			September		
		CTL	WARM	Δ	CTL	WARM	Δ	CTL	WARM	Δ
HYDROLOGICAL CYCLE										
Precipitation	mm/day	4.03	4.35	+0.32	3.50	3.44	-0.07	2.10	2.08	-0.02
Evaporation	mm/day	-3.47	-3.63	-0.16	-3.69	-3.95	-0.25	-2.16	-2.35	-0.19
Runoff	mm/day	-0.79	-0.85	-0.06	-0.52	-0.52	+0.00	-0.21	-0.19	+0.01
Snowmelt	mm/day	0.00	0.00	+0.00	0.00	0.00	+0.00	0.00	0.00	+0.00
Soil moisture	mm	438.5	440.1	+1.6	403.3	405.8	+2.5	383.6	378.2	-5.3
(root zone)	% sat	60.9	61.1	+0.3	55.8	56.2	+0.5	53.1	52.3	-0.8
Soil moisture	mm	1079.8	1085.5	+5.8	1028.4	1035.5	+7.1	981.6	978.4	-3.3
(total)	% sat	74.3	74.7	+0.4	70.8	71.2	+0.5	67.6	67.3	-0.2
SURFACE ENERGY BUDGET										
SWI	W/m^2	235.5	230.0	-5.5	262.1	267.5	+5.3	161.9	172.6	+10.6
SWO	W/m^2	-38.6	-37.8	+0.8	-44.0	-44.8	-0.8	-27.4	-29.4	-2.0
SWN	W/m^2	196.9	192.3	-4.6	218.1	222.6	+4.5	134.5	143.1	+8.6
LWI	W/m^2	323.0	342.1	+19.0	371.3	389.4	+18.1	337.5	354.8	+17.3
LWO	W/m^2	-387.5	-399.9	-12.4	-439.7	-454.8	-15.1	-397.3	-415.2	-17.9
LWN	W/m^2	-64.5	-57.8	+6.7	-68.4	-65.4	+3.0	-59.8	-60.4	-0.6
NR	W/m^2	132.4	134.4	+2.0	149.7	157.3	+7.5	74.7	82.7	+8.0
SH	W/m^2	-26.0	-23.7	+2.3	-43.0	-42.6	+0.4	-18.0	-20.5	-2.5
LH	W/m^2	-102.9	-107.5	-4.7	-109.5	-117.0	-7.5	-63.9	-69.6	-5.7
SURFACE CLIMATE										
TS	°C	14.3	16.6	+2.3	23.5	26.0	+2.5	16.1	19.3	+3.2
RHA	%	80.2	80.8	+0.6	70.1	67.4	-2.7	78.4	74.1	-4.3

TABLE 2.3: Overview of the mean hydrological cycle (10 years) in Wetherald and Manabe (1995) based on simulations using a GCM with idealized geography for $1xCO_2$ (300 ppmv) and $4xCO_2$ (1200 ppmv, fully interactive experiment) equilibrium conditions. The figures represent averages for the continental region 45°N to 60°N. Sign conventions as in Table 2.2.

Fields	Units	May			July			September		
		$1xCO_2$	$4xCO_2$	Δ	$1xCO_2$	$4xCO_2$	Δ	$1xCO_2$	$4xCO_2$	Δ
Precipitation	mm/day	3.33	3.89	+0.57	2.27	1.90	-0.37	2.40	2.73	+0.33
Evaporation	mm/day	-2.87	-3.61	-0.74	-3.19	-3.07	+0.13	-1.52	-1.63	-0.11
Runoff	mm/day	-2.65	-1.13	+1.52	-0.25	-0.11	+0.14	-0.18	-0.10	+0.08
Snowmelt	mm/day	1.76	0.00	-1.80	0.00	0.00	+0.0	0.04	0.00	+0.0
Soil moisture	mm	134.7	125.5	-9.2	61.9	35.3	-26.6	45.8	29.9	-15.9
(150 mm bucket)	% bucket	89.8	83.7	-6.1	41.3	23.5	-17.8	30.5	19.9	-10.6

of 0.3 mm/day, while they are up to two or three times larger in the simulations of WM95 (Table 2.3). Particularly striking are the differences in spring evapotranspiration: while our simulations present an evapotranspiration increase of only 0.16 mm/d in May (Table 2.2), WM95 report an almost five time larger increase for this month (0.74 mm/d, Table 2.3). Moreover, runoff is almost unaffected in our simulations while very sensitiv in WM95.

Evapotranspiration is higher in the WARM experiments than in the CTL integrations in all the months simulated. Precipitation is higher in the WARM experiments from March to June due to an enhancement of convective activity during these months (see later). Later in the year (from July to September), precipitation differences between the CTL and WARM simulations are negligible.

The temporal evolution of the net input of water in the soil (precipitation-evaporation-runoff) over the Midwest subdomain is shown in Figure 2.8a. From March to June, the precipitation increase is higher than the evapotranspiration increase; in May for instance, it is twice as high (Table 2.2). As the soil is not at saturation (Figure 2.8b), this extra input of water can thus be stored in the soil. In July, the increase in evapotranspiration remains substantial, while precipitation is the same as in the CTL integrations. For this reason, there is an enhanced depletion of soil moisture during this month, but due to the higher storage of water during spring, soil moisture in the WARM simulations reaches lower values than in the CTL simulations by the end of August only. This sequence of events is well apparent in Figure 2.8b which displays the temporal evolution of the soil moisture saturation in the root zone. Overall the differences between the CTL and WARM experiments are again very small. The highest (positive or negative) changes are of the order of 0.5-0.8 % of soil saturation, corresponding to 2.5-5.5 mm in the root zone, the soil layer of relevance for plant growth (see Table 2.2 for exact values). In the total soil column, changes range from +7.1 mm (July) to -3.3 mm (September). In comparison, WM95 report mean soil moisture decreases of the order of 10 to 30 mm (see Table 2.3).

Figure 2.9 displays the geographical distribution of mean summer (June to August) soil moisture differences in the root zone (1 to 2 m depth) between WARM and CTL. There is no important drying in the focus region. Indeed, the highest drying peaks observed in the Midwest are of the order of 2% of the saturation water content, corresponding to 10-20 mm. Furthermore, many parts of this region display no changes in soil moisture at all, or even some signs of soil wetting (for instance in the states of Missouri, Kansas, and South and North Dakota). A possibly interesting feature is the large drying observed in the western Gulf Coast region around 30°N which is caused by a large decrease of summer precipitation (not shown).

Figure 2.10 displays the hydrological changes between the CTL and WARM experiments individually for each simulated year. The behaviour observed for the average of the simulations is again noticeable in 1986, 1988, and 1993: in all three years, there is an enhancement of precipitation in spring leading to slightly wetter soil moisture conditions, which is followed by a gradual depletion of the additional soil water storage during the course of the summer. The applied scenario leads to an enhancement of the 1993 flood, while the 1988 drought conditions are not markedly different in the CTL and WARM integrations. In 1990, precipitation fails to increase sufficiently in spring to counterbalance the increase in evapotranspiration due to a decrease in large-scale precipitation in May; for this reason, somewhat enhanced summer drying occurs during this year. The opposite behaviours observed in the "normal" years (1986 and 1990) illustrate well the importance

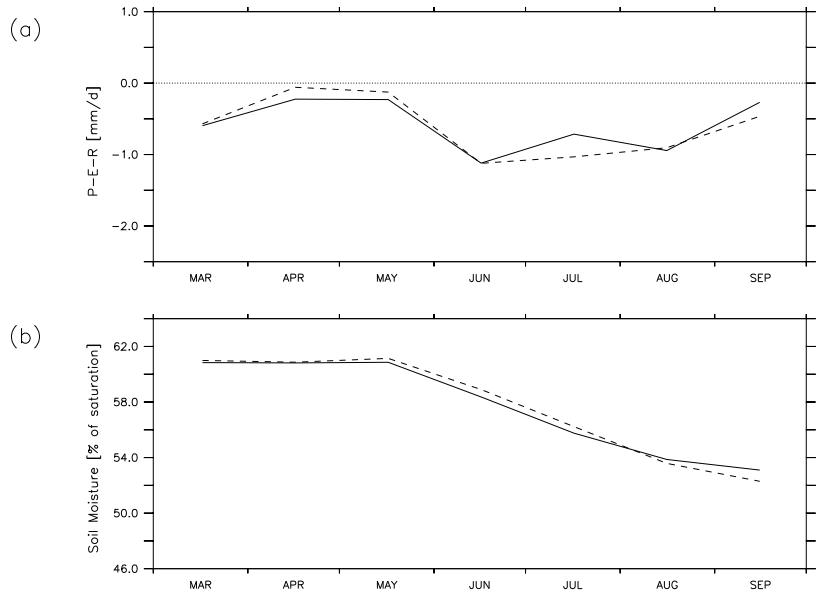

FIG. 2.8: (a) Net input of water in the soil (precipitation-evapotranspiration-runoff) in mm/day. (b) Temporal evolution of the relative soil moisture content in the root zone in % of saturation. The values are averaged over the Midwest subdomain (outlined in Fig. 2.3) and represent means of the CTL (solid lines) and WARM (dashed lines) integrations.

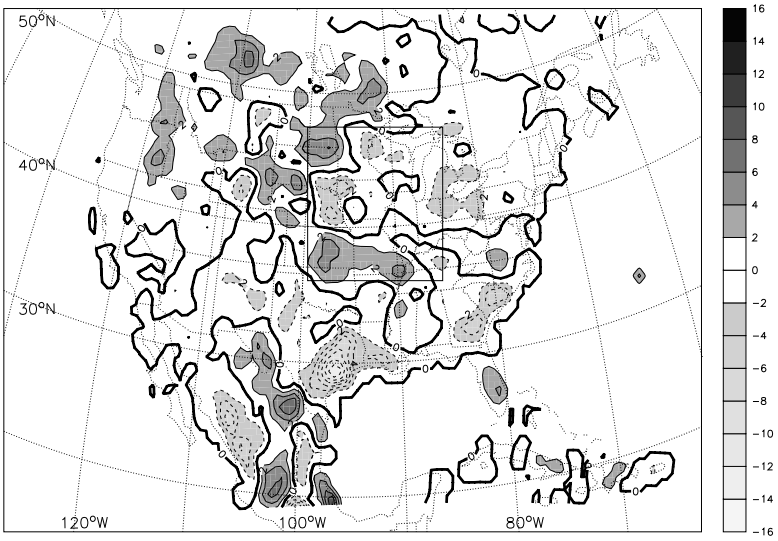

FIG. 2.9: Average summer (June-August) changes in relative soil moisture content [% of saturation] in the root zone (1-2 m depth) for the 4 years simulated (WARM-CTL). Shading occurs above and below differences of +2% and -2% of saturation. A weak spatial smoothing has been applied for display purposes. The outlined box is the Midwest analysis region.

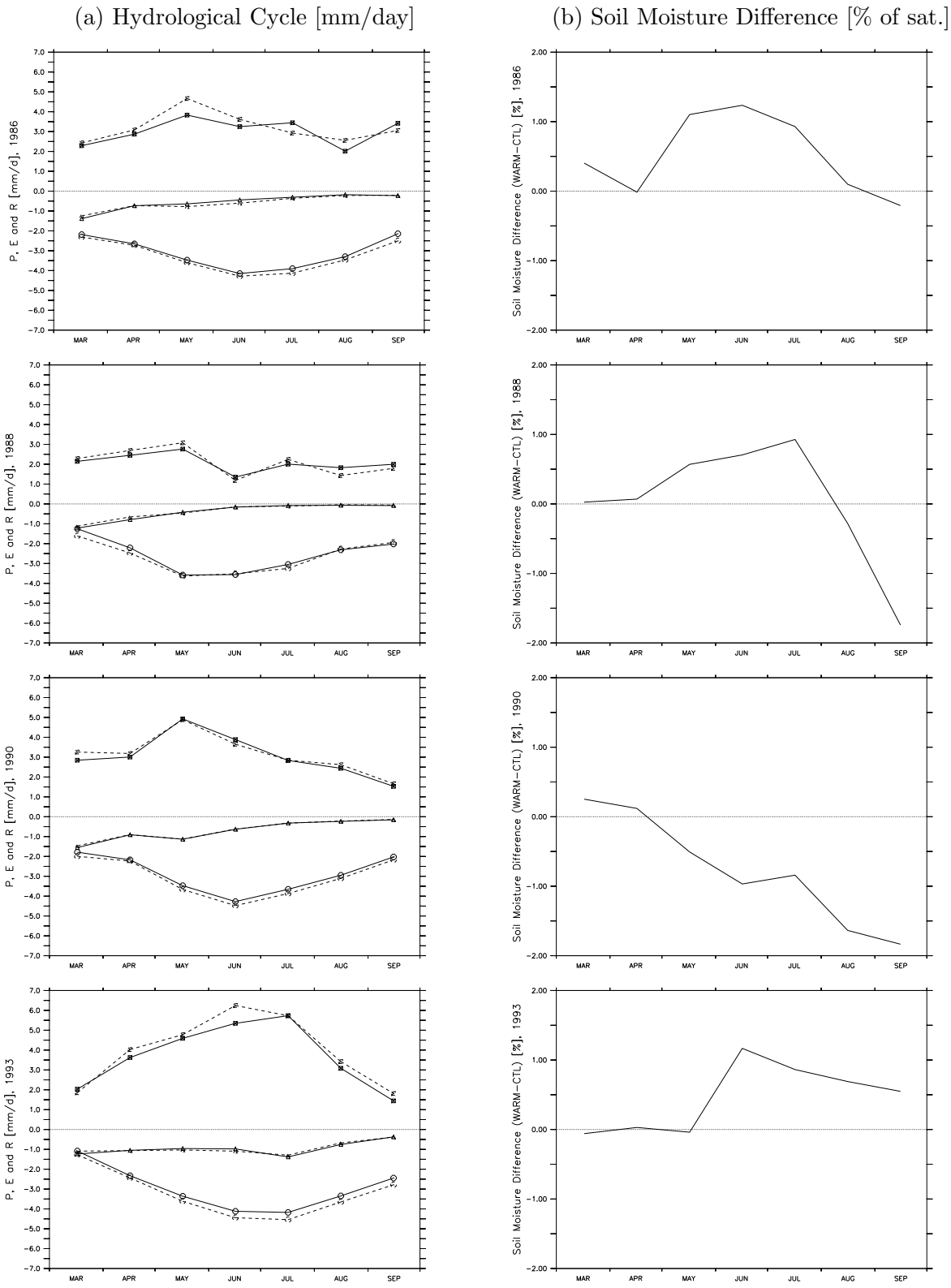

FIG. 2.10: (a) Temporal evolution of precipitation (squares), evapotranspiration (circles), and runoff (triangles) in the simulations CTL (solid) and WARM (dashed) in mm/day. (b) Temporal evolution of the soil moisture differences in the root zone (WARM-CTL) in % of saturation. The values are spatial averages over the box outlined in Figure 2.3. The panels represent 1986 (top row), 1988 (second row), 1990 (third row), and 1993 (bottom row).

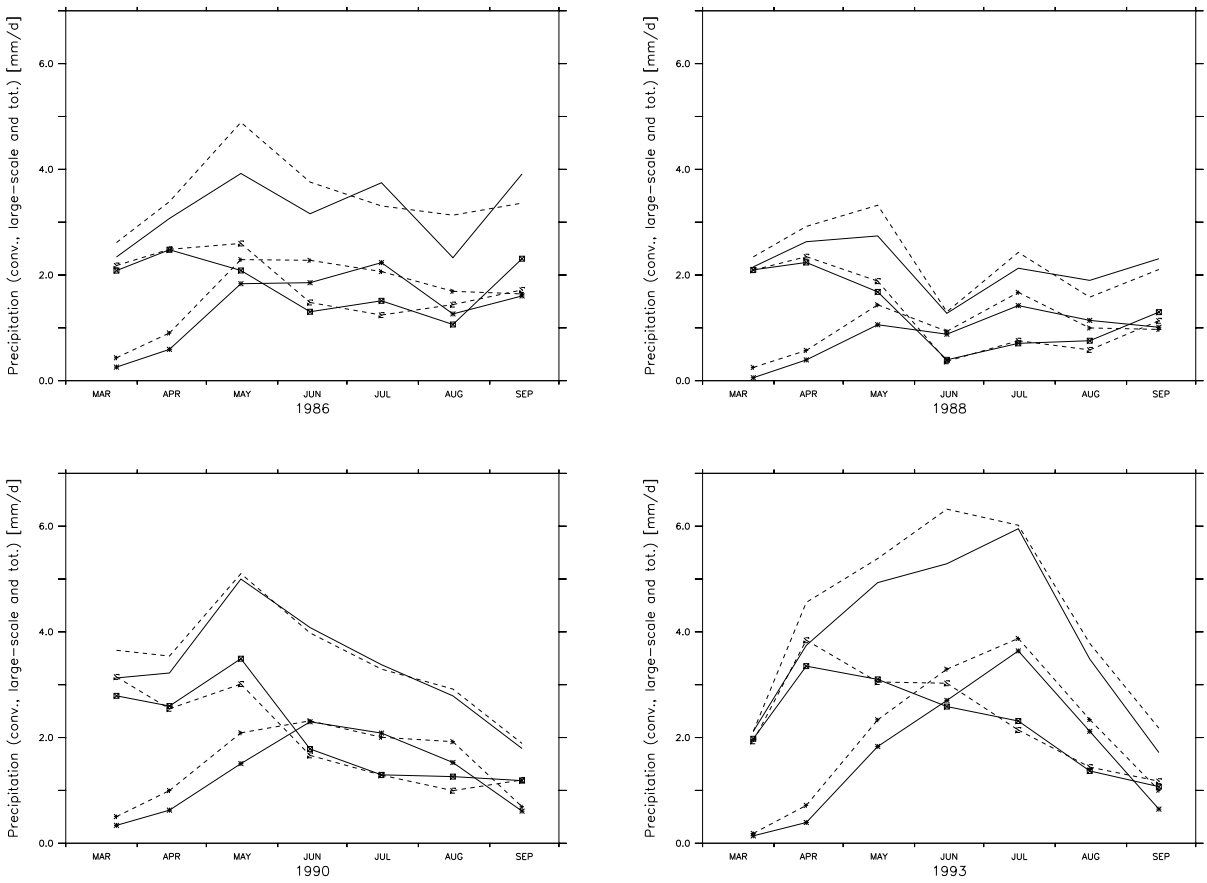

FIG. 2.11: Temporal evolution of total (no symbols), non-convective (squares), and convective rainfall (asterisks) in the simulations CTL (solid) and WARM (dashed) in 1986, 1988, 1990, and 1993 [mm/day]. The values are spatial averages over the Midwest subdomain (outlined in Figure 2.3).

of the precipitation increase in spring. If the precipitation increase in spring is not high enough, then some minor summer drying might occur. Regardless of this effect, however, the absolute changes in soil moisture are of small magnitude in all four years considered.

A more detailed look at the temporal evolution of the convective and non-convective parts of precipitation (Fig. 2.11) shows that convective rainfall increases from March to June/July in all years. The precipitation increase observed in spring is therefore mainly due to increases in convection. Some changes in large-scale precipitation are observed in 1986 (increase) and 1990 (decrease). In May 1990, there is a significant decrease of large-scale precipitation, which is responsible for the absence of total precipitation increase in spring, and hence for the mild increase in summer drying observed in this year.

In summary, the hydrological changes in the WARM experiments are as follows: The simulations are generally characterized by a wetter spring with enhanced convective activity (from March to June/July), followed by a period with drier climatic conditions (July-September). Due to the higher infiltration associated with the enhanced spring precipitation and the relatively moderate increase in evapotranspiration, the simulated soil

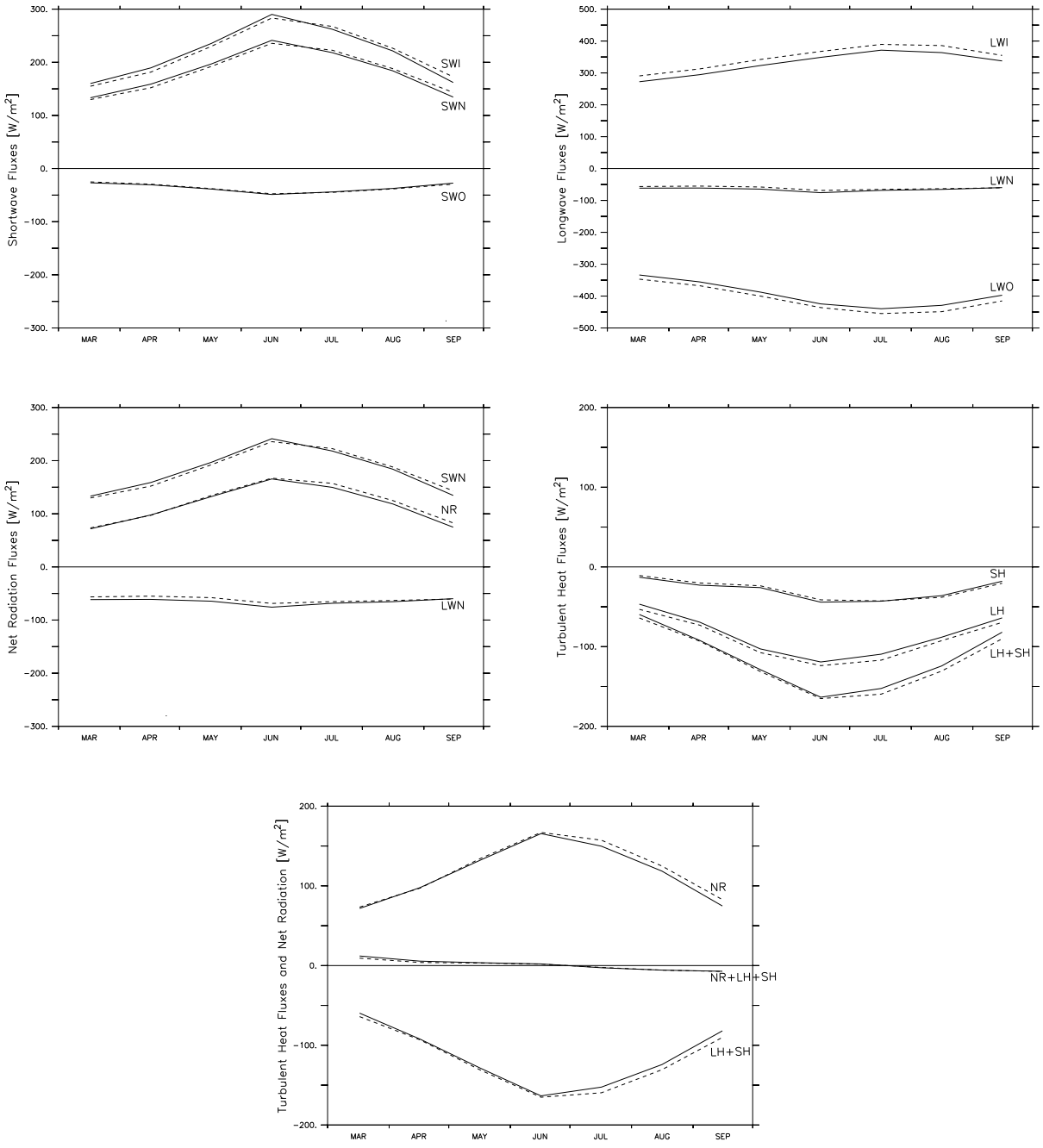

FIG. 2.12: Temporal evolution of the various components of the surface energy budget in the simulations CTL (solid lines) and WARM (dashed lines) over the Midwest [W/m^2]. The values are spatial averages over the box outlined in Figure 2.3. SWI denotes incident shortwave (SW) radiation, SWO outgoing SW, SWN net SW, LWI incident longwave (LW) radiation, LWO outgoing LW, LWN net LW, LH latent heat flux, SH sensible heat flux, and NR net radiation. Downwards directed fluxes are counted positive.

moisture changes are in general of very small magnitude. These results are independent of the choice of the closure assumption in the convection scheme, since additional experiments conducted with the Arakawa and Schubert (1974) closure assumption (not shown) were in qualitative agreement with the simulations presented.

2.5.b WARM experiments: Surface energy budget

Figure 2.12 presents the mean temporal evolution of the various components of the surface energy budget in the CTL and WARM integrations over the Midwest region. The differences for the net longwave radiation, the net shortwave radiation, the sensible heat flux, and the latent heat flux are shown in Figure 2.13.

The average changes in the energy budget components are consistent with the changes observed in the hydrological cycle. There is a reduction of the incident shortwave radiation in spring. This is in agreement with the increase in convective activity observed in the WARM experiments and appears to be mainly induced by an increase of the low-level cloud amount and relative humidity, while the high cloud amount is decreased (not shown). As seen in the previous section, the latent heat flux (which is proportional to evapotranspiration) is increased for all the duration of the simulations due to the enhanced air temperature.

From March to June, the increase in latent heat flux occurs at the expense of sensible heat as the net radiation is almost equal in the two sets of integrations. The increase in incoming longwave radiation induced by the change in greenhouse gases (CO_2 and water vapour) is indeed almost entirely compensated by the combined effects of the enhanced outgoing longwave radiation (associated with the higher surface temperature) and the

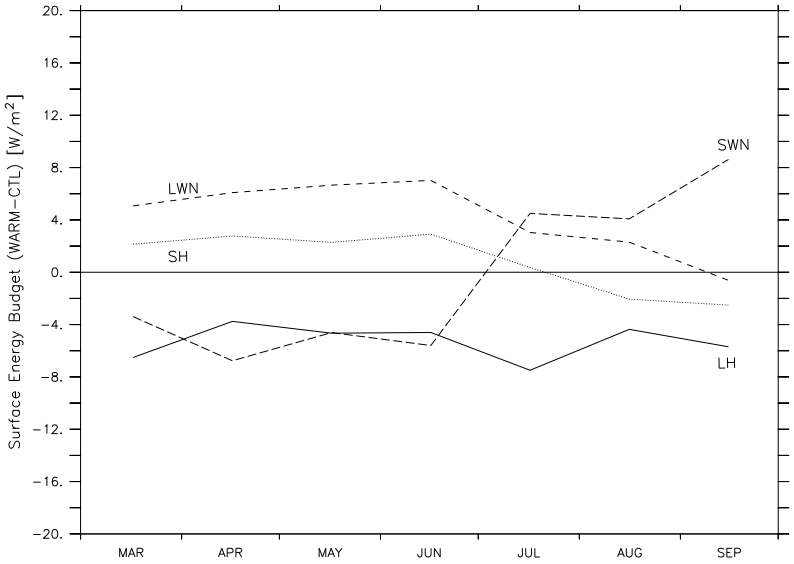

FIG. 2.13: Differences of various components of the surface energy budget between the CTL and WARM integrations over the Midwest in W/m^2 (WARM-CTL). The values are spatial averages over the box outlined in Figure 2.3. SWN denotes net shortwave radiation, LWN net longwave radiation, LH the latent heat flux, and SH the sensible heat flux. Downwards directed fluxes are counted positive.

decrease in incoming shortwave radiation (due to increased low-level cloud cover and relative humidity).

From June onwards, there is an enhancement of the net radiation in the WARM experiments due to an increase in incident shortwave radiation; the latter is caused by a significant decrease in cloud amount, particularly in the lower part of the atmosphere (not shown). The increase in net radiation is almost entirely converted into sensible heat, while latent heat does not markedly increase any further.

2.5.c *BUCKTRA experiments*

Comparisons between the BUCKTRA and standard (CTL and WARM) experiments show that these two sets of experiments are similar in 1986, 1990, and 1993, but markedly distinct for the drought year 1988. Figure 2.14 displays the temporal evolution of transpiration and soil moisture in the root zone in 1988 for the simulations CTL, WARM,

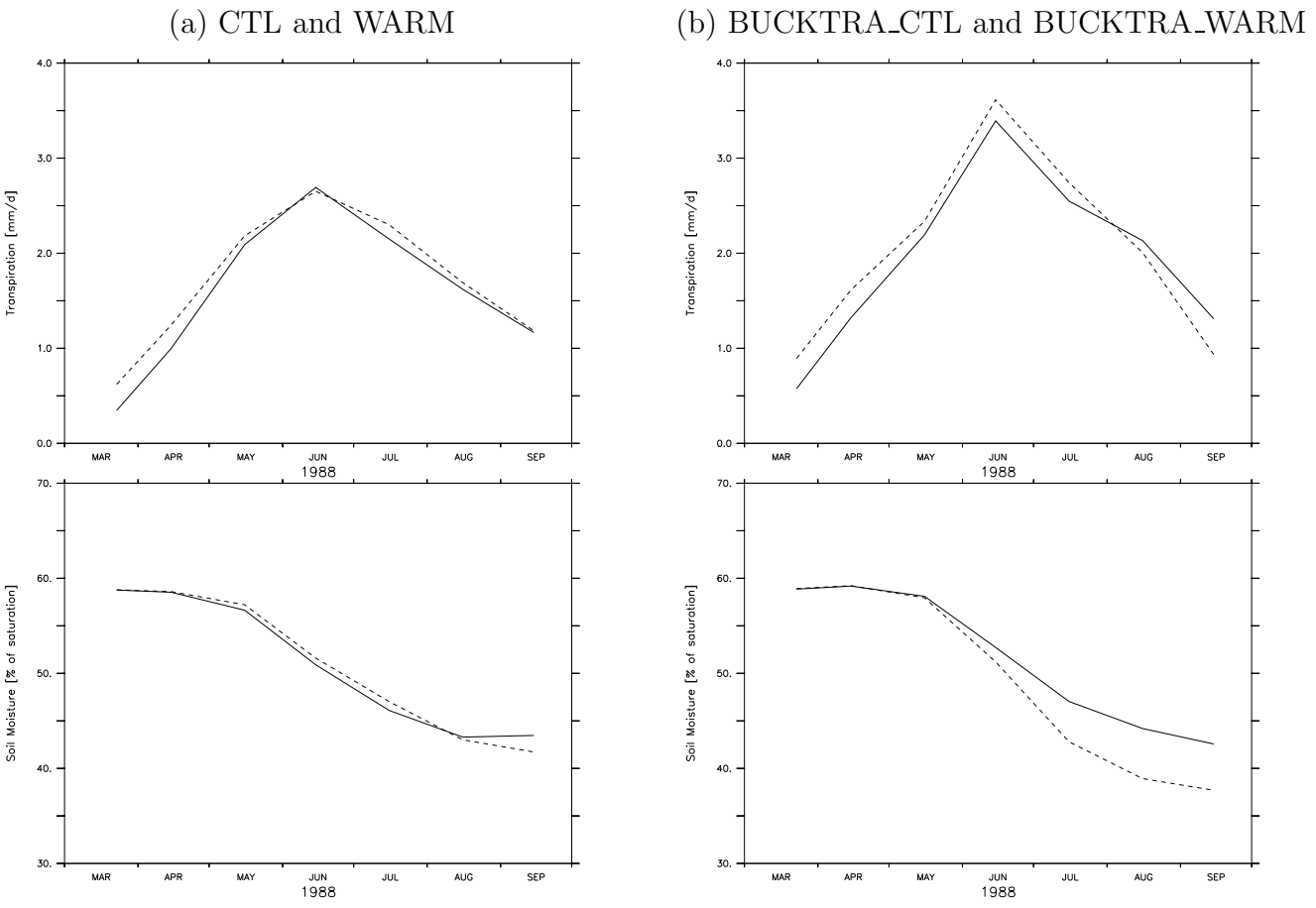

FIG. 2.14: Temporal evolution of transpiration [mm/d] (top) and soil moisture content in the root zone [% of saturation] (bottom) in 1988: (a) Simulations CTL (solid) and WARM (dashed); (b) Simulations BUCKTRA_CTL (solid) and BUCKTRA_WARM (dashed). The values are spatial averages over the Midwest subdomain (outlined in Figure 2.3).

BUCKTRA_CTL, and BUCKTRA_WARM. For this year, transpiration is higher with the bucket-type formulation than with the standard BATS parameterization, both in the control (CTL, BUCKTRA_CTL) and warmer climate (WARM, BUCKTRA_WARM) runs. The BUCKTRA experiments display a large sensitivity to the applied climate change scenario, contrary to the experiments with the standard BATS parameterization: Transpiration is markedly enhanced both in spring and summer, leading to a strong drying of the soil (see Figure 2.14b, bottom). The drying starts in May, and attains about -5% of saturation (approximately -32 mm) until September. These figures are similar in magnitude to the changes reported by WM95. Note, however, that the differences for the average of the four years are much smaller, as the two sets of experiments differ significantly in 1988 only.

The fact that the performed changes only impact the results for 1988, the drought year, suggests that the vegetation control on transpiration in BATS (through root and stomatal resistances) mostly comes into play under water stress conditions. Conversely, this also suggests that the bucket model might not be appropriate for investigating drought-like conditions.

As mentioned in Section 2.3, the changes performed in the BUCKTRA experiments do only mimic some of the characteristics of the bucket model; other aspects, such as the available water capacity and the treatment of runoff and groundwater drainage, would also need investigation. Despite these limitations, the results of the BUCKTRA experiments suggest that the more realistic land-surface scheme employed in our simulations might explain at least part of the differences observed between our study and earlier studies on this issue.

2.5.d NOCO$_2$ experiments

Figure 2.15a displays the mean temporal evolution of the incident longwave radiation in the simulations CTL, WARM, and NOCO$_2$. The increase in incident longwave radiation exhibited by the WARM experiments (about +18 W/m^2) is primarily induced by the enhanced moisture content of the atmosphere (80-90% of total change) rather than by the increase in atmospheric CO$_2$. This result is consistent with theory (e.g. Ramanathan 1981) and observations (e.g. Raval and Ramanathan 1989, Rind et al. 1991), since water vapour is known to be a much more effective greenhouse gas than CO$_2$. The total increases in incident longwave radiation for both sets of simulations are also consistent with the results from GCM climate change simulations presented by Garatt et al. (1999). Their analysis of transient CO$_2$ experiments with three coupled climate models reveals indeed on a global average a mean increase of about 20 W/m^2 in incident longwave radiation for a 3 K increase in temperature.

Due to the limited impact of the differences in CO$_2$ concentrations, the results of the NOCO$_2$ experiments are therefore relatively similar to those of the WARM integrations, and are mostly characterized by their insensitivity to the performed changes. As an example, the temporal evolutions of the soil moisture differences in the root zone for WARM-CTL and NOCO$_2$-CTL are presented in Figure 2.15b. As with the WARM simulations, the absolute change in soil moisture is very small (less than 2% of saturation). An analysis of the other fields shows that the amplitudes of the differences to the CTL runs are of similar magnitude (not shown).

(a) Incident Longwave Radiation [W/m^2] (b) Soil Moisture Diff. in Root Zone [%]

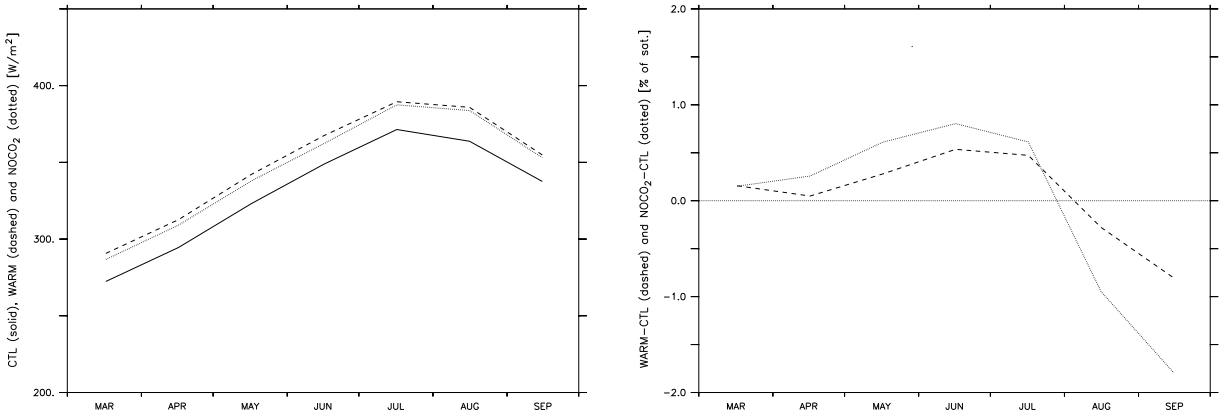

FIG. 2.15: (a) Temporal evolution of the incident longwave radiation in the simulations CTL (solid line), WARM (dashed line), and $NOCO_2$ (dotted line) in W/m^2 (average over all years). (b) Temporal evolution of the soil moisture differences in the root zone for WARM-CTL (dashed line) and $NOCO_2$-CTL (dotted line) in % of saturation (average over all years). The values are spatial averages over the box outlined in Figure 2.3.

We can conclude from this analysis that on the spatial and temporal scales considered, the differences between the WARM and CTL experiments can be mainly explained by the changes in temperature and specific humidity (through temperature advection and water vapour greenhouse effect), while the change in the atmospheric CO_2 concentration has an almost negligible impact.

2.6 Summary and conclusions

The present study uses a regional climate model with a surrogate climate change scenario to investigate the mechanisms potentially leading to enhanced summer dryness in the Midwestern United States under warmer climatic conditions. The control integrations of four spring and summer seasons generally agree with observations in terms of their water cycle and precipitation distribution.

The WARM experiments are generally characterized by a wetter spring with enhanced convective activity (from March to June/July), followed by a period with somewhat drier climatic conditions (July-September). These changes are mostly induced by the modifications in temperature and humidity advection, rather than by local changes in atmospheric CO_2 concentrations. This is apparent from the comparison between the WARM and $NOCO_2$ experiments.

Although the summertime depletion of soil moisture in the WARM experiments is somewhat higher than in the CTL integrations, it is generally compensated by the higher infiltration in spring, when convective precipitation is enhanced. On average, the WARM integrations start showing weak signs of soil drying by late August only. There are, however, some noticeable year-to-year variations. In 1993, the flood year, the applied scenario leads to a net wetting of the soil. The highest drying is observed in 1990, a

"normal" year, due to a decrease in large-scale precipitation in May.

Whether positive or negative, these soil moisture changes are nonetheless of very small magnitude (of the order of 1 to 2% of saturation at most); in this light, even the drying occurring in the 1990 experiment would thus represent a rather mild scenario. Overall, our results suggest that the risks of enhanced drying might possibly be smaller than suggested by earlier studies (e.g. WM95, Kattenberg et al. 1996).

The relatively mild changes observed in our simulations can mainly be explained by two factors. First, the soil is not fully saturated in spring and can thus absorb extra precipitation occurring during this season. In contrast, in the simulations of WM95, there are no compensating effects for the increases in evapotranspiration, as most of the enhanced spring precipitation is lost to runoff. Second and perhaps more importantly, increases in evapotranspiration are relatively moderate, thus restricting soil moisture depletion occurring in summer. This behaviour appears to be tied to the use of a land-surface scheme of intermediate complexity (BATS). The simpler bucket model as used in earlier studies is known to generally overestimate latent heat flux in various regimes (see introduction), a fact which might exaggerate the simulated summer drying in some climate change simulations. This problem was also recognized by WM95, who stated: "In assessing the present results, one should recognize that the GCM used here employs a simple "bucket model" parameterization of land-surface processes. Because of this simplified formulation, it is possible that the midlatitude summer dryness discussed in this study may not be realized in the actual climate system.". Since our model uses a more sophisticated representation of the land-surface processes, it is possible that the mild changes observed in our simulations might be closer to reality. The results of the BUCKTRA experiments, in which the BATS parameterization of transpiration was replaced with a bucket-type formulation, seem to confirm this hypothesis. They display a large drying in 1988, the drought year, which suggests that vegetation control on transpiration (through the stomatal and root resistances) might play an important part in counteracting an enhancement of summer drying when soil water gets scarce.

However, also our simulations entail various simplifications, which might question some of the results. First, our methodology does not allow for global changes in the synoptic-scale circulation patterns. Possible shifts in the storm tracks could be important features of climate change and are at present still difficult to predict (e.g. Kattenberg et al. 1996, Cubasch et al. 2001). Second, the simulations are only performed for the spring and summer seasons; it is possible that changes in fall precipitation or in the onset of snowmelt could significantly impact the hydrological cycle in warmer climatic conditions. Third, slight moisture deficits such as those displayed by the WARM experiments towards the end of the summer might add up and lead to a stronger drying in multi-year simulations. Last, some factors which were not accounted for in the present simulations (e.g. changes in aerosol concentrations, adaptative response of vegetation to climate change) could also be of relevance for this issue. Potential vegetation feedbacks which were not investigated here, such as changes in stomatal resistance (e.g. Henderson-Sellers et al. 1995), rooting depth (Milly 1997) and plant physiology (e.g. Sellers et al. 1996), or shifts in vegetation distribution patterns (e.g. Betts et al. 1997, Levis et al. 2000), might be of key importance in modulating the response of the climate system to changes in greenhouse gases and local climate.

Despite the aforementioned limitations, our study underlines the importance of land-

surface processes in climate integrations, and the potential role of enhanced spring precipitation in substantially reducing a possible enhancement of summer dryness in mid-latitudes.

Acknowledgements

We would like to acknowledge and thank Eric Small for his very valuable assistance at the beginning of this study. Many thanks are due to Christoph Frei, Oliver Fuhrer, Reto Stöckli, Pier Luigi Vidale, Pedro Viterbo and Martin Wild for their very helpful comments and suggestions. We would also like to express our sincere thanks to Richard Wetherald for kindly providing us with the data of the WM95 study as well as for his pertinent and constructive comments, which substantially contributed to improving the manuscript. Useful comments from an anonymous reviewer are also gratefully acknowledged. Special thanks are due to Eric Müller (Computing Services ETH) for technical support. In addition, we thank Filippo Giorgi for providing RegCM, Erik Kluzek (NCAR) for providing the framework necessary to implement the NCEP Reanalysis boundary conditions, NOAA-CIRES Climate Diagnostics Center for providing the NCEP Reanalysis data, and Daniel Lüthi for aid with the implementation of the rotated Mercator projection in the model and the generation of NetCDF output.

Financial support for this study was provided by the MIT/ETH/UT Alliance for Global Sustainability, and by the Swiss National Science Foundation through the NCCR Climate programme.

Chapter 3

Inferring Changes in Terrestrial Water Storage: The Mississippi River Basin

Inferring changes in terrestrial water storage using ERA-40 reanalysis data: The Mississippi River basin[†]

Sonia I. Seneviratne[1*], Pedro Viterbo[2], Daniel Lüthi[1], and Christoph Schär[1]

[1]*Atmospheric and Climate Science, ETH Zurich, Switzerland*
[2]*European Center for Medium-Range Weather Forecasts, Reading, UK*

ABSTRACT

Terrestrial water storage is an essential part of the hydrological cycle, encompassing crucial elements of the climate system such as soil moisture, groundwater, snow, and land ice. On a regional scale, it is however not a readily measured variable and observations of its individual components are scarce. This study investigates the feasability of estimating monthly terrestrial water-storage variations with the water-balance method, using the following three variables: water vapour flux convergence, atmospheric water content, and river runoff. The two first variables are available with high resolution and good accuracy in present reanalysis datasets, and river runoff is commonly measured in most parts of the world. The applicability of this approach is tested in a 10-year (1987-1996) case study for the Mississippi river basin. Data used include ERA-40 reanalysis data from the European Centre for Medium-Range Weather Forecasts (water vapour flux and atmospheric water content) and runoff observations from the United States Geological Survey.

Results are presented for the whole Mississippi River basin and its subbasins, and for a smaller domain covering Illinois, where direct measurements of the main components of the terrestrial water storage (soil moisture, groundwater level, and snow cover) are available. The water-balance estimates of monthly terrestrial water-storage variations show excellent agreement with observations taken over Illinois. The mean seasonal cycle as well as interannual variations are captured with notable accuracy. Despite this excellent agreement, it is not straightforward to integrate the computed variations over longer time periods, as there are small systematic biases in the monthly changes. These biases likely result from inaccuracies of the atmospheric assimilation system used to estimate the atmospheric water vapour convergence. Nevertheless, the results suggest that the critical domain size for water-balance computations using high resolution reanalysis data such as ERA-40 is much smaller than for raw radiosonde data. The Illinois domain has a size of only $\sim 2\text{x}10^5$ km^2 and is shown to be suitable for the computation of the water-balance estimates. A comparison for other regions would be needed in order to confirm this result.

[†]Journal of Climate, submitted.

[*]Corresponding author: Sonia I. Seneviratne, Atmospheric and Climate Science ETH, Winterthurerstr. 190, CH-8057 Zurich, Switzerland. E-mail: sonia.seneviratne@ethz.ch

3.1 Introduction

Terrestrial water storage is an essential part of the hydrological cycle, encompassing crucial elements of the climate system such as soil moisture, groundwater, snow and land ice, as well as surface water and biomass water. Beside their key role in the climate system, soil moisture and groundwater are also of essential importance for agriculture and the supply of freshwater. Despite its relevance for both climate and human civilisation, continental and sub-continental terrestrial water storage is not a readily measured quantity and little knowledge is available on its individual components, most of the available observations being of very limited temporal or spatial scope.

In the tropics and the mid-latitudes, soil moisture is generally the main element contributing to seasonal changes in terrestrial water storage. Its key role for the global- and regional-scale climate (through its impact on the partitioning of the sensible and latent heat fluxes) has been recognized in various observational (e.g. Betts et al. 1996, Findell and Eltahir 1997) and modelling studies (e.g. Shukla and Mintz 1982, Milly and Dunne 1994, Schär et al. 1999, Koster et al. 2000). More recently, it has also been shown to significantly impact numerical weather predictions (e.g. Beljaars et al. 1996, Viterbo and Betts 1999a, Fukutome et al. 2001, see also Viterbo and Beljaars 2003 for a review). Soil moisture is moreover important for assessing impacts of climate change, but its potential evolution with greenhouse gas warming is still unclear (Wetherald and Manabe 1999, Seneviratne et al. 2002).

In view of its relevance for climate, recent initiatives have tried to palliate the lack of information available on soil moisture. The few observational datasets (mostly for the State of Illinois, the former Soviet Union, Mongolia and China) have recently been regrouped and are now distributed on the internet by the Soil Moisture Data Bank at Rutgers University (Robock et al. 2000). The Global Soil Wetness Project (GSWP), an ongoing modeling activity of the International Satellite Land-Surface Climatology Project (ISLSCP), is another project aiming at obtaining additional information on soil moisture (Dirmeyer et al. 1999). Its goal is to produce large-scale datasets of soil moisture, temperature, runoff, and surface fluxes, by driving uncoupled land-surface schemes using externally specified surface forcings and standardized soil and vegetation distributions. The results of its first initiative (GSWP1) for the years 1987 and 1988 show that all the tested land surface schemes have problems in reproducing the actual soil moisture value for the studied regions (Entin et al. 1999). A second phase of the project (GSWP2) has been recently started to seek an improvement of the produced datasets.

Groundwater is another important component of terrestrial water storage in the tropics and mid-latitudes. There are, however, very few long-term measurements of this variable, and no project comparable to the Soil Moisture Data Bank has been initiated for groundwater as yet. With the exception of water-balance estimates from the Soviet Literature (Zekster and Loaiciga 1993), there is little information available on large-scale seasonal and interannual groundwater variations.

Snow is the only other component of the total terrestrial water storage which can induce similar variations as soil moisture and groundwater in mid- and high-latitude regions. Measurements of snow areal extent and snow depth are available for various areas, however the relevant variable for hydrological modelling is the snow mass per unit area or snow mass (snow water equivalent), which is not measured. The ratio of snow

mass to the depth of snow cover depends greatly on the snow type, age, amount of melt and compaction, as well as on the temperature and atmospheric humidity at the time of snowfall (Pomeroy and Gray 1995), and can not be precisely inferred from snow depth without corresponding snow density measurements. Land ice only plays an important part in mountainous areas and in polar regions, while changes in surface water and biospheric water are comparatively negligible.

Although little information is available on terrestrial water storage at the moment, this might change in the future. Soil moisture, for instance, is measured and studied in various new projects such as the Oklahoma mesonet (Basara and Crawford 2000). Moreover, remote sensing based on microwave radiometry is now able to provide datasets of near-surface soil moisture (e.g. Jackson et al. 1999), and data assimilation techniques can be used to infer root zone soil water from these measurements (Calvet and Noilhan 2000). Remote sensing also holds promise for additional observations of snow cover: Mapping of snow areal extent is already performed operationally with visible satellite imagery, and further developments of microwave techniques should enable the monitoring of snow mass (Rango 1996). A currently ongoing satellite project, the Gravity Recovery and Climate Experiment (GRACE) launched in 2001, might even provide estimates of variations in total terrestrial water storage (Wahr et al. 1998). Nevertheless, effective use of remote sensing data to estimate geophysical quantities requires a-priori estimates which, in the case of globally distributed soil water budgets, can only come from model estimates. Another caveat of new remote-sensing techniques is their restriction to the future climate states, while past variations must be assessed from existing observations.

This study investigates the combined atmospheric and terrestrial water balance approach for obtaining estimates of changes in terrestrial water storage for continental and sub-continental areas. The basic concept of using atmospheric data to estimate the terrestrial water balance was first presented in the 1950s, in the pioneer studies by Benton and Estoque (1954) and Starr and Peixoto (1958). It was used in various subsequent studies (e.g. Rasmusson 1968, Alestalo 1983) and has received more attention in recent years, thanks to the availability of high-resolution atmospheric data (e.g. Oki et al. 1995, Matsuyama and Masuda 1997, Yeh et al. 1998, Berbery and Rasmusson 1999, Masuda et al. 2001). The advantage of this method is that it is based on variables which have been routinely measured for decades.

Here, we present a 10-year case study for the Mississippi river basin using the new reanalysis product from the European Center for Medium-Range Weather Forecasts (ECMWF), ERA-40 (Simmons and Gibson 2000), and streamflow data from the United States Geological Survey (USGS). Computed estimates of monthly variations in terrestrial water storage are presented for the Mississippi River basin and its major subbasins, as well as for a smaller domain covering the State of Illinois, where observations of various components of the terrestrial water storage are available (soil moisture, groundwater, and snow cover). This study is meant as a pilot study and aims at establishing the validity of the approach, but application to other catchments and continents is currently underway.

The paper is structured as follows. The tested methodology, the investigated region, and the employed datasets are presented in section 3.2. The observations from Illinois used for the validation are presented in section 3.3. The computed estimates of terrestrial water-storage variations for the investigated domains are presented in section 3.4, and the validation for the Illinois domain is discussed in section 3.5. For comparison purposes,

the ERA-40 soil moisture in Illinois is shortly discussed in Section 3.6. A summary of the main results and the conclusions are provided in section 3.7.

3.2 Methodology

3.2.a The water balance equations

This section presents the terrestrial, atmospheric, and combined water balance equations. Good reviews on this topic are given in Peixoto and Oort (1992, Chapter 12), Yeh et al. (1998) and Oki (1999).

The terrestrial branch of the hydrological cycle is governed by the following equation:

$$\frac{\partial S}{\partial t} = -R_s - R_u + (P - E) \quad , \tag{3.1}$$

where S represents the terrestrial water storage of the given area, R_s the surface runoff, R_u the subterreanean runoff, P the precipitation, and E the evapotranspiration.

Within a given river basin, most of the area groundwater runoff can be considered to be discharged into streams and hence measured together with surface runoff (Rasmusson 1968). For large areas, (3.1) can thus be simplified to:

$$\left\{\overline{\frac{\partial S}{\partial t}}\right\} = -\left\{\overline{R}\right\} + \left\{\overline{P} - \overline{E}\right\} \quad , \tag{3.2}$$

where the overbar denotes a temporal average (e.g. monthly means), $\{\}$ a spatial average over the region, and $\overline{R} \cong \overline{R}_s + \overline{R}_u$ is the measured runoff.

The water balance for the atmospheric branch of the hydrological cycle is given as follows:

$$\frac{\partial W}{\partial t} + \frac{\partial W c}{\partial t} = -\nabla_H \cdot \mathbf{Q} - \nabla_H \cdot \mathbf{Q}_c - (P - E) \quad , \tag{3.3}$$

where W represents the column storage of water vapour (sometimes refered to as precipitable water), W_c the column storage of liquid and solid water, $\mathbf{Q}$ the vertically integrated two-dimensional water vapour flux, and $\mathbf{Q}_c$ the vertically integrated two-dimensional water flux in the liquid and solid phases. The term $(\nabla_H \cdot)$ represents the horizontal divergence. $\mathbf{Q}$ is the vapour flux vector and is defined as follows:

$$\mathbf{Q} = \int_0^{p_0} q\mathbf{v}\frac{dp}{g} \quad , \tag{3.4}$$

where q, $\mathbf{v}$, g, p and p_0 represent the specific humidity, wind vector, gravitational acceleration, pressure, and surface pressure at the ground.

Generally, both the time rate of change of the liquid and solid water in clouds and their horizontal transports can be neglected (Peixoto and Oort 1992), and equation (3.3) simplifies to:

$$\frac{\partial W}{\partial t} = -\nabla_H \cdot \mathbf{Q} - (P - E) \tag{3.5}$$

Averaging (3.5) in space and time over a large area (similarly as in (3.2)) leads to following equation:

$$\left\{\overline{\frac{\partial W}{\partial t}}\right\} = -\left\{\overline{\nabla_H \cdot \mathbf{Q}}\right\} - \left\{\overline{P} - \overline{E}\right\} \tag{3.6}$$

The term $\left\{\overline{P} - \overline{E}\right\}$ can be eliminated between equations (3.6) and (3.2) to give:

$$\left\{\overline{\frac{\partial S}{\partial t}}\right\} = -\left\{\overline{\nabla_H \cdot \mathbf{Q}}\right\} - \left\{\overline{\frac{\partial W}{\partial t}}\right\} - \left\{\overline{R}\right\} \tag{3.7}$$

In this combined equation, the monthly variations in terrestrial water storage of the studied region can be expressed as the sum of three terms: the water vapour flux convergence, the changes in atmospheric vapour content, and the measured river runoff. The term $\left\{\overline{\frac{\partial W}{\partial t}}\right\}$ is usually negligible for annual means, but not for monthly means, particularly during spring and fall (Rasmusson 1968).

Note that for long-term means (multi-year averages) the tendency terms are negligible, and (3.7) simplifies to:

$$\left\{\overline{R}\right\} = -\left\{\overline{\nabla_H \cdot \mathbf{Q}}\right\} \quad , \tag{3.8}$$

i.e. for any climate equilibrium within a given hydrologic unit, the long-term water input from the atmosphere (vapour flux convergence) has to be balanced by the long-term net water output at the surface (runoff). In studies using combined atmospheric and terrestrial water-balance computations, (3.8) can be viewed as a criterion for evaluating the agreement between the atmospheric and hydrological data on the spatial scale under consideration (Yeh et al. 1998).

The accuracy of atmospheric water-balance computations is highly dependent on the size of the area investigated. Early studies by Rasmusson (1968, 1971) using raw radiosonde data over North America suggested that for this type of data water-balance computations can give reliable estimates of $\left\{\overline{P} - \overline{E}\right\}$ when averaging over areas of $2 \times 10^6\,\mathrm{km}^2$ or larger, but can become quite erratic as the size of the area is reduced to less than $10^6\,\mathrm{km}^2$. The limiting factors for capturing regional-scale features were identified as the density of rawinsonde observations and their sampling frequency (Berbery and Rasmusson 1999).

Although the rawinsonde network over North America has not changed much in the last decades, there is now a large amount of new data available, such as wind and temperature observations from aircraft, data from the wind profiler demonstration network, and various types of surface data (Berbery et al. 1996). Reanalysis data which optimally combine these sources of information with model integrations provide comparatively high resolution atmospheric vapour flux data, which are likely to allow reliable water-balance computations for domains smaller than the critical size of $10^6\,\mathrm{km}^2$. This is confirmed by results of recent studies making use of reanalysis data for atmospheric water-balance computations, which suggest that the critical size limit with such data might be lowered to 5×10^5 km^2 (Berbery and Rasmusson 1999) or even 1×10^5 km^2 (Yeh et al. 1998).

3.2.b Investigated region

The Mississippi River basin was chosen for the testing of the proposed methodology, based on various reasons. First, it is a well studied region characterized by abundant meteorological and hydrological datasets; it is for instance the focus area of the Global Energy and Water Cycle Experiment (GEWEX) Continental-Scale International Project (GCIP; see Coughlan and Avissar 1996 for an overview). Second, the existence of comprehensive observations of terrestrial water storage in Illinois (soil moisture, groundwater and snow measurements, see section 3.3) is another asset of this region. Finally, various studies have investigated combined water-balance computations for some of the Mississippi subbasins or Illinois (e.g. Gutowski et al. 1997, Yeh et al. 1998, Berbery and Rasmusson 1999), which allows some comparisons with our results.

The Mississippi River basin is divided in 5 main subbasins (Fig. 3.1): 1) The Arkansas and Red River basins, 2) the Missouri basin, 3) the upper Mississippi basin, 4) the Ohio and Tennessee River basins, and 5) the lower Mississippi River basins. Note that there are no actual runoff measurements for domain 5, where runoff can only be computed as the difference between the total runoff of the whole Mississippi River basin (station Vicksburg) and the runoff measured for the other subbasins. Therefore, we only focus on the four first subbasins, on the sum of all 5 subbasins (whole Mississippi River basin), and on a smaller domain approximately covering Illinois (domain 6, Fig. 3.1). Note that all 6 domains are smaller than the Rasmusson threshold of 2×10^6 km^2 (Table 3.1), but larger than the critical size of 1×10^5 km^2 identified by Yeh et al. (1998) for their water-balance computations over Illinois. The datasets used for the atmospheric vapour flux, the changes in atmospheric water content, and the areal runoff are described in section 3.2.c.

3.2.c Datasets

ERA-40: Computed water vapour flux divergence and atmospheric water content

Vertically integrated water vapour fluxes and atmospheric water-content estimates are taken from the latest ECMWF reanalysis data product ERA-40 (Simmons and Gibson 2000). The ERA-40 project, which is still in its running phase, aims at creating a complete reanalysis dataset covering more than 40 years (from mid-1957 to 2001). Here we use 10 years of data, covering the period 1987 to 1996. The ERA-40 data which is employed here is part of stream 1 of the reanalysis, which covers the years 1987-2001. Note that the years 1987 and 1988 are test years and will be rerun at the end of the ERA-40 project.

The ERA-40 model uses a T159 spherical harmonic representation of the atmospheric dynamical and thermodynamical fields, and a grid-point representation of humidity and cloud variables, using the so-called reduced Gaussian grid (Hortal and Simmons 1991). This grid has an almost uniform distribution of grid points on the sphere, with a grid-spacing of 112 km. There are 60 levels in the vertical, with a hybrid sigma-pressure coordinate between the surface and 0.1 hPa. Given its importance for the transport of water vapour, it is worth mentioning the high vertical resolution in the lower troposphere: The lowest model level is at 10 m above the surface, and there are 8, 11, 15, 17, and 22 levels below 500, 1000, 2000, 3000, and 5000 m, respectively. The reanalysis uses a three-dimensional variational assimilation system (Courtier et al. 1998) with a 6-hour analysis

cycle. Documentation of the Integrated Forecast System (IFS), cycle 23r4, is available at http://www.ecmwf.int/research/ifsdocs/index.html. A summary and discussion of the observations available at different times during the 40-year reanalysis period is available at http://www.ecmwf.int/research/era/Observations/.

Trenberth (1997) thoroughly discusses issues related to budget computations from analysis fields. In particular, vertically integrated budgets based on pressure level fields have several disadvantages (see also Trenberth and Guillemot 1995): (a) Insufficient detail to resolve model transport in the lower troposphere, particularly detrimental for moisture transport; (b) the equation of continuity is not fully satisfied by the assimilation cycle, with the consequence that all budget values will see artificial sources/sinks of mass (Trenberth et al. 1995); (c) the lower boundary condition is more complex to formulate than in terrain-following coordinates; and (d) extrapolation below the earth's surface is arbitrary and pollutes the budget values near orography. The obvious alternative is to compute the budgets from the fields defined on the model (hybrid) vertical coordinates. However, model level computations must be performed at maximum resolution. Truncation of model level data is an ill-defined operation, since the vertical coordinate changes with the truncation (Trenberth 1995).

For all the above reasons, the computation of the divergence of the water vapour flux is done as follows. The wind components on terrain-following model levels are transformed from spherical harmonics into the grid-point space (reduced Gaussian grid) and multiplied by the specific humidity at each level. The horizontal fluxes are then integrated over the whole depth of the atmosphere. In order to compute the divergence, and since the reduced Gaussian grid is irregular in latitude-longitude, the fluxes are transformed into spectral space for the computation of the divergence. The resulting spectral field is transformed back to obtain the divergence of the integrated water vapour flux on the reduced Gaussian grid. Note that no truncation or interpolation (either vertical or horizontal) is involved. We calculate the vapour flux divergence for each analysis cycle, i.e. at 00, 06, 12 and 18. All figures shown in the paper are based on longer-term averages of these data.

The water-vapour flux divergence and the atmospheric water content are averaged for the chosen domains using latitude-longitude quadrilaterals, following the same procedure as Betts et al. (1998, 1999, 2003). The quadrilaterals are pictured in Figure 3.1 and listed in Table 3.1.

USGS surface streamflow data

The daily streamflow data was downloaded from the USGS web site (http://water.usgs.gov/nwis). The stations used here are listed in Table 3.2. For the Mississippi subbasins, measurements from the following 6 stations are used: Arkansas River at Van Buren, Red River at Index, Missouri River at Kansas City, Missouri River at St. Louis, Ohio River at Metropolis, and Mississippi River at Vicksburg. These stations are the same as the ones used by Betts et al. (1999); the streamflow of domains 1-4 and of the whole Mississippi river basin is computed in the same way as in their study (Table 3.3).

For the computation of the mean runoff in Illinois, we use the same procedure as Yeh et al. (1998). Daily discharge measurements are used from the three following hydrological stations: Illinois River at Valley city, Rock River near Joslin, and Kaskaskia River near

FIG. 3.1: Major Mississippi subbasins and their approximation in the ECMWF reanalysis model (domains 1-5); domain 6 covers the State of Illinois. Model grid points are represented by closed circles (land) and open squares (sea). (adapted from Betts et al. 2003)

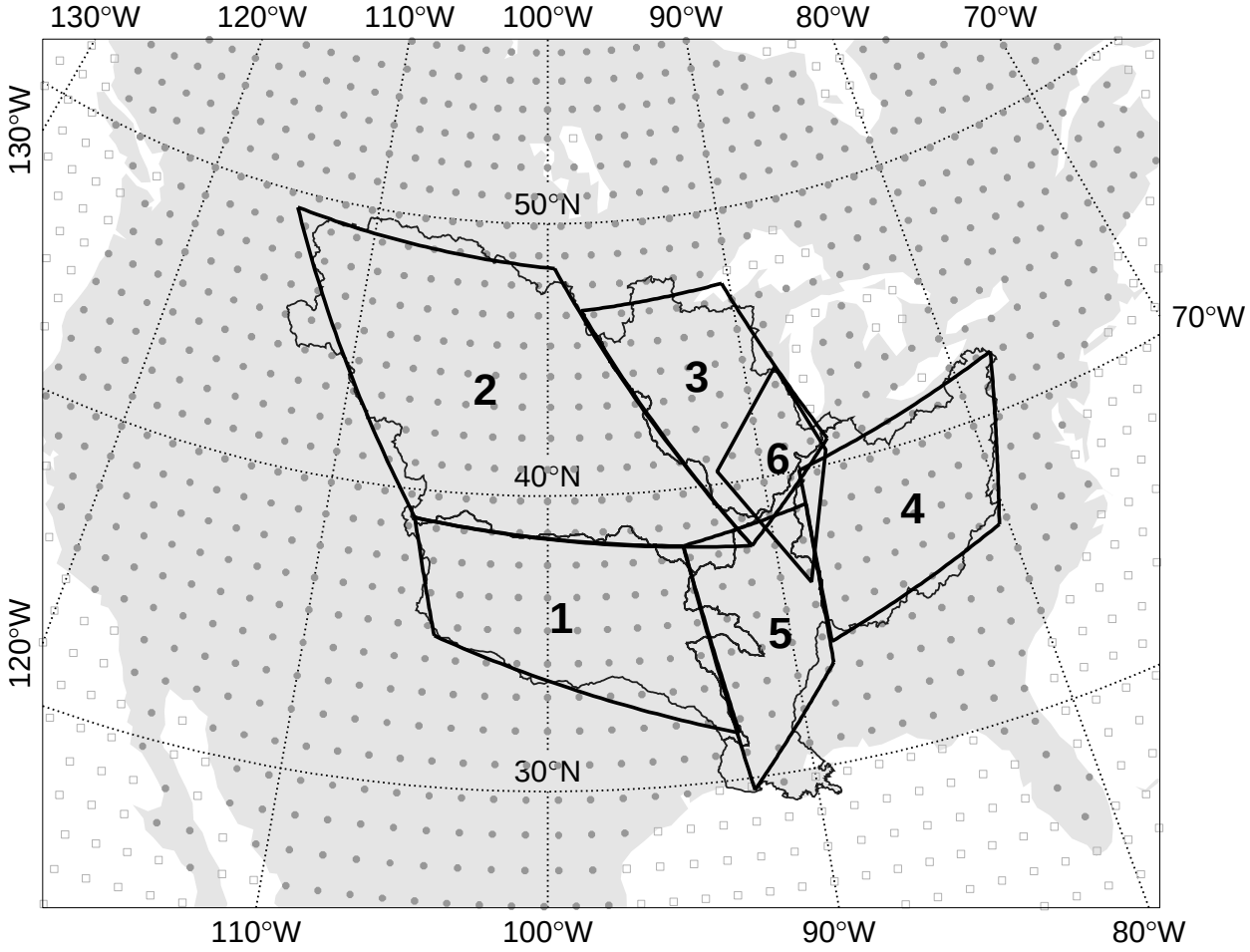

TABLE 3.1: Quadrilaterals used for the computation of the ERA-40 domain mean fields

	Domain	Quadrilateral coordinates	Number of Grid points[1]	Quadrilateral Area [km^2]
1	Arkansas-Red	106.0W, 39.0N; 94.0W, 38.0N; 92.6W, 31.5N; 104.7W, 35.0N	43	604,054
2	Missouri	114.7W, 49.4N; 99.6W, 48.3N; 91.0W, 37.7N; 106.0W, 39.0N	94	1,299,229
3	Upper Mississippi	98.2W, 46.7N; 90.4W, 47.2N; 86.7W, 40.9N; 91.0W, 37.7N	37	512,722
4	Ohio-Tennessee	88.3W, 40.0N; 78.0W, 42.1N; 80.4W, 36.3N; 88.4W, 34.0N	34	462,521
5	Lower Mississippi	94.0W, 38.0N; 88.3W, 38.8N; 88.5W, 33.3N; 92.3W, 29.6N	27	382,664
	Whole Mississippi	– sum of quadrilaterals 1-5 –	235	3,261,190
6	Illinois	92.0W, 40.5N; 88.5W, 43.5N; 87.0W, 40.5N; 88.5W, 36.0N	15	203,549

[1]reduced Gaussian grid

Venedy Station (Table 3.2). These three streamflow-gauging stations are located as far downstream as possible, with the largest drainage areas along the three major rivers in Illinois (Yeh et al. 1998). Their integrated monthly discharges in mm/d are weighted by drainage areas in order to obtain an estimation of average streamflow in Illinois (Table 3.3).

TABLE 3.2: Employed streamflow data (USGS)

		River	Station	Basin Area [km^2]
Mississippi Subbasins (domains 1-5)	(a)	Arkansas	Van Buren, Arkansas	389,900
	(b)	Red	Index, Arkansas	124,300
	(c)	Missouri	Kansas City, Missouri	1,256,100
	(d)	Missouri	St. Louis, Missouri	1,804,500
	(e)	Ohio	Metropolis, Illinois	525,500
	(f)	Mississippi	Vicksburg, Mississippi	2,952,600
Illinois (domain 6)	(g)	Illinois	Valley City, Illinois	69,200
	(h)	Rock	near Joslin, Illinois	24,700
	(i)	Kaskaskia	near Venedy Stn, Illinois	11,400

TABLE 3.3: Computation of streamflow for the domains 1-4, for the whole Mississippi River basin (sum of domains 1-5), and for Illinois (domain 6). Note that there are no actual runoff measurements for domain 5 (see section 3.2.b).

	Domain	Computation of Domain streamflow[1]	Drainage area [km^2]
1	Arkansas-Red	(a)+(b)	514,200
2	Missouri	(c)	1,256,100
3	Upper Mississippi	(d)-(c)	548,400
4	Ohio-Tennessee	(e)	525,500
5	Lower Mississippi	-	108,400
	Whole Mississippi Basin	(f)	2,952,600
6	Illinois	*(g),(h),(i)* [2]	-

[1]the letters refer to the streamflow at the gauging stations listed in Table 3.2

[2]for Illinois, areal runoff is computed as the sum of the area-weighted runoff of the three considered catchments

3.3 Observed terrestrial water storage in Illinois

Illinois has a unique and comprehensive collection of hydrological datasets, including measurements of soil moisture, groundwater, and snow cover. Therefore, it is an ideal region for the validation of the methodology presented in this study. Here we briefly describe the datasets used for the validation and the observed values of terrestrial water storage computed based on these datasets.

3.3.a Soil moisture

The soil moisture dataset was collected by the Illinois State Water Survey (ISWS). It is described in Hollinger and Isard (1994) and can be downloaded from the web site of the Global Soil Moisture Data Bank (Robock et al. 2000). The dataset includes 19 (mostly grass-covered) sites scattered throughout the State of Illinois. Nine of the time series begin in 1981, seven in 1982, two in 1986, and one in 1991. The measurements are realised with neutron probes calibrated by the gravimetric technique. They are taken once (November through February) to twice (March through October) a month at 11 different soil layers down to 2 m below the surface.

3.3.b Groundwater

The ISWS also has an extensive network of groundwater measurements in Illinois (Changnon et al. 1988). Here, we use shallow well data from the ISWS Water and Atmospheric Resource Monitoring (WARM) Program, consisting of monthly measurements of shallow groundwater levels at 17 wells located far away from pumping stations and streams. The wells range in depth from 3 to 24 m and are in communication with the local unconfined aquifer. The average water table levels range between 1 and 10 m below the surface. The measurements are generally conducted at the end of each month (Ken Hlinka, ISWS, personal communication, 2002). We therefore compute the monthly changes in groundwater level as the value of the given month minus the value of the preceding month. Missing data are replaced by interpolated values.

The change in groundwater storage $\frac{\partial S_{GW}}{\partial t}$ can be computed from the change in groundwater level with the following equation:

$$\frac{\partial S_{GW}}{\partial t} = S_y \frac{\partial H}{\partial t} \quad , \tag{3.9}$$

where H is the groundwater level and S_y is the specific yield, i.e. the fraction of water volume that can be drained by gravity in an unconfined aquifer (Domenico and Schwartz 1990).

For regional-scale time averaged values, one can assume (Yeh et al. 1998):

$$\left\{ \overline{\frac{\partial S_{GW}}{\partial t}} \right\} = \{S_y\} \left\{ \overline{\frac{\partial H}{\partial t}} \right\} \tag{3.10}$$

Here, we use $\{S_y\} = 0.08$ as a mean value for Illinois as in the study by Yeh et al. (1998). Their choice of $\{S_y\}$ was based on existing measurements of S_y at various small Illinois watersheds and on soil texture considerations (silt loam in most parts of the state).

3.3.c Snow

The snow dataset employed was provided by the Midwest Regional Climate Center (MRCC, http://mrcc.sws.uiuc.edu/). It includes observations of snowfall, snow depth, precipitation and temperature for 32 stations within Illinois. The choice of the stations was based on the following criteria: 1) the availability of precipitation and temperature measurements for the whole time period 1961-2000, and 2) less than 10% of missing data either in snow depth or snowfall.

A snow density value of $100\,\mathrm{kg/m^3}$ is used to convert the monthly changes in snow depth into changes in snow mass. This is a rather low value which is normally more appropriate for fresh snow. Therefore we also made a comparison with a conversion depending on snow depth using the equations described in Pomeroy and Gray (1995). The values obtained with this second method are about twice as large (not shown), but do not induce any significant change in the computed total terrestrial water storage and its monthly variations due to the very small values of snow mass compared to soil moisture and groundwater (see next section). In their study of the hydroclimatology of Illinois, Yeh et al. (1998) mention the state's location upwind of Lake Michigan as the main cause for the comparatively low snow amounts in this region.

3.3.d Total terrestrial water storage

Figure 3.2 displays time series of the Illinois observations of soil moisture, groundwater storage, and snow mass, as well as of their total, for the years 1987 to 1996. The groundwater storage is displayed relative to its deepest value within the time series (in October 1988).

The main components contributing to changes in total terrestrial water storage in Illinois are soil moisture and groundwater, while the contribution of the snow reservoir is negligible in comparison. Soil moisture and groundwater are characterized by very similar temporal evolutions in most years. The late spring drought of 1988, the drought of 1991, and the summer flood of 1993, can be easily recognized in both datasets. Interestingly, the computed total terrestrial water storage compares well with the results of Rodell and Famiglietti (2001) for the same region, though they use a different method for the computation of the groundwater storage. They also account for the water stored in the intermediate zone and for occasional overlaps of the soil moisture and groundwater layers when the water table rises above 2 m depth, two aspects which are not considered here. Therefore, these effects are likely to be small relative to the computed total terrestrial water storage.

The monthly mean annual cycle of terrestrial water storage, as well as the standard deviation of the monthly values for the 10 years considered, are displayed in Table 3.4. On average, terrestrial water storage in Illinois is highest in April and lowest in October. Year-to-year variations are lowest in April and have their highest spread in October.

Figure 3.3 displays the monthly variations of terrestrial water storage and its components in Illinois. The monthly variations in soil moisture and groundwater are of the same order of magnitude, while the contribution of the snow reservoir is negligible in comparison. Note that the peaks in groundwater storage tend to lag those in soil moisture.

As mentioned in section 3.2.a, variations in terrestrial water storage should cancel out

for long-term averages (equation 3.8). The time scale on which this occurs is generally assumed to be of the order of one (e.g. Oki et al. 1995) to several years (e.g. Gutowski et al. 1997). Table 3.5 displays annual and 10-year means of the observed variations in terrestrial water storage in Illinois. As expected, the 10-year mean storage variations clearly cancel out, however, annual mean variations can be significant mostly due to the contribution from groundwater storage. In 1988 and 1990, for instance, the yearly variations in terrestrial water storage (groundwater) amount to -0.37 mm/d (-0.31 mm/d) and +0.43 mm/d (+0.26 mm/d), respectively. This represents about 50% of the average streamflow and convergence in Illinois (see section 3.4.b), confirming that it is generally not feasible to neglect annual changes in basin water storage when inferring mean streamflow from vapour flux convergence for a given year (e.g. Oki et al. 1995).

TABLE 3.4: Mean annual cycle of terrestrial water storage in Illinois (1987-1996)

	mean [mm]	standard deviation
January	841.4	69.0
February	872.2	57.8
March	889.2	42.3
April	907.0	33.3
May	894.3	45.5
June	863.4	76.3
July	804.6	83.9
August	763.4	77.5
September	720.6	75.8
October	718.2	94.2
November	723.3	78.8
December	800.1	71.7

TABLE 3.5: Long-term variations of terrestrial water storage in Illinois (1987-1996).

	annual mean storage variations [mm/d]										mean absolute	10-year
	87	88	89	90	91	92	93	94	95	96	annual variations	mean
Soil moisture	0.00	-0.07	-0.11	0.17	-0.01	0.04	-0.01	-0.04	-0.11	0.09	0.06	0.00
Groundwater	0.00	-0.31	0.06	0.26	-0.06	0.13	0.04	-0.13	-0.13	0.06	0.12	-0.01
Snow depth	0.01	0.01	-0.01	0.00	-0.01	0.00	0.01	0.00	0.00	0.00	0.00	0.00
Total	0.01	-0.37	-0.06	0.43	-0.08	0.17	0.03	-0.17	-0.23	0.15	0.17	-0.01

FIG. 3.2: Observations [mm] of soil moisture, snow mass, and groundwater storage (groundwater level*$\{S_y\}$) in Illinois (left), and their total (terrestrial water storage, right).

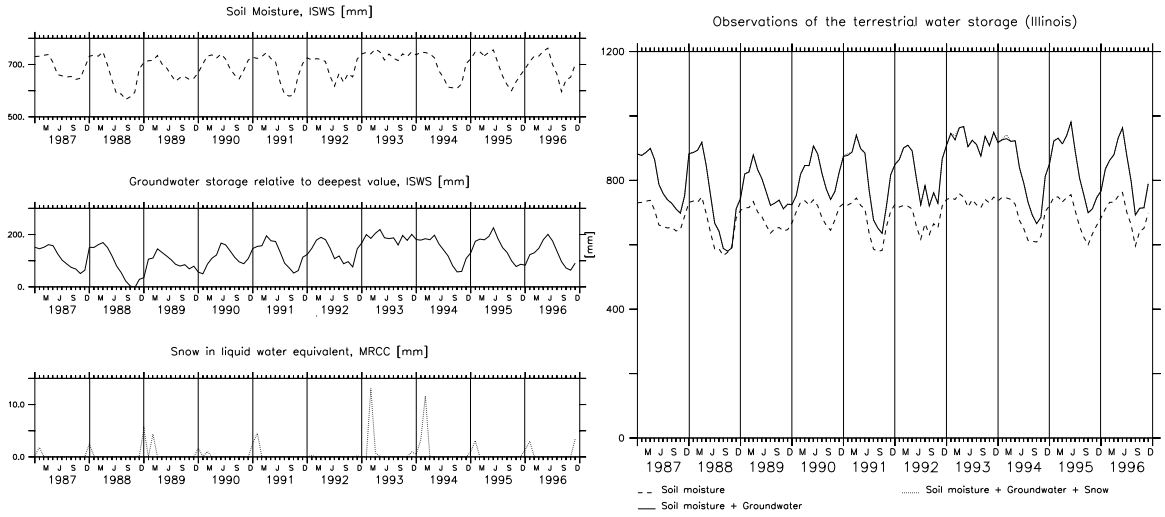

FIG. 3.3: Observed monthly variations [mm/d] of soil moisture, snow mass, and groundwater storage (groundwater level*$\{S_y\}$) in Illinois (left), and the associated total terrestrial water storage (right).

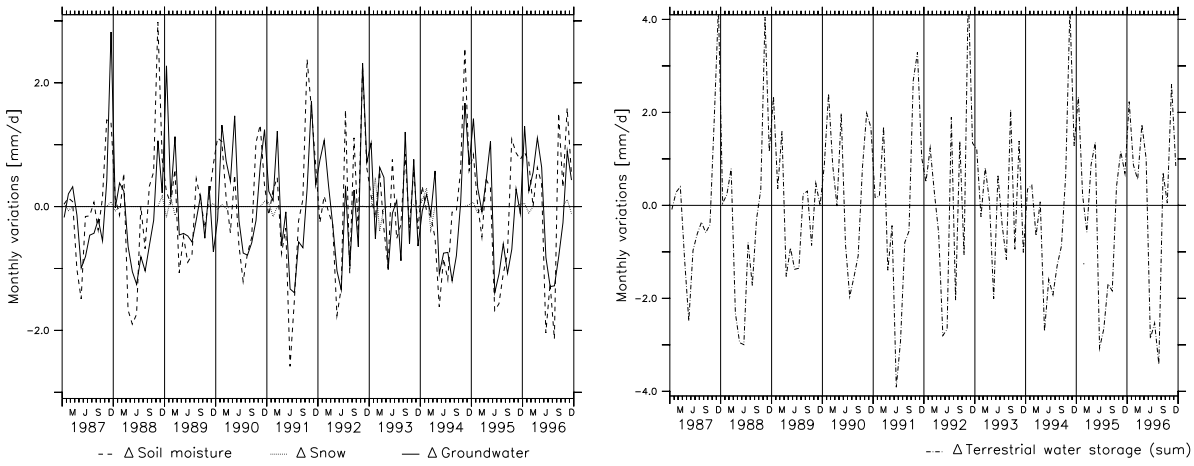

3.4 Results: Water-balance estimates of terrestrial water-storage variations

The outline of this section is as follows. First, the ERA-40 water vapour flux and its divergence are briefly analysed (section 3.4.a). The computed monthly terrestrial water-storage variations for the 10-year climatology and the individual years are then presented in subsections 3.4.b and 3.4.c, respectively. Finally, subsection 3.4.d discusses the long-term imbalances between the computed vapour flux convergence and the measured streamflow, comparing the present results with other water-balance studies investigating some of the domains considered here.

3.4.a ERA-40 water vapour flux and flux divergence over the United States

This section gives a short description of the ERA-40 water vapour flux and flux divergence over the United States in annual, winter (DJF), and summer (JJA) means for the years 1987-1996 (see Figure 3.4). The maps represent means of analysis values sampled 4 times a day.

In the annual mean, the dominant vapour flux occurs over the Gulf Coast states, a region of comparatively large moisture convergence. There is also a substantial vapour flux from the Pacific Ocean to the Northwest. Convergence values dominate over land, while there is significant vapour flux divergence over sea. As one expects, divergence over sea is largest in tropical and subtropical regions.

The winter mean vapour flux presents regions of large convergence, mainly in the Pacific Northwest as well as in the Gulf Coast states. There is a sharp land-sea gradient in vapour flux divergence along the East Coast during this season. Over land, the flux is almost always convergent, while it is divergent over the sea areas, except in the Northwestern Pacific.

The picture is very different in summer, where there is divergence in many regions over land and convergence over sea off the East Coast. Some convergence also appears west of the Mexican Sierra Madres. One of the main features of the summer moisture circulation over the United States is the large vapour flux from the Gulf of Mexico into the central United States associated with the North American Monsoon system. Despite this circulation, most of the central United States exhibits a net export of moisture during the summer season.

On the whole, these features are consistent with what is known about the climate and circulation characteristics of the United States and are similar to the patterns of vapour flux and vapour flux convergence described by Roads et al. (1994) in their analysis of vapour flux divergence from the NCEP/NCAR (National Center for Environmental Prediction/National Center for Atmospheric Research) analysis data for the years 1984 to 1990.

3.4.b Computed estimates: 10-year climatology

Figure 3.5 displays the 10-year mean annual cycle of vapour flux convergence, observed runoff, monthly variations in atmospheric water content, and computed monthly variations in terrestrial water storage for the regions investigated: the Mississippi subbasins

FIG. 3.4: Water vapour flux [kg m^{-1} s^{-1}] and flux divergence [mm/d] over North America in ERA-40: (a) annual mean, (b) winter mean (DJF), and (c) summer mean (JJA) fields for the years 1987-1996. A light smoothing has been applied for display purposes.

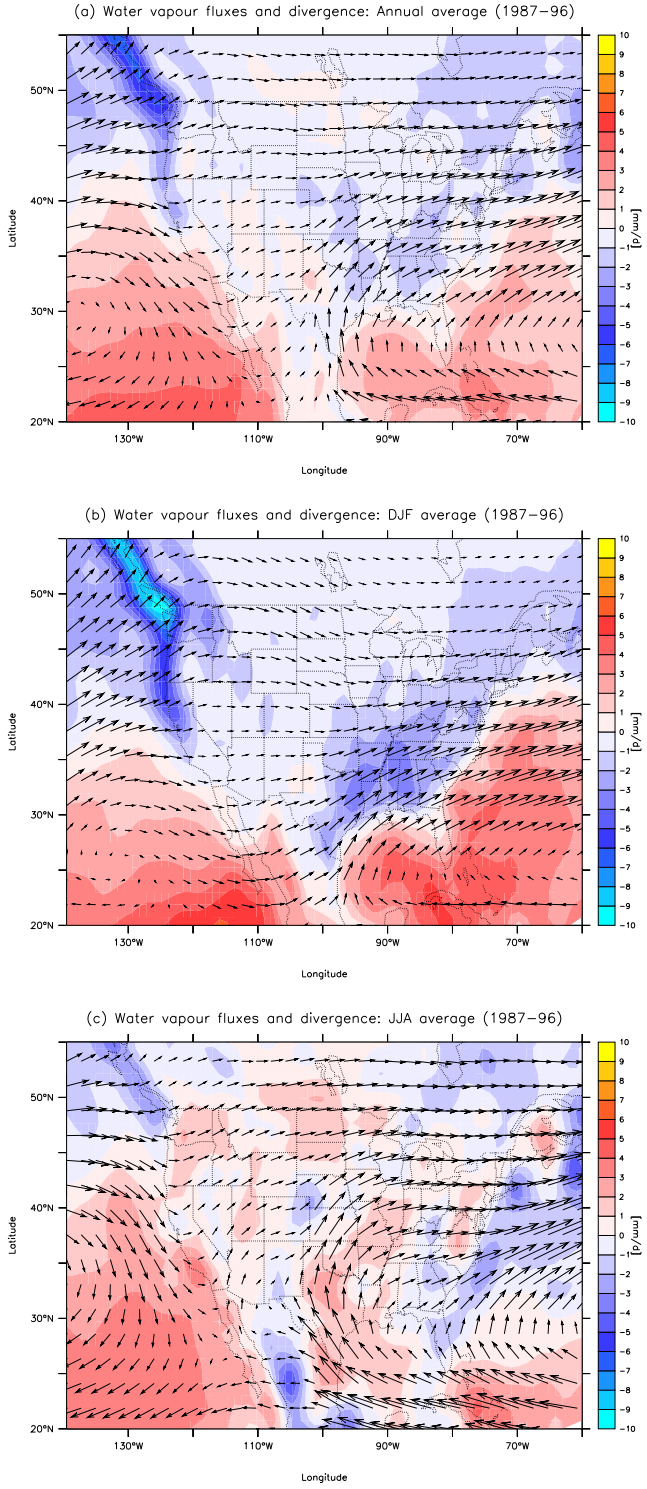

Arkansas-Red, Missouri, upper Mississippi and Ohio-Tennessee (domains 1-4), the whole Mississippi river basin (sum of domains 1-5), and Illinois (domain 6).

In most domains, the vapour flux convergence is positive from the fall until the middle of spring. It generally presents two distinctive peaks, one in November-December and the other in spring (in March in the Ohio-Tennessee River basin, in April in the upper Mississippi River basin, and in May in the Missouri River basin). In summer, there is divergence in most domains. The Ohio-Tennessee River basin (situated in the large moisture convergence region of the Gulf Coast, see section 3.4.a) has unique characteristics: It exhibits large water vapour convergence in most months, and divergence in one month (August) only. This is due to the important orographic effects of Appalachian Mountains which are responsible for the heavy precipitation typical of this region (e.g. Pardé 1930, Berbery and Rasmusson 1999).

Streamflow strongly varies in magnitude between the considered domains. It is comparatively negligible in the Arkansas-Red and Missouri River basins, while it attains very large values in the Ohio-Tennessee River basin (in relation with the heavy precipitation in this region). It is generally largest in spring, at the time of the peak in vapour flux convergence.

The variations in atmospheric water content are generally smaller than the other water-balance components. Their mean annual cycle is very similar for all 6 domains, and presents a net increase in spring and a decrease in the fall.

The mean annual cycle of the computed monthly variations in terrestrial water storage (the residual of the other three variables) is relatively similar for the 6 domains considered. Storage depletion occurs in spring and summer (generally from April-May to September), with a peak between June and August. In most domains, there is a recharge peak in November, associated with the peak in vapour flux convergence occurring during this month. The Missouri River basin also presents an additional recharge peak in spring, which again closely follows the peak in vapour flux convergence. This is probably a realistic feature as it is known that a large part of the recharge occurs as snow accumulation in this region (e.g. Pardé 1930). In the other domains, the spring peak in vapour convergence only partly goes into terrestrial water recharge, the remaining going into runoff.

3.4.c Computed estimates: Interannual variability

Figure 3.6 displays the temporal evolution of the computed monthly variations in terrestrial water storage for the investigated regions. As for the climatological means, the estimates generally follow the vapour flux convergence, while runoff and the changes in atmospheric water content are usually comparatively small. Runoff, however, can be significant in years with large vapour flux convergence (for instance in 1993 in the upper Mississippi River basin and Illinois), and is especially large in the Ohio-Tennessee River basin, where it amounts to similar values as the vapour flux convergence (see also previous section).

Note that, contrary to what is seen in the other domains, there is almost no lag-correlation between vapour flux convergence and the observed river runoff in the Ohio-Tennessee River basin, which suggests that the soil is close to saturation in this region or that precipitation is very localized and instantly directed into streams. As most of the

FIG. 3.5: Ten-year (1987-1996) mean annual cycle [mm/d] of vapour flux convergence (denoted $-\nabla Q$; blue line), of the changes in atmospheric water content (denoted ΔTCW; green line), of runoff (red line), and of the computed changes in terrestrial water storage (black line), for the Arkansas-Red, Missouri, upper Mississippi, and Ohio-Tennessee River basins, the whole Mississippi River basin, and Illinois (see Fig. 3.1 and Table 3.1 for the definition of the domains).

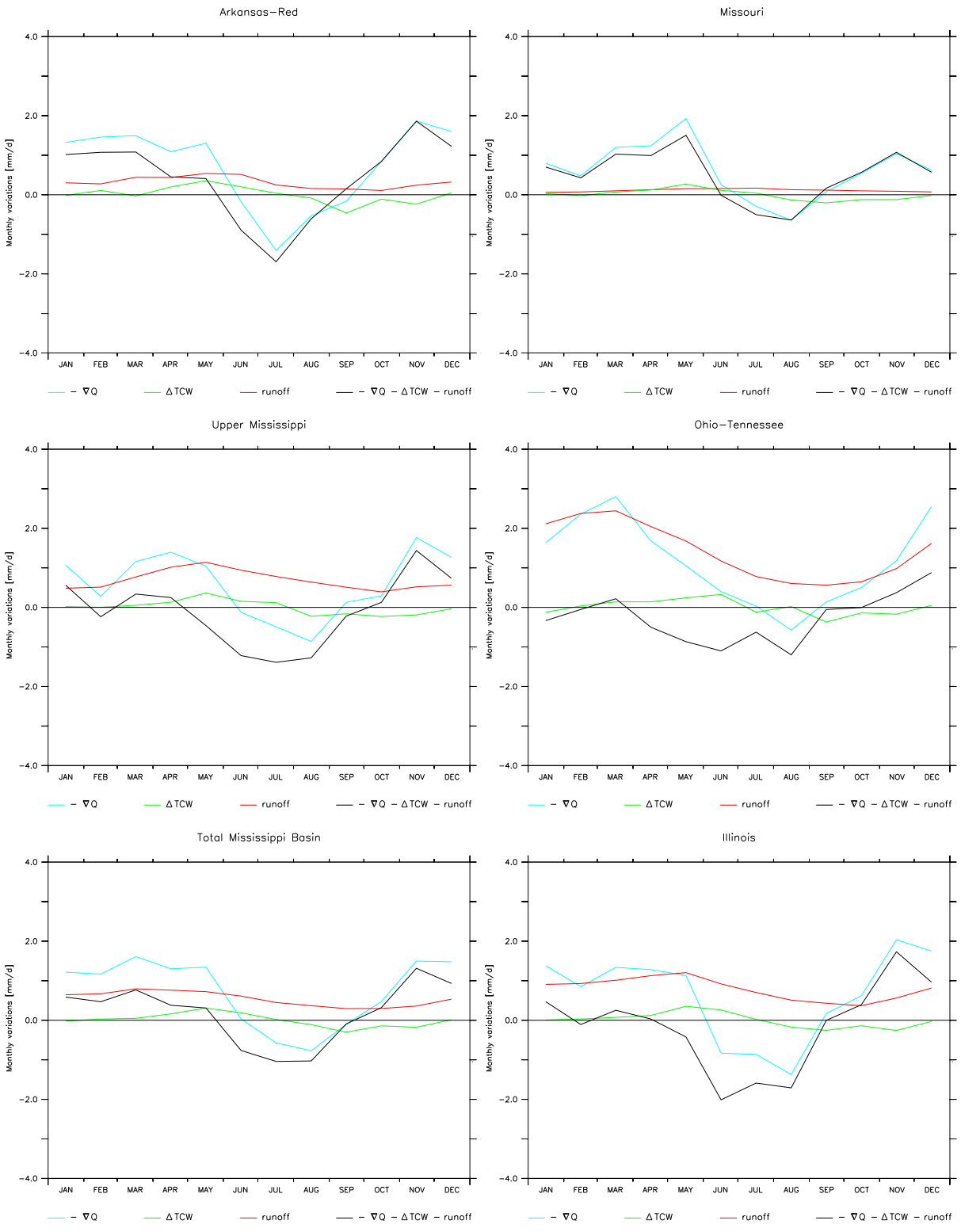

FIG. 3.6: Monthly water-balance components for the Arkansas-Red, Missouri, upper Mississippi, Ohio-Tennessee, and whole Mississippi River basins, and for Illinois [mm/d]: vapour flux convergence (denoted $-\nabla Q$; blue line), changes in atmospheric water content (denoted ΔTCW; green line), runoff (red line), and computed estimates of changes in terrestrial water storage (black line).

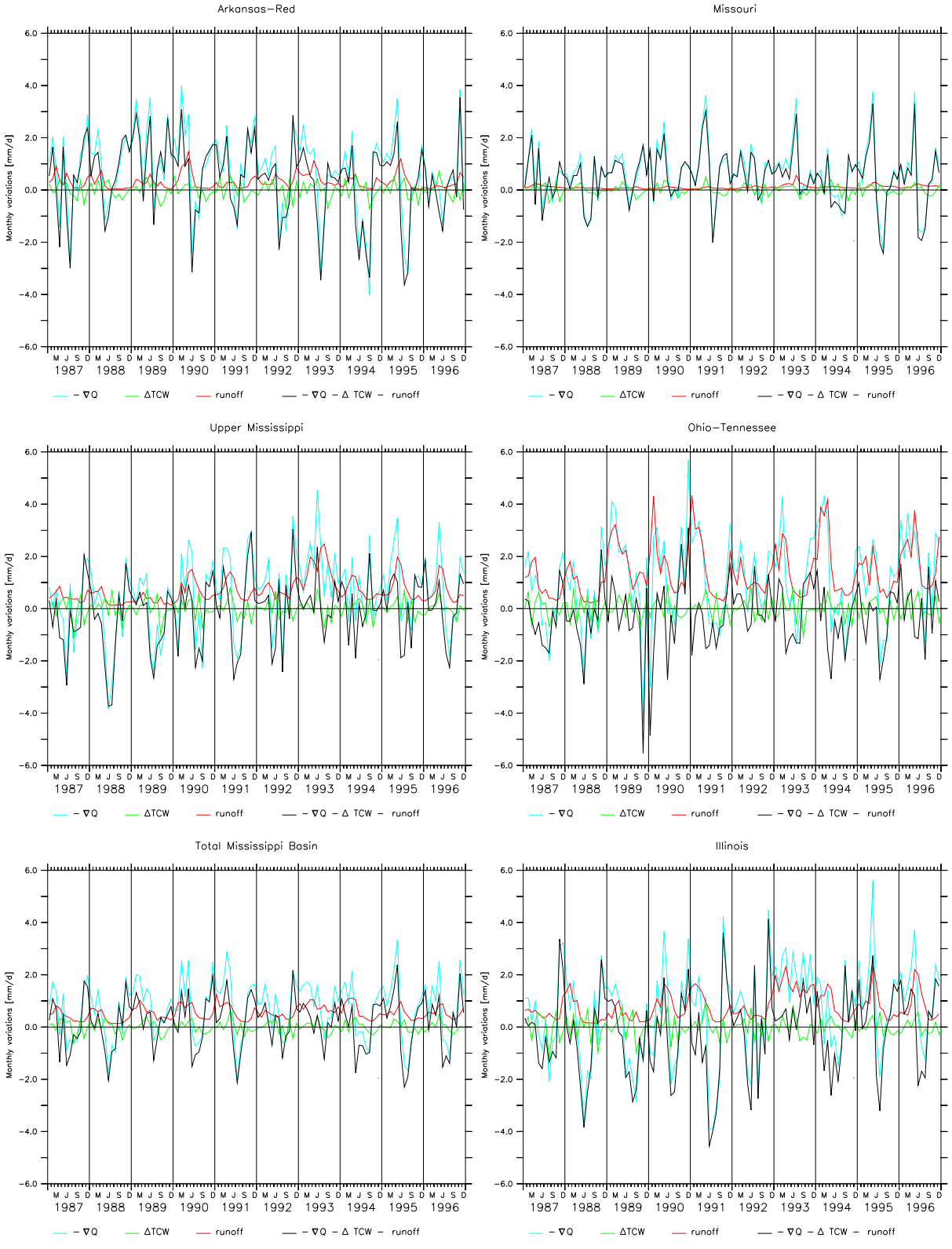

vapour flux convergence goes into river runoff, the computed changes in terrestrial water storage are a mere residual of two large values and may be rather inaccurate for this subbasin.

In the other domains, the temporal evolution of the estimates is generally characterized by a clear seasonal cycle, with storage depletion in spring and summer, and recharge during the rest of the year. Note that individual events such as the late spring 1988 drought and the summer 1993 flood in the Midwest are clearly captured in the regions concerned (Upper Mississippi, Illinois).

3.4.d Computed estimates: Long-term imbalances

Though the mean vapour flux convergence should equate areal runoff for long-term averages (see equation (3.8), section 3.2.a), this is not the case for the investigated domains (Table 3.6), and correspondingly the 10-year average of the computed variations in terrestrial water storage do not cancel out (contrary to the variations in atmospheric water content). Such imbalances are a common problem of studies investigating atmospheric water balances, both with raw radiosondes data (e.g. Rasmusson 1968, Ropelewski and Yarosh 1998) and modelling products (e.g. Roads et al. 1994, Oki et al. 1995, Gutowski et al. 1997). They are likely due to errors in the determination of the regional vapour flux divergence, as streamflow measurements are known to be accurate within a few percent (e.g. Gutowski et al. 1997).

For illustration, results from other studies using analyses for the computation of vapour flux convergence in some of the domains investigated, are presented in Table 3.6. Gutowski et al. (1997) and Yeh et al. (1998) use NCEP reanalysis data, Berbery and Rasmusson (1999) Eta Data Assimilation System (EDAS) analyses. In the case of Berbery and Rasmusson (1999), we computed the mean streamflow for the relevant time period from the USGS dataset, as comparisons with streamflow data were not provided in their study. Note, moreover, that our domain 2 "Missouri" corresponds to the sum of their domains "Missouri" and "Lower Missouri", and that we averaged the data of these two domains for the present comparison.

From the results of these four studies, it is apparent that the long-term imbalances between the ERA-40 vapour flux convergence and the measured streamflow is comparable as (and in general smaller than) for other analysis products. Note, however, that the results of Berbery and Rasmusson (1999) are available for only two years of data, which might explain the large imbalances between the vapour flux convergence and streamflow in their study.

It is difficult to identify the exact causes for the imbalances between the reanalysis data and the measured streamflow. Possible explanations for biases in the vapour flux convergence could be related to: 1) the intrinsic difficulty in accurately reconstructing regional vapour flux divergence based on scattered radiosonde measurements, 2) possible errors in the radiosonde measurements themselves, 3) inaccuracies introduced by the assimilation procedure (notably the lack of water conservation due to the analysis increments), or 4) systematic biases of the analysis model. An open issue is the extent to which the non-accounting of the groundwater fluxes at the domains' lateral boundaries might impact the computed estimates.

TABLE 3.6: Ten-year (1987-1996) average values of vapour flux convergence, runoff, changes in atmospheric water content, and changes in terrestrial water storage of the present study (left column), and long-term averages of vapour flux convergence, runoff, and corresponding imbalances in the studies of Gutowski et al. 1997 (G97), Yeh et al. 1998 (Y98), and Berbery and Rasmusson 1999 (BR99). All values in [mm/d].

	ERA-40 present study (87-96)				NCEP G97(84-93)*, Y98(83-94)**			EDAS BR99 (05/95-04/97)		
	$-\overline{divQ}$	$\overline{R}$	$\overline{\frac{\partial W}{\partial t}}$	$\overline{\frac{\partial S}{\partial t}}$	$-\overline{divQ}$	$\overline{R}$	Imb^1	$-\overline{divQ}$	$\overline{R}$	Imb^1
Arkansas-Red	0.72	0.31	0.002	0.41	-	-	-	-1.07	0.30	-1.37
Missouri	0.60	0.11	0.002	0.49	-	-	-	-0.18	0.16	-0.34
Upper Mississippi	0.58	0.69	0.000	-0.11	1.0	0.72	0.28 *	0.41	0.76	-0.35
Ohio-Tennessee	1.10	1.42	0.003	-0.27	0.89	1.33	-0.44*	2.11	1.74	0.37
Whole Mississippi	0.72	0.54	0.002	0.18	-	-	-	-	-	-
Illinois	0.62	0.79	0.001	-0.17	0.80	0.86	-0.06**	-	-	-

[1] Imbalance ($-\overline{divQ} - \overline{R}$): This term corresponds to $\overline{\frac{\partial S}{\partial t}} + \overline{\frac{\partial W}{\partial t}}$ in the first column.

For the whole Mississippi basin, the total imbalance is relatively small due to a compensation between the positive and negative imbalances of the various subbasins. Such compensations between regional biases could explain why atmospheric water-balance computations for larger domains tend to be more accurate as discussed in Rasmusson (1968, 1971; see also section 3.2.a). Note, however, that the imbalance is small for Illinois as well, despite the very small size of this domain. In the NCEP reanalysis, the imbalance in Illinois is even lower, possibly due to a similar compensation between negative and positive imbalances, as the NCEP reanalysis imbalances switch sign in this region (W.J. Gutowski, personal communication, 2002).

Preliminary results for other river basins suggest that, beside domain size, also regional climate characteristics might impact the occurrence and magnitude of the mentioned imbalances (see this thesis, chapter 4). In the case of the Mississippi River basin, it appears that the vapour flux convergence tends to be overestimated in the western domains (Arkansas-Red, Missouri), and underestimated in the eastern domains (Upper Mississippi, Ohio-Tennessee, Illinois). Interestingly, Betts et al. (2003) found a similar subdivision of the Mississippi subbasins relative to precipitation forecasts in ERA-40, with a tendency for overestimation of summer precipitation in the east (and slight underestimation in the west). It is possible that these biases are related, but a more detailed analysis would be needed in order investigate such links.

3.5 Results: Validation against observations in Illinois

3.5.a Monthly estimates

Figure 3.7 compares the water-balance estimates of the terrestrial water-storage variations in Illinois with the available observations, for the ten years investigated (top) and their climatology (bottom). The estimates are close to the observations in most years, with the

FIG. 3.7: Computed and observed variations in terrestrial water storage in Illinois [mm/d].

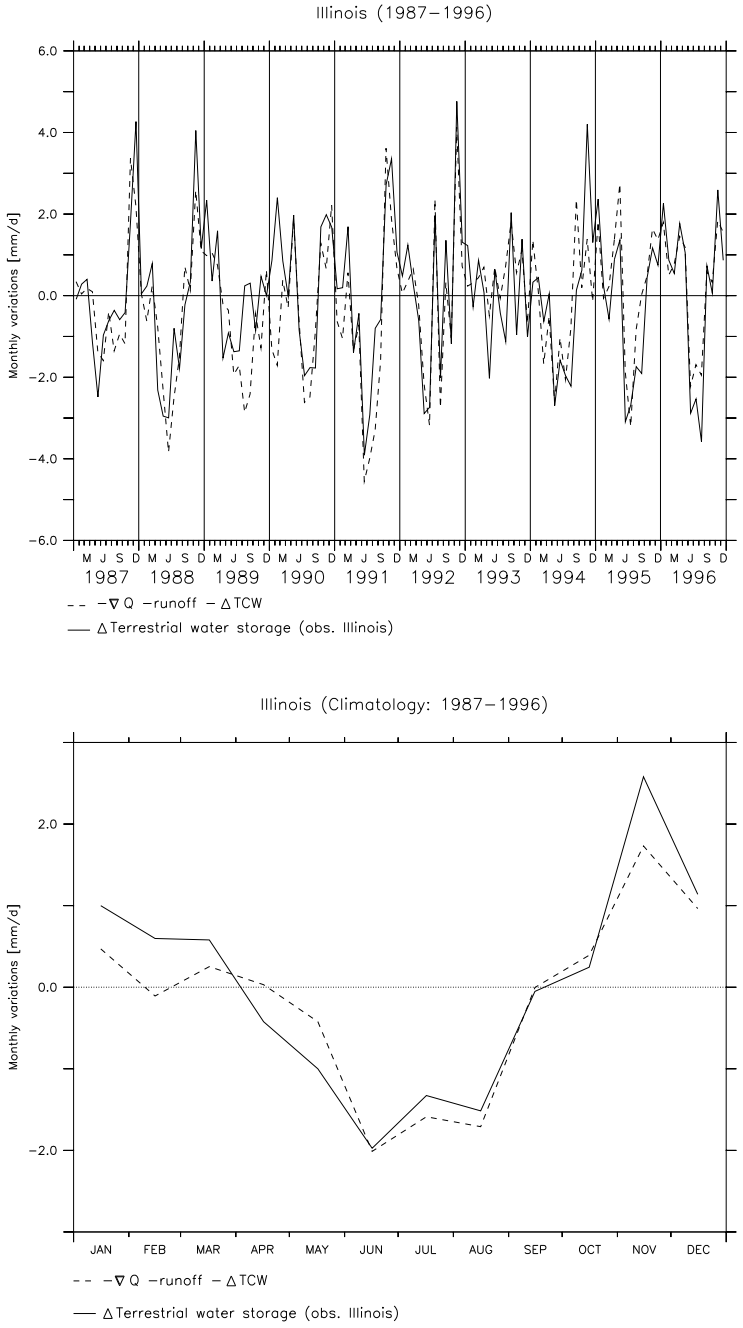

partial exception of 1989 and 1990. Important features such as the late spring drought of 1988 and the summer flood of 1993 are well captured (as is the drought of 1991), a sign that the interannual variability of the vapour flux convergence is well represented in ERA-40 (as seen in section 3.4.c). The mean climatology of the terrestrial water-storage variations for the ten years investigated is also well captured, although there is a slight negative bias in late fall and winter.

Figure 3.8 shows a scatter diagram of the computed estimates of monthly terrestrial water-storage variations versus the observational values in Illinois. The correlation between both time series is equal to 0.8, with a slope of 0.76, i.e. a slight tendency to underestimate observed changes. Although the agreement between the monthly water-balance estimates and the observations is not perfect, there is a clear correlation between them, suggesting that reasonably reliable estimates of monthly terrestrial water-storage variations can be obtained using the tested methodology with the ERA-40 reanalysis data.

FIG. 3.8: Scatter diagram of the computed and observed monthly variations in terrestrial water storage in Illinois [mm/d].

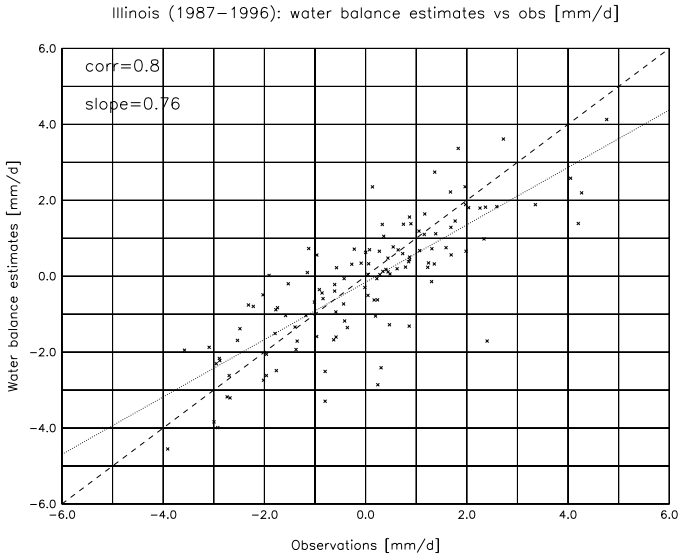

3.5.b Seasonal changes in terrestrial water storage

An important issue is the possibility to obtain estimates of the yearly amplitude of terrestrial water storage, as there is little consistent information on this critical hydrological quantity. Heck et al. (2001) found for instance that the amplitude of the soil moisture cycle between April and September can be as disparate as ∼100 mm and ∼300 mm in Europe (average for Spain, years 1987-1992), depending on the dataset considered (ERA-15 and NCEP reanalysis, respectively). Similar inconsistencies are also found in the United States (see this thesis, chapter 4).

Table 3.7 displays the mean observed and estimated seasonal changes in terrestrial water storage in Illinois for various time ranges. Interestingly, the water-balance estimates show a good correlation with the observations for periods of 4-5 months (from April 1

TABLE 3.7: Computed mean (1987-1996) seasonal change in terrestrial water storage vs. observations for various time ranges [mm] in Illinois.

	observations	estimates			
	change [mm]	change [mm]	bias [mm]	bias [%]	corr
Aug1-Apr1	-144	-122	+22	-15.2	0.94
Sep1-Apr1	-186	-175	+12	-6.2	0.82
Oct1-Apr1	-189	-175	+14	-7.3	0.72
Nov1-Apr1	-184	-163	+21	-11.4	0.66

to August 1/September 1). For longer times ranges, the correlation is lower, although the 10-year mean estimated storage depletion is generally close to the observations (but always slightly underestimated).

3.5.c Long-term integration of the estimates

Figure 3.9a displays the integrated monthly estimates of terrestrial water-storage variations for Illinois and the whole Mississippi River basin, compared with the absolute values of the observations, for the whole 10-year period. A striking feature is the drift of the integrated estimates that starts around 1988 for both regions (with opposite sign), and which can be directly related to the water-balance imbalances discussed in section 3.4.d.

FIG. 3.9: (a) Integrated estimates of terrestrial water-storage variations for Illinois and the whole Mississippi River basin compared against observations in Illinois [mm]; (b) Detrended integrated estimates for Illinois compared against observations [mm].

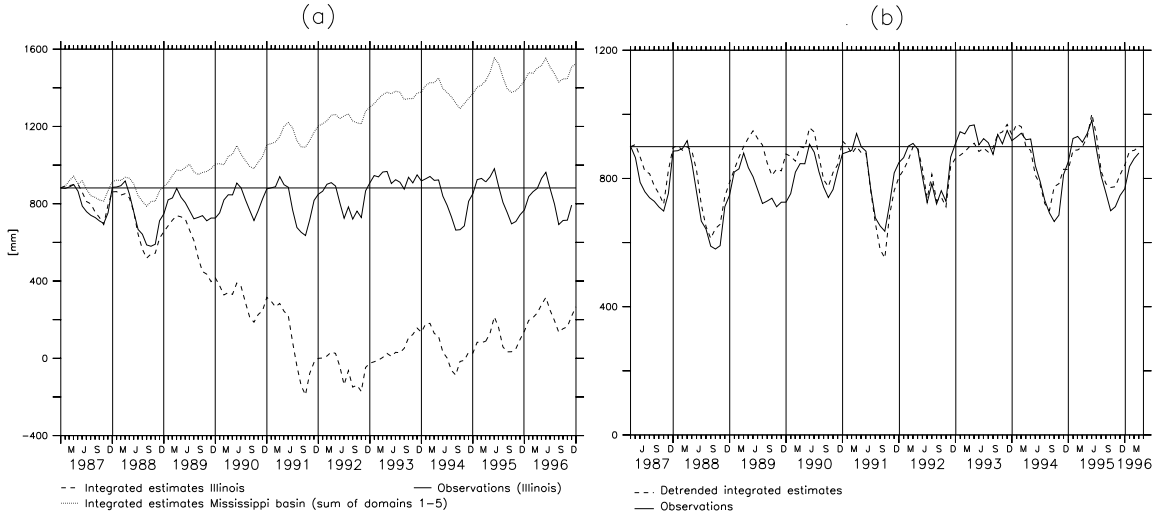

In order to correct for such drifts, the detrending procedure that is usually applied consists of a uniform monthly correction factor (e.g. Rasmusson 1968, Oki et al. 1995, Ropelewski and Yarosh 1998). As is apparent from Figure 3.9a, such a correction would not correctly suppress the drift, as some years present more drift than others, and most

of all due to the fact that the drift changes sign during the considered period over Illinois. Therefore, we correct the annual drift separately for each year, under the assumption of unchanged terrestrial water storage for annual means. As discussed in section 3.3.d (see also Table 3.5), this approximation is likely to lead to relatively significant biases in some years. In order to minimize the error induced by this approximation, we chose April as reference month, since it exhibits the smallest spread in yearly values of observed terrestrial water storage (Table 3.4). The constant of integration (mean terrestrial water storage in April) is taken from the 10-year climatology of the observations. Note that this method could also be applied for inferring storage changes in years where no observations are available, under the assumption that the mean climatological conditions of the observational period is representative for the investigated time frame.

Figure 3.9b displays the integrated values of the so-obtained detrended estimates for Illinois compared with the observations. In general, the detrended integrated estimates exhibit a good agreement with the observations, except in 1989, the only year where the monthly water-balance estimates agree rather poorly with the observations (see Fig. 3.7). In the other years, the detrending appears to give relatively correct values, but there is an underestimation of the seasonal amplitude of terrestrial water storage. This is due to the fact that the detrending is applied uniformly over all months, while most of the negative bias in the estimates occurs in fall and winter (Fig. 3.7).

3.6 Soil moisture simulation in ERA-40

For comparison purposes, this section briefly describes the ERA-40 fields of soil moisture in Illinois. The reanalysis soil moisture is available at 4 levels: from 0 to 7 cm, from 7 to 28 cm, from 28 to 100 cm, and from 100 to 289 cm. As the soil moisture observations are available for a 2-meter soil layer, we scaled the soil moisture content of the lowermost layer to a depth of 1 m and summed this value together with the moisture content of the other three layers.

The monthly variations in soil moisture show good agreement with the observations (Figures 3.10a and 3.10b). The interannual variability is in general well captured, however the reanalysis underestimates both soil moisture depletion in summer and soil moisture recharge in the fall (Fig. 3.10c), leading to a damping of the annual cycle (see hereafter). The absolute soil moisture content is underestimated (Figure 3.10d), but the temporal evolution shows again a good agreement with the observations, with a relatively high correlation (Figure 3.10e). Note that the reanalysis tends to underestimate extreme values of soil moisture (slope of 0.59, Fig. 3.10e) as well as the mean amplitude of the annual soil moisture changes: Between April and October the net decrease in soil moisture amounts to $\sim$50 mm in ERA-40, compared to $\sim$100 mm for the observations (Figure 3.10f).

In summary, the ERA-40 soil moisture appears to be consistent with the observations, presents relatively accurate monthly variations, but has a damped yearly cycle and an underestimation of the absolute storage. The damping of the yearly cycle is likely attributable to the increments in soil water, which supply water in summer and remove water in winter and early spring (Betts et al. 2003).

Note that the simulated monthly variations in soil moisture do not correlate as well with the observations as the water-balance estimates of terrestrial water-storage variations discussed in the preceding sections. A combination of the information entailed in both

FIG. 3.10: Monthly variations (left-hand panels, [mm/d]) and values (right-hand panels, [mm]) of ERA-40 soil moisture (scaled to 2 m) over Illinois compared against observations: (a,d) temporal evolution, (b,e) scatter plot, and (c,f) mean climatology.

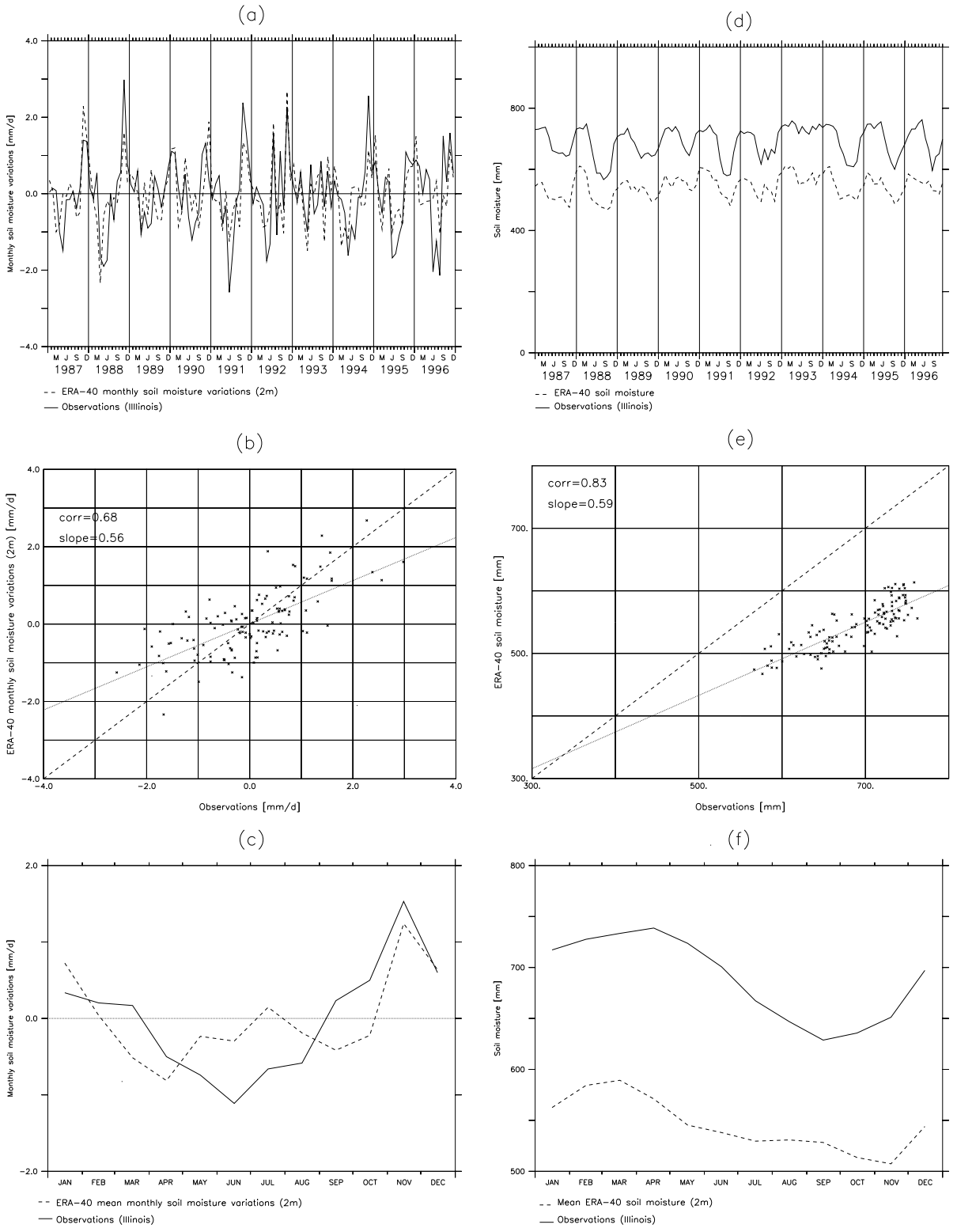

timeseries could perhaps be used in order to obtain optimal estimates of soil moisture values. In Illinois for instance, groundwater and soil moisture are clearly correlated, and snow amounts are small (see section 3.3.d, and Figs. 3.2 and 3.3), therefore it should be possible to scale the estimated changes in terrestrial water storage to obtain information on soil moisture for this region. As soil moisture has a more direct impact on climate than terrestrial water storage as a whole, this could represent particularly useful information.

3.7 Summary and conclusions

This study investigates the feasibility of estimating monthly variations in terrestrial water storage from water-balance computations, using atmospheric water vapour convergence from the ERA-40 reanalysis data and conventional runoff data. The results are very promising, as the computed estimates of the terrestrial water-storage variations appear realistic for the various domains within the Mississippi River basin and show very good agreement with observations in Illinois. The mean seasonal cycle is well represented for the studied period and the interannual variability is in general well captured.

In the long-term average, the computed variations in terrestrial water storage do not cancel out due to imbalances between the ERA-40 vapour flux convergence and the measured streamflow, which are likely due to systematic biases in the computed vapour flux convergence. Due to these biases, an estimation of the temporal evolution of terrestrial water storage over time periods longer than 4-6 months is possible only with an appropriate detrending. The simple detrending procedure applied here yields reasonably good results, allowing a correct estimation of absolute terrestrial water storage in most years.

An important result is that the critical domain size for water-balance computations using high resolution reanalysis data appears to be much smaller than for raw radiosonde data (e.g. Rasmusson 1968, 1971). The Illinois domain has a size of only $\sim 2\text{x}10^5$ km^2 and is shown to be suitable for the computation of the water-balance estimates. Yeh et al. (1998) come to similar conclusions in their study of the hydroclimatology of Illinois.

One should note that Illinois is a region with flat and homogeneous terrain, and that this methodology might not be as accurate for areas presenting more horizontal and vertical heterogeneities, or other climatic characteristics. We are not aware of other regions with such comprehensive observational datasets of terrestrial water storage as Illinois, and it might thus not be possible to perform such a detailed validation for other river basins, but further validation studies for regions with observations of at least some components of the terrestrial water storage would be very useful.

As discussed in section 3.2.c, the ERA-40 reanalysis project is still in its running phase. Once the full reanalysis data becomes available, it will be possible to compute 40-year timeseries of the proposed estimates for various regions of the world, as recent runoff measurements are available for most major river basins. A study focusing on several European and Asian river basins has recently been started (Hirschi 2002; this thesis, chapter 4).

Finally, water-balance estimates computed with this methodology could be compared with results obtained with other methodologies, such as the model-computed soil moisture from the phase 2 of the GSWP project (see Dirmeyer et al. 1999), or remote sensing measurements of the GRACE mission (Wahr et al. 1998), which will provide estimates of changes in terrestrial water storage for the entire globe.

Acknowledgements

Many thanks to the respective teams of the Global Soil Moisture Data Bank, of the Illinois State Water Survey (ISWS), of the Midwest Regional Climate Center (MRCC), and of the United States Geological Survey (USGS) for the observational datasets made available to us. We would like to thank in particular Ken Hlinka (ISWS WARM Program), as well as Jon Burroughs and Maria Peters (MRCC) for numerous helpful comments. We are also most grateful to Pat Yeh for his pertinent and helpful answers to numerous questions on the hydrology of Illinois. Sincere thanks as well to Alan Betts, Kirsten Findell, Christoph Frei, Oliver Fuhrer, Sophie Fukutome, Bill Gutowski, Martin Hirschi, Wolfgang Kinzelbach, Matt Rodell, Reto Stöckli, and Pier Luigi Vidale for their useful comments on this study. Financial support was provided by the Swiss National Science Foundation through the NCCR Climate programme.

Chapter 4

Some Preliminary Applications

4.1 Introduction

This chapter investigates various aspects completing the analyses of the studies presented in chapters 2 (Seneviratne et al. 2002) and 3 (Seneviratne et al. 2003). In the rest of this chapter, the two studies will be referred to as S02 and S03, respectively. Section 4.2 presents an application of the methodology presented in S03 to several European and North-Asian river basins. Section 4.3 compares the simulated soil moisture in study S02 with the Illinois observations and the water-balance estimates described in S03.

4.2 Estimated variations in terrestrial water storage: Europe and Northern Asia

In a recent diploma thesis, Hirschi (2002) computed water-balance estimates of changes in terrestrial water storage for various European and North-Asian river basins using the same methodology as S03. This section summarizes and extends some of the analysis presented in his study. The employed datasets include the ERA-40 reanalysis (vapour flux convergence and monthly changes in atmospheric moisture content) as well as conventional streamflow data from the Global Runoff Data Center and national hydrological services. The river basins analysed are depicted in Figure 4.1 and listed in Table 4.1. For simplicity, they are again represented as a combination of quadrilaterals.

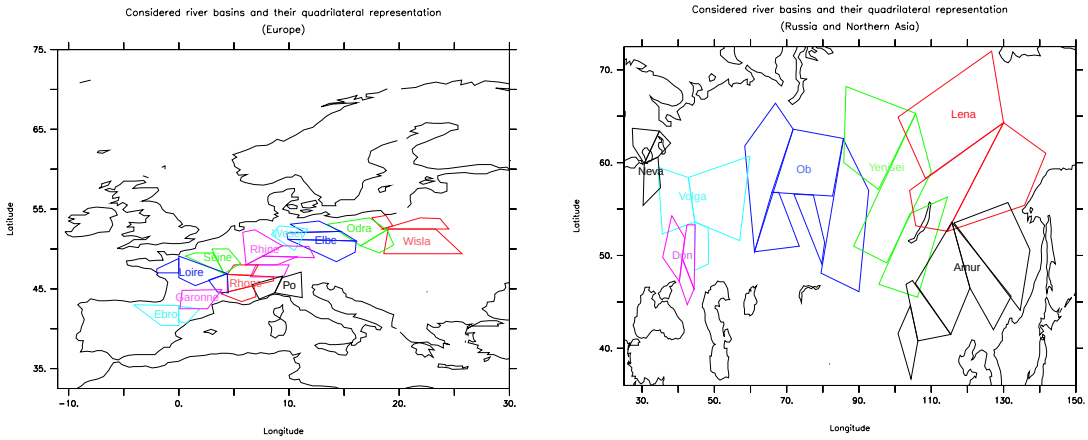

FIG. 4.1: Quadrilateral representation of the basins investigated: European river basins (top) and Russian and North-Asian river basins (bottom). (after Hirschi 2002)

4.2.a Long-term averages of water-balance components

The long-term average values of vapour flux convergence, runoff, drift in atmospheric moisture content, and drift in terrestrial water storage are presented in Table 4.2 for each basin. Note that the averages are computed for the longest period free of missing data within each timeseries (between 3 and 10 years depending on the basin considered).

TABLE 4.1: Domains analysed.

River basin/region	Station	Basin area [km^2]
Europe (without Russia)		
Ebro	Tortosa	84,230
Elbe	Neu-Darchau	131,950
Garonne	Mas-d'Agenais	52,000
Loire	Montjean	110,000
Odra	Gozdowice	109,730
Po	Pontelagoscuro	70,090
Rhine	Rees	159,680
Rhone	Beaucaire	95,590
Seine	Normandie	65,000
Weser	Intschede	37,790
Wisla	Tczew	194,380
Central Europe[a]		482,270
Eastern Europe[b]		436,060
Russia and Northern Asia		
Amur	Komsomolsk	1,730,000
Don	Razdorskaya	378,000
Lena	Stolb	2,460,000
Neva	Novosaratovka	281,000
Ob	Salekhard	2,950,000
Volga	Volgograd	1,360,000
Yenisei	Igarka	2,440,000

[a] Garonne, Loire, Seine, Rhone and Rhine

[b] Elbe, Odra, and Wisla

TABLE 4.2: Long-term average values of vapour flux convergence, runoff, drift in atmospheric moisture content, and drift in terrestrial water storage in mm/d for the basins listed in Table 4.1.

River basin/region	$-\overline{divQ}$	$\overline{R}$	$\overline{\frac{\partial W}{\partial t}}$	$\overline{\frac{\partial S}{\partial t}}$	Years considered[a]
Europe (without Russia)					
Ebro	-1.2	0.27	-0.008	-1.5	1990-92
Elbe	-1.1	0.44	-0.004	-1.5	1987-96
Garonne	0.53	1.0	-0.004	-0.47	1987-96
Loire	0.48	0.54	-0.010	-0.04	1987-92
Odra	-0.26	0.35	-0.000	-0.62	1987-93
Po	1.1	1.5	0.004	-0.49	1987-90
Rhine	1.1	1.2	-0.003	-0.17	1987-96
Rhone	1.5	1.6	-0.002	-0.07	1987-96
Seine	0.82	0.61	-0.002	0.21	1987-95
Weser	0.09	0.77	-0.003	-0.67	1987-96
Wisla	0.13	0.39	-0.001	-0.26	1987-93
Central Europe	0.72	0.98	-0.007	-0.24	1987-92
Eastern Europe	-0.36	0.39	-0.001	-0.74	1987-93
Russia and Northern Asia					
Amur	0.31	0.57	-0.001	-0.26	1987-90
Don	0.13	0.13	0.000	-0.01	1987-90
Lena	0.58	0.55	0.000	0.03	1987-94
Neva	0.88	0.83	0.003	0.04	1987-90
Ob	0.41	0.36	0.002	0.05	1987-94
Volga	0.64	0.53	0.001	0.11	1987-90
Yenisei	0.55	0.68	0.000	-0.13	1987-95

[a]Longest continuous period between 1987 and 1996 without missing runoff data

Interestingly, the European river basins exhibit much larger long-term drifts ($\overline{\frac{\partial S}{\partial t}} + \overline{\frac{\partial W}{\partial t}}$) than the basins considered in Russia and Northern Asia. A possible explanation for these differences is the comparatively small size of the European basins. They lie below the Rasmusson (1968, 1971) threshold of 2x10^6 km^2 by more than one order of magnitude, and are thus even smaller than the Illinois domain considered in S03 ($\sim$ 2x10^5 km^2). Figure 4.2 displays the imbalances of the investigated domains in Europe and North-Asia as well as for the 6 Mississippi (sub-)basins analysed in S03. Though a relationship between domain size and the accuracy of the long-term water balances seems to apply at first sight, it is notable that the large imbalances for domains of small size ($\leq$ 5x10^5 km^2) are only observed in Central Europe. For the Mississippi and the river basins in Russia and Northern Asia, the imbalances are almost independent of the domain size, and in general of small magnitude. Note in particular the extreme accuracy of the computed long-term water balances in Russia and Northern Asia, even at spatial scales lower than 5x10^5 km^2.

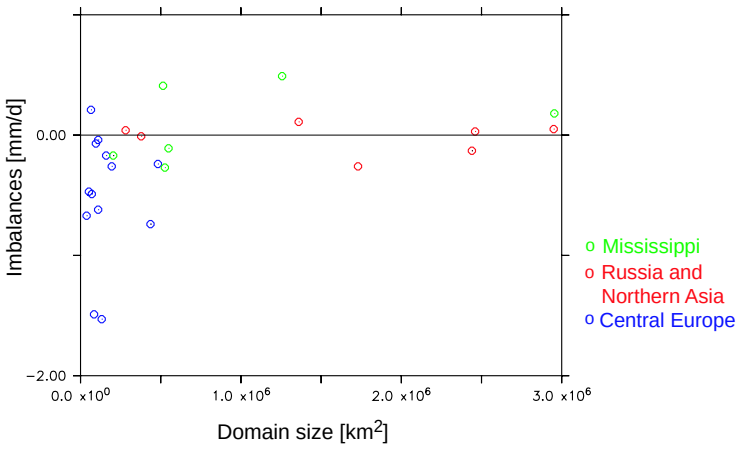

FIG. 4.2: Long-term imbalances ($\overline{\frac{\partial S}{\partial t}} + \overline{\frac{\partial W}{\partial t}}$) vs. domain size for the European (blue), and the Russian and North-Asian (red) domains listed in Table 4.2, as well as for the 6 Mississippi sub-domains (green) investigated in S03 (see chapter 3, Table 3.6).

This analysis suggests that the magnitude of the imbalances can also depend on regional characteristics of the domains investigated. Beside the small size of the considered river basins (and their coarse representation in quadrilaterals), possible further explanations for the drifts in Europe are the importance of topographic effects and heterogeneous climate features in this region, in comparison with the relatively homogeneous climatic conditions of both Western Russia and Siberia. Note that the Amur basin, similarly to Central Europe, has an important relief and high moisture in-flow, and is also the only domain of Russia and Northern Asia presenting a relatively large long-term imbalance of moisture convergence and streamflow. Another possible source of errors in mid-latitudes is linked to the complex role of vegetation in this climatic zone, and to the related difficulties in accurately modelling its interaction with climate (e.g. Heck et al. 2001, Vidale et al. 2003). In high-latitudes, the water balance is mostly determined by the accumulation and melting of the snow cover, which are possibly easier to represent.

An interesting feature is the consistent negative imbalances exhibited by all European river basins but the Seine. Due to the consistent sign of the imbalances, combining single river basins into larger domains does not yield a cancelling out of the individual drifts, as is apparent from the computed water balances for Central and Eastern Europe (Table 4.2). A negative imbalance implies an underestimation of moisture convergence relative to streamflow in these domains (see equations 3.7 and 3.8). This might be due to the high variations in topography (e.g. Alps, Pyrenees), which are not fully resolved by the reanalysis model. It is therefore possible that the reanalysis has a tendency for underestimating moisture convergence in mountainous regions, a problem which might be particularly relevant in coastal regions, where there are also high imports of atmospheric moisture. Note that the imbalances tend to be of the opposite sign for the Mississippi, suggesting that other mechanisms might explain the drifts in this region.

In summary, the critical size for combined atmospheric and terrestrial water-balance computations might lie between 2-5x10^5 km^2 for reanalysis data with a resolution comparable to ERA-40, but is likely to significantly vary along with regional climate features. Despite the mentioned drifts in some of the domains, ERA-40 appears well suitable for the computation of combined atmospheric and terrestrial water balances, as the computed moisture convergence generally shows less long-term imbalance with observed streamflow than for other similar datasets (e.g. Oki et al. 1995, Gutowski et al. 1997, Berbery and Rasmusson 1999).

4.2.b Mean annual cycle

In the rest of the analysis, we focus on 10 river basins representative of very diverse climate conditions and which present low to moderate long-term imbalances. The selected domains are the Loire, Rhine, Rhone, Seine, Don, Lena, Neva, Ob, Volga, and Yenisei River basins. Figures 4.3 and 4.4 display the long-term mean annual cycle of vapour flux convergence, of the changes in atmospheric moisture content, of runoff, and of the computed changes in terrestrial water storage, for the chosen river basins.

The Western European river basins (Loire, Rhine, Rhone, Seine) all have a similar river flow regime, characterized by a late winter peak of streamflow and a minimum in summer (pluvial oceanic flow regime according to the classification of Pardé 1947, see also Krasovskaia 1996). This flow regime is mainly determined by evaporation, which explains the maximum in the cold season and the minimum in the warm season. The Loire and the Seine Rivers present typical pluvial oceanic flow regimes, while the Rhine and the Rhone have more complex regimes including ice- and snowmelt effects, as well as influences from the mediterranean climate in the case of the Rhone. In these 4 river basins, there is atmospheric moisture convergence in the cold season and moisture divergence in summer, due to the high evaporation. Correspondingly, the computed changes in terrestrial water storage are positive in the cold season and negative in the summer.

The Don and the Neva Rivers, both situated west of the Ural mountains, show small monthly variations in runoff. In the Don River basin, streamflow is very low, and the computed change in terrestrial water storage follows closely the moisture convergence. In the case of the Neva, streamflow is relatively abundant and appears mostly induced by snowmelt. The absence of a clear snowmelt-induced peak of streamflow (contrary to what is observed for the Volga, Ob, Lena, and Yenisei Rivers) comes from the fact that the

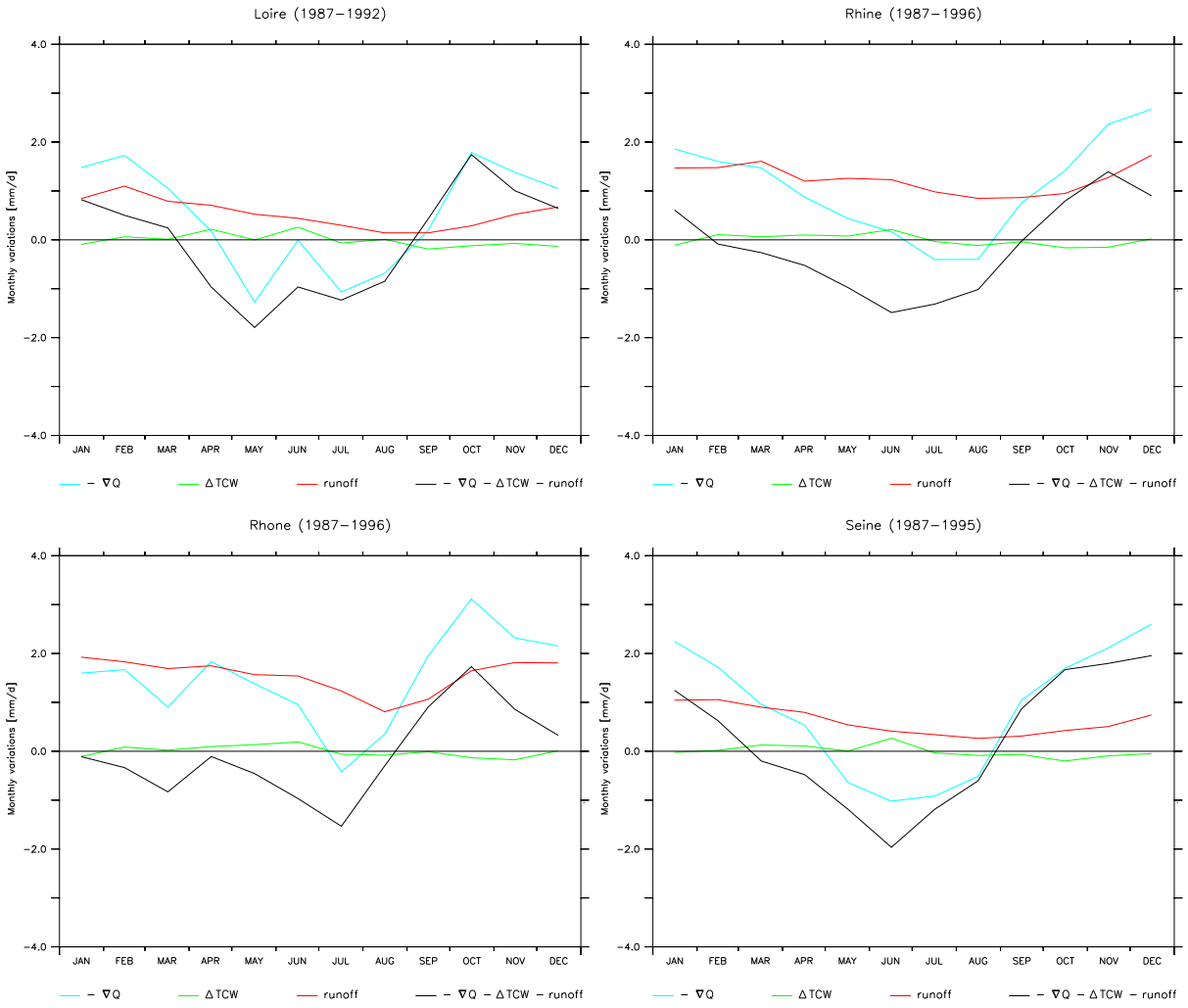

FIG. 4.3: Long-term mean annual cycle [mm/d] of vapour flux convergence ($-\nabla Q$), of the changes in precipitable water content (ΔTCW), of runoff, and of the computed changes in terrestrial water storage, for the Loire, Rhine, Rhone, and Seine River basins.

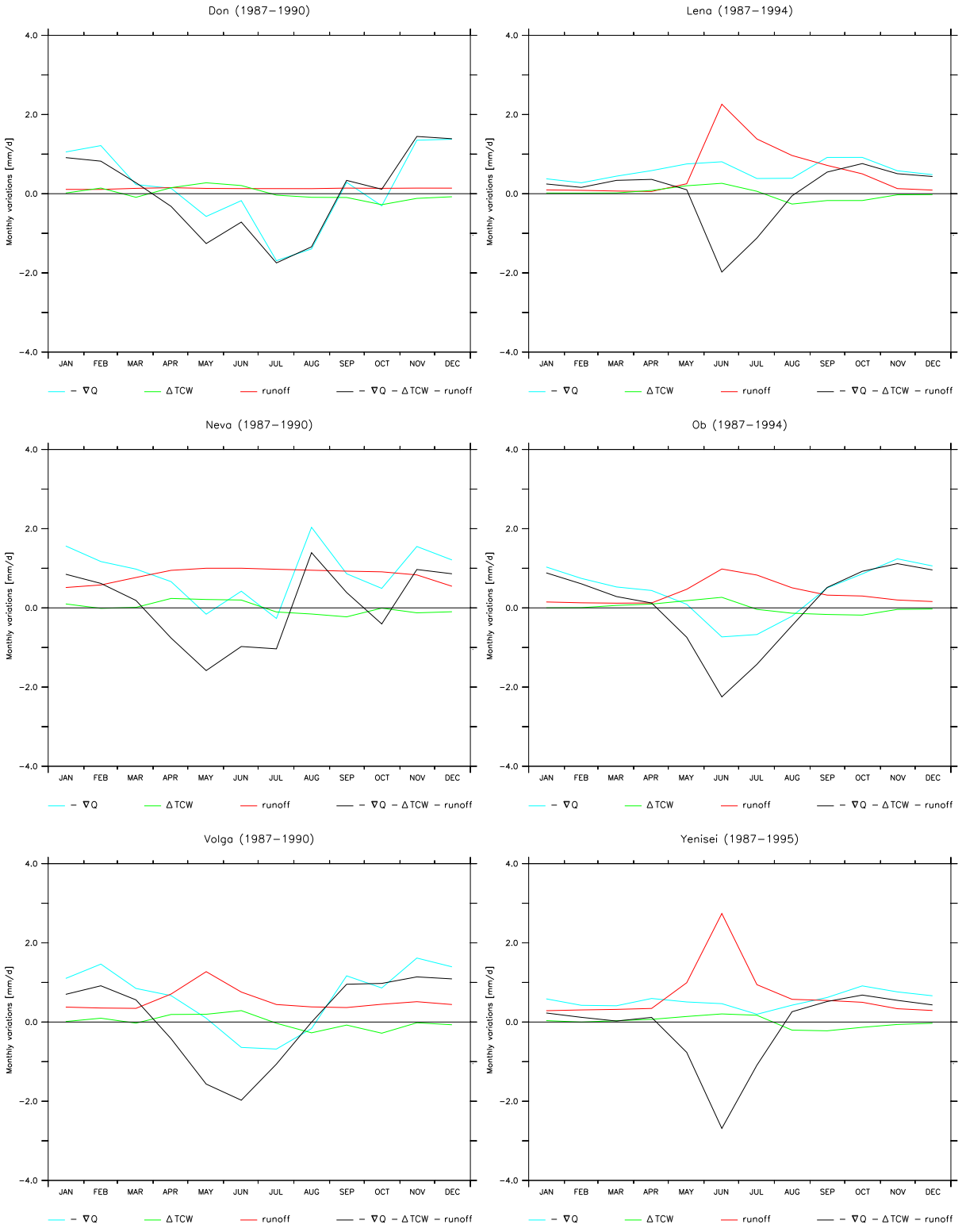

FIG. 4.4: Same as Figure 4.3 for the Don, Lena, Neva, Ob, Volga, and Yenisei River basins.

Neva and its tributaries flow through a series of lakes which have a damping effect on the maximum (Pardé 1947). As for the Don River basin, the computed variations of terrestrial water storage for the Neva River basin are closely correlated with the moisture convergence, due to the low seasonal variations of runoff.

The other Russian rivers show a clear nival river flow regime (Pardé 1947), with a very large streamflow peak occurring in May (Volga) or June (Ob, Lena, Yenisei). The timing of the streamflow peak depends on the local temperature conditions, occurring later in colder regions. The Volga and the Ob Rivers present some moisture divergence in summer, which also contributes to the terrestrial water-storage depletion. To the contrary, the Lena and Yenisei River basins show moisture convergence in all months. In these domains, the computed changes in terrestrial water storage appear to be mostly determined by changes in snow amounts. Note that the computed changes in terrestrial water storage for the Volga are qualitatively similar to the results that Matsuyama and Masuda (1997) obtained for this region using the four-dimensional data assimilation (4DDA) operational analysis data from the ECMWF.

In summary, in all the considered basins, the computed changes in terrestrial water storage are negative in the warm season and positive in the cold season. Regions with a very short warm season (Ob, Lena, Yenisei) present a short but sharp peak of storage depletion, mostly due to snowmelt. In warmer regions, storage depletion is mostly induced by evaporation (Central and Eastern Europe). Replenishment due to moisture convergence occurs in fall and spring in most regions. In long-term average, the computed monthly changes in terrestrial water storage generally appear realistic and compare well with the results of other long-term water-balance studies (e.g. Matsuyama and Masuda 1997, Masuda et al. 2001).

4.2.c Comparison with soil moisture observations

As for the Mississippi River basin, it would be desirable to compare the computed changes in terrestrial water storage with observations. Unfortunatly, there are to our knowledge no large-scale soil moisture datasets for Western Europe. Soil moisture measurements are available from countries of the former Soviet Union (Robock et al. 2000), however there are no corresponding groundwater measurements, and the available snow measurements do not match the years investigated. For comparison purposes, the available soil moisture observations and the computed changes in terrestrial water storage are displayed in Figure 4.5) for the relevant river basins. Though the agreement is not good for most basins, there is, however, some correlation between both datasets for the Ob and the Volga River basins. The poor agreement between the estimated terrestrial water-storage variations and the observed soil moisture is likely due to the omission of the observed changes in snow and groundwater in the comparison. As mentioned earlier, snow plays a very important part in the water balance of these regions, contrary to what is observed in Illinois (S03). This is confirmed by the high summer mismatch for Ob (1987,1988), Neva (1988), and Volga (1987).

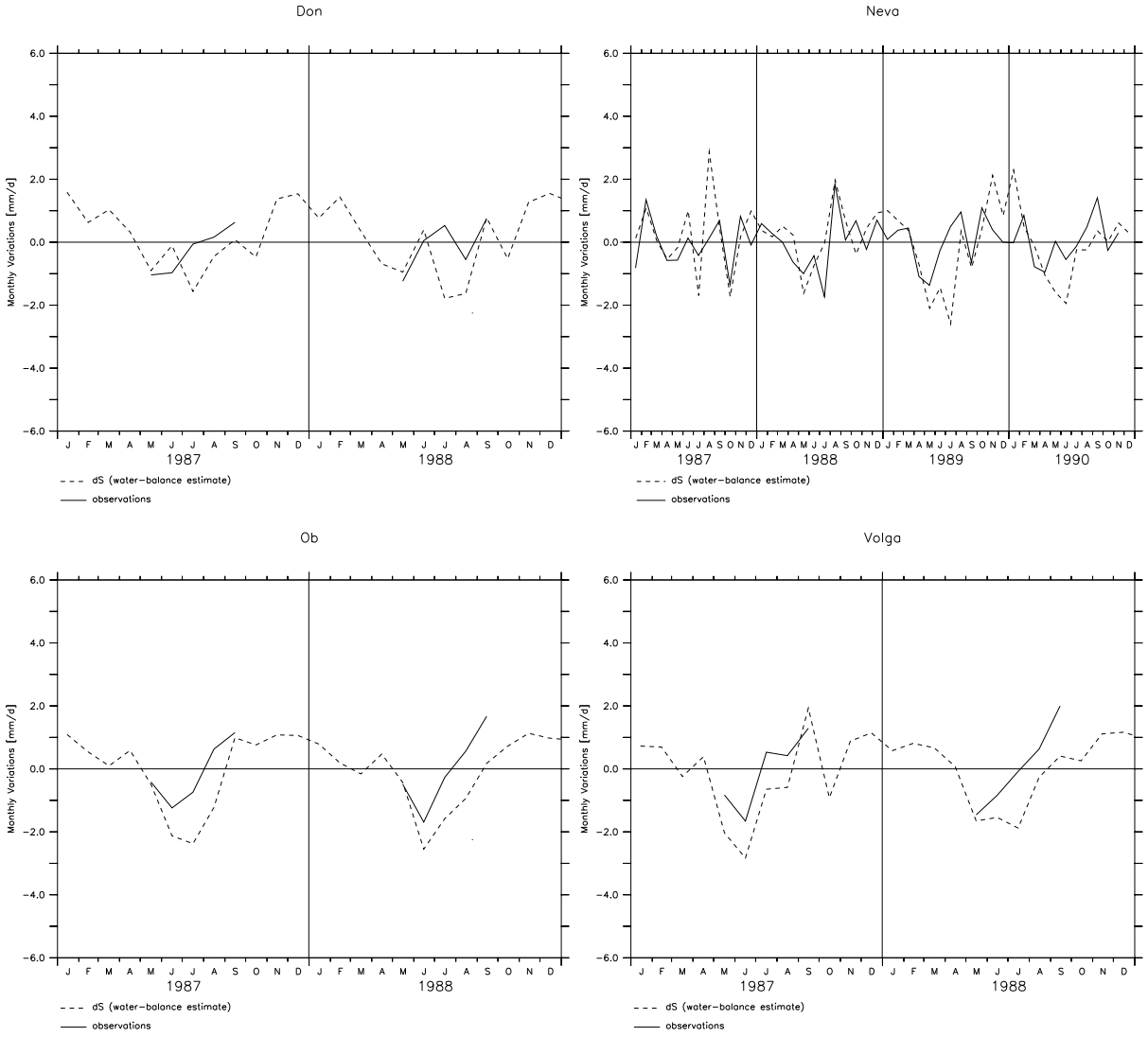

FIG. 4.5: Comparison of estimated changes in terrestrial water storage with observed monthly changes of soil moisture for the Don, Neva, Ob, and Volga River basins [mm/d]. Note that the soil moisture observations in the Don, Ob, and Volga River basins are only available from April 8 to October 28). (from Hirschi 2002)

4.2.d Comparison with CHRM simulation over Europe

In this section, seven years (1987-1993) from a 15-year control simulation performed with the Climate High Resolution Model (CHRM) over Europe (RAD simulation of Vidale et al. 2003, see also appendix A) is compared with the ERA-40 soil moisture and the computed changes in terrestrial water storage (raw and detrended estimates; see S03 for a description of the detrending procedure). The CHRM is a regional climate model covering the European region, and it is driven by the previous ERA-15 reanalysis at its lateral boundaries.

Figure 4.6 displays the annual mean changes in soil moisture and estimated terrestrial water storage between April and October for the CHRM domains France and Germany. The depth of the soil moisture storage in the CHRM is 1.70 m. The integrated raw and detrended estimates of terrestrial water-storage variations are summed over the relevant river basins (Rhone, Seine, Loire and Garonne for France, and Rhine, Weser, and Elbe for Germany), using area-weighted averages. Soil moisture from ERA-40 for the total depth of the reanalysis (3 m) and scaled to 1.70 m (by scaling the lowermost layer to 70 cm) is also displayed for comparison. Note as in the previous section that the estimates of terrestrial water-storage variations entail information on changes in groundwater storage and snow amounts, and not only on changes in soil moisture. This should be kept in mind in the following discussion.

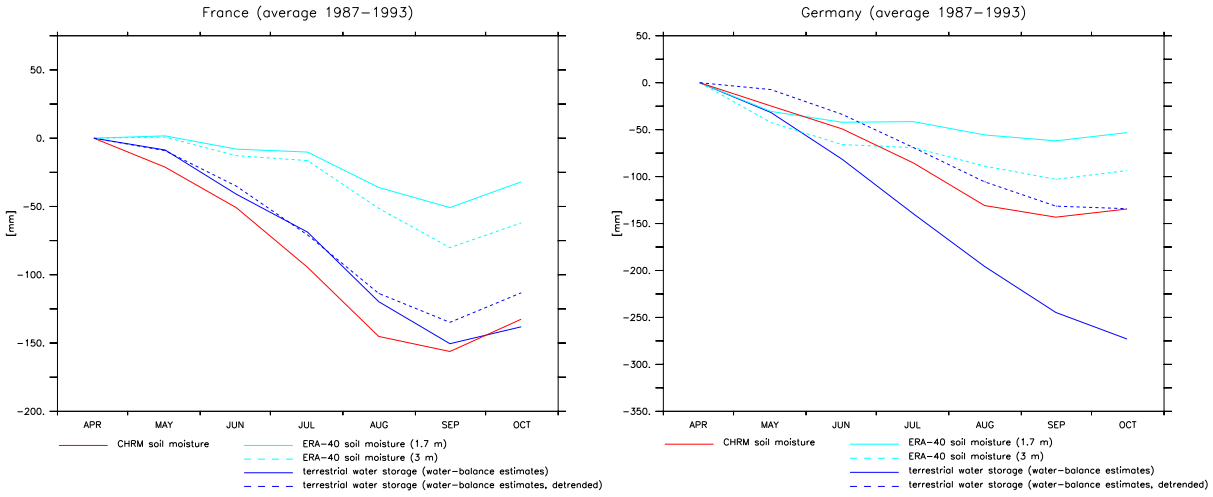

FIG. 4.6: Soil moisture (CHRM, ERA-40 for 1.7 m and 3 m depth) and terrestrial water storage (water-balance estimates, raw and detrended) relative to April value in France (Rhone, Seine, Loire, Garonne) and Germany (Rhine, Weser, Elbe) in [mm].

The CHRM simulation exhibits higher seasonal changes in soil moisture than ERA-40 in the two domains (both for the 1.70 m and the 3 m reanalysis soil moisture). The amplitude of the soil moisture changes in ERA-40 appears relatively small, similar to what is seen in Illinois (S03). Note that this is the case even for the 3 m soil moisture. The detrended estimated changes in terrestrial water-storage and the CHRM soil moisture exhibit similar seasonal amplitudes both in France and Germany. The raw estimates are close to the detrended values over France, but show a large drift in Germany, mainly due

to the large imbalances in the Elbe river basin (see Table 4.2). Therefore, the observed values of terrestrial water storage are likely to be closer to the detrended estimates. In the absence of such observations, it is difficult to assess where the true soil moisture values might lie. As the snow amounts in France and Germany are not likely to change in a significant way during the spring and summer, the representativeness of the terrestrial water-storage estimates for changes in soil moisture depends on the amplitude of the groundwater changes in these regions. Though the CHRM might somewhat overestimate the seasonal changes in soil moisture, its good agreement with the water-balance estimates gives some confidence in the performed simulations. Note, however, that some of the agreement might be due to the ERA-15 driving fields at the model boundaries, which are likely to have a similar vapour flux convergence as ERA-40.

4.3 Validation of RegCM simulations over Illinois

This section gives a brief validation of the S02 simulations with regards to soil moisture in Illinois. Figure 4.7 compares the soil moisture of the S02 CTL simulations with the observations from the Illinois State Water Survey (ISWS; Hollinger and Isard 1994, see S03 for a description), the ERA-40 soil moisture, and the National Center for Environmental Prediction (NCEP) reanalysis (Kalnay et al. 1996) soil moisture. The soil moisture of these time series are displayed for the top 2 m of the soil; the values were scaled to this depth when necessary. Note that no ERA-40 output is available for 1986 at the moment.

Overall, the S02 CTL simulations agree very well with the observations, except in 1988, which presents a somewhat exaggerated drying in summer. Remarkably, the model appears to perform better than both reanalyses in all the years considered. While the ERA-40 reanalysis has a relatively correct amplitude of the soil moisture cycle, it exhibits, however, a constant underestimation of soil moisture content in Illinois (see also S03). The NCEP reanalysis has a correct value of early spring soil moisture, but strongly overestimates the late spring and summer soil moisture depletion. The overestimation of the yearly soil-moisture cycle is a well known problem of the NCEP reanalysis in the central United States (Lenters et al. 2000, Kanamitsu et al. 2002), which also appears to occur in southern Europe (Heck et al. 2001).

The very good perfomance of the S02 simulations gives some added confidence in the results of this study. Note, however, that the soil moisture of the integrations is initialized with a dataset based in part on the ISWS observations. This likely explains why the spring soil moisture level is generally correct. Notwithstanding, the soil moisture evolution in late spring and summer, which is determined by the model, is quite satisfactory as well, suggesting a correct representation of the relevant hydrological processes within the employed model.

Interestingly, the BUCKTRA integrations, in which the BATS-parameterization of transpiration is replaced with a bucket-type formulation of evaporation, do not perform very differently from the standard runs in the control-climate simulations (Figure 4.8). As mentioned in S02, the two formulations only perform differently for the 1988 WARM-case scenario. Therefore, two parameterizations behaving similarly in present climate conditions, might exhibit different responses to climate-changes conditions. (Note, however, that the results of our study concerning the different sensitivity of the bucket- and BATS land surface schemes are based on only one pair of simulations. Simulations with ensemble

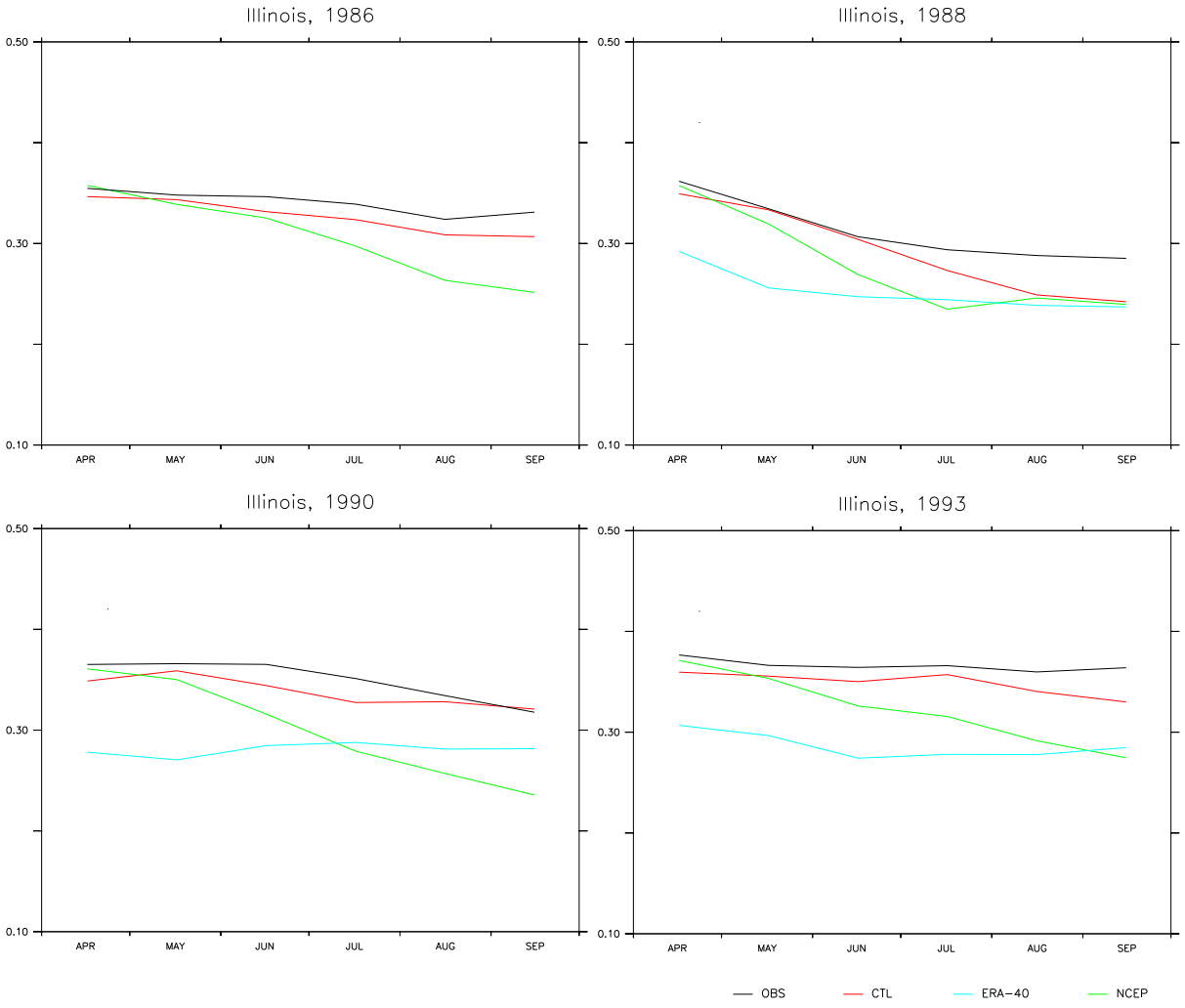

FIG. 4.7: Volumetric soil moisture content (0-2 m depth) over Illinois in the observations from the ISWS (black line), in the S02 CTL simulations (red line), in the ERA-40 reanalysis (light blue line), and in the NCEP reanalysis (green line) [m/m].

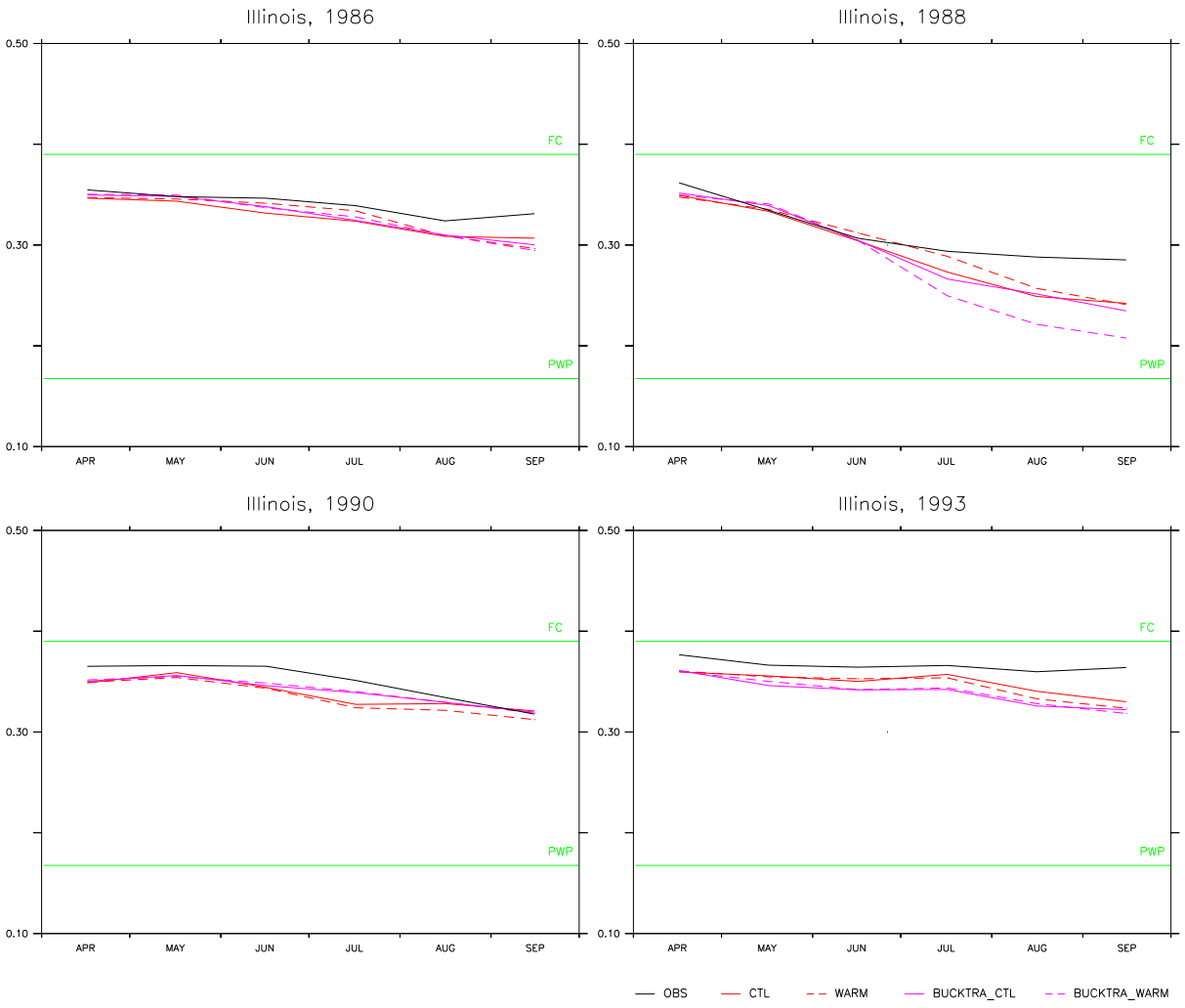

FIG. 4.8: Volumetric soil moisture content (0-2 m depth) over Illinois in the S02 simulations CTL (red solid line), WARM (red dashed line), BUCKTRA_CTL (pink solid line) and BUCKTRA_WARM (pink dashed line), compared with the observations from the ISWS (black solid line) [m/m]. The green lines represent the values of the field capacity (FC) and permanent wilting point (PWP) as defined in the Biosphere-Atmosphere Transfer Scheme (BATS) for this region. See S02 for a detailed description of the simulations.

runs, or multi-year integrations would be needed in order to test the robustness of these results.)

As mentioned earlier, the terrestrial water-storage variations computed with the methodology presented in S03 cannot be used as surrogates for soil moisture variations, at least in regions where groundwater storage or changes in snow cover are important (see S03 and section 4.2). However, they might still have some value for comparison purposes, which is what we would like to assess in the following paragraphs.

Figure 4.9 displays the monthly absolute changes in soil moisture (observations, S02 CTL simulations, ERA-40 and NCEP reanalyses) and estimated terrestrial water storage (raw and detrended, see S03) in Illinois, relative to the April value of the corresponding time series for the years 1988, 1990 and 1993, and their average. As expected from the preceding analysis, the S02 CTL simulations are closest to the observations. ERA-40 performs relatively well, has however a tendency to underestimate the soil moisture depletion in the warm season. As seen earlier, the NCEP reanalysis has a marked overestimation of soil drying in summer. Compared with the reanalyses, the computed estimates of terrestrial water-storage variations (raw and detrended) show a relatively good agreement with the soil moisture measurements both in average and for the individual years (see also Table 4.3). General tendencies (dry, normal or wet years) can be clearly recognized from both sets of estimates.

TABLE 4.3: Seasonal changes (August15-April15) in soil moisture (observations, S02 CTL simulations, ERA-40, and NCEP reanalysis) and in S03 water-balance estimates of terrestrial water storage [mm].

	OBS (ISWS)	CTL	ERA-40	NCEP	Water-balance estimates raw	Water-balance estimates detrended
1988	-147.3	-200.6	-107.0	-223.2	-299.1	-261.1
1990	-61.9	-41.1	6.1	-207.6	-83.4	-64.7
1993	-33.7	-38.3	-58.0	-159.3	25.4	-16.1

For most regions, reanalysis products such as ERA-40 or the NCEP reanalysis are the only sources of information on (inferred) soil moisture evolution. In this respect, the methodology presented by S03 for computing estimates of terrestrial water-storage variations represents a valuable alternative to existing datasets for inferring changes in seasonal soil water.

Overall, the very disparate behaviours of the ERA-40 and NCEP reanalyses over Illinois, as well as their respective biases compared with the observations, underline the need for added observations of soil moisture and a better understanding of its role within the climate system. Recognizing this issue, NCEP is currently releasing a new reanalysis product (the NCEP/DOE reanalysis 2) which has as one of its main purposes the improvement of its soil moisture representation (Kanamitsu et al. 2002). The ECMWF forecast model has undergone several improvements with regards to its land surface parameterization (e.g. Viterbo and Beljaars 2002), which should significantly improve the performance of ERA-40 compared to ERA-15. Similarly, much effort is currently invested into the improvement of the terrestrial water cycle in regional and global climate models (e.g. Vidale et al. 2003).

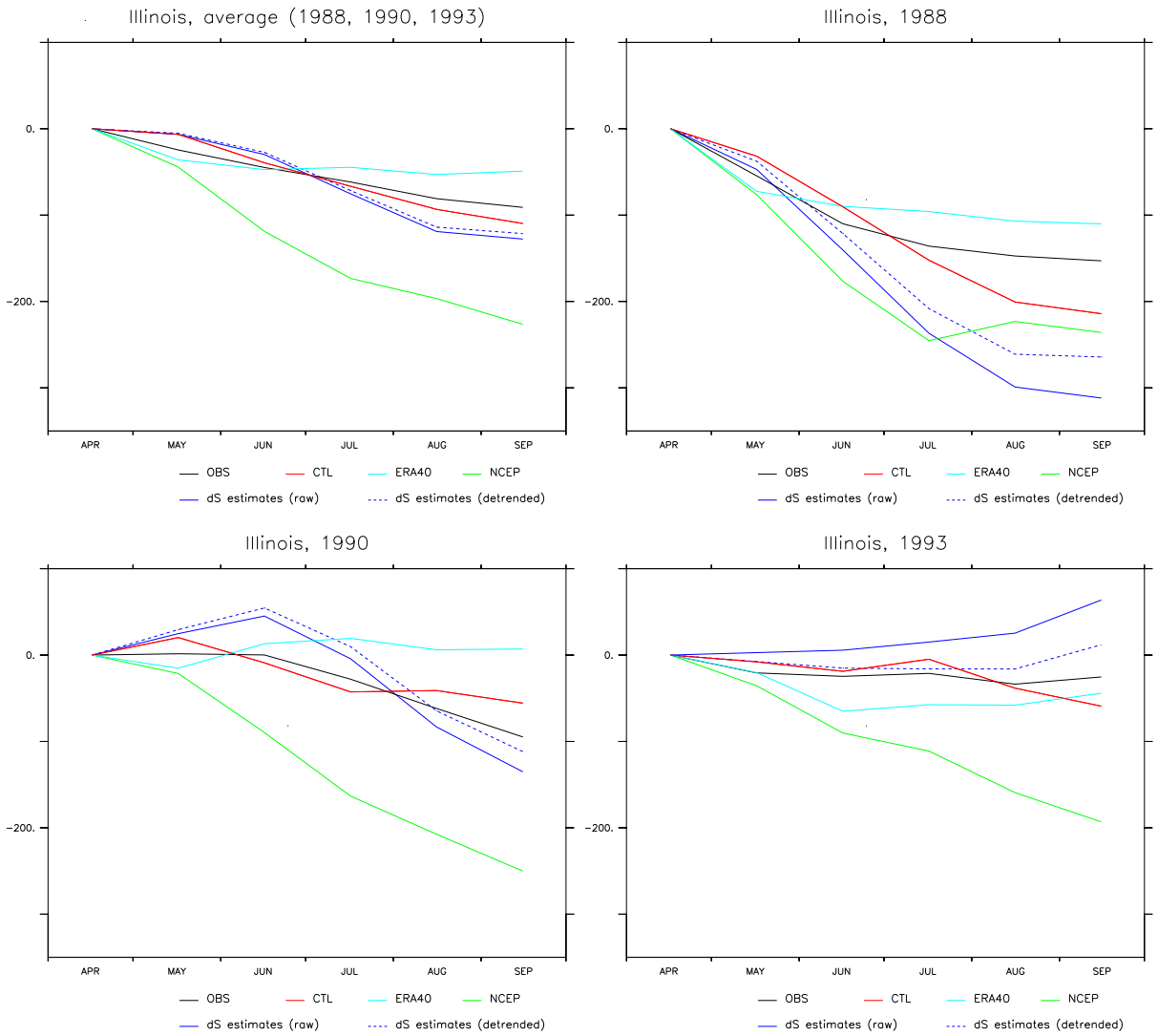

FIG. 4.9: Soil moisture within top 2 meters of soil (ISWS observations, S02 CTL simulations, ERA-40, NCEP) and terrestrial water storage (water-balance estimates, raw and detrended) relative to April value in Illinois.

In the absence of adequate measurement networks of soil moisture, the computed water-balance estimates of terrestrial water-storage variations can offer some information on soil water evolution at continental and sub-continental scales, which can contribute to the continuing improvement of the reanalysis data products, to the better understanding of the soil-atmosphere interactions, and to the further development of climate models.

4.4 Summary

This chapter has investigated various applications of the estimates of terrestrial water-storage variations computed with the methodology described in S03. Over Europe and Northern Asia, the computed estimates show very varying performance, with some large long-term imbalances in most Central-European river basins, but almost no drift in Russia and Northern Asia (section 4.2.a). Though the imbalances in Central Europe are certainly due in part to the small size of the river basins considered (and to their rough approximation using quadrilaterals), it has been hypothesized that some of the regional variations in the performance of the water-balance computations might be due to unresolved topography within the reanalysis model or to the difficulty in accurately modelling land surface processes in regions where the vegetation has a large impact on climate. An accurate representation of the large-scale atmospheric moisture fields in the reanalysis is likely easier to obtain in regions showing homogeneous terrain and climatic conditions.

Whether the estimated changes in terrestrial water-storage variations can be used as surrogates for soil moisture observations in areas where no measurements are available is an open question. The agreement of the computed water-balance estimates with soil moisture measurements from the former Soviet Union (Section 4.2.c) is not good, probably due to the importance of snow cover in this region. In Illinois, however, the computed seasonal changes in terrestrial water storage are shown to be useful for obtaining rough estimates of the seasonal changes in soil moisture, and are generally closer to observations than the reanalysis data (Section 4.3). This is the case despite the fact that the groundwater variations are important in this region (see S03), possibly because of the correlation of the temporal evolutions of soil moisture and groundwater. Changes in snow cover, however, have a different mean annual cycle, which might explain the low correlation of the estimates with soil moisture measurements in high latitudes.

Finally, the CHRM control simulation over Europe (Vidale et al. 2003) exhibits a realistic seasonal amplitude of soil moisture compared with the amplitude of the estimated changes in terrestrial water storage (Section 4.2.d), and the CTL simulations of the S02 study show very good agreement with the soil moisture observations of the ISWS (Section 4.3). This gives some added confidence in the results of these two studies.

Chapter 5

Conclusions and Outlook

In the present thesis, various aspects linked to terrestrial water storage and its role in climate were investigated. Here, a brief summary of the main results is presented, and possible directions for future research are discussed.

- The first study (chapter 2) investigates the role of land surface processes for mid-latitude climate change, focusing on the risk of enhanced summer droughts in these regions. Present and warmer-climate simulations are conducted over North America, using a regional climate model forced by observed and modified lateral boundary conditions. The results suggest that studies with GCMs including the so-called bucket model might have overestimated the risk of enhanced summer droughts in mid-latitudes, due to its lack of vegetation control on evapotranspiration. These results point to the importance of an accurate representation of land surface processes for the simulation of mid-latitude climates and call for a more detailed investigation of the role of vegetation for climate change. Note, however, that the experimental set-up used in this study also has its limitations, as it does not account for potential circulation changes associated with global warming.

- The second study (chapter 3) investigates the water-balance method for estimating monthly variations in terrestrial water storage, using atmospheric reanalysis data (ERA-40) and traditional streamflow measurements. The computed monthly estimates show very good agreement with observations in Illinois. The mean seasonal cycle is well represented and the interannual variability is in general well captured. When integrated over longer time scales (several months to several years), the estimates present some drift, due to the presence of small systematic biases in the monthly values. An estimation of the temporal evolution of terrestrial water storage over longer time scales appears nonetheless feasible, provided a proper detrending is performed. In view of the lack of reliable information available on terrestrial water storage, these are very promising results with a range of potential applications.

- The results from chapter 4 show that this method also gives realistic results over Europe and Northern Asia. The accuracy of the obtained estimates appears to be both dependent on the size and regional climate characteristics of the considered domains. The validation of the simulations of chapter 2 with the soil moisture observations from Illinois shows that the model performs well for the studied region, giving added confidence to the results of that study.

- Finally, the co-authored paper presented in the Appendix A also underlines the importance of a sound representation of the hydrological cycle for long-term simulations of soil moisture in present mid-latitude climate, showing that uncertainties stemming from differing model formulations are generally predominant compared to uncertainties originating from intrinsic predictability limitations.

In summary these results underline the importance of an appropriate representation of the land surface processes for simulations investigating soil moisture in mid-latitude climates and suggest that reliable estimates of changes in terrestrial water storage can be obtained with the method presented in chapter 3, a promising perspective given the lack of measurements of this variable.

The following projects based on this study are currently underway:

- Various follow-up investigations are planned to the study presented in chapter 2. Multi-year simulations with a similar set-up have been conducted for Europe with the CHRM model, and will be performed over the United States. The questions addressed will include the importance of winter processes and of cumulative year-to-year effects for the studied issue as well as the investigation of further characteristics of the bucket model which were not considered in this study.
- A project currently underway at our institute is the application of the method presented in chapter 3 to further river basins, possibly on all continents. To this end a more accurate procedure for averaging the atmospheric moisture divergence fields over the considered river basins will be developed using Geographical Information System (GIS) techniques. This will allow the creation of a global dataset of monthly terrestrial water-storage variations for the entire ERA-40 period.

Future research could also include the following aspects:

- It would be interesting to rerun the experiments of the chapter 2 study with yet a more advanced land surface scheme (e.g. SiB2.5, Vidale and Stöckli 2003). As presented in the introduction, the employed land surface parameterization (BATS) belongs to the land surface models of intermediate complexity, i.e. including a comprehensive representation of biophysical processes, but not including physiological processes such as carbon assimilation. This latter aspect is likely to play an important part in climate change, as plants might adapt to the enhanced CO_2 concentrations, with associated changes in evapotranspiration.
- A limitation of the experiments of chapter 2 is their idealized set-up which does not allow for changes in large-scale circulation potentially associated with global warming. A similar investigation using a GCM could therefore clarify whether such aspects are relevant to the investigated issue.
- A systematic intercomparison of the estimates obtained with the method presented in chapter 3 with results from other studies would be very desirable, in particular with the new soil moisture datasets that will be produced by the Global Soil Wetness

Project 2 (GSWP2), with the remote sensing estimates of terrestrial water-storage variations that will be available from the Gravity Recovery and Climate Experiment (GRACE), and with the future products from the Global Land Data Assimilation System (GLDAS).

- As the soil moisture dataset in Illinois is available since 1981, the validation of the presented method could be extended to 20 years of data (1981-2001). If another region with large-scale datasets of soil moisture, snow depth and groundwater can be identified, the validation of the method for a region with other climatic characteristic would also be very useful.

- The snow and groundwater datasets in Illinois are available for the whole ERA-40 period. Therefore, the proposed method could be possibly used to obtain estimates of soil moisture variations in Illinois for the time period without soil moisture measurements (1960-1981). As the method has been shown to be accurate for this region, it should be possible to obtain reliable estimates of this variable for the period considered.

- The ERA-40 monthly fields of atmospheric moisture divergence could be used to obtain estimates of monthly evapotranspiration in regions with good rain gauge measurement networks (atmospheric moisture divergence being a measure of P-E). Evapotranspiration being a flux, the identified drift is not expected to represent a major issue for this variable (as the values do not need to be integrated over long time periods). Since evapotranspiration is just as much an unknown variable as soil moisture, such estimates would also be of great use for the research community.

- An important issue is the possible identification of the causes for the mentioned drifts. In order to separate biases coming from the assimilation procedure from other sources of errors, it would be useful to analyse the atmospheric moisture increments applied by the assimilation scheme, and to compare atmospheric moisture divergence computed with the forecast fields (background) with the values obtained when using the reanalysis data.

- Finally, new techniques could be developed in order to combine various sources of information on terrestrial water storage and soil moisture (e.g. water-balance estimates, remote sensing data, modelling datasets, and the few available observational datasets) in order to obtain reliable global datasets of these variables.

This work also points to further issues and questions of more general scope:

- An accurate representation of soil moisture is likely to play a crucial role for extended range forecasts (10-60 days) and seasonal forecasting, an issue that should be further investigated.

- Groundwater storage has been shown to contribute to similar changes in terrestrial water storage as soil moisture in Illinois; however, it is generally not represented in current land surface schemes. It can however act as a long-term memory reservoir, an effect which might need to be parameterized in order to simulate soil water storage in an accurate way (see also Yeh et al. 1998).

- As discussed in the introduction, there have been various key LSP developments in the last decades, however the present climate models still have difficulties in accurately predicting soil moisture, even with LSPs of enhanced complexity. Recent findings have suggested that the characteristic behaviour of the parameterizations for evapotranspiration and runoff and their interaction is more important for the resulting soil moisture than their absolute sophistication (Koster and Milly 1997). The identification of the key processes determining soil moisture and the required amount of complexity needed for accurately representing them could be a next major step in the development of LSPs.

In conclusion, this study has shown that there are still many open questions regarding the parameterization of the land surface processes in climate models and that more research effort should be invested in the examination of the exact role of vegetation for climate change. It is hoped that the presented method for estimating monthly and seasonal variations in terrestrial water storage will help validate present and future land surface schemes, and will contribute to a better understanding of the processes determining terrestrial water storage in mid-latitudes. Finally, it should be stressed that, however useful, no indirect estimates are likely to fully replace "true" observations, and that it would be therefore highly desirable to set up more comprehensive measurement networks of terrestrial water storage in various regions of the world.

Appendix A

Predictability and Uncertainty in a Regional Climate Model

Predictability and Uncertainty in a Regional Climate Model. †

Pier Luigi Vidale*, Daniel Lüthi, Christoph Frei, Sonia I. Seneviratne, and Christoph Schär

Atmospheric and Climate Science, ETH Zurich, Switzerland

ABSTRACT

The evaluation of the quality and usefulness of climate modeling systems is dependent upon an assessment of both the limited predictability of the climate system and the uncertainties stemming from model formulation. In this study a methodology is presented that is suited to assess the performance of a regional climate model (RCM), based on its ability to represent the natural interannual variability on monthly and seasonal time scales. The methodology involves carrying out multi-year ensemble simulations (to assess the predictability bounds within which the model can be evaluated against observations) and multi-year sensitivity experiments using different model formulations (to assess the model uncertainty).

As an example application, experiments driven by assimilated lateral boundary conditions and sea surface temperatures from the ECMWF re-analysis project (ERA-15, 1979-1993) were conducted. While the ensemble experiment demonstrates that the predictability of the regional climate varies strongly between different seasons and regions, being weakest during the summer and over continental regions, important sensitivities of the modeling system to parameterization choices are uncovered. In particular, compensating mechanisms related to the long-term representation of the water cycle are revealed, in which summer dry and hot conditions at the surface, resulting from insufficient evaporation, can persist despite insufficient net solar radiation (a result of unrealistic cloud-radiative feedbacks).

†JGR-Atmospheres, accepted.

*Corresponding author: Pier Luigi Vidale, Atmospheric and Climate Science ETH, Winterthurerstr. 190, CH-8057 Zurich, Switzerland. E-mail: vidale@geo.umnw.ethz.ch

A.1 Introduction

Modern climate models are highly complex numerical constructs, encoding the laws of dynamics and thermodynamics for relevant geophysical fluids. Also, in these models, because of computational and theoretical limitations, explicitly resolved dynamical mechanisms co-exist with parameterized physical processes. As stated by Palmer (2000), "the predictability of weather and climate forecasts is determined by the projection of uncertainties in both initial conditions (ICs) and model formulation onto flow-dependent instabilities of the chaotic climate attractor". Loss of predictability occurs not only because of uncertainties in initial conditions (usually thought particularly relevant for weather forecasting), but also due to model formulation (particularly relevant to climate modeling). It is difficult to separate these two kinds of sources of error, and this seriously hampers the evaluation of climate modeling systems. In fact, the response of a climate model to parameterization changes can lead to unexpected biases, and the tuning, validation and improvement of these complex tools represents a difficult challenge to climate modelers. Improving validation methodologies is thus an important target of future climate research (IPCC 2001, see Chapter 10).

Of particular concern in this context is the compensation between model errors: such compensation may well produce seemingly correct results for incorrect reasons. A recent and still largely unresolved example is the representation of the seasonal water cycle over continental-scale land surfaces. Many atmospheric models currently suffer from an artificial summer drying and warming over major mid-latitude continents. Some investigators (e.g. Machenhauer et al. 1998) suggest that the causes may be ascribed to large-scale biases inducing subsidence; others have focused on physical parameterizations, addressing radiation and land surface processes (e.g. Betts et al. 1996; Wild et al. 1996; Murphy 1999; Seneviratne et al. 2002, Hagemann et al. 2002). The range of these investigations suggests that many different physical processes are probably relevant to the problem.

The mutual interaction of physical mechanisms, as represented by physical parameterizations within the models, has been the focus of the European Union project MERCURE (Modeling European Regional Climate: Understanding and Reducing Errors), spanning the ECMWF Re-Analysis (ERA-15, Gibson et al. 1997). Specific MERCURE studies have addressed a detailed analysis and intercomparison of models' energy and water balance (Hagemann et al. 2002); causes behind model warming and drying in summer (Hagemann et al. 2001); and precipitation at daily resolution (Frei et al. 2003). Previous studies of European climate, including the assessment of the performance of RCM formulation, include Giorgi and Marinucci (1991, 1996), Christensen et al. (1996), Jones et al. (1995), Noguer et al. (1998).

The development of Regional Climate Models (RCMs) has come historically from the idea of physically-based downscaling tools, in which a limited-area climate model is driven by time-dependent lateral boundary data, either from an analysis or from a coarser-meshed general circulation model (e.g. Giorgi, 1990; Jones et al. 1995). Recently, however, the concept of the RCMs has evolved into also applying them as tools for process studies (e.g. Frei et al. 1998; Giorgi and Mearns 1999), so that the relevance of the role of physical processes in the representation of the climate has become more prominent.

The goal of this paper is to develop an improved methodology for the assessment of the quality of an RCM system in the presence of limited predictability. Here the

term predictability is intended as sensitivity to ICs in the context of an RCM, that is, a Limited Area Model (LAM) with prescribed Lateral Boundary Conditions (BCs). In order to pursue our investigation's goals, a detailed analysis of one RCM's ability to represent the natural interannual variability on monthly and seasonal time-scales within the ERA-15 period 1979-1993 is undertaken. The RCM is driven at its lateral boundaries by the observed synoptic-scale variability, and the model is evaluated for its ability to reproduce climatic fluctuations on monthly and seasonal time scales, within predictability bounds derived from an ensemble experiment. A previous version of this methodology has been used earlier in month-long integrations (Lüthi et al. 1996, Fukutome et al. 1999), and more recently in Giorgi and Shields (1999), Small et al. (1999) and Dutton and Barron (2000).

The validation of a climate modeling system relative to the interannual variability has two major advantages. Firstly, unlike the validation based on seasonal or yearly climate means, the method is much less permissive with respect to the practice of model tuning and associated misleading effects. In fact, even a hypothetical perfectly-tuned model with an excellent representation of the longer-term mean climate may still exhibit deficiencies in representing interannual variations. Secondly, the methodology implicitly assesses simulated climatic differences (such as differences between warm and cold winters), and this may to some extent be taken as a surrogate for climatic changes. A validation based on interannual variability can also assess the role of model biases in the simulation of climatic differences, one of the major open issues when using a modeling system for the simulation of climate change (IPCC 2001).

The main disadvantage of our validation methodology is its restricted applicability to modeling systems that contain some degree of determinism. In an RCM, the monthly mean climate is largely controlled by the forcing at the lateral boundaries and by long-term memory effects (such as those associated with soil moisture and snow cover) in the interior (Jones et al. 1995), as well as model formulation. In contrast, our methodology is not applicable to a coupled atmosphere-ocean GCM simulation, where comparison with observations on a month-to-month basis is not meaningful, due to the lack of deterministic forcing. To some extent, however, our methodology is closely related to AMIP-type (Gates et al. 1999) studies on seasonal predictability in the tropics, driven by prescribed SST conditions.

The RCM used in this study is the Climate High-Resolution Model (CHRM), described in section 2, which had previously been used extensively for the study of continental-scale interannual climate variability (Lüthi et al. 1996, Fukutome et al. 1999), as well as land-surface and precipitation processes (Schär et al. 1996, Frei et al. 1998, Schär et al. 1999, Heck et al. 2001). Model inter-comparison studies addressing other aspects of the CHRM experiments presented in this paper, also in comparison with other European models, include Hagemann et al. (2002) and Frei et al. (2003).

The interannual variability methodology of Lüthi et al. (1996) is here extended to cover a set of continuous simulations with durations of 15 years and to include a treatment of uncertainty due to both model formulation and to predictability limitations. Special consideration will be given to the processes relating to the water cycle, due to its importance for the climate system, but also due to its significance in the event of climate change and their sensitivity to the parameterization of physical processes. Such ensembles of long experiments, in which different combinations of physical parameterization options are ac-

tivated, while long-term memories in the climate system are retained, can yield important insight into the underlying physical processes (see also recommendations in Giorgi and Bi, 2000). Ensembles of (short) RCM experiments including different model formulations have also recently appeared in Yang et al. (2002).

The outline of the paper is as follows: In section 2, the most recent modeling changes introduced into the CHRM are documented; section 3 discusses the model's mean climate, including its ability to represent current climate variability, followed by a comparative assessment of the model's predictability and uncertainties; finally section 4 provides an interpretation of the mechanisms uncovered by the sensitivity studies, together with some concluding considerations.

A.2 Methods

A.2.a The CHRM Regional Climate Model

The CHRM is a climate version of the former mesoscale weather forecasting model of the German and Swiss meteorological services, known as the HRM (High Resolution Model) or formerly EM (Europa-Modell). This model has been used until recently as an operational Numerical Weather Preditcion (NWP) model at the Swiss and German weather services (Majewski 1991, Majewski and Schrodin, 1994) and had been modified by Lüthi et al. (1996) for application as a regional climate model. The model grid is a regular latitude/longitude grid (Arakawa type C) with a rotated pole and a hybrid vertical coordinate (Simmons and Burridge 1981). It includes a full package of physical parameterizations, including a mass-flux scheme for moist convection (Tiedtke 1988); Kessler-type microphysics (Kessler 1969, Lin et al. 1983); a radiation package (Ritter and Geleyn 1992) including interaction with partial cloud cover (of the type described in Slingo, 1987); a land surface scheme (Dickinson 1984) with three soil moisture layers; an 'extended force-restore' soil thermal model (Jacobsen and Heise 1982), also capable of interacting with accumulated snow at the soil surface); and vertical diffusion and turbulent fluxes based on the flux-gradient approach (of the classic Louis et al. (1982), type in the surface layer, Mellor and Yamada (1974), in the boundary layer and above).

Recent changes in our regional climate modeling suite, in relation to previous work (Lüthi et al. 1996, Schär et al. 1999, Heck et al. 2001) were inspired by the need to address longer simulation periods than used in the NWP context, and have come in three individual areas:

Land surface and soil processes

The Soil-Vegetation-Atmosphere Transfer Scheme (SVATS) and deep soils upgrades were motivated by the need to simulate the land surface balances of heat, water and momentum in a realistic and sustainable fashion in the context of decadal simulations over a very heterogeneous region. In particular, the soil water storage capacity had to be increased from the standard (shallow) NWP profile because soil water is never corrected in the RCM after initialization. Three soil moisture levels are therefore used to reach a total depth of 1.7m. The soil profiles are initialized (never nudged) with ERA-15 data, retaining a "climatological" layer from 1.7 to 3.4m, which acts as a fixed boundary condition, but is

only accessed in case the root zone layer dries further than the air dryness point (ADP). In terms of soil thermal processes, the original "extended force-restore method" of Jacobsen and Heise (1982) was modified in order to control winter soil surface temperatures by including a representation of soil moisture freezing, similar to Lunardini (1981), which imposes a latent heat release/uptake barrier in a 1 degree interval around the freezing point, as is also done in the BATS 1e (Dickinson et al. 1993) and LSM (Bonan 1996).

Parameterization of the surface layer

The use of Beljaars and Viterbo (1996) surface layer parameterization, in lieu of the more standard Louis et al. (1982), was motivated by the desire to eliminate a well-known model cold bias in stable situations. Corresponding improvements, using alternative analytical stability functions formulations, had been reported for the ECMWF and other models (Holstlag and Boville 1993, Hess and McAveney 1997).

The optional Xu and Randall (1996) cloud diagnostics scheme

The Ritter and Geleyn radiation package is of the delta-two stream type and was originally conceived as a fairly comprehensive package, useful for both NWP and climate studies. For such a purpose it retains the interaction of three short-wave and five long-wave bands of radiation with cloud droplets (not yet with ice species), gases (H_2O, a composite CO_2 ensemble and O_3) and five aerosol species. The key of the parameterization's interaction with clouds lies in the definition of the model's integrated grid box liquid water content, which is then used inside the radiation module to distinguish eight different clouds types and respective drop-size distributions (thus prescribing relative optical properties), as is described in Ritter and Geleyn (1992) and originally formulated in Stephens (1979). The model is thus capable of representing the cloud-radiation interaction in a variety of climatic conditions, including future climate scenarios, since the abundance and distribution of all radiatively active agents can meaningfully be represented: in particular, for cloud water, different atmospheric conditions will immediately feed back onto radiation and vice-versa. In the CHRM suite of models this is accomplished by combining contributions from both grid-scale and sub-grid scale clouds and performing a weighted average in this fashion:

$$q^l_{RAD} = q^l_{SGS} \cdot PCC_{SGS} + q^l_{GS} \cdot PCC_{GS} \cdot (1 - PCC_{SGS}) \tag{A.1}$$

where q^l_{RAD} is the total liquid water passed to radiation (gkg^{-1}); $q^l_{SGS}$is the total liquid water content of sub-grid scale clouds; q^l_{GS} is the total liquid water content of grid scale clouds ; PCC_{SGS} and PCC_{GS} are the fractional covers of sub-grid scale and of grid scale clouds, respectively.

Equation (A.1) shows how the cloud-radiation feedbacks are dependent on the convection and stable precipitation parameterizations. For the grid-scale liquid water content the standard model formulation employs an approach based solely on relative humidity (Slingo 1987), while the sub-grid scale portion is based on the diagnostic liquid water content provided by the convection scheme. The following is the standard CHRM implementation of the grid-scale Partial Cloud Cover (PCC_{GS}):

$$PCC_{GS} = \left(\frac{\frac{q_{GS}^{TOT}}{q_w^*(T)} - RH_{crit}}{RH_{r3} - RH_{crit}} \right)^2 \quad ; \quad 0 \leq PCC_{GS} \leq 1 \tag{A.2}$$

Where $q_{GS}^{TOT} = q_{GS}^v + q_{GS}^l$ is the total water at a grid point; $q_w^*(T)$ is the saturation mixing ratio over water at temperature T; the critical relative humidity at model layer σ is $RH_{crit} = 0.95 - RH_{r1}\sigma(1-\sigma)(1 + RH_{r2}(\sigma - 0.5))$, with $RH_{r1} = 0.8$; $RH_{r2} = \sqrt{3}$; $RH_{r3} = 1.0$.

Recently, as a result of detailed analysis of the CHRM surface energy balance (see Hagemann et al. 2002), it was decided to implement the Xu and Randall (1996) cloud diagnostics parameterization as a CHRM option, so that it could be used to test how a more physically-based cloud cover diagnostic scheme (and associated liquid water path) would affect the atmospheric extinction of radiation and thus the surface energy balance. According to Xu and Randall, we have introduced the following alternative definition for PCC_{GS}:

$$PCC_{GS} = \begin{cases} RH^p \left[1 - \exp\left(\frac{-\alpha_0 q_{GS}^l}{[(1-RH)q_w^*(T)]^\gamma} \right) \right] & ; \ 0 < RH < 1 \\ 1 & ; \ RH \geq 1 \end{cases}$$

where q_{GS}^l is the grid scale liquid water (gkg^{-1}); RH is the relative humidity; $q_w^*(T)$ is the saturation mixing ratio over water at temperature T; $p = 0.25$; $\alpha_0 = 100$; $\gamma = 0.49$ are the dimensionless coefficients as in Xu and Randall (1996).

The two alternative formulations in equations (A.2) and (A.3) have been tested in different model realizations and will be contrasted later in the results section.

Model setup for the numerical experiments

The experiments were integrated over a standard European domain (Fig. A.1), already used in earlier studies (Lüthi et al 1996, Schär at al.1999, Heck et al. 2001), with a grid spacing of approximately 56 km and a time step of five minutes. Twenty levels were used in the atmosphere and three layers in the soil. Land surface physiography and phenology were imposed every six hours by interpolating in space and time the monthly ISLSCP I (Sellers et al. 1994) climatological fields (e.g. LAI, vegetation cover fraction). The only other substantial data ingestion deviations from the operational NWP modeling system are due to the use of ERA-15 data for the lateral boundaries forcing, with an updating frequency of six hours, using the Davies (1976) relaxation technique for temperature, atmospheric water and wind. Moreover, in the NWP operation of the HRM model, the soil water profile is calculated by the driving GCM and used to initialize and nudge the model, with the intent of controlling 2m temperatures through a Bowen ratio approach, and not with multi-year soil water conservation objectives in sight. The nature of the climate simulations presented here requires more careful specification of the soil model framework and of the yearly evolution of surface and sub-surface parameters and processes. For this purpose the deep soil temperature boundary condition is set to reflect the 1979-1993 surface temperature average at each grid-point, as is recommended for the extended force-restore soil model (Jacobsen and Heise 1982).

Three incremental CHRM model formulations are introduced, all based on the common model described so far: the first, SOIL (CHRM 2.1), makes use of an earlier configuration of the original NWP version of the soil model. In this version, as a result, infiltration of precipitation is hindered by the numerics of the vertical grid stretching (with soil layers corresponding to 2, 8 and 190cm), and by physical limitations in the form of artificial impermeabilization deriving from soil (cold) temperature barriers affecting soil water conductivity. As previous studies had not included the full yearly cycle, the lack of appropriate soil moisture recharge had only been noted recently.

The second model formulation, HYD (CHRM 2.2), by contrast, relaxes all artificial in-soil water flux constraints (and the normal soil grid stretching), resulting in a more regular recharge and normalized latent heat fluxes, including a reasonable seasonal contribution of transpiration originating in the root zone.

Model version RAD (CHRM 2.3) is a further development from HYD and addresses climatologically significant negative surface short-wave radiative biases that are present in SOIL and HYD, with the intent of studying the mechanisms and feedbacks behind the well-known surface cold bias in the model. The method used here, rather than resorting to the tuning of the liquid water path fed to the radiation scheme, consists in calculating the radiatively active cloud liquid water estimation by using the Xu and Randall (1996) parameterization. The setup of simulation RAD preserves therefore the treatment of soil moisture fluxes in simulation HYD and includes the alternative PCC_{GS} formulation presented in equation (A.3).

The model version used in the ensemble experiment with different initial conditions (section 2.2) is RAD (CHRM 2.3).

A.2.b Predictability in a RCM

In order to test the sensitivity to initial conditions (ICs) prescribed at integration start time (normally 1 January 1979) we have designed an ensemble experiment composed of four members, one comprising the first four years of the standard 15-year simulation performed with model RAD, the other three consisting in simulations started on 2,3,6 January 1979 and continued until 31 December 1982, but otherwise identical. While the same initial conditions and lateral nudging data were applied to the model formulation experiments, initial conditions from the same ERA-15 data set were therefore extracted for the ensemble experiment. The set of initial conditions includes all prognostic variables and also all land surface (snow/ice cover), soil (complete temperature and moisture profiles) at initial time and at every grid point. The simulation start dates were chosen as would be done in a typical NWP environment, so that individual simulations would be related through a common synoptic situation and very similar in terms of soil moisture and snow cover states. However, our analysis (section 3.3) discards year 1 of the integration and during this time substantial soil and snow anomalies are allowed to develop in response to the spread in atmospheric evolutions in the ensemble. This IC-based approach differs from the approach taken in Christensen et al. (2001) for the estimation of model internal variability, where the ensemble was composed of seven 1-year ensemble members (re-applying lateral boundaries from a single year) and only soil moisture was allowed to retain its memory of initial conditions; it also differs from the approach in Giorgi and Bi (2002), where different combinations of initial (but atmosphere-only) and boundary

conditions were perturbed in generating sets of seasonal ensemble members. The spread in model solution thus generated in our ensemble (as illustrated in section 3.3) will be used to estimate the predictability limitations in our modeling system, as dependent on uncertainties in initial conditions, and will be presented together with the results from different model formulations in sections 3.4 and 3.5.

A.2.c Observational data

Data sets used for validation purposes were mainly extracted from the Climatic Research Unit analyses (New et al. 1999) and the Alpine precipitation data set (Frei and Schär 1998), both at 50 km and available exclusively over land. Additionally, ERA-15 reanalysis data at T106 truncation (excluding of course the fields used for the nudging) were also used for validation purposes in the interior of the domain, although only in instances in which other data from independent origins were not available. All data were available at monthly intervals for the entire simulation period.

A.3 Results

The common integration domain is shown in Fig. A.1, along with the sub-domains to be used for time-series calculations. The two letter labels have been in use historically at ETH, and are listed in the caption, summarily reminding of European political and geographical regions.

A.3.a Mean climate

Previous month-long integrations with the EM family of models, e.g. Christensen et al. 1997, have shown that monthly precipitation biases were at most 1-2 mm day^{-1} in winter (EA, FR, AL and SP sub-domains) and -2 to -1 mm day^{-1} in summer (AL, DA sub-domains). The corresponding biases in temperature were at most -6 to -2 ^{o}C in winter (SW, AL, DA) and +2 to +4 ^{o}C in summer (FR, ME), while over the DA region the summer bias was between +2 and +6 ^{o}C. Another study by Lüthi et al. (1996), concentrating on ensembles of January and July simulations, reported a similar geographical distribution of errors for precipitation, but the magnitude of the biases was smaller than in Christensen et al. (1997), mostly positive in winter (0.6 to 0.8 mm day^{-1} over SW, GE and AL) and negative in summer (-0.6 mm day^{-1} over GE and AL). In these studies the model also showed a clear tendency to produce too much rain in the northern part of the domain, while becoming too dry in the southern part of the domain.

In the new set of CHRM simulations the model has been run continuously for the 1979-1993 period, so that direct comparison to the aforementioned studies is complicated by spin-up and re-initialization issues: the current model needs to rely much more on the long-term behavior of its physical parameterizations than was the case with month-long and seasonal simulations. This is particularly relevant for root-zone soil moisture, which is characterized by a pronounced seasonal cycle and may contribute to the month-to-month "memory" of precipitation (see also the discussion in Schär et al. 1999).

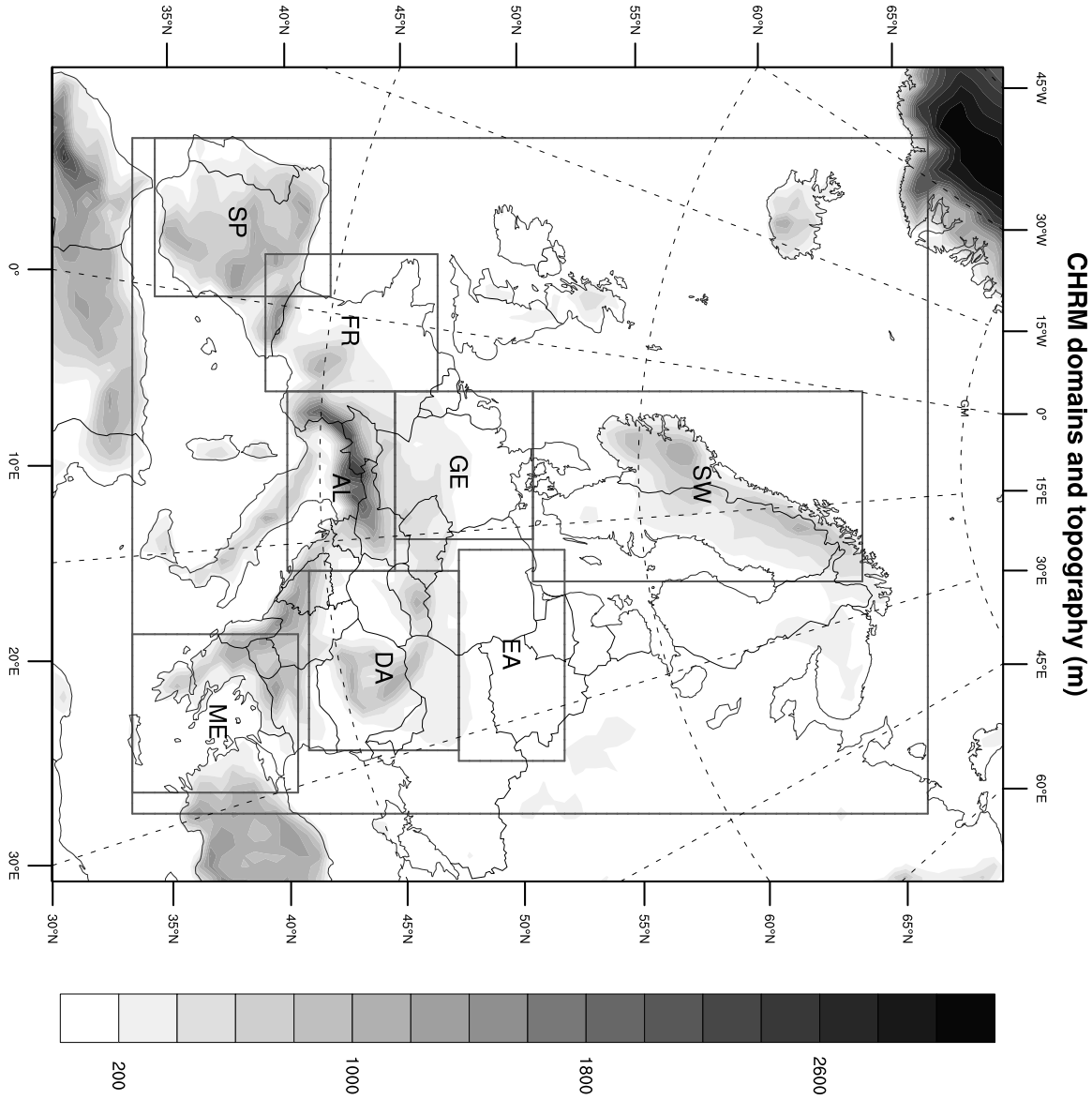

FIG. A.1: The CHRM domain and sub-domains (boxes), superposed on the model orography (m). The domain comprises 81 (longitudinally) by 91 (latitudinally) grid points. The sub-domain labels will be used subsequently in area-average plots. AL is an abbreviation for Alpine region, DA for Danube catchment, EA for East Europe, FR for France, GE for Germany, ME for South-East Mediterranean, SP for Spain (Iberian Peninsula), SW for Sweden (Scandinavia). The model is relaxed to the driving data within the 8-point rim delimited by the outermost convex box, which marks the internal (free) integration region.

Figure A.2 shows maps of 15-year mean precipitation. Our simulation results are shown in the right-hand panels and compared with the CRU observed precipitation and the results of the ERA-15 reanalysis. Comparison shows that the yearly precipitation fields produced by simulations SOIL and RAD (which are the two extremes in this set of model formulations) are both reproducing the correct distribution and amount of precipitation, especially in the region of localized maxima in northern UK, Scandinavia, the Alps and the Balkans. These maxima are fairly accurately positioned, despite some local differences in magnitude and extent. The north-south distribution tends to point to a slight over-estimation in the north and under-estimation in the south. The analysis in the ERA-15 data set is of coarser resolution and cannot reproduce some of the narrow regions of precipitation in the CRU and simulation fields, especially near coastlines. The southwards extent of the region with significant precipitation tends to be insufficient in both our simulations and seems to reflect a tendency for Mediterranean dryness. This bias is also present in the ERA-15 data.

Figures A.3 and A.4 show the precipitation bias for the entire domain, calculated as deviations from CRU data for the 1979-1993 period and averaged for winter and summer. The winter (DJF) precipitation bias maps show that the model has a small positive bias in the north, amounting to less than 1 mm day^{-1} and under-estimation in coastal areas and over the south, with a typical bias around -1 mm day^{-1} over Portugal. Some localized regions, over the north of the UK and the Alps (where a North-South dipole is visible), show a locally enhanced pattern, but this is in fact due to 1-2 grid points shifts in the simulated precipitation in relation to the observed simulation. A large portion of the domain shows a bias contained in the -0.5 to 0.5 mm day^{-1} interval and differences between model versions are very small and localized. The ERA-15 precipitation is fairly successful over coastal areas (except for Norway) but overestimates precipitation in an extensive region in the northern part of the domain.

The summer (JJA) bias in Fig. A.4, on the other hand, shows that SOIL has a drying problem in large portions of central Europe and in particular in the Danube and Alpine regions, with a bias exceeding -1 mm day^{-1} and -2 mm day^{-1} respectively. The bias is clearly more pervasive in simulation SOIL, covering most of central Europe, while being geographically more contained in simulations HYD and RAD. A very scattered positive bias of less than 1 mm day^{-1} is present in some part of Scandinavia, which is somewhat worse in the model versions HYD and RAD with a larger soil moisture availability and correspondingly larger evapo-transpiration, as will be seen later in this section. The ERA-15 analysis also shows discrepancies in relation to CRU data, in particular over the Alps (negative bias) and the UK, but is very successful in the Danube catchment region. In this regard, however, it should be recalled that the ERA-15 assimilation applies soil moisture increments which change the seasonal cycle (Douville et al. 2000), despite the soil model being fully interactive.

Figure A.5 shows the complementary horizontal distributions of winter (DJF) temperature bias, which is generally negative (especially so over the Alps) and clearly extends to the entire domain, including small portions of the southern regions with local values as low as -4K. Northern Scandinavia is an exception, with a local warm bias of about 2K. The bias over the Alps is smallest in simulation RAD while there are some indications that the bias over the UK and Scandinavia is smallest in simulation HYD. The CRU and

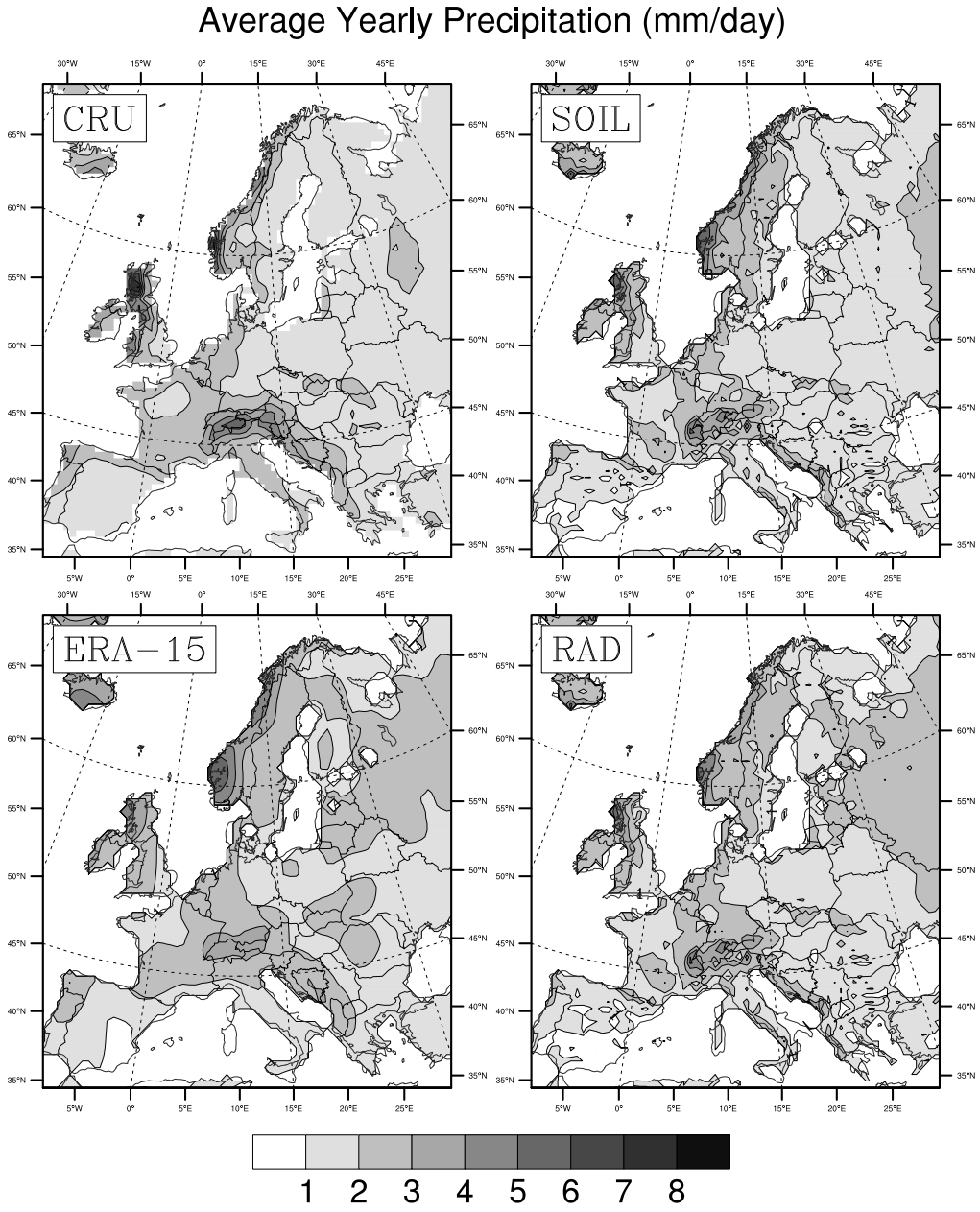

FIG. A.2: Yearly mean total precipitation (mm day^{-1}) for the entire simulation period (1979-1993) for the CRU analysis (top left), the ERA-15 assimilation (bottom left), and CHRM simulations SOIL (top right) and RAD (bottom right). All plots were masked with the CRU data coverage.

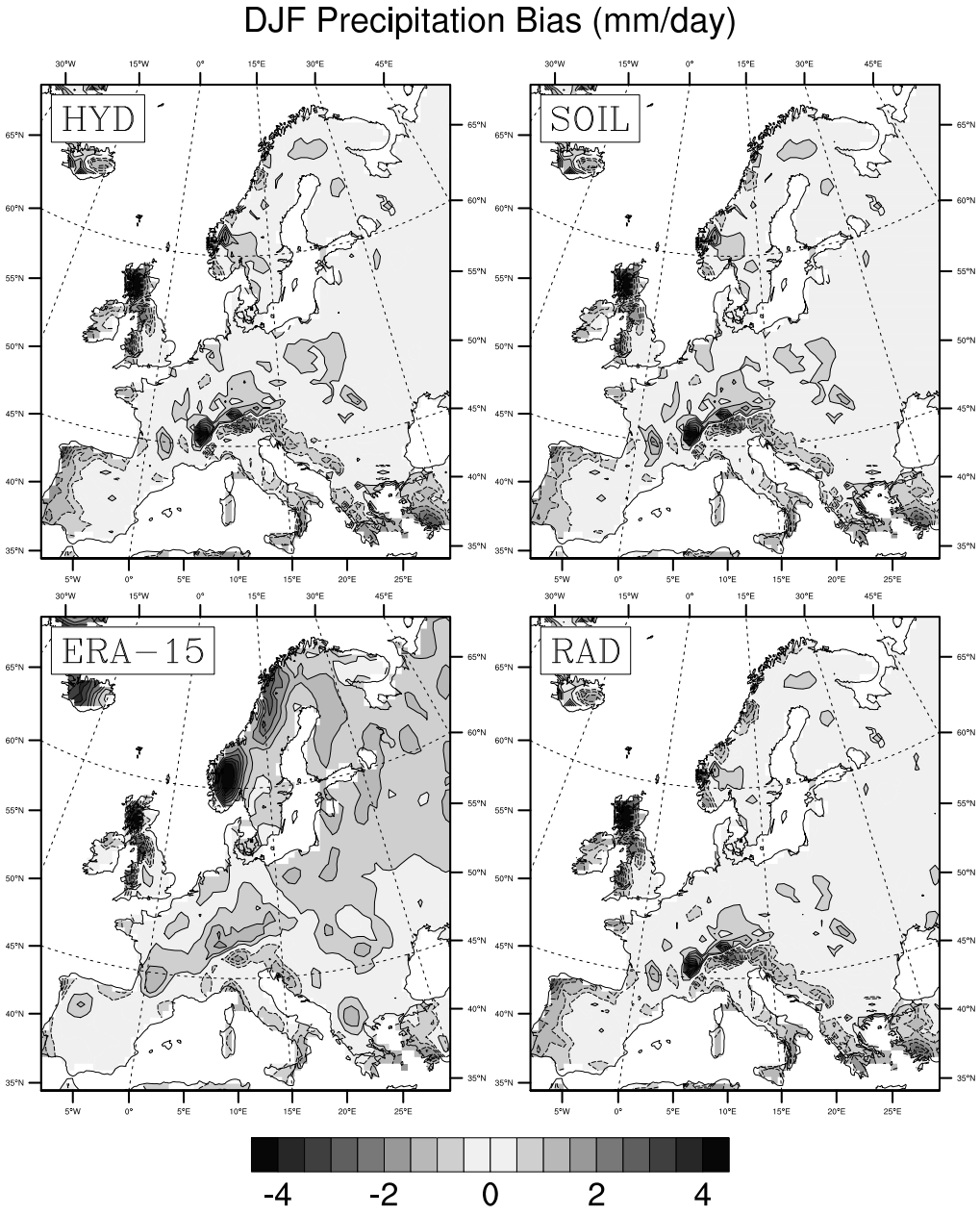

FIG. A.3: Maps of precipitation bias (relative to the CRU analysis, in mm day^{-1}) for winter (DJF) over the 1979-1993 period for ERA-15 (bottom left) and simulations HYD (top left), SOIL (top right) and RAD (bottom right). Positive contour lines are continuous, negative contours are dashed.

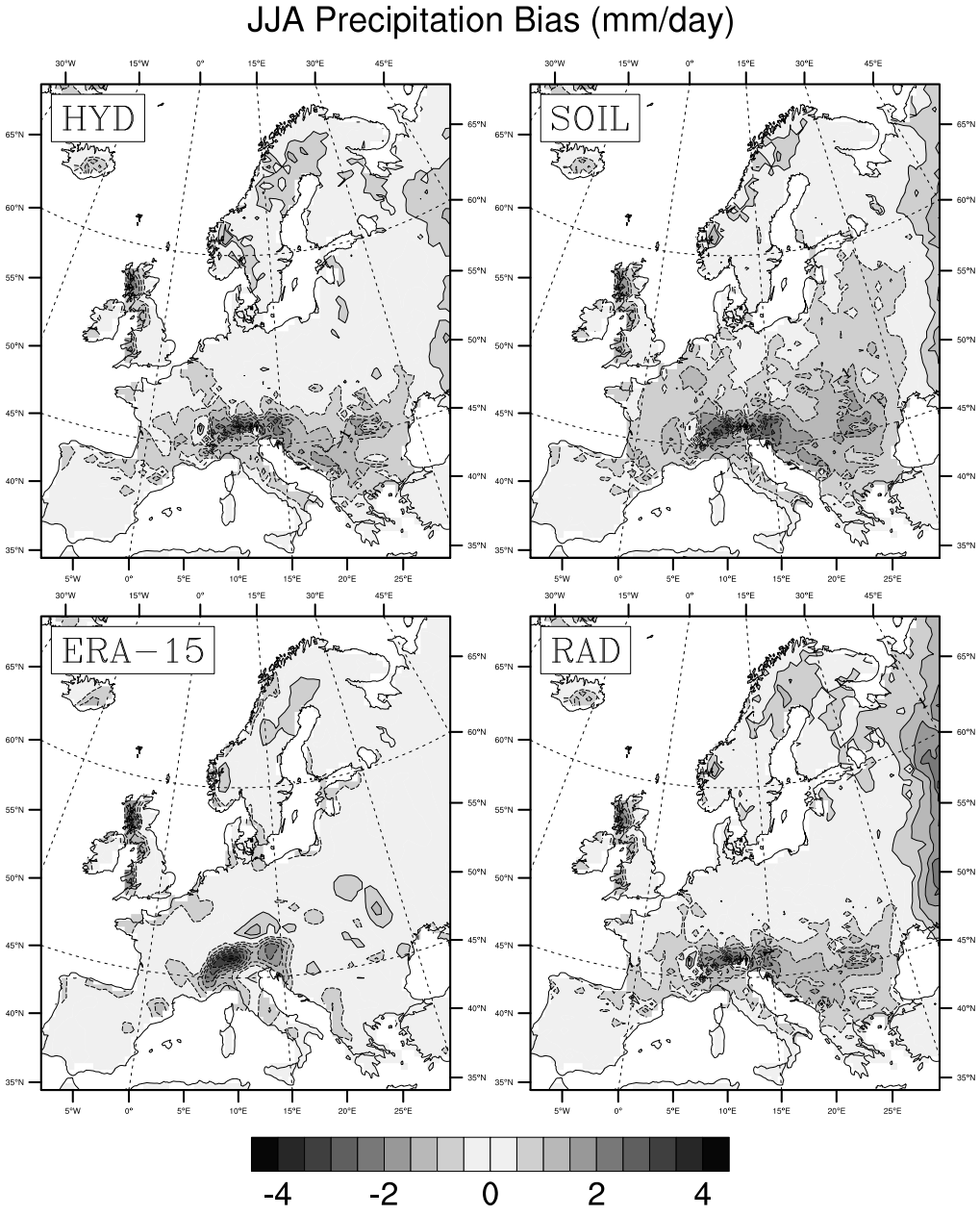

FIG. A.4: As in Fig. A.3, but for the summer precipitation bias (JJA).

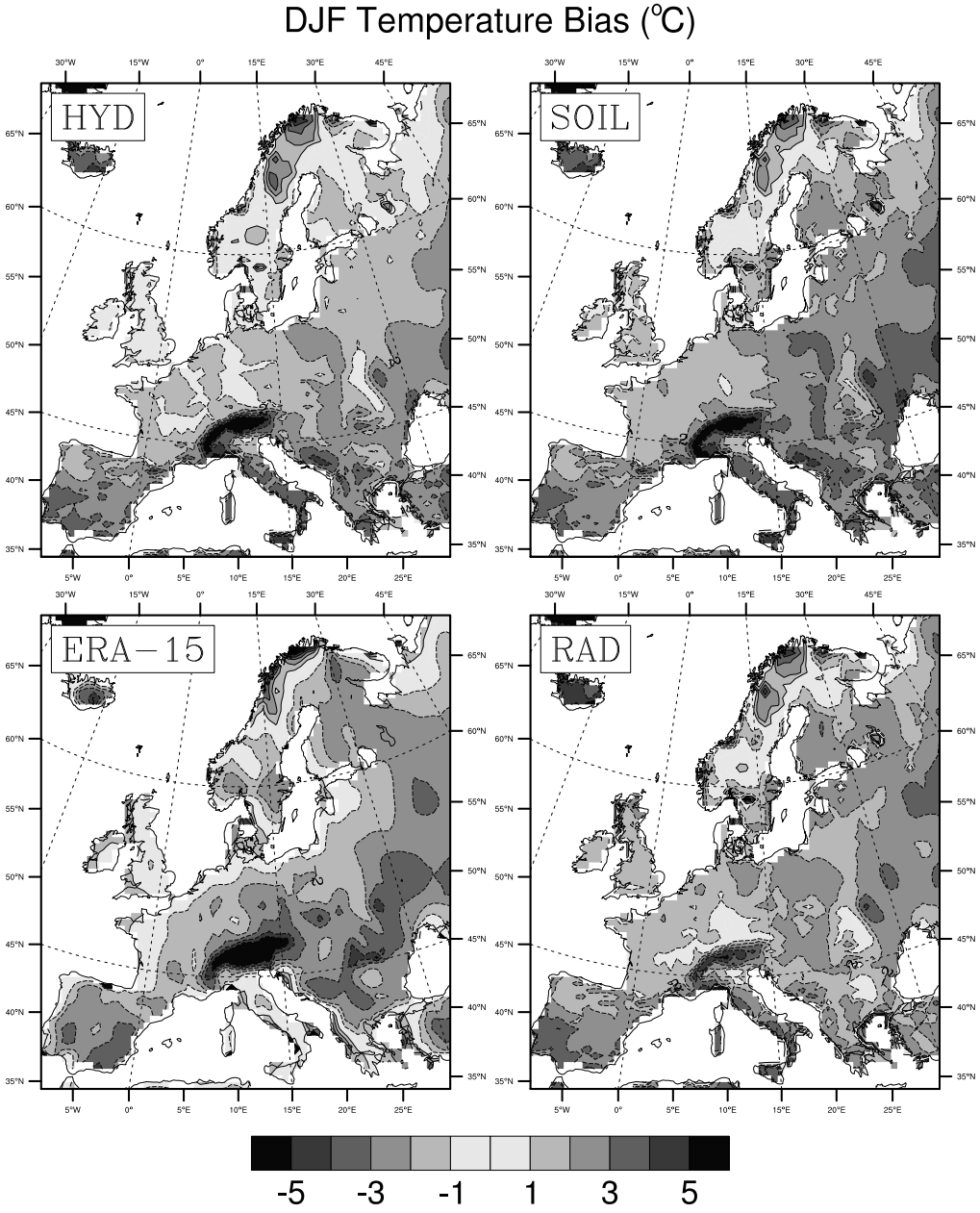

FIG. A.5: As in Fig. A.3, but for the winter temperature bias (DJF) in ^{o}C.

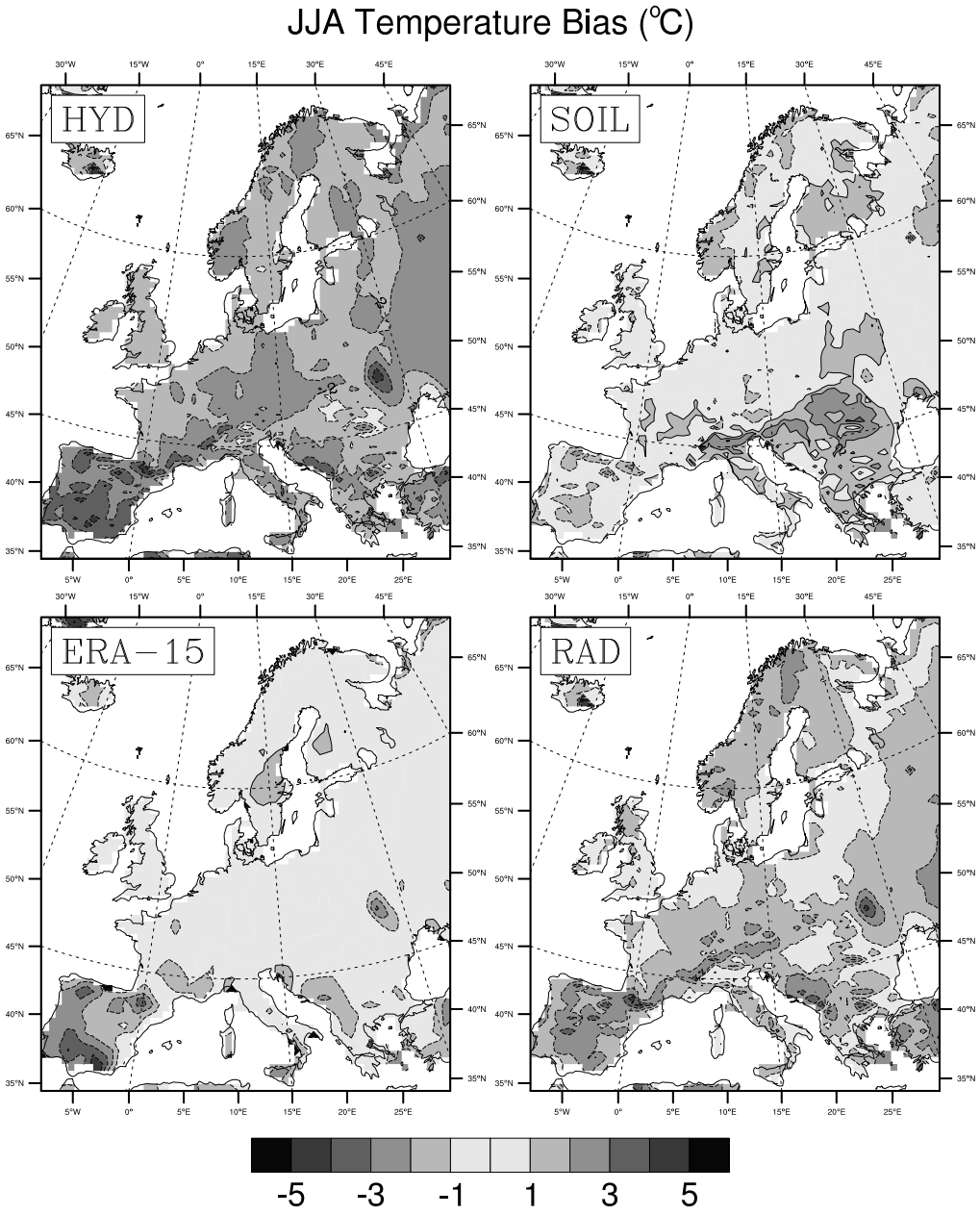

FIG. A.6: As in Fig. A.3, but for the summer temperature bias (JJA) in ^{o}C.

ERA-15 temperatures were treated as in Christensen et al. (1997) to correct for differences in underlying orography (using CHRM orography as reference), using a 6.5 $\mathrm{K\,km^{-1}}$ lapse rate. The bias in the ERA-15 analysis (also reported in Viterbo et al., 1999) is very similar to that found in our model simulations, both in magnitude and in geographical distribution, especially so over the Iberian Peninsula and the Alps.

For the summer (JJA), Fig. A.6 shows how the bias is more differentiated between individual simulations: It is most prominent in magnitude and horizontal extent in HYD where there is a large-scale negative bias between -1 and -3 K, especially noticeable over the Iberian peninsula and Central Europe, while simulation SOIL displays a very large region of positive bias over the SE portion of the domain, often exceeding +2K. Simulation RAD appears to clearly reduce the warm bias seen in SOIL, while reducing the cold bias over most of the domain in relation to HYD, despite remaining slightly cold over most of the in-land regions and over the Iberian Peninsula, when compared to SOIL. ERA-15 data show excellent agreement with CRU data, except over the Iberian Peninsula, where the analysis indicates an underestimation very similar to the one in the CHRM results.

A.3.b Soil moisture evolution

Before delving into the analysis of interannual variability, which complements and expands the bias analysis, it is important to include an excursion into the soil moisture evolution in the three model formulation experiments, which is essential for their interpretation. As an example of a regional soil moisture evolution, Fig. A.7 compares the soil moisture levels from the first and last year of the three simulations, averaged over the Alps subdomain (see Fig. A.1). Bearing in mind that 1992 and 1993 were years of extremely low precipitation in this region (see Figs. A.9-A.10), while 1978-79 was a very wet winter, the January 1979 initial condition, imposed from ERA-15 analysis, shows all three model versions very near the field capacity level (shown as a weighted average over the domain with continuous lines). Already by inspecting the soil water levels in December 1979, it is clear, however, that the soil moisture in the root zone is not re-charged equally in the three simulations, with SOIL recharging least and RAD recharging most. Simulations HYD and RAD achieve a stable, repeating soil moisture cycle between the first and fourth simulation years, depending on location, by exclusively interacting with the atmospheric water cycle. In simulation SOIL, on the contrary, the soil is losing water as a result of underestimating the recharge, despite sizable access to the climatological layer, the latter to prevent soil moisture values under the ADP. This behavior has a cumulative effect over the course of the fifteen years: simulation SOIL is clearly achieving a much lower water level by 1993 (about 100 mm less over the domain average, much more pronounced locally), with a smaller amplitude of the yearly cycle, than either HYD or RAD. The difference between simulations RAD and HYD can be ascribed to a slightly more vigorous water cycle in RAD and to the warmer temperatures, which help water infiltration into the soil due to the less frequent triggering of soil impermeabilization by freezing.

A.3.c Predictability of seasonal means

Prior to analyzing the interannual characteristics of the simulations (including biases and sensitivities to different physical parameterization choices), the predictability of seasonal

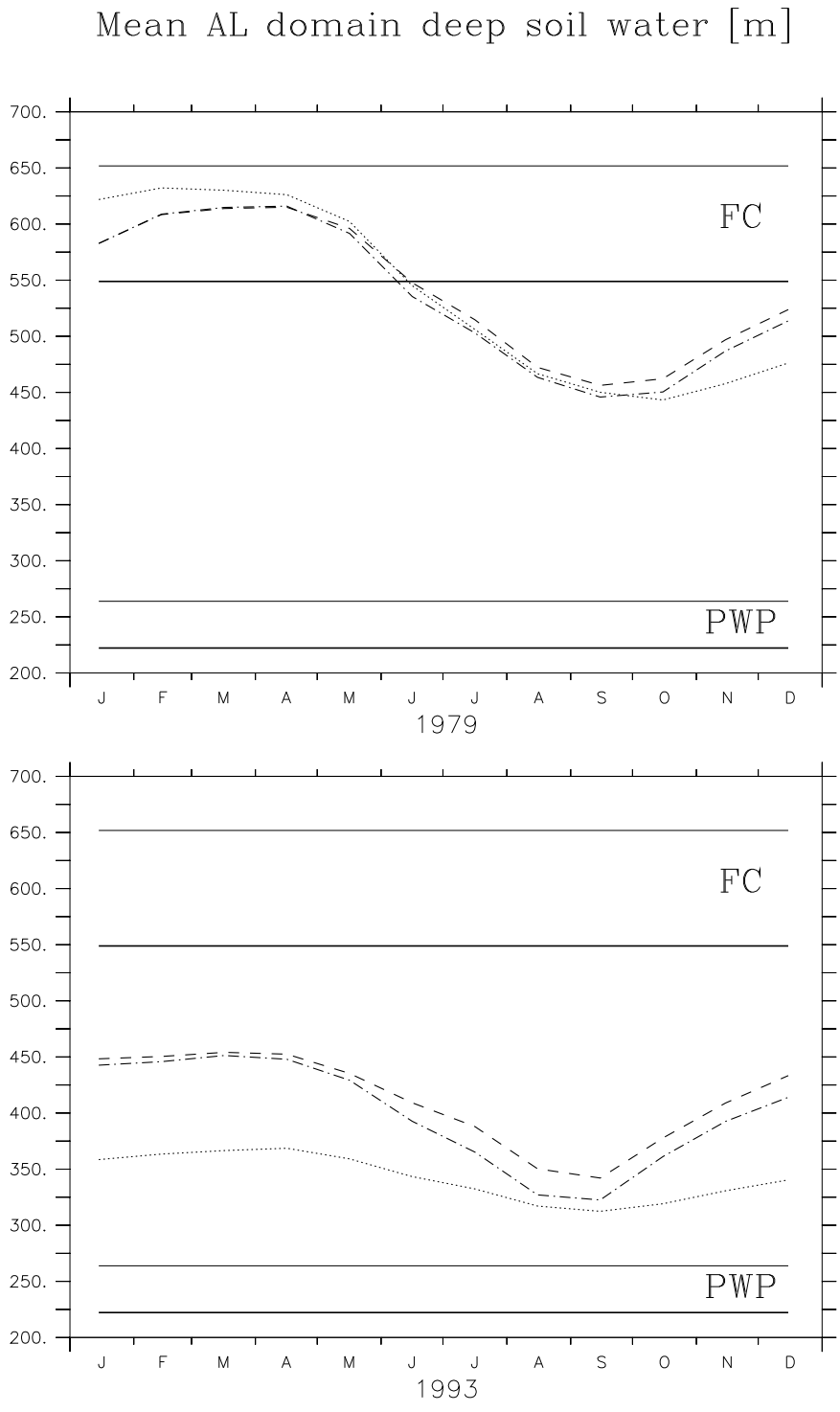

FIG. A.7: Time series plot of domain-average deep soil water for the initial year (1979, top panel) and the final year (1993, bottom panel) of the simulations in mm. Simulations SOIL, HYD and RAD are represented by dotted, dash-dot and dashed lines respectively. The average field capacity (FC) and Plant Wilting Point (PWP) for the domain are also shown as a vertical range corresponding to the two soil model formulations.

means by a given model version is assessed using an ensemble experiment in which the model formulation is kept fixed (RAD).

Examples of results are shown in Fig. A.8, in the form of scatter diagrams, representing the seasonal mean responses of the four ensemble members over one particular sub-domain (Alps), and illustrating the procedure used to estimate the uncertainty associated with alternative initial conditions. Each data point represents a spatial average for a particular ensemble member over a particular season (left panels are for winter, right panels for summer), for total precipitation (top, mm day^{-1}) and for 2m temperature (bottom, ^{o}C), respectively. The results in Fig. A.8 show that, given an initial (Jan 79) model spread of about 0.4 mm day^{-1} (and corresponding soil moisture and snow cover values) together with a 1.6 K temperature range, the summer precipitation uncertainties arising from the model's predictability are contained in a 0.2 to 0.8 mm day^{-1} interval, while temperature uncertainties in the summer range from 0.3 to 0.6 K. The behavior of individual model realizations is in no way systematic, be it by variable or by season. The vertical spread between data points is a measure of the limited predictability due to the chaotic nature of the model's dynamics; this uncertainty estimate will be later contrasted with the uncertainties stemming from alternative model formulations.

To this end, we consider only the years 1980 to 1982, since January 1979 is made special by spin-up issues and also contaminated by different simulation lengths: Even a single storm, missed by starting the model on subsequent days, could locally affect the monthly means and prevent comparability with 1980-1982 winter means. After removing the interannual variability, which was done by calculating the yearly anomalies of each ensemble mean by season (with respect to the 1980-1982 mean), the resulting 12 values were used to calculate an anomaly variance at each grid point. Sub-domain standard deviations were thus derived and applied to the comparative analysis of model uncertainties stemming from model formulation (Figs. A.9 through A.12, which are introduced in the next section).

A.3.d Interannual variability of precipitation

Previous EM-CHRM studies considering interannual variability (e.g. Christensen et al. 1997, Lüthi et al. 1996, Fukutome et al. 1999, Heck et al. 2001) have focused on ensembles of short, 1-5 month simulations, also establishing its skill at representing interannual variability of precipitation and temperature. In particular, Lüthi et al. (1996) have shown that, in general, the model retains skill at representing interannual variability of precipitation in winter, when the simulated signal is large, while not being able to achieve the same level of skill in summer, when the performance of the model has to rely more on the quality of its physical parameterizations.

In this subsection we analyze the interannual variability in precipitation for the 1979-1993 period and the ability of the CHRM model to regionally represent it. The results are presented in the form of scatter diagrams of model and observed (CRU) sub-domain seasonal averages. Before proceeding, we use the top-left panel of Fig. A.9 (sub-domain SW) to explain their use. On the abscissa are CRU observational data, while on the ordinate are model results. In each panel, the results from the three simulations SOIL, HYD and RAD as well as the ERA-15 reanalysis are represented (using different symbols and a common year label), while each of the three simulations, together with ERA-15

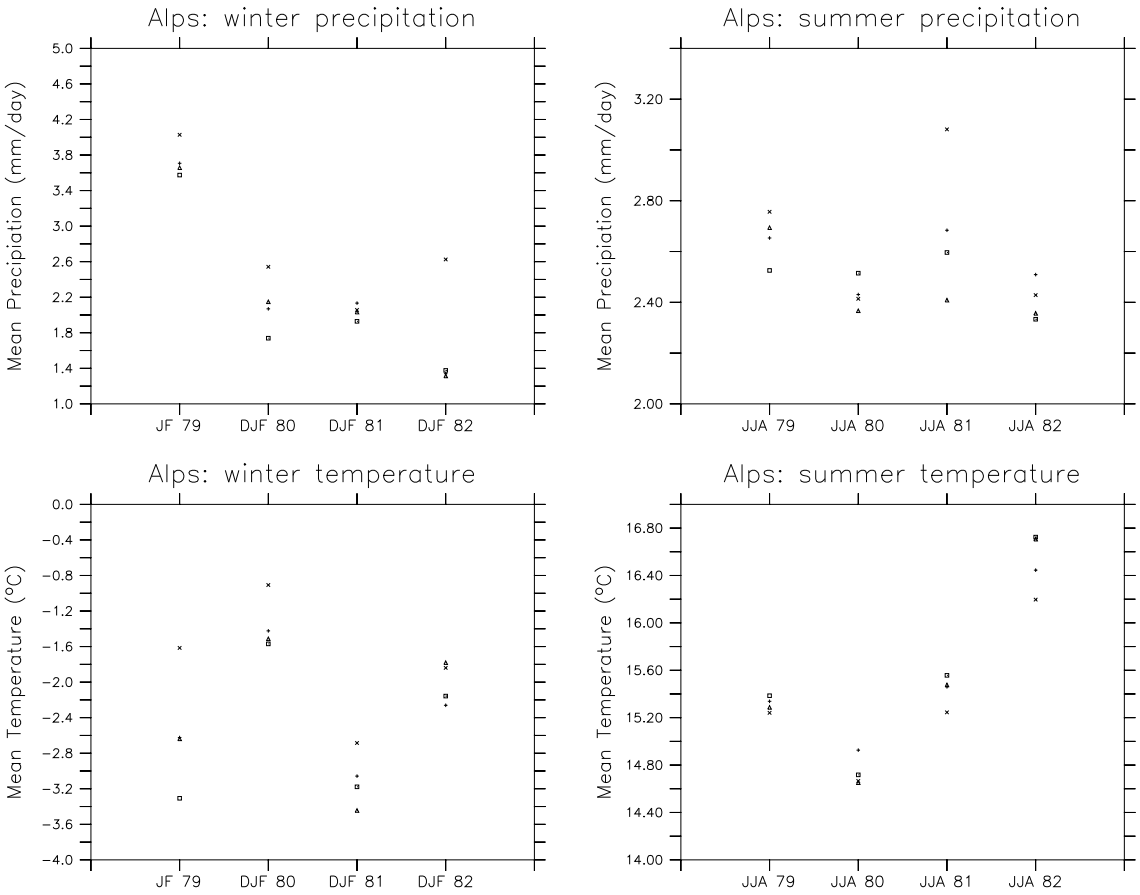

FIG. A.8: Scatter plots of spatially averaged results (Alps sub-domain) from the four ensemble members: precipitation (top panels, mm day^{-1}) and temperature (bottom panels, ^{o}C) during the winter (DJF, left panels) and the summer (JJA, right panels) seasons. The individual years (1979 to 1982) are represented on the abscissa; the data corresponding to the individual realizations are represented by symbols.

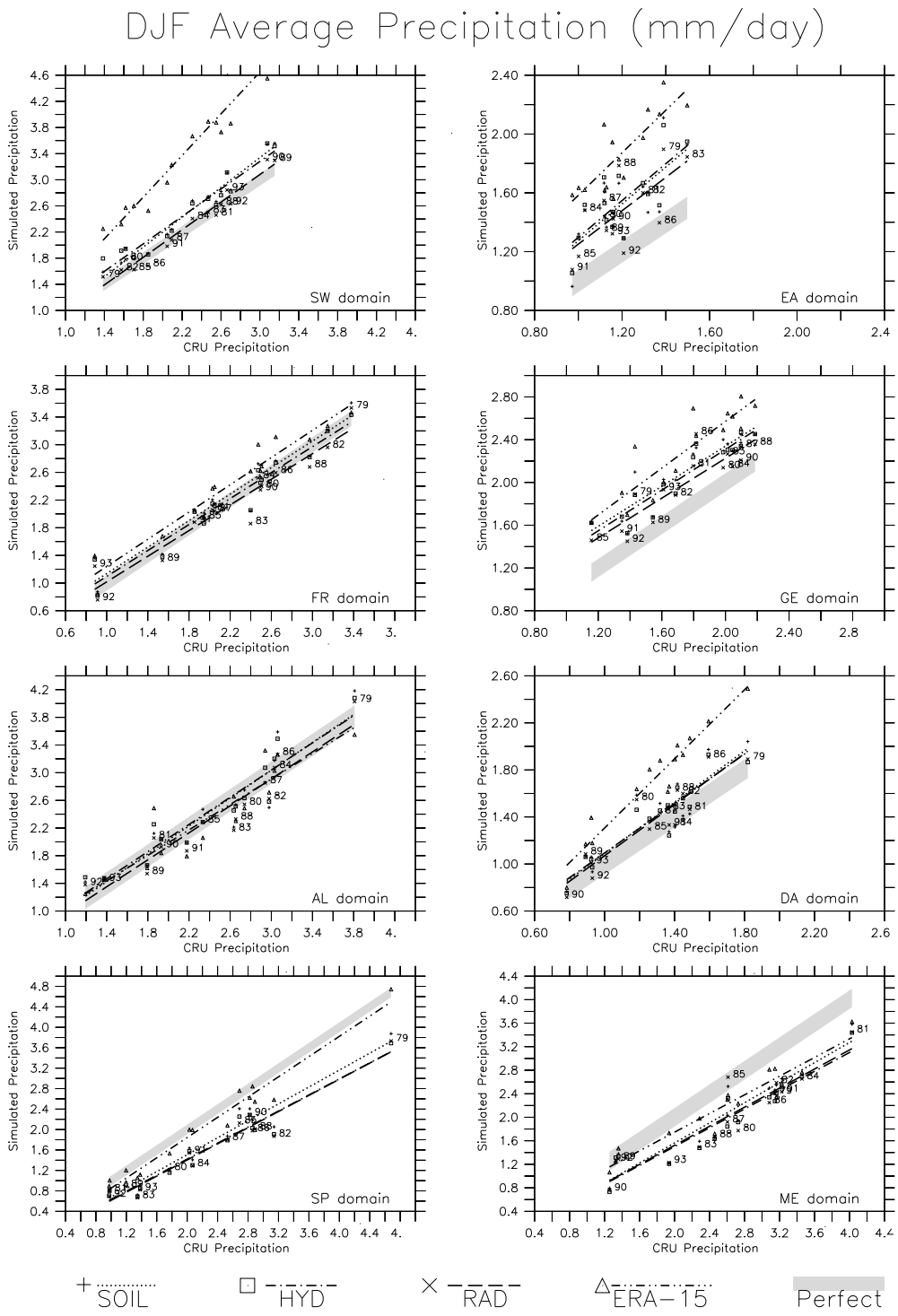

FIG. A.9: Winter (DJF) scatter plots of precipitation (mm day^{-1}) showing monthly domain means of simulations (ordinate) versus observations (CRU, abscissa) for the sub-domains shown in Fig. A.1 and the 1979-1993 period. Each data set is represented by symbols and a regression line: ERA-15: triangles and double-dot-dashed line; SOIL: plus symbols and dotted line; HYD: square symbols and dash-doted line; RAD: (x) symbols and dashed lines. Individual data points for the RAD data set are also identified by year labels. "Perfect simulation" data would lie on a diagonal line across the plot (bottom left to top right). The uncertainty related to the predictability of the system is represented by the grey area straddlng this diagonal.

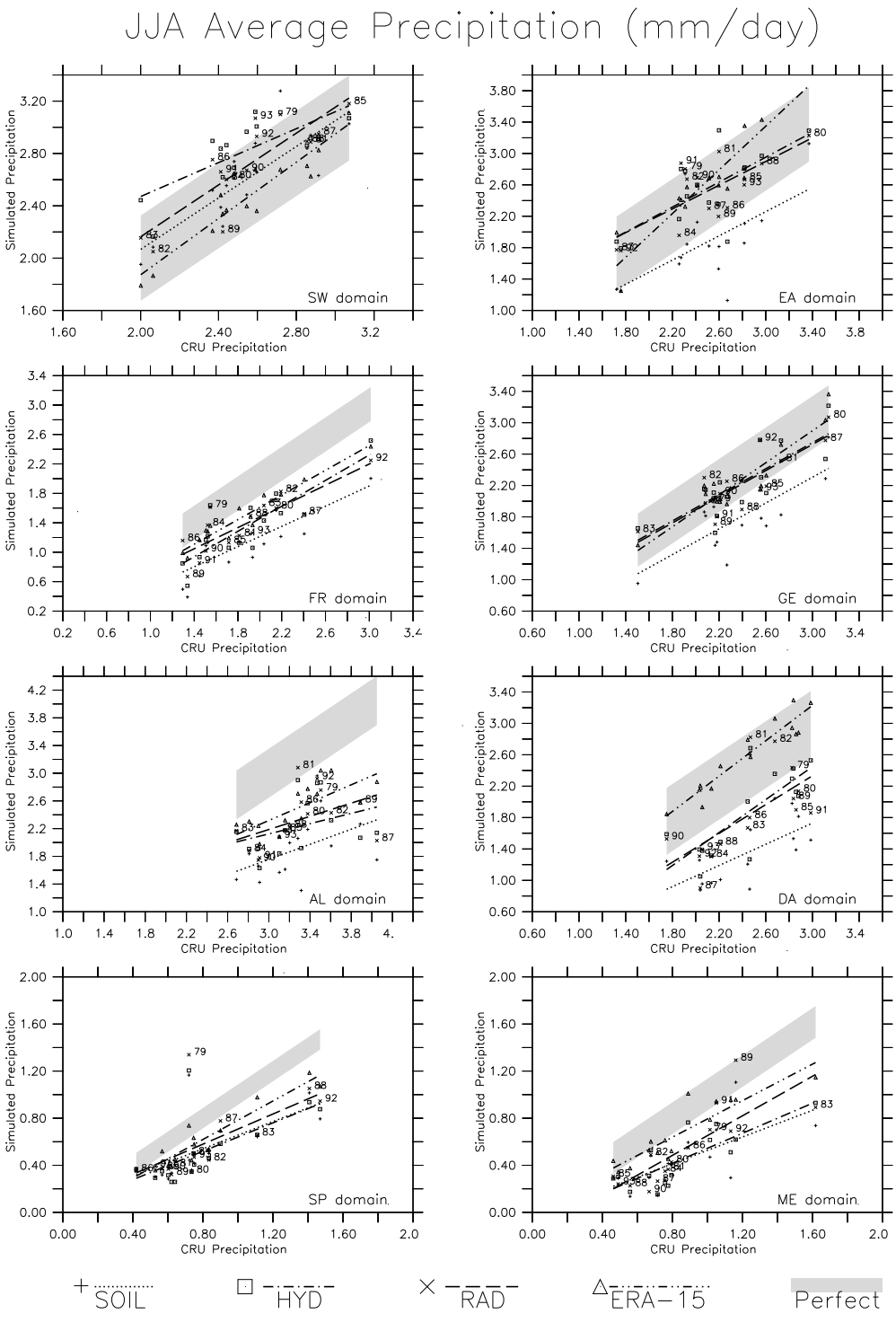

FIG. A.10: Same as Fig. A.9, but for JJA.

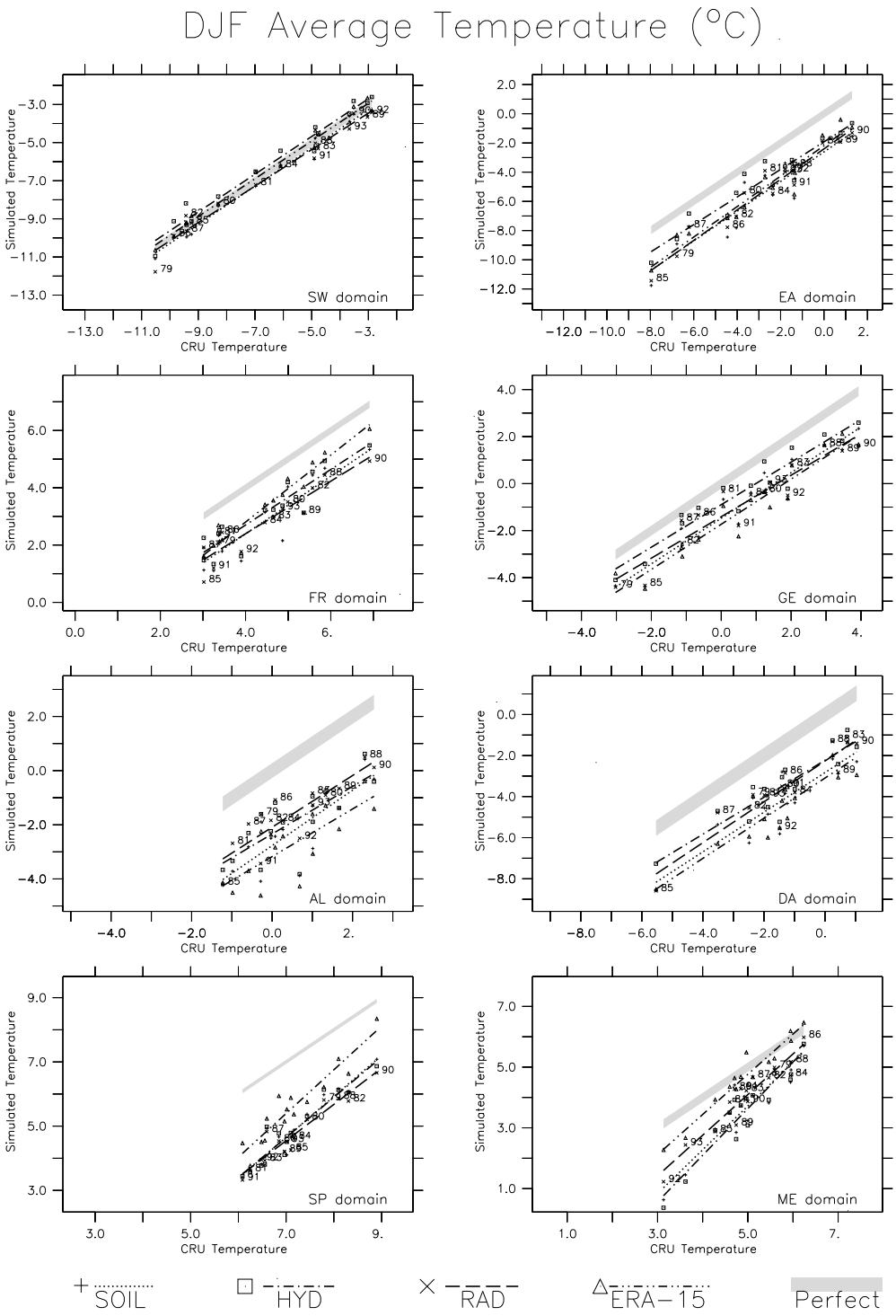

FIG. A.11: Same as Fig. A.9, but for DJF temperature (^{o}C).

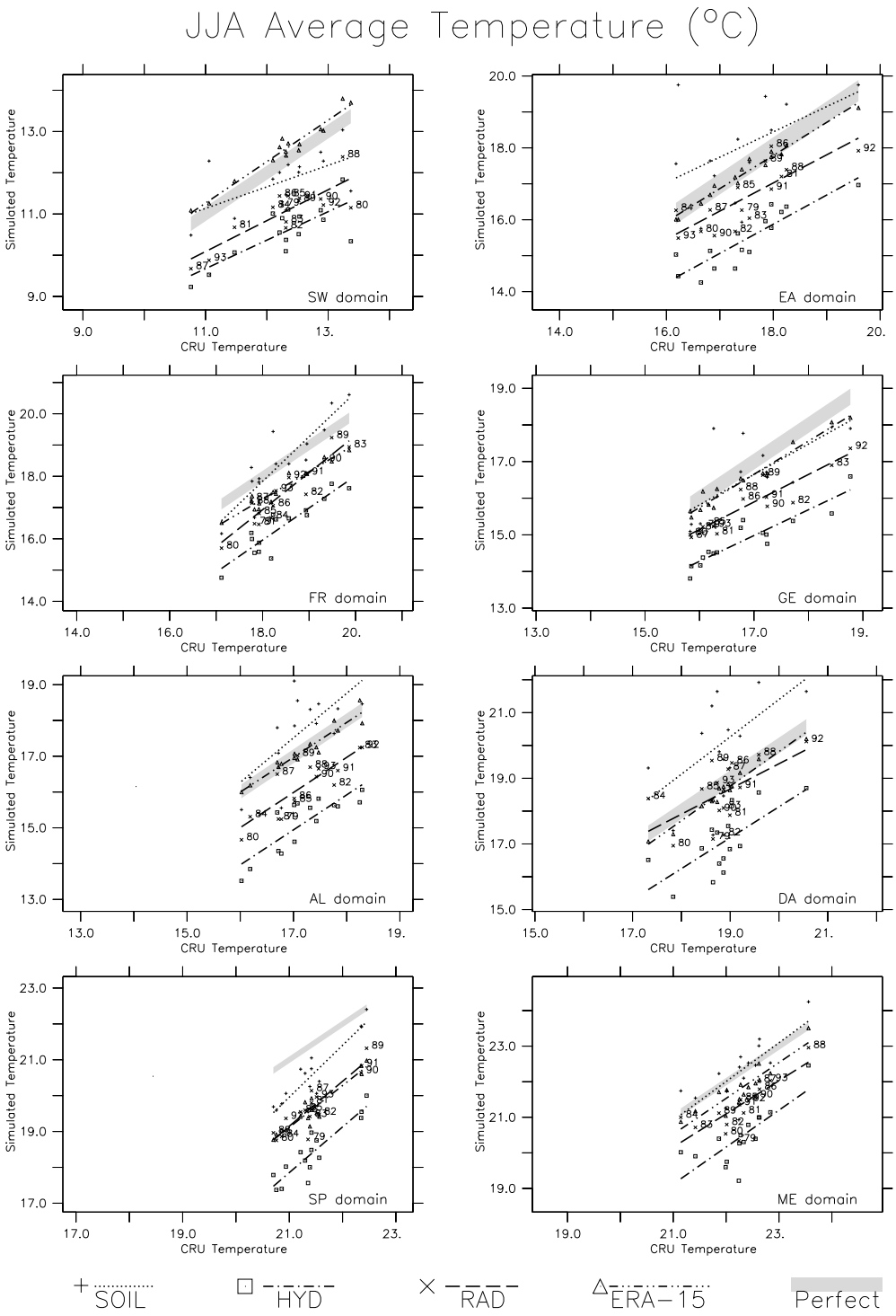

FIG. A.12: Same as Fig. A.11, but for JJA temperature (^{o}C).

analysis, is summarized by its regression line. Perfect simulation data would be located on a diagonal line (left bottom to right top) across each panel. This type of plot allows distinguishing three different types of error. First, an overall wet or dry bias can be identified from a location of the regression line above or below the diagonal (e.g. ERA-15 and RAD). Second, a systematic bias in representing the interannual variability is present when the slope of the regression line does not match that of the diagonal (e.g. ERA-15 has a tendency to overestimate precipitation more in wet years than dry years in absolute terms, albeit not necessarily so in relative terms). This behavior will be referred to as a misrepresentation of the "precipitation sensitivity", and it pinpoints a problem in simulating differences (here between wet and dry seasons). This kind of consideration may be relevant to assess the suitability of a model for conducting climate change scenarios, as is recommended in the latest IPCC (2001) report. Third, the scatter of individual data points around the regression line represents an unsystematic error contribution. This error contribution may partly be explained by the limited predictability of the system (see the previous section), which is summarized for each variable and region by the grey polygon of height $2 \cdot \sigma$ (standard deviation of ensemble results from the previous section) straddling the "perfect simulation" diagonal across each diagram. A "perfect model", that is a model with perfect physics and dynamics, would produce results contained in this grey area.

The winter precipitation in Fig. A.9 shows very good skill of the model at reproducing interannual variability, as data lie principally along the diagonal over most regions. The sub-domains with the best reproduction of the signal are the Alps and France, for which both precipitation amount and sensitivity are almost perfectly represented for all four data sets. Germany, Spain, SE Mediterranean and the Danube region show good simulation quality, but slightly less so in years of high precipitation, which are overestimated in the North and under-estimated in the South; Scandinavia (SW) and the East (EA) domains display the largest errors, with pronounced over-estimation in SW (but less so than ERA-15) and poor slope of the regression line for SP and ME. Modeled precipitation regression lines over sub-domains SW, EA, GE, DA show some degree of overestimation, but at the same time lie between ERA-15 and CRU estimates. It is of interest to note that for most of the data sets, the slope of the regression line corresponds very closely to reality (is parallel to the diagonal), but remains poorest in the south. The uncertainty associated with alternative initial conditions ranging from 0.2 to 0.6 mm day^{-1}, is most relevant in sub-domains further from the entry point of storms (NW), but tends to be comparatively important since individual model versions produce solutions that are very nearly identical.

During summer (Fig. A.10) the grey area is much thicker in response to the reduced predictability. The results nevertheless show how the SOIL simulation tends to be consistently too dry, especially in the south and southeast, and also how the slope of the regression line (the precipitation sensitivity) is generally underestimated. The dry bias is substantially reduced in simulation HYD and RAD over most domains, while the underestimation of the precipitation sensitivity is not or only marginally improved. The regions displaying the most pronounced dry bias are the Alps and the Danube; Germany and France are relatively better represented, while Spain and the Mediterranean show surprisingly good skill at the representation of interannual variability despite the small signal and the identified bias. Simulation RAD is closest to the observational data in the majority of sub-domains, except in SW and FR. The uncertainty stemming from alternative initial

conditions is larger than in winter, ranging from 0.2 to 1 mm day^{-1}, but is comparable to the one stemming from model formulation in some sub-domains, since individual model versions produce quite different bias and precipitation sensitivity results. The magnitude of the uncertainty is generally larger in the east and near mountain ranges.

In general, it is quite clear how the signal under study displays enough interannual variability as to allow the (1979-1993) model errors to be relatively large while still enabling the model to claim skill at representing this variability over most sub-domains over the entire yearly cycle. The skill, however, is least in the summer period and furthest from the principal entry point of storms, at the NW corner of the domain.

A.3.e Interannual temperature variability.

The winter temperature scatter diagrams in Fig. A.11 show for most domains a good skill at representing the temperature sensitivity (the slope of the regression lines), while there is a cold bias as large as -2K in several domains (e.g. France, Spain and Alps). Differences between individual simulations are quite small, but comparisons to the uncertainty associated with predictability (ranging from 0.1 to 0.6 K) indicate that model formulation is a more important source of uncertainty for this variable in winter.

Summer temperature scatter diagrams in Fig. A.12 show how most data are roughly aligned parallel to the diagonal (thus correctly representing temperature sensitivity), but the systematic errors are quite large, as much as 2K. The temperature field displays the largest differences between simulations, with simulation SOIL always much warmer and simulation HYD much colder than the other two. Over the Danube region, simulation SOIL is systematically over 1 K warmer than CRU, while simulation HYD is systematically 1K colder; simulation RAD has the least bias, well in agreement with ERA-15. The regression line of simulation SOIL is closest to the diagonal in several domains, but this is a clear case of error compensation and occurs at the expense of pronounced underestimation of summer precipitation in most areas (contrast with Fig. A.10). Simulation HYD is generally the coldest, while simulation RAD is a clear improvement over HYD in all sub-domains, being the one with the least bias over the Danube region, and being within 1K error bars over the Alps, Sweden, Germany, France and the SE Mediterranean, with the exception of Spain. It is also noteworthy that ERA-15 has quite an excellent behavior over most sub-domains, with the exception of Spain, which shows a bias signature very similar in geographic distribution and magnitude to the one in our model.

The uncertainty stemming from model predictability (0.2 to 0.6 K) is comparatively much less important for a variable and period in which large discrepancies exist between solutions produced by alternative model configurations, and especially so in the south.

A.3.f Surface energy and water fluxes effects

The soil-atmosphere feedbacks in the water cycle, which affect the land surface temperature and precipitation budgets, can be better understood by considering the surface energy and water fluxes and contrasting them in all three model formulation experiments. The fields that are mostly affected in the three different simulations are the surface net short wave flux and the surface latent heat flux. The three experiments are compared with the ERA-15 fluxes in Figs. A.13 and A.14, this time in the form of the mean seasonal

cycle of the 15-year period, again organized by region. The use of ERA-15 solar fluxes as a proxy for observations is justified by Wild et al. (1998), who showed that the incoming solar radiation is in general well reproduced by ERA-15 and well amenable to this type of basic validation in regional climate studies. It must be remembered, however, that the latent heat fluxes in ERA-15 are mostly a model product, despite the continuous data assimilation.

The absorbed solar radiation of simulation SOIL (Fig. A.13) is in good agreement with the fluxes of ERA-15, with a maximum local over-estimation of 20 Wm^{-2} in sub-domain DA (corresponding to summer positive temperature biases) and an under-estimation over sub-domain SW (-40 Wm^{-2} at the peak). Most sub-domains exhibit however significant drying (in several regions as much as 40 Wm^{-2} at the peak of the growing season), as evident from the depressed latent heat flux simulated by the model (Fig. A.14), also associated with a general attenuation of the soil moisture annual cycle, as was seen in Fig. A.7.

The surface latent heat fluxes (seen in Fig. A.14) in model HYD are in better agreement with those of ERA-15 than those in SOIL (except over SW and GE where some over-estimation is present). However, this extra water flux into the atmosphere feeds the almost exclusive growth of low-level clouds (not shown) which have the general effect of depressing the net surface short wave over the growing season by 10-30 Wm^{-2}: in Sweden the June biases of -40 Wm^{-2} are made to be about -60 Wm^{-2} in this model formulation.

Model RAD, with about the same total water content as HYD but a different diagnostic of cloud cover by layer (and correspondingly liquid water path), displays solar radiation with the opposite tendency, substantially correcting the bias by almost 40 Wm^{-2}over Sweden and also over Germany, in eastern Europe and the Alps. The corrections due to RAD are most pronounced in central and northern Europe and are also found (although with slightly smaller magnitude) in the net radiation plots (not shown), so that the response to the introduction of the Xu and Randall cloud diagnostic is clearly of benefit to the surface energy balance and explains the improved results in the temperature plots. The representation of the surface latent heat fluxes in RAD is very similar to that in HYD.

The short wave plots for the southern domains (SP, ME) show that radiation is rather well represented in this region and insensitive to model formulation. The latent heat flux systematic difference from ERA-15 for these regions are also significant, but also evidence spring and fall errors in the initiation and termination of vegetation activity. It is noteworthy that the static phenology in the ERA-15 land surface parameterization is mostly responsible for the differences in latent heat flux during spring and fall, which helps explain the ERA-15 cold bias during the cold season in the southern portions of the domain (especially Spain), where sufficient energy is available but vegetation should be dormant instead of transpiring.

A.4 Discussion of the simulated water and energy cycles

A.4.a Comparison of results from predictability and model formulation experiments

The comparison of the uncertainties originating from model predictability and those originating from alternative model formulations indicates that the latter are mostly predomi-

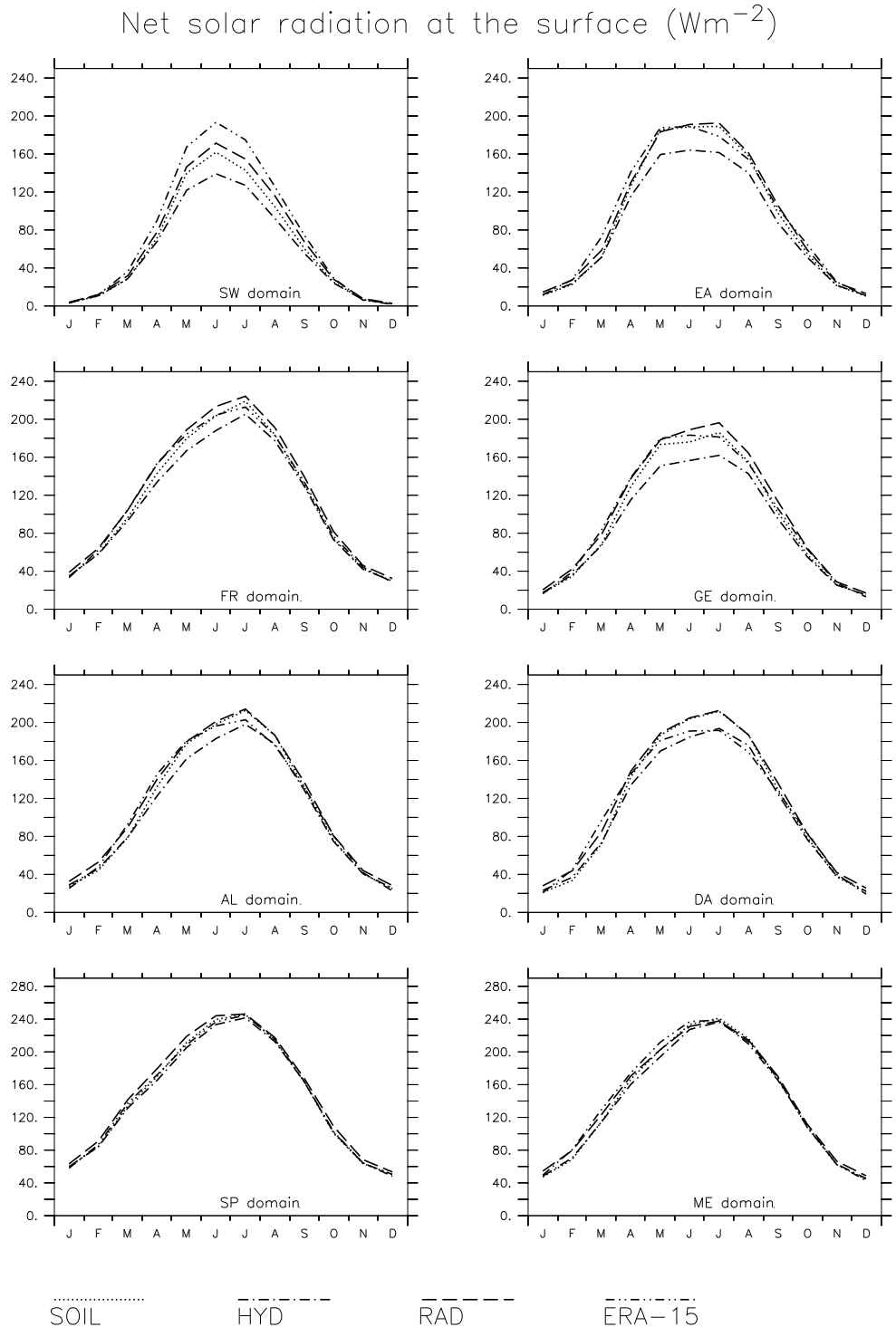

FIG. A.13: Mean seasonal cycle (1979-1993) of net solar radiation at the surface, averaged over sub-domains (Wm^{-2}).

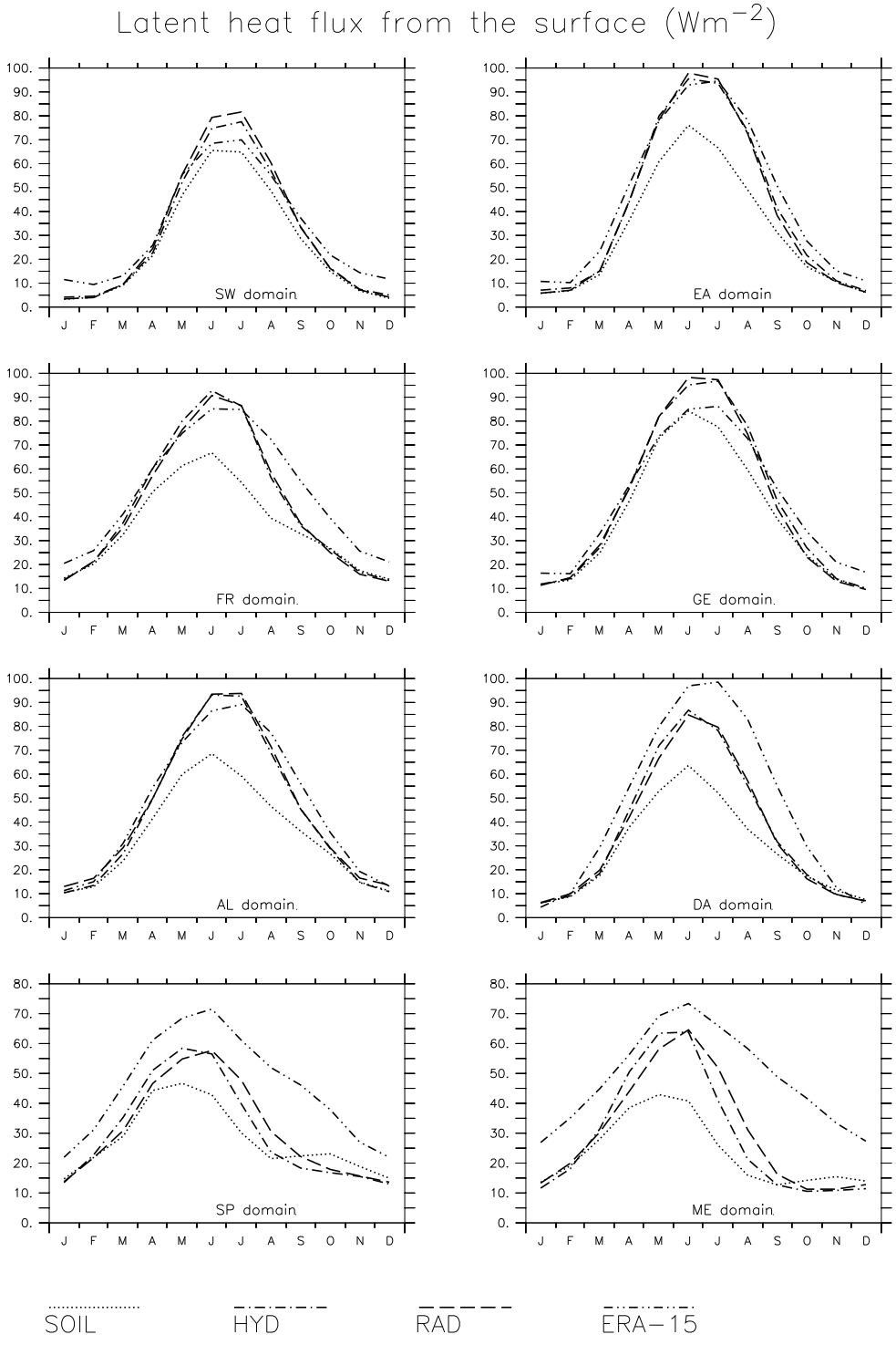

FIG. A.14: Mean seasonal cycle of latent heat flux from the surface, averaged over subdomains (Wm^{-2}).

nant. Unlike the results from experiments with alternative model formulations, no systematic behavior was uncovered in the time frame of the ensemble simulation, with a spread of solutions continuously converging and diverging, depending on location, variable and season, but no defined bias or trend. The summer precipitation field appears to be the one with the greatest sensitivity to initial conditions (although in general of comparable or smaller magnitude than the sensitivity to model formulation), arising from soil moisture and snow cover memory effects, the time scales of which will need to be investigated further.

A.4.b Mechanisms uncovered

The results of the experiments with alternative model formulations uncovered clear mechanisms associated with the water cycle: a compromised soil moisture recharge (in SOIL) causes systematic early depletion of soil water, leading to a dry warm bias in summer. Comparatively less low-level cloud formation in the growing season and limited latent heat fluxes also contribute to a warmer summer climate. A more realistic, self-sustaining, water cycle (in HYD) also enhances summer precipitation, at the cost of allowing excessive interplay of low-level cloud-radiation feedbacks, which, together with the enhanced latent heat fluxes over the growing season, produces a balance climate significantly colder than the observed climate. An alternative cloud-radiation feedback intensity, achieved by altering the cloud diagnostic (in RAD) and the resulting short wave attenuation throughout the troposphere, produces a more reasonable radiative balance at the surface (and associated temperatures) while being still successful at producing a sustainable water cycle.

A.4.c Biases and their sources

Interpreting these results in terms of biases and related compensation of model errors, it is clear that model SOIL is producing good growing season diagnostics of surface temperatures (except over the DA region, one of the "raisons d'être" of the MERCURE project) by compromising the soundness of its water cycle. This is characterized, for instance, by the significant dry biases and the serious depletion of the soil moisture reservoir. The resulting representation of precipitation displays substantial biases, which are more severe over the east of the domain and in years in which more abundant precipitation was observed. The representation of the energy and water cycles inter-play appears compromised and many of the good results are attributable to wrong reasons.

Model HYD, on the other hand, is capable of representing a sound and self-sustaining water cycle, mostly addressing the precipitation, latent heat flux and soil moisture errors in model SOIL, but at the cost of introducing a severe surface cold bias, partly explained by an underestimation of short wave radiation at the surface.

Model RAD comparatively retains the best ability in the representation of both energy and water cycles, with the smallest net short wave and latent heat flux biases, co-existing with a sustainable soil moisture cycle and one of the best representations of precipitation, in both seasons. The summer temperature bias is still significant, but represents an important improvement over the biases in models SOIL and HYD, while it also derives from a more meaningful net surface radiative balance.

It is particularly interesting to notice that the increase in solar radiation between simulations HYD and RAD, and the increase in evapo-transpiration between simulation SOIL and HYD, are just about the same and occur over the same regions. This again confirms the diagnostic of error compensation in the treatment of the soil-water and energy cycles in SOIL. The Xu and Randall corrections are also limited to regions where the yearly cycle of cloudiness is evolving around a high average value, such as Scandinavia, and is much smaller in regions of infrequent cloud cover, such as Spain, so that temperature biases are virtually unaffected. The summer positive bias in net short wave, which is present in model RAD over the DA sub-domain, corresponds to the largest deficit in latent heat flux over the domain. The same observation applies, with smaller involved amplitudes, to sub-domains SP and ME.

The uncovered mechanisms and related error compensations however do not explain all biases. A reasonable interpretation of the winter surface (2m) temperature bias is that it partially reflects the winter error in the ERA-15 data (which consists in a domain-wide -2K bias, see Viterbo et al., 1999), an argument which may come to mind by observing the geographical and temporal distributions of the CHRM and ERA-15 biases. A more complete explanation needs to also take into account the characteristics of the force-restore soil model used in the CHRM, which has only two layers, and therefore introduces large phase and amplitude errors at time scales other than diurnal and annual (see also the discussion in Jacobsen and Heise 1984). The model cannot retain sufficient memory of the summer heat storage (and is also influenced by a too cold boundary condition at the lowermost level, corresponding to the 15-year surface temperature average in ERA-15) and therefore tends to quickly reflect and respond to the cold bias in the driving data traveling through the domain from the lateral boundaries. Moreover, the model has a tendency to develop a too narrow diurnal cycle of temperature (confirmed by a separate analysis of diurnal temperature range climatology versus CRU data), so that maximum diurnal temperatures are too cold and minimum nighttime temperatures are too warm. The bias is in general concentrated more in the maximum (daytime) 2m temperature field, both in summer and winter (albeit almost exclusively in the southern extremes of the domain for winter) which is the field mostly affected both by the evapo-transpiration corrections in HYD and the cloud-radiation alterations in RAD. The impact of the grid-scale liquid water diagnostics scheme, revealed by differences in simulation RAD versus simulation HYD, is also concentrated almost exclusively to daytime maximum temperatures.

Over the summer, when local conditions prevail, and when the ERA-15 bias is much smaller, the model is free to achieve its own surface energy balance, which is much more meaningful under the new conditions imposed by the Xu and Randall cloud diagnostics, despite the fact that its partitioning into sensible and latent heat is locally still favoring too high Bowen ratios.

As expected, winter precipitation appears to be well represented, despite some local over-estimation, and appears to be unaffected by the physical parameterization changes introduced.

A.5 Conclusions and outlook

Consideration of both the predictability of the climate system and the uncertainties related to model formulation are at the same time necessary and useful in testing, understanding

and improving a climate modeling system. The methodology presented here includes both approaches and expands the interannual variability method already applied in Lüthi et al. (1996), presenting results from multi-year integrations of different model formulations and with alternative initial conditions. The nature of the methodology, and the involved computational costs, indicate that RCMs can provide sound and affordable test-beds for physical parameterization packages in the context of climate studies. The following was found in analysis of our simulation results:

1. The model has skill at representing interannual variability in precipitation and surface temperature, more so in winter, despite fairly sizeable (but within the state of the art) biases in both precipitation and temperature;

2. The analysis of precipitation sensitivity favors a correct representation of dryer years, especially so in summer and the south, while temperature sensitivity is generally well represented;

3. The comparison of model predictability and uncertainties stemming from different model formulations indicates that the latter are relatively more important over most of the European region, except for precipitation in summer, where some subdomains indicate a moderate loss of predictability. The relevance of local physical processes is of course enhanced at times when the large scale driving has less influence, most notably in summer, and farther from the entry region of storms, but it is not exclusive of those periods;

4. Severe limitations to the in-soil water flux, resulting in significant drying of the soil after few years into the simulation, create corresponding deficits in precipitation and large positive temperature biases in most central European regions, especially in the Danube catchment region;

5. Correcting the large deficit in surface solar radiation has allowed the model to achieve a good balance between the energy and the water cycles, especially in summer; this is also true, in winter, of elevated regions such as the Alps.

The new series of simulations that will be undertaken in the course of the next year will use driving data from HadAM3 and ECHAM5 simulations for current climate conditions, and also, as soon as available, from ERA-40 data; this should allow for better understanding of the influence of the lateral boundary forcing on the remaining biases. Tests will also be performed with an expanded domain, in order to study the ability of the model to develop its own solution in a larger interior region. Furthermore, a more advanced and comprehensive SVATS will be coupled, including a multi-layer diffusive soil thermal model, which should isolate the inadequacies of the force-restore method for this type of long term studies.

Acknowledgements

This research was supported by the 5th Framework Program of the European Union (project MERCURE, contract No. ENV4-CT97-0485), by the Swiss Ministry for Education and Science (BBW contracts Nr. 97.008) and by the Swiss National Science Foundation (NCCR Climate Project 2.2). We are extremely grateful to the German Weather

Service (DWD) for allowing use of the HRM base model. Special thanks to D. Majewski, B. Ritter and E. Heise for numerous suggestions and practical help with the code. This work could not have been accomplished without the fundamental support of Mr. B. Loepfe and the staff of ID-ETH, who provided assistance in data transfer and guaranteed continuous and reliable supercomputer operations. The authors wish to acknowledge use of the NCAR Graphics and Ferret softwares for analysis and graphics in this paper. NCAR Graphics is a product of University Corporation for Atmospheric Research; Ferret is a product of NOAA's Pacific Marine Environmental Laboratory.

Appendix B

Uncertainty Range of the Illinois Validation Datasets

B.1 Introduction

This appendix investigates the uncertainty range of the observational data employed for the validation of the estimates presented in Seneviratne et al. 2003 (chapter 3). Section B.2 discusses the standard error range of the mean soil moisture, both for the absolute values and the monthly variations. The errors of the mean groundwater storage and storage variations are discussed in section B.3.a, and the sensitivity of the groundwater values and monthly variations on the choice of the areal mean specific yield $\{S_y\}$ is discussed in section B.3.b. Finally, section B.4 assesses the total uncertainty range for the computed mean values of observed terrestrial water storage, comparing the obtained values with the water-balance estimates of chapter 3. A summary of the main findings is given in section B.5.

B.2 Soil moisture measurements

Figure B.1 displays the location of the 19 soil moisture measurement sites in Illinois. The names of the sites are given in Table B.1, together with their coordinates, altitude, permanent wilting point (PWP), field capacity (FC), and potential plant available moisture (FC-PWP). Note that the sites are well distributed throughout the State of Illinois.

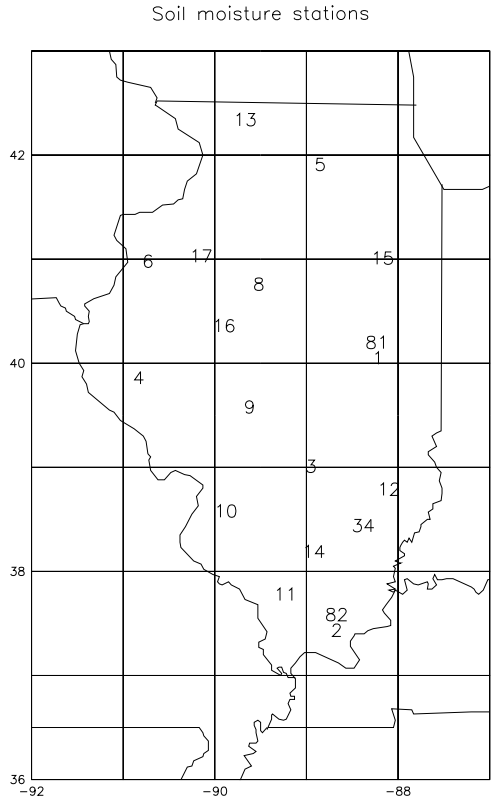

FIG. B.1: Location of the soil moisture measurement sites in Illinois. See Table B.1 for a description of the sites.

TABLE B.1: Soil moisture measurement sites in Illinois. PWP denotes the permanent wilting point of the 2 m soil column, FC its field capacity, and FC-PWP the corresponding potential plant available moisture (values summed over 11 soil levels).

No.	Name	Code	Lat. [^{o}N]	Lon. [^{o}W]	Altitude [m]	PWP [mm]	FC [mm]	FC-PWP [mm]
1	Bondville	BVL	40.05	88.22	213	502.5	866.7	364.2
2	Dixon Springs - Bare soil	DXB	37.45	88.67	165	540.4	846.3	305.8
3	Brownstown	BRW	38.95	88.95	177	492.0	832.1	339.9
4	Orr Center (Perry)	ORR	39.80	90.83	206	496.2	879.4	384.1
5	De Kalb	DEK	41.85	88.85	265	440.5	764.8	324.4
6	Monmouth	MON	40.92	90.73	229	484.3	784.4	300.0
8	Peoria	ICC	40.70	89.52	207	529.7	903.3	400.1
9	Springfield	LLC	39.52	89.62	177	638.9	853.3	214.4
10	Belleville	FRM	38.52	89.88	133	559.9	757.8	398.0
11	Carbondale	SIU	37.72	89.23	137	504.4	879.3	375.0
12	Olney	OLN	38.73	88.10	134	577.8	794.6	177.0
13	Freeport	FRE	42.28	89.67	265	471.6	916.3	444.9
14	Rend Lake (Ina)	RND	38.13	88.92	130	642.0	798.7	156.6
15	Stelle	STE	40.95	88.17	213	429.1	804.5	375.4
16	Topeka - Loamy sand	MTF	40.30	89.90	152	147.9	400.2	252.3
17	Oak Run	OAK	40.97	90.15	229	519.3	837.9	318.6
34	Fairfield	FAI	38.38	88.38	136	566.5	763.1	196.5
81	Champaign	CMI	40.08	88.23	219	452.7	727.0	274.2
82	Dixon Springs - Grass	DXG	37.45	88.67	165	540.4	846.3	305.8

Most sites have similar land cover and soil characteristics. The texture is generally of type silt-loam, or silt-clay-loam, with the exception of site 16 (Topeka) which has a loamy sand soil (Hollinger and Isard 1994). Note that PWP and FC are correspondingly markedly distinct at this site (low values), though the range FC-PWP, which denotes the potential plant available moisture, is similar in magnitude to the values from the other sites. Most sites are grass-covered (Hollinger and Isard 1994), and one location (Dixon springs) has both a bare-soil (2) and a grass-covered (82) site.

Due to these varying characteristics, some spread can be expected in the soil moisture measurements at the 19 sites. In addition, there may be geographical variations due to variability of precipitation. These two error sources will be addressed using a statistical analysis. Under the assumption that the deviations from sample mean at the measurement sites are independent and follow a Gaussian distribution, the standard error (se) in the mean ($\overline{x_i}$) of the measurements x_i can be estimated from the Central Limit Theorem by:

$$se(\overline{x_i}) = \frac{\hat{\sigma}}{\sqrt{n}} \quad , \tag{B.1}$$

where $\hat{\sigma}$ is the standard deviation of the sample and n the number of measurements.

In the presence of outliers, a more robust estimator of spread such as the median absolute deviation, $\hat{\sigma}_{MAD}$, is generally preferable to the standard deviation. The $\hat{\sigma}_{MAD}$ estimator is defined as (e.g. Venables and Ripley 1997):

$$\hat{\sigma}_{MAD} = med(|x_i - med(x_i)|)/0.6745 \quad , \tag{B.2}$$

where *med* is the median function. Note that $\hat{\sigma}_{MAD}$ is asymptotically consistent with the normal standard deviation, i.e. for Gaussian distributions $\hat{\sigma}_{MAD} \approx \hat{\sigma}$. This estimator presents the advantage of being very resistant to outliers in the data (e.g. Venables and Ripley 1997). In the following, we use both $\hat{\sigma}$ and $\hat{\sigma}_{MAD}$ for the computation of the standard error $se(\overline{x_i})$. Close values of the two estimators can be interpreted as a sign that the deviations from sample mean approximately follow a Gaussian distribution and do not entail significant outliers.

Figure B.2 displays the mean absolute values and mean monthly variations of observed soil moisture, and the corresponding standard error ranges computed with both estimators for each time available. The temporal-mean standard errors se($\hat{\sigma}$) and se($\hat{\sigma}_{MAD}$) amount

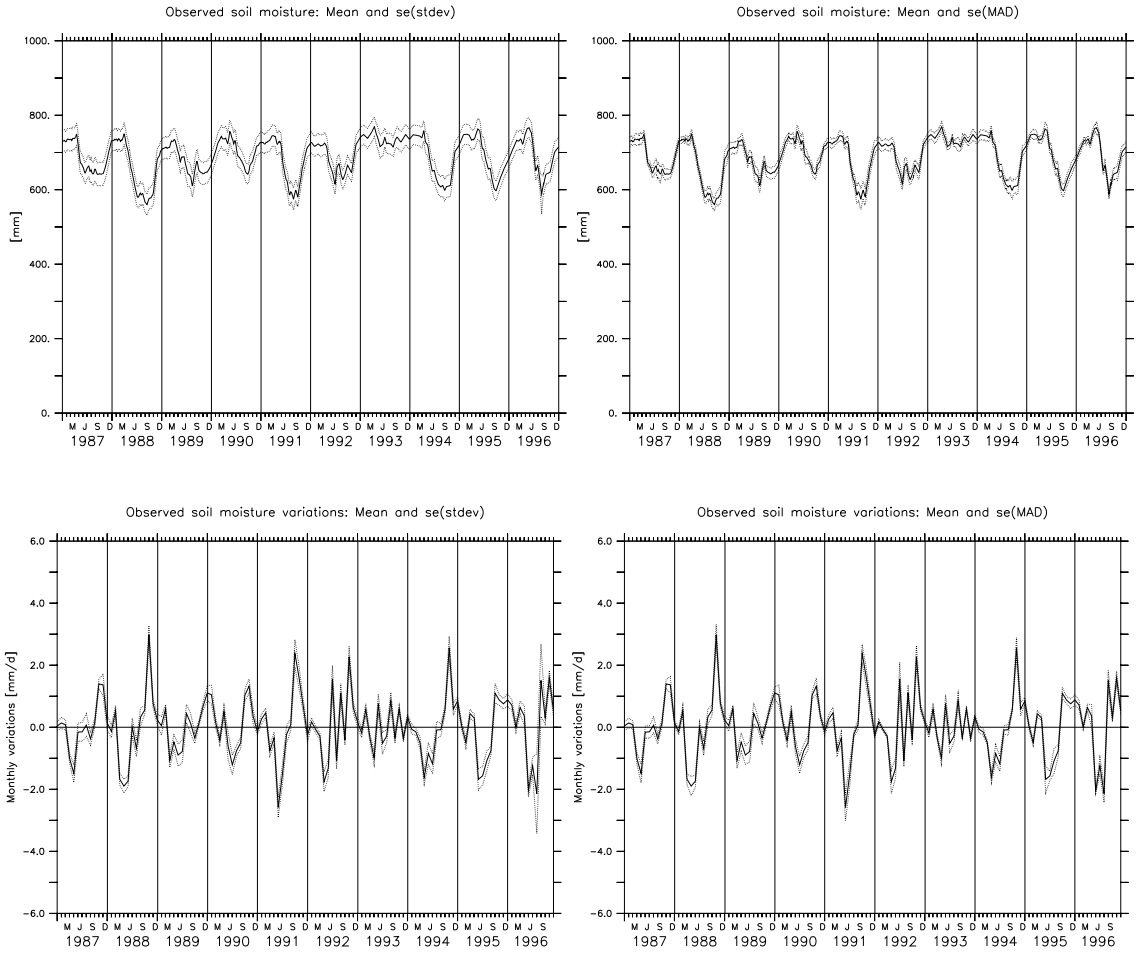

FIG. B.2: (top) Observed soil moisture in Illinois [mm]: Mean of the 19 stations (solid line) and standard error ranges (dotted lines); $\pm se(\hat{\sigma})$ (left) and $\pm se(\hat{\sigma}_{MAD})$ (right). (bottom) Observed monthly soil moisture variations in Illinois [mm/d]: Mean monthly variations at the 19 stations (solid line) and standard error ranges (dotted lines); $\pm se(\hat{\sigma})$ (left) and $\pm se(\hat{\sigma}_{MAD})$ (right).

to 27.8 mm and 14.0 mm for the mean of the absolute soil moisture values, and to 0.24 mm/d and 0.19 mm/d for the mean of the monthly variations. Interestingly, the mean monthly variations (contrary to the absolute values) exhibit a small standard error and little differences between both deviation estimators. This suggests that even though absolute soil moisture content can differ significantly from site to site (and probably entail some outliers), soil moisture depletion and recharge are similar at all sites, and are thus more directly dependent on the atmospheric forcing than on the local characteristics (e.g. soil texture). Hollinger and Isard (1994) found concordant results in their comparison of long-term time series of soil moisture at Topeka (site 16: plainfield loamy sand soil) and Bondville (site 1: poorly drained, silt-loam soil), showing that the relative soil moisture evolution was very similar at the two sites, despite large differences in absolute soil moisture level due to the differing soil texture and structure.

In conclusion, the standard errors of mean areal soil moisture amount to 15-30 mm for the absolute soil moisture, and to 0.20-0.25 mm/d for the monthly variations. Note that the uncertainty ranges computed here are likely to be underestimates, as further sources of uncertainty such as measurement errors, can also be relevant. For the Illinois measurement network, the measurement uncertainty is for instance of the order of 10-20 % (Hollinger and Isard 1994). Moreover, despite the comparative homogeneity of this region, it is possible that the sample of stations does not cover the full variability of soil moisture in Illinois, as most of the measurement sites are located in grass-covered agricultural areas.

B.3 Groundwater measurements

In the following sections, we discuss two main sources of errors for the computed mean groundwater storage and storage variations. Section B.3.a analyses the standard error of the mean groundwater storage and storage variations, and section B.3.b assesses the uncertainty resulting from the choice of the mean areal specific yield $\{S_y\}$. Measurements errors in the groundwater level are of the order of 0.1 foot or 30 mm (Ken Hlinka, personal communication, 2003), which corresponds to only 2.5-3 mm of effective groundwater storage, and can therefore be neglected.

B.3.a Standard error of the mean groundwater storage and storage variations

Figure B.3 displays the location of the 17 groundwater measurement sites in Illinois (see also Table B.2 for a list of the stations). Note that the sites are relatively well distributed throughout Illinois, but that there are comparatively less stations available in the north-eastern part of the state.

As for the soil moisture measurements, we first compute the standard error of the mean values using equation (B.1) and the two deviation estimators $\hat{\sigma}$ and $\hat{\sigma}_{MAD}$ (Fig. B.4). The mean standard errors $se(\hat{\sigma})$ and $se(\hat{\sigma}_{MAD})$ are equal to 51.1 mm and 29.8 mm for the mean absolute values, and to 0.30 mm/d and 0.21 mm/d for the mean monthly variations. As for soil moisture (section B.2), the absolute values have a larger discrepancy between se($\hat{\sigma}$) and se($\hat{\sigma}_{MAD}$) than the monthly variations, which suggests that they might

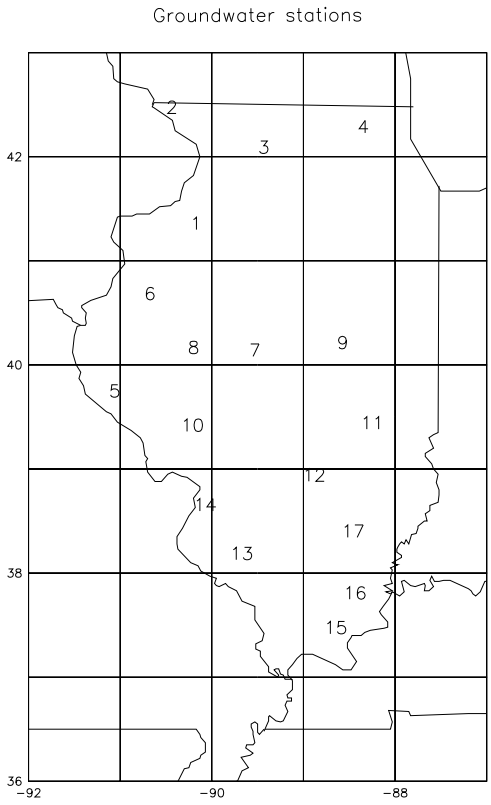

FIG. B.3: Location of the groundwater measurements sites in Illinois (see also Table B.2).

TABLE B.2: Groundwater measurement sites in Illinois.

Number	Name	Lat. (^{o}N)	Lon. (^{o}W)
1	Cambridge	41.30	90.17
2	J. Hudson, Galena	42.42	90.44
3	Mt. Morris	42.03	89.43
4	SWS No. 1, Crystal Lake	42.23	88.35
5	Coffman	39.69	91.06
6	Good Hope No. 2	40.63	90.68
7	Middletown	40.08	89.53
8	Snicarte	40.11	90.20
9	Swartz	40.16	88.57
10	Greenfield No. 2	39.36	90.21
11	Janesville No. 3	39.38	88.25
12	St. Peter No. 3	38.88	88.88
13	Sparta	38.13	89.68
14	SWS No. 2	38.60	90.07
15	Dixon Springs	37.42	88.65
16	S.E. Illinois College	37.75	88.44
17	Boyelston	38.34	88.46

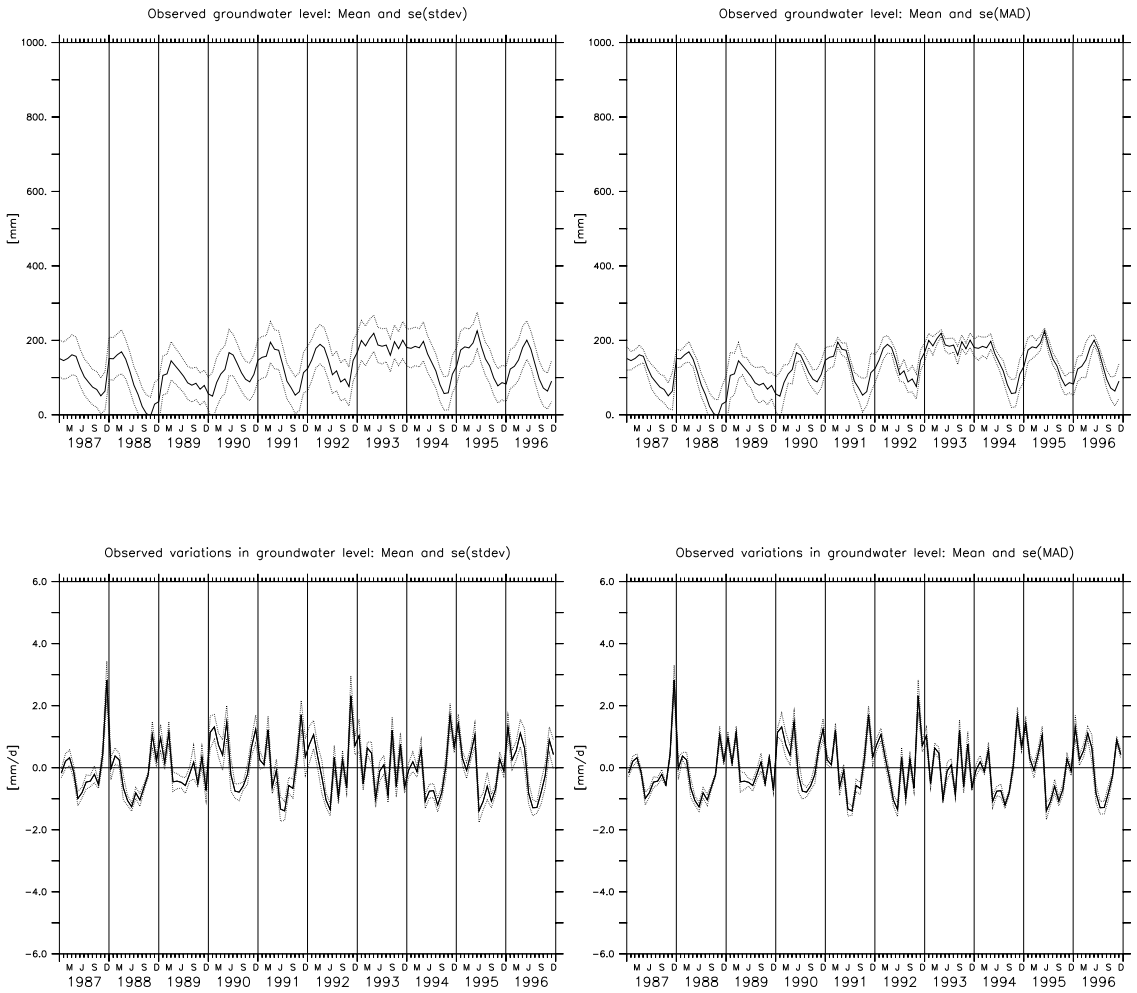

FIG. B.4: (top) Observed groundwater storage (groundwater level relative to deepest value $* S_y$) in Illinois [mm]: Mean of the 17 stations (solid line) and standard error ranges (dotted lines); $\pm se(\hat{\sigma})$ (left) and $\pm se(\hat{\sigma}_{MAD})$ (right). (bottom) Observed monthly groundwater variations in Illinois [mm/d]: Mean monthly variations at the 17 stations (solid line) and standard error ranges (dotted lines); $\pm se(\hat{\sigma})$ (left) and $\pm se(\hat{\sigma}_{MAD})$ (right).

entail more outliers. Note that the standard errors in the computed mean groundwater values are somewhat larger than for soil moisture, particularly in the case of the absolute values.

B.3.b Dependence on $\{S_y\}$

The chapter 3 study (Seneviratne et al. 2003) uses a value of 0.08 for the areal mean specific yield $\{S_y\}$ in Illinois. This choice was based on the study of Yeh et al. (1998), who use the same value for the computation of their water-balance estimates of evapotranspiration in Illinois (see also section 3.3.b). They suggest that the representative $\{S_y\}$ should range

between ∼0.05 and 0.1. Here, we test the sensitivity of the computed groundwater storage to variations in this parameter.

Figure B.5 displays timeseries of the mean groundwater storage (relative to the lowest value within the timeseries) and storage variations, for $\{S_y\}$ values of 0.08, 0.05, and 0.1. The uncertainty induced in the absolute values is relatively large and is of similar magnitude as the standard error (see Fig. B.4). For the monthly variations, it amounts on average to only ±0.17 mm/d and ±0.26 mm/d for $\{S_y\}$ values of 0.1 and 0.05, respectively.

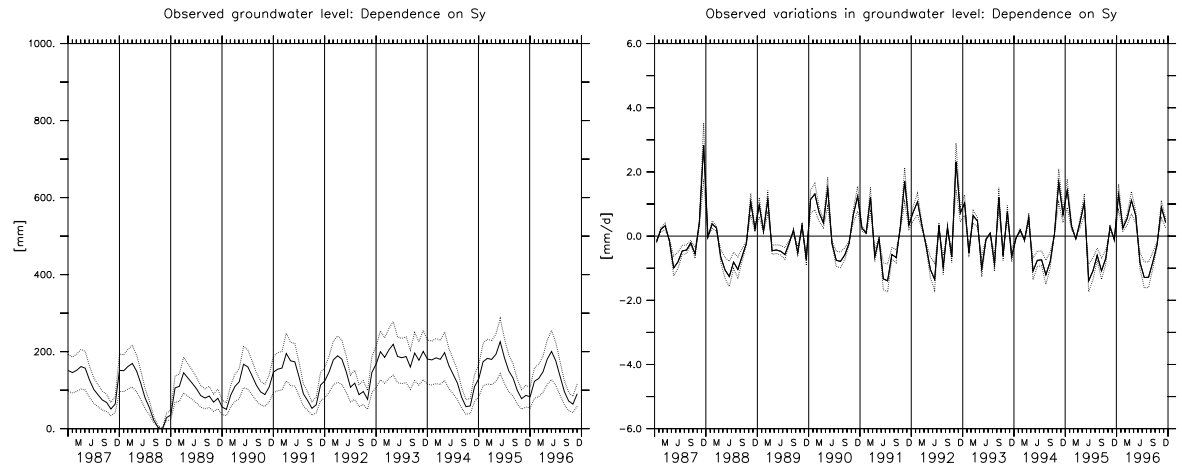

FIG. B.5: Dependence on $\{S_y\}$: (Left) Groundwater storage (relative to the lowest value within the timeseries) [mm] computed with $\{S_y\}$ values of 0.08 (solid line), 0.05 and 0.1 (dotted lines). (Right) Groundwater storage variations [mm/d] computed with $\{S_y\}$ values of 0.08 (solid line), 0.05 and 0.1 (dotted lines).

B.4 Total terrestrial water storage

In this section, we look at the cumulated uncertainty of the three considered uncertainty ranges for the total terrestrial water storage: the standard errors in the computed mean values of soil moisture and groundwater storage values, and the uncertainty range in the $\{S_y\}$ parameter. Uncertainties in the snow measurements are not discussed here, as the snow amounts are negligible in comparison with the soil moisture and groundwater storage (see section 3.3.c).

Figure B.6 displays the observed values of terrestrial water storage in Illinois with the cumulated uncertainty ranges for $\{S_y\}$ and the standard errors in the mean soil moisture and groundwater storages (left plot: standard errors computed with $\hat{\sigma}$; right plot: standard errors computed with $\hat{\sigma}_{MAD}$). The two uncertainty ranges are qualitatively similar, but smaller when including $se(\hat{\sigma}_{MAD})$ instead of $se(\hat{\sigma})$, as can be expected from the results of the preceding sections. The total uncertainty range is of the order of ±100-120 m, depending on the choice of the deviation estimator.

Figure B.7 displays the observed monthly variations of terrestrial water storage with the cumulated error range for the three investigated sources of uncertainty ($\{S_y\}$ range,

and standard errors $se(\hat{\sigma}_{MAD})$ of the mean soil moisture and groundwater variations computed with the median absolute deviation). Note that the results for $se(\hat{\sigma})$ are very similar, except that the uncertainty range is somewhat larger (not shown). Strikingly, the water-balance estimates (red curve) are within the uncertainty range in most years, with the only exception of 1989, and the first months of 1990. Considering that additional uncertainties should also be taken into account (in particular the uncertainty of the soil moisture measurements), this suggests an excellent agreement between the computed water-balance estimates and the observations.

B.5 Discussion and summary

This appendix has assessed the magnitude of the uncertainty range of the observed terrestrial water storage in Illinois. The standard errors of the mean absolute soil moisture and groundwater storage are generally relatively large: of the order of 15-30 mm for soil moisture, and 30-50 mm for groundwater. The absolute values also appear to entail some outliers, as their median absolute deviation $\hat{\sigma}_{MAD}$ is on average much smaller than their standard deviation $\hat{\sigma}$.

For their part, the mean monthly variations of both soil moisture and groundwater storage appear quite robust, as they exhibit similar values of $\hat{\sigma}$ and $\hat{\sigma}_{MAD}$, and have relatively small uncertainty ranges (of the order of 0.20-0.25 mm/d for soil moisture, and 0.20-0.30 mm/d for groundwater). It is interesting that the monthly variations of soil moisture and groundwater storage are more homogeneous than the absolute values; this suggests that they are more directly dependent on the atmospheric forcing than on the local characteristics, unlike the absolute values. This is possibly one of the explanations for the good agreement between the computed water-balance estimates and the observations.

The uncertainty range associated with $\{S_y\}$ for the absolute values and monthly variations of groundwater storage is of similar magnitude as for the standard error, but is characterized by higher seasonal variations. Added together with the standard error, it implies a relatively large uncertainty in the mean of the groundwater measurements, most of all for the absolute values.

Finally, the comparison of the monthly water-balance estimates of chapter 3 with the observations and computed uncertainty range shows that they are close or within the uncertainty range in most years, an excellent agreement given that the uncertainty range is probably underestimated. The results thus provide confidence in the accuracy of the computed monthly estimates.

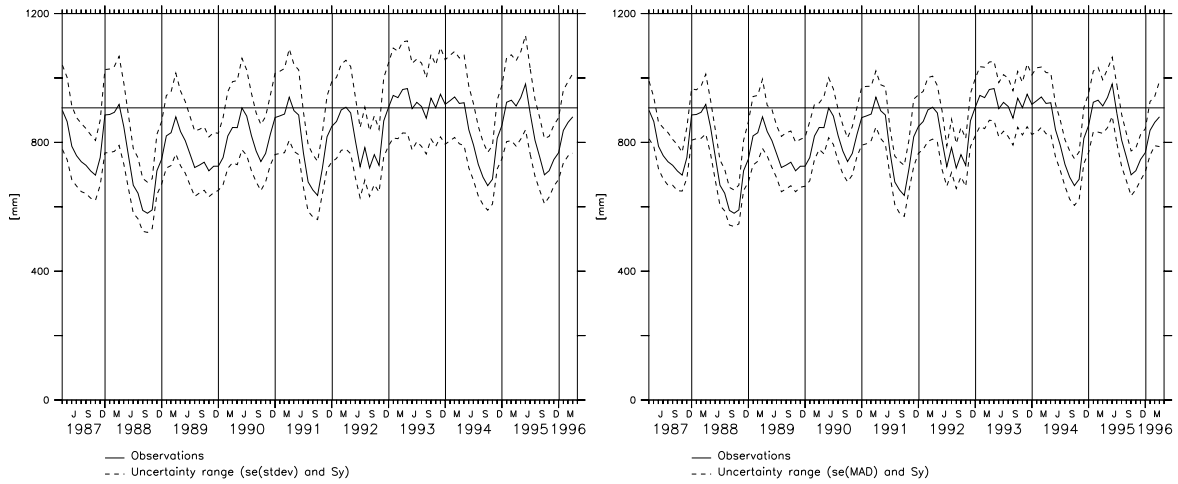

FIG. B.6: Observed terrestrial water storage in Illinois (solid line) and cumulated uncertainty ranges (dashed lines) for $\{S_y\}$ and the standard errors of the mean soil moisture and groundwater values computed with $\hat{\sigma}$ (left) and $\hat{\sigma}_{MAD}$ (right).

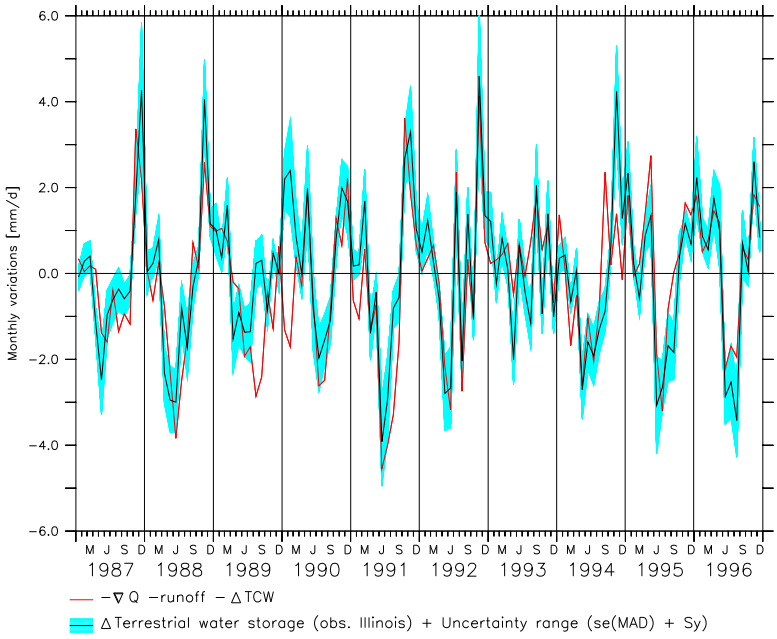

FIG. B.7: Monthly variations in terrestrial water storage [mm/d]: Observations (black line) with error range (blue), and water-balance estimates (red line). The error range includes the standard errors of the mean soil moisture and groundwater measurements (computed with $\hat{\sigma}_{MAD}$), and the uncertainty range for $0.05 \leq \{S_y\} \leq 0.1$.

References

Alestalo, M., 1983: The atmospheric water vapour budget over Europe. In: *Variations in the Global Water Budget*, A. Street-Perrot et al. (eds.), pp. 67-79. D. Reidel Publishing Company.

Anthes, R., E. Hsie, and Y. Kuo, 1987: Description of the Penn State/NCAR Mesoscale Model Version 4 (MM4). Technical report TN-282+STR, NCAR, Boulder, Colorado, 66 pp.

Arakawa, A., and W.H. Schubert, 1974: Interaction of a cumulus cloud ensemble with the large-scale environment, Part I. J. Atmos. Sci., 31, 674-701.

Ball, J.T., 1988: An analysis of stomatal conductance. Ph. D. thesis, Stanford University, 89 pp.

Basara J.B., and T.M. Crawford, 2000: Improved installation procedures for deep-layer soil moisture measurements. Journal of Atmospheric and Oceanic Technology, 17 (6), 879-884.

Beljaars, A.C.M. and P. Viterbo, 1998: The role of the boundary layer in a Numerical Weather Prediction model. In: *Clear and Cloudy Boundary Layers*, A.A.M. Holstlag and P.G. Duynkerke (eds.), pp. 287-304. Royal Netherlands Academy of Arts and Sciences.

Beljaars, A.C.M, P. Viterbo, M.J. Miller, and A.K. Betts, 1996: The anomalous rainfall over the United States during July 1993: Sensitivity to land surface parameterization and soil moisture anomalies. Mon. Wea. Rev., 124, 362-383.

Benton, G.S., and M.A. Estoque, 1954: Water-vapor transfer over the North American continent. J. Meteorol., 462-477.

Berbery, E.H., E.M. Rasmusson, and K.E. Mitchell, 1996: Studies of North American continental scale hydrology using Eta Model forecast products. JGR-Atmosphere, 101 (D3), 7305-7319.

Berbery, E.H., and E.M. Rasmusson, 1999: Mississippi moisture budgets on regional scale. Mon. Wea. Rev., 127, 2654-2673.

Betts, A.K., J.H. Ball, A.C.M. Beljaars, M.J. Miller, and P.A. Viterbo, 1996: The land-surface atmosphere interaction: A review based on observational and global modeling perspectives. JGR-Atmospheres, 101 (D3), 7209-7225.

Betts, A.K., P. Viterbo, and E. Wood, 1998: Surface energy and water balance for the Arkansas-Red River basin from the ECMWF reanalysis. J. Climate, 11 (11), 2881-2897.

Betts, A.K., J.H. Ball, and P. Viterbo, 1999: Basin-scale surface water and energy budgets for the Mississippi from the ECMWF reanalysis. JGR-Atmospheres, 104 (D16), 19'293-19'306.

Betts, A.K., J.H. Ball, M. Bosilovich, P. Viterbo, Y.-C. Zhang, and W.B. Rossow, 2003: Intercomparison of water and energy budgets for five Mississippi Sub-basins between ECMWF reanalysis (ERA-40) and NASA-DAOfvGCM for 1990-1999. JGR-Atmospheres, in press.

Betts, R.A., P.M. Cox, S.E. Lee, and F.I. Woodward, 1997: Contrasting physiological and structural vegetation feedbacks in climate change simulations. Nature, 387, 796-799.

Bonan, G., 1996: The NCAR land surface model (LSM version 1.0) coupled to the NCAR community climate model. Technical Report NCAR/TN-429 + STR, NCAR Boulder, Colorado.

Budyko, M.I.,1956: The heat balance of the Earth's surface (in Russian). Gidrometeoizdat, Leningrad (translation: Budyko, M.I. 1958: The heat balance of the Earth's surface. U.S. Department of Commerce, 259 pp.)

Budyko, M.I., 1974: Climate and life. Academic Press, 510 pp.

Calvet, J.C., and J. Noilhan, 2000: From near-surface to root-zone soil moisture using year-round data. J. Hydrometeor., 1, 393-411.

Chahine, M.T., 1992: The hydrological cycle and its influence on climate. Nature, 359, 373-380.

Changnon, S.A., F.A. Huff, and C.F. Hsu, 1988: Relations between precipitation and shallow groundwater in Illinois. J. Climate, 1, 1239-1250.

Chen, F., R.A. Pielke Sr., and K. Mitchell, 2001: Development and application of land-surface models for mesoscale atmospheric models: Problems and promises. Water Science and Application, 3, 107-135.

Christensen, J.H., B. Machenhauer, R.G. Jones, C. Schär, P.M. Ruti, M. Castro, and G. Visconti, 1997: Validation of present-day regional climate simulations over Europe: LAM simulations with observed boundary conditions, Clim. Dyn., 13, 489-506.

Christensen, O.B., M.A. Gaertner, J.A. Prego, J. Polcher, 2001: Internal variability of a regional climate model. Clim. Dyn., 17, 875-887.

Claussen, M., 2003: Feedbacks, synergisms, multiple equilibria, and teleconnections. Chapter A3.1, In: *Vegetation, Water, Humans and the Climate: A New Perspective on an Interactive System*, M. Claussen et al., Eds, Springer-Verlag, New York, to appear.

Coughlan, M., and R. Avissar, 1996: The Global Energy and Water Cycle Experiment (GEWEX) Continental-Scale International Project (GCIP): An overview. JGR-Atmospheres, 101 (D3), 7139-7147.

Courtier, P., E. Andersson, W. Heckley, J. Pailleux, D. Vasiljevic, M. Hamrud, A. Hollingsworth, F. Rabier, and M. Fisher, 1998: The ECMWF implementation of three dimensional variational assimilation (3D-Var). Part I: Formulation. Quart. J. Roy. Meteor. Soc., 124, 1783-1808.

Cubasch, U., G.A. Meehl, G.J. Boer, R.J. Stouffer, M. Dix, A. Noda, C.A. Senior, A. Raper, and K.S. Yap, 2001: Projections of future climate change. In: Climate change 2001: The scientific basis. Contribution of working group I to the third assessment report of the Intergovernmental Panel on Climate Change. Houghton, J.T., and others (eds.), 525-582. Cambridge University Press.

Davies, H.C., 1976: A lateral boundary formulation for multi-level prediction models. Quart. J. Roy. Meteor. Soc., 102, 405-418.

Davies, H.C., and R. Turner, 1977: Updating prediction models by dynamical relaxation: An examination of the technique. Quart. J. Roy. Meteor. Soc., 103, 225-245.

Déqué, M., P. Marquet, and R.G. Jones, 1998: Simulation of climate change over Europe using a global variable resolution general circulation model. Clim. Dyn., 14, 173-189.

Dickinson, R.E., 1984: Modeling evapotranspiration for three-dimensional global climate models. In: *Climate processes and climate sensitivity.* Geophys. Monogr. Am. Geophys. Union, 29, 58-72.

Dickinson, R.E., and A. Henderson-Sellers, 1988: Modelling tropical deforestation: A study of GCM land-surface parametrizations. Quart. J. Roy. Meteor. Soc., 114, 439-462.

Dickinson, R.E., 1991: Evapotranspiration models with canopy resistance for use in climate models, a review. Agric. For. Meteorol., 54, 373-388.

Dickinson, R.E., A. Henderson-Sellers, and P.J. Kennedy, 1993: Biosphere-atmosphere transfer scheme (BATS) version 1e as coupled to the NCAR community climate model. NCAR technical note, 72 pp.

Dingman, S.L., 1993: Physical hydrology. Prentice Hall, New Jersey.

Dirmeyer, P.A., A.J. Dolman, and N. Sato, 1999: The pilot phase of the Global Soil Wetness Project. Bull. Am. Met. Soc., 80 (5), 851-878.

Domenico, P.A., and F.W. Schwartz, 1990: Physical and chemical hydrogeology (2nd ed.). John Wiley and Sons, Inc., New York, 1990.

Dorman, J.L., and P.J. Sellers, 1989: A global climatology of albedo, roughness length and stomatal resistance for atmospheric general circulation models as represented by the simple biosphere model (SiB). J. Appl. Met., 28, 833-855.

Douville, H., P. Viterbo, J.F. Mahfouf, and A.C.M. Beljaars, 2000: Evaluation of the optimum interpolation and nudging techniques for soil moisture analysis using FIFE data. Mon. Wea. Rev., 128, 1733-1756.

Dutton, J.F., and E.J. Barron, 2000: Intra-annual and interannual ensemble forcing of a regional climate model. JGR-Atmospheres, 105 (D24), 29523-29538.

Eamus, D. and P.G. Jarvis, 1989: The direct effects of increase in the global atmospheric CO_2 concentration on natural and commercial temperate trees and forests. Advances in Ecological Research, 19, 1-55.

Easterling, D.R., G.A. Meehl, C. Parmesan, S.A. Changnon, T.R. Karl, and L.O. Mearns, 2000: Climate extremes: Observations, modeling, and impacts. Science, 289, 2068-2074.

Eltahir, E.A.B., 1998: A soil moisture-rainfall feedback mechanism. 1. Theory and observations. Wat. Res. Res., 34, 3, 765-776.

Entin, J.K., A. Robock, K.Y. Vinnikov, V. Zabelin, S. Liu, A. Namkhai, and Ts. Adyasuren, 1999: Evaluation of Global Soil Wetness Project soil moisture simulations. J. Met. Soc. of Japan, 77 (1B), pp 183-198.

Fajer, E.D. and Bazzaz, F.A., 1992: Is carbon dioxide a good greenhouse gas? - Effects of increasing carbon dioxide on ecological systems. Global Environmental Change - Human and Policy Dimensions, 2, 301-310.

Findell, K., and E.A.B. Eltahir, 1997: An analysis of the soil moisture-rainfall feedback, based on direct observations from Illinois. Wat. Res. Res., 33(4), 725-735.

Foley, J.A., C.I. Prentice, N. Ramankutty, S. Levis, D. Pollard, S. Sitch, and A. Haxeltine, 1996: An integrated biosphere model of land surface processes, terrestrial carbon balance, and vegetation dynamics. Global Biogeochem. Cycles, 10, 603-628.

Frei, C., and C. Schär, 1998: A precipitation climatology of the Alps from high-resolution rain-gauge observations. Int. J. Climatol., 18, 873-900.

Frei, C., C. Schär, D. Lüthi, and H.C. Davies, 1998: Heavy precipitation processes in a warmer climate. Geophys. Res. Lett., 25, 9, 1431-1434.

Frei, C., J.H. Christensen, M. Déqué, D. Jacob, R.G. Jones, and P.L. Vidale, 2003: Daily precipitation statistics in regional climate models: Evaluation and intercomparison for the European Alps. JGR-Atmospheres, in press.

Fritsch, J.M., and C.F. Chappell, 1980: Numerical prediction of convectively driven mesoscale pressure systems. Part I: Convective parameterization. J. Atmos. Sci., 37, 1722-1733.

Fukutome, S., C. Frei, D. Lüthi, and C. Schär, 1999: The interannual variability as a test ground for regional climate simulations over Japan. J. Meteor. Soc. Japan, 77, 649-672.

Fukutome, S., C. Prim, and C. Schär, 2001: The role of the soil in medium-range weather predictability. Nonlinear Proc. Geoph., 8 (6), 373-386.

Garatt, J.R., 1993: Sensitivity of climate simulations to land-surface and atmospheric boundary-layer treatments - A review. J. Climate, 6, 419-449.

Garratt, J.R., D.M. O'Brien, M.R. Dix, J.M. Murphy, G.L. Stephens, and M. Wild, 1999: Surface radiation fluxes in transient climate simulations. Global and Planetary Change, 20, 33-55.

Gates, W.L., A. Henderson-Sellers, G.J. Boer, C.K. Folland, A. Kitoh, B.J. McAvaney, F. Semazzi, N. Smith, A.J. Weaver, and Q.C. Zeng, 1996: Climate models - evaluation. in: Climate Change 1995, The science of climate change, Contribution of working group I to the second assessment report of the Intergovernmental Panel on Climate Change. Houghton, J.T., and others (eds.), 285-357. Cambridge University Press.

Gates, W.L., J.S. Boyle, C. Covey, C.G. Dease, C.M. Doutriaux, R.S. Drach, M. Fiorino, P.J. Gleckler, J.J. Hnilo, S.M. Marlais, T.J. Phillips, G.L. Potter, B.D. Santer, K.R. Sperber, K.E. Taylor, and D.N. Williams, 1999: An overview of the results of the Atmospheric Model Intercomparison Project (AMIP I), Bull. Am. Met. Soc., 80, 29-55.

Gibson, J.K., P. Kallberg, S. Uppala, A. Hernandey, A. Nomura, and E. Serano, 1997: ERA description. ECMWF Reanalysis Project Report Series (Reading UK), 1, 66 pp.

Giorgi, F., 1990: On the simulation of regional climate using a limited area model nested in a general circulation model. J. Climate, 3, 941-963.

Giorgi, F., and M.R. Marinucci, 1991: Validation of a regional atmospheric model over Europe – Sensitivity of wintertime and summertime simulations to selected physics parametrizations and lower boundary conditions. Quart. J. Roy. Meteorol. Soc., 117, 1171-1206.

Giorgi, F., M.R. Marinucci, and G.T. Bates, 1993a: Development of a second-generation regional climate model (RegCM2). Part I: Boundary-layer and radiative transfer processes. Mon. Wea. Rev., 121, 10, 2794-2813.

Giorgi, F., M.R. Marinucci, G.T. Bates, and G. De Canio, 1993b: Development of a second-generation regional climate model (RegCM2). Part II: Convective Processes and assimilation of lateral boundary conditions. Mon. Wea. Rev., 121, 10, 2814-2832.

Giorgi, F., and M.R. Marinucci, 1996: Improvements in the simulation of surface climatology over the European region with a nested modeling system. Geophys. Res. Lett., 23, 273-276.

Giorgi, F., and L.O. Mearns, 1999: Introduction to special section: Regional climate modeling revisited. JGR-Atmospheres, 104 (D6), 6335-6352.

Giorgi, F., and C. Shields, 1999: Tests of precipitation parameterizations available in the latest version of NCAR regional climate model (RegCM) over continental United States. JGR-Atmospheres, 104 (D6), 6353-6375.

Giorgi, F., and X. Bi, 2000: A study of the internal variability of a regional climate model. JGR-Atmospheres, 105 (D24), 29503-29521.

Gregory, J.M., J.F.B. Mitchell, and A.J. Brady, 1997: Summer drought in Northern midlatitudes in a time-dependent CO_2 climate experiment. J. Climate, 10, 662-686.

Grell, G., 1993: Prognostic evaluation of assumptions used by cumulus parameterizations. Mon. Wea. Rev., 121, 764-787.

Grell, G.A., J. Dudhia, and D.R. Stauffer, 1994: A description of the fifth generation Penn State/NCAR Mesoscale Model (MM5), NCAR Technical Note, NCAR/TN-398+STR, p.121.

Gutowski Jr., W.J., Y. Chen, and Z. Ötles, 1997: Atmospheric water vapor transport in NCEP-NCAR reanalyses: Comparison with river discharge in the central United States. Bull. Am. Meteorol. Soc., 78 (9), 1957-1969.

Hagemann, S., M. Botzet, and B. Machenhauer, 2001: The summer drying problem over south-eastern Europe: Sensitivity of the limited area model HIRHAM4 to improvements in physical parameterization and resolution. Physics and Chemistry of the Earth Part B, Vol. 26/5-6, 391-396.

Hagemann, S., B. Machenhauer, O.B. Christensen, M. Déqué, D. Jacob, R.G. Jones, and P.L. Vidale, 2002: Intercomparison of water and energy budgets simulated by regional climate models applied over Europe. Max-Planck-Institute for Meteorology, Report 338, Hamburg, Germany.

Heck P., D. Lüthi, H. Wernli, and C. Schär, 2001: Climate impacts of European-scale anthropogenic vegetation changes: A sensitivity study using a regional climate model. JGR-Atmospheres, 106 (D8), 7817-7835.

Henderson-Sellers, A., K. McGuffie, and C. Gross, 1995: Sensitivity of global climate model simulations to increased stomatal resistance and CO_2 increases. J. Climate, 8, 1738-1756.

Henderson-Sellers, A., K. McGuffie, and A.J. Pitman, 1996: The Project for Intercomparison of Land-Surface Parametrization Schemes (PILPS): 1992 to 1995. Clim. Dyn., 12, 849-859.

Hess, G.D., and B.J. McAvaney, 1997: Note on computing screen temperatures, humidities and anemometer-height winds in large-scale models. Aust. Met. Mag., 46, 109-115.

Hirschi, M., 2002: Abschätzung der terrestrischen Wasserspeicheränderung mit Wasserbilanzen und ERA-40 Reanalysedaten in Einzugsgebieten von Flüssen in Asien und Europa. Diploma thesis, Atmospheric and Climate Science ETH.

Hollinger, S.E., and S.A. Isard, 1994: A soil moisture climatology of Illinois. J. Climate, 4, 822-833.

Holtslag, A.A.M., E.I.F. de Bruijn, and H.L. Pan, 1990: A high resolution air mass transformation model for short-range weather forecasting. Mon. Wea. Rev., 118, 1561-1575.

Holstlag, A.A.M., and B.A. Boville, 1993: Local versus non-local boundary-layer diffusion in a global climate model. J. Climate, 6, 1825-1842.

Hortal, M., and A.J. Simmons, 1991: Use of reduced Gaussian grids in spectral models. Mon. Wea. Rev., 119, 1057-1074.

Huang, J., H.M. van den Dool, and K. Georgakakos, 1996: Analysis of model-calculated soil moisture over the U.S. (1931-93) and application in long-range temperature forecasts. J. Climate, 9, 1350-1362.

IPCC, 2001: Climate Change 2001, The scientific basis. Contribution of Working Group I to the third assessment report of the Intergovernmental Panel on Climate Change. Houghton, J.T. and others (eds.), Cambridge University Press, Cambridge, England, 881 pp.

Iselin, J.P., and W.J. Gutowski Jr., 1997: Water vapor layers in STORM-FEST rawinsonde observations. Mon. Wea. Rev., 125, 1954-1963.

Jackson, T.J., D.M. Le Vine, A.Y. Hsu, A. Oldak, P.J. Starks, C.T. Swift, J.D. Isham, and M. Haken, 1999: Soil moisture mapping at regional scale using microwave radiometry: The southern great plains hydrology experiment. IEEE transactions on geoscience and remote sensing, 37 (5), 2136-2151.

Jacquemin, B., and J. Noilhan, 1990: Sensitivity study and validation of a land surface parameterization using the HAPEX-MOBILHY data set. Boundary-Layer Meteorology, 52, 93-134.

Jacobsen, I., and E. Heise, 1982: A new economic method for the computation of the surface temperature in numerical models. Beitr. Phys. Atm., 55, 128-141.

Jarvis, P., 1976: The interpretation of the variations in leaf water potential and stomatal conductance found in canopies in the field. Philos. Trans. Roy. Soc. London B, 273, 593-610.

Jones, R.G., J.M. Murphy, and M. Noguer, 1995: Simulation of climate change over Europe using a nested regional-climate model I: Assessment of control climate, including sensitivity to location of lateral boundaries. Quart. J. Roy. Meteorol. Soc., 121, 1413-1449.

Kalnay, E. et al., 1996: The NCEP/NCAR 40-year reanalysis project. Bull. Am. Meteorol. Soc., 77 (3), 437-471.

Kanamitsu, M., W. Ebisuzaki, J. Woollen, S.K. Yang, J.J. Hnilo, M. Fiorino, G.L. Potter, 2002: NCEP-DOE AMIP-II reanalysis (R-2). Bull. Am. Meteorol. Soc. 83 (11), 1631-1643.

Karl, T.R., T.N. Williams Jr., T.N. Quinlan, and T.A. Boden, 1990: United States Historical Climate Network (HCN) serial temperature and precipitation data. *Technical Report Environmental Science Division, Publication No. 3404,* Oak Ridge National Laboratory, Oak Ridge, TN. 389 pp.

Kattenberg, A., F. Giorgi, H. Grassl, G.A. Meehl, J.F.B. Mitchell, R.J. Stouffer, T. Tokioka, A.J. Weaver, and T.M.L. Wigley, 1996: Climate models - projections of future climate. In: *Climate Change 1995, The science of climate change, Contribution of working group I to the second assessment report of the intergovernmental panel on climate change,* Houghton, J.T. and others (eds.), pp. 285-357. Cambridge University Press.

Kessler, E., 1969: On the distribution and continuity of water substance in atmospheric circulation models. Meteor. Monographs, 10, Americ. Meteor. Soc. Boston, MA.

Kiehl, J.T., J.J. Hack, G.B. Bonan, B.A. Boville, D.L. Williamson, and P.J. Rasch, 1998: The National Center for Atmospheric Research Community Climate Model: CCM3. J. Climate, 11, 1131-1149.

Korzun, V.I., (ed.), 1978: World water balance and water resources of the earth – Studies and reports in Hydrology, 75, 663pp. Paris (UNESCO), translated from Russian.

Koster, R.D., and P.C.D. Milly, 1997: The interplay between transpiration and runoff formulations in land surface schemes used with atmospheric models. J. Climate, 10, 1578-1591.

Koster, R.D., M.J. Suarez, and M. Heiser, 2000: Variance and predictability of precipitation at seasonal-to-interannual timescales. J. Hydrometeor., 1, 26-46.

Krasovskaia, I., 1996: Stability of river flow regimes. Rapport nr.5 Oslo 1996, ISSN 0803-8848.

Kunkel, K., S. Changnon, and J. Angel, 1994: Climatic aspects of the 1993 Upper Mississippi River Basin flood. Bull. Am. Meteorol. Soc. 75, 811-822.

Lenters, J.D., M.T. Coe, and J.A. Foley, 2000: Surface water balance of the continental United States, 1963-1995: Regional evaluation of a terrestrial biosphere model and the NCEP/NCAR reanalysis. JGR-Atmospheres, 105(D17), 22393-22425.

Levis, S., J. Foley, and D. Pollard, 2000: Large-scale vegetation feedbacks on a doubled CO_2 climate. J. Climate, 13, 1313-1325.

Lin, Y.-L., R.D. Farley, and H.D. Orville, 1983: Bulk parameterization of the snow field in a cloud model. J. Clim. Appl. Meteor., 22, 1065-1092.

Louis, J.F., M. Tiedkte, and J.F. Geleyn, 1982: A short history of the operational PBL parameterization at ECMWF. Proc. ECMWF Workshop on Boundary Layer parameterizations, ECMWF, 59-79.

Lunardini, V.J., 1983: Heat transfer in cold climates. Van Nostrand Reinhold, New York.

Lüthi, D., A. Cress, H.C. Davies, C. Frei, and C. Schär, 1996: Interannual variability and regional climate simulations. Theor. Appl. Climatol., 53, 185-209.

Machenhauer, B., M. Windelband, M. Botzet, J.H. Christensen, M. Déqué, R.G. Jones, PM. Ruti, and G. Visconti, 1998: Validation and analysis of regional present-day climate and climate change simulations over Europe. MPI Report 275, Max Planck Institute, Hamburg, 87pp. and figures.

Majewski, D., 1991: The Europa Modell of the Deutscher Wetterdienst. ECMWF Seminar Proceedings on Numerical Methods in Atmospheric Models, 16-18 Sept. 1991, VOL II., 147-191.

Majewski, D., and R. Schrodin, 1994: Short description of the Europa-Modell (EM) and Deutschland-Modell (DM) of the Deutscher Wetterdienst (DWD) (Quarterly Bulletin, April).

Manabe, S., 1969: Climate and ocean circulation. Part I: The atmospheric circulation and the hydrology of the earth's surface. Mon. Wea. Rev., 97 , 739-774.

Manabe S., R.T. Wetherald, and R.J. Stouffer, 1981: Summer dryness due to an increase of atmospheric CO_2 concentrations. Clim. Change, 3, 347-386.

Masuda, K., Y. Hashimoto, H. Matsuyama, and T. Oki, 2001: Seasonal cycle of water storage in major river basins of the world. Geophys. Res. Lett., 28 (16), 3215-3218.

Matsuyama, H., and K. Masuda, 1997: Estimates of continental-scale soil wetness and comparison with the soil moisture data of Mintz and Serafini. Clim. Dyn., 13, 681-689.

Mays, L.W., 1996: Water resources handbook. McGraw-Hill, New York.

Mellor, G.L., and T. Yamada, 1974: A hierarchy of turbulent closure models for planetary boundary layers. J. Atmos. Sci., 31, 1791-1806.

Milly, P.C.D., and K.A. Dunne, 1994: Sensitivity of the global water cycle to the water-holding capacity of the land. J. Clim. 7, 506-526.

Milly, P.C.D., 1997: Sensitivity of greenhouse summer dryness to changes in plant rooting characteristics. Geophys. Res. Lett., 24, 3, 269-271.

Mo, K.C., J. Nogues Paegle, and R.W. Higgins, 1997: Atmospheric processes associated with summer floods and droughts in the central United States. J. Climate, 10, 3028-3046.

Murphy, J.M., 1999: An evaluation of statistical and dynamical techniques for downscaling local climate. J. Climate, 12, 2256-2284.

National Research Council, 1986: Global Change in the Geosphere-Biosphere, 91. National Academy Press, Washington DC.

New, M., M. Hulme, and P. Jones, 1999: Representing twentieth-century space-time climate variability. Part I: Development of a 1961-90 mean monthly terrestrial climatology. J. Climate, 12, 829-856.

Noguer, M., R.G. Jones, and J.M. Murphy, 1998: Sources of systematic errors in the climatology of a regional climate model over Europe. Clim. Dyn., 14, 691-712.

Oki, T., K. Musiake, H. Matsuyama, and K. Masuda, 1995: Global atmospheric water balance and runoff from large river basins. Hydrological Processes, 9, 655-678.

Oki, T, 1999: The global water cycle. In: Global Energy and Water Cycle. K. Browning and R. Gurney (eds.), pp. 10-27. Cambridge University Press.

Palmer, T.N, 2000: Predicting uncertainty in forecasts of weather and climate. Rep. Prog. Phys., 63, 71-116.

Pardé, M., 1930: Le régime du Mississippi. Revue de Géographie Alpine, vol. 18 (4).

Pardé, M., 1947: Fleuves et rivières. Collection Armand Colin (eds.), 2nd edition.

Pal, J.S., E.E. Small, and E.A.B. Eltahir, 2000: Simulation of regional scale water and energy budgets: Importance of subgrid cloud and precipitation processes within RegCM. JGR-Atmospheres, 105, D24, 29579-29594.

Pal, J.S., 2001: Modeling of the soil moisture-rainfall feedback mechanism. PhD Thesis, MIT, Cambridge, USA.

Pal, J.S., and E.A.B. Eltahir, 2001: Pathways relating soil moisture conditions to future summer rainfall within a model of the land-atmosphere system. J. Climate, 14, 1227-1242.

Peixoto, J.P., and A.H. Oort, 1992: Physics of climate. Am. Inst. of Phys. Press, Woodbury, New York.

Pomeroy, J.W., and D.M. Gray, 1995: Snow cover - Accumulation, relocation and management. National Hydrology Research Institute Science Report No. 7, Saskatoon, Canada, 144 pp.

Ramanathan, V., 1981: The role of ocean-atmosphere interactions in the CO_2 climate problem. J. Atmos. Sci., 38, 918-930.

Rango, A., 1996: Spaceborne remote sensing for snow hydrology applications. Hydrological Sciences Journal, 41 (4), 477-494.

Rasmusson, E.M., 1968: Atmospheric water vapor tranport and the water balance of North America. II. Large-scale water balance investigations. Mon. Wea. Rev. 96, 720-734.

Rasmusson, E.M., 1971: A study of the hydrology of eastern North America using atmospheric vapor flux data. Mon. Wea. Rev., 99, 119-135.

Raval, A., and V. Ramanathan, 1989: Observational determination of the greenhouse effect. Nature, 342, 758-761.

Rind, D., E.W. Chiou, W. Chu, J. Larsen, S. Oltmans, J. Lerner, M.P. McCormick, and L. McMaster, 1991: Positive water vapour feedback in climate models confirmed by satellite data. Nature, 349, 500-503.

Rind, D., R. Goldberg, J. Hansen, C. Rosenzweig, and R. Ruedy, 1990: Potential evapotranspiration and the likelihood of future drought. JGR-Atmospheres, 95 (D7), 9983-10,004.

Ritter, B., and J.F. Geleyn, 1992: A comprehensive radiation scheme for numerical weather prediction models with potential applications in climate simulations. Mon. Wea. Rev., 120, 303-325.

Roads, J.O., S.C. Chen, A.K. Guetter, and K.P. Georgakakos, 1994: Large-scale aspects of the United States hydrological cycle. Bull. Am. Meteorol. Soc., 75 (9), 1589-1610.

Roads, J.O., S.C. Chen, M. Kanamitsu, and H. Juang, 1999: Surface water characteristics in NCEP global spectral model and reanalysis. JGR-Atmospheres, 104 (D16), 19307-19327.

Robock, A., K.Y. Vinnikov, G. Srinivasan, J.K. Entin, S.E. Hollinger, N.A. Speranskaya, S. Liu, and A. Namkhai, 2000: The Global Soil Moisture Data Bank. Bull. Amer. Meteorol. Soc., 81, 1281-1299. Web site: http://climate.envsci.rutgers.edu/soil_moisture/ .

Rodell, M., and J.S. Famiglietti, 2001: An analysis of terrestrial water storage variations in Illinois with implications for the Gravity Recovery and Climate Experiment (GRACE). Wat. Res. Res., 37 (5), 1327-1339.

Rogers, H.H., S.A. Prior, G.B. Runion, and R.J. Mitchell, 1996: Root to shoot ratio of crops as influenced by CO2. Plant and soil, 187 (2), 229-248.

Ropelewski, C.F., 1988: The global climate for June-August 1988: A swing to the positive phase of the Southern Oscillation, drought in the United States and abundant rain in monsoon areas. J. Climate, 1, 1153-1174.

Ropelewski, C.F., and E.S. Yarosh, 1998: The observed mean annual cycle of moisture budgets over the central United States (1973-92). J. Climate, 11, 2180-2190.

Rowntree, P.R., and J.A. Bolton, 1983: Simulation of the atmospheric response to soil moisture anomalies over Europe. Quart. J. Roy. Meteorol. Soc., 109, 501-526.

Rowntree, P.R., 1991: Atmospheric parameterization schemes for evaporation over land: Basic concepts and climate modeling aspects. In: Land Surface Evaporation, T.S. Schmugge and J.C. André (eds.), pp. 5-29.

Schär, C., C. Frei, D. Lüthi, and H.C. Davies, 1996: Surrogate climate-change scenarios for regional climate models. Geophys. Res. Lett., 23, 6, 669-672.

Schär, C., D. Lüthi, U. Beyerle, and E. Heise, 1999: The soil-precipitation feedback: A process study with a regional climate model. J. Climate, 12, 722-741.

SCOWAR (Scientific Committee on Water Research: Afouda, A., R. Bhatia, A. Becker, S. Cairncross, M. Falkenmark, J. Kindler, W. Kinzelbach, R.J. Naiman, L. Oyebande, W.J. Shuttleworth, K. Takeuchi, G. Vachaud, J.A. Veltrop, and A. Verwey), 1997: Water resources research: trends and needs in 1997. Hydrological Sciences - Journal - des Sciences Hydrologiques, 43(1).

Sellers, P.J., Y. Mintz, Y.C. Sud, and A. Dalcher, 1986: A simple biosphere model (SiB) for use within general-circulation models. J. Atmos. Sci., 43 (6), 505-531.

Sellers, P.J., 1992: Biophysical models of land processes. In: *Climate System Modeling*, Trenberth, K.E. (ed), Cambridge University Press, Cambridge, England.

Sellers, P.J., S.O. Los, C.J. Tucker, C.O. Justice, D.A. Dazlich, G.J. Collatz, and D.A. Randall, 1994: A global 1 by 1 degree NDVI data set for climate studies. Part 2: The generation of global fields of terrestrial biophysical parameters from the NDVI. Int. J. Rem. Sens., 15 (17), 3519-3545.

Sellers, P.J., Bounoua, L., Collatz, G.J, Randall, D.A, Dazlich, D.A., Los, S.O., Berry, J.A., Fung, I., Tucker, C.J., Field, C.B. and Jensen, T.G., 1996a: Comparison of radiative and physiological effects of doubled atmospheric CO_2 on climate. Science, 271, 1402-1406.

Sellers, P.J., D.A. Randall, G.J. Collatz, J.A. Berry, C.B. Field, D.A. Dazlich, C. Zhang, G.D. Collelo, and L. Bounoua, 1996b: A revised land surface parameterization (SiB2) for atmospheric GCMs .1. Model formulation. J. Climate, 9 (4), 676-705.

Sellers, P.J., R.E. Dickinson, D.A. Randall, A.K. Betts, F.G. Hall, J.A. Berry. G.J. Collatz, A.S. Denning, H.A. Mooney, C.A. Nobre, N. Sato, C.B. Field, and A. Henderson-Sellers, 1997: Modeling the exchanges of energy, water, and carbon between continents and the atmosphere. Science, 275, 502-509.

Seneviratne S.I., J.S. Pal, E.A.B. Eltahir, and C. Schär, 2002: Summer dryness in a warmer climate: A process study with a regional climate model. Clim. Dyn., 20, 69-85.

Seneviratne, S.I., P. Viterbo, D. Lüthi, and C. Schär, 2003: Inferring changes in terrestrial water storage using ERA-40 reanalysis data: The Mississippi river basin. J. Climate, submitted.

Shiklomanov, I.A., 1993: World fresh water resources. In: *Water in Crisis*, P. Gleick (ed.), Oxford University Press, Oxford, New York.

Shiklomanov, I.A., and A.A. Sokolov, 1983: Methodological basis of world water balance investigation and computation. In: *New Approaches in Water Balance Computations.* International Association for Hydrological Sciences Publication No. 148. (referenced in Dingman 1993).

Shukla, J., and Y. Mintz, 1982: Influence of land-surface evaporation on the Earth's climate. Science, 215, 1498-1501.

Simmons, A.J., and D.M. Burridge, 1981: An energy and angular momentum conserving vertical finite-difference shceme and hybrid vertical coordinates. Mon. Wea. Rev., 109, 758-766.

Simmons, A.J., and J.K. Gibson, 2000: The ERA-40 Project Plan. ERA-40 Project Report Series, No. 1, 62 pp. Available from ECMWF.

Slingo, J.M., 1987: The development and verification of a cloud prediction scheme for the ECMWF model. Quart. J. Roy. Meteor. Soc., 116, 435-460.

Small, E.E., F. Giorgi, and L.C. Sloan, 1999: Regional climate model simulation of precipitation in central Asia: Mean and interannual variability. JGR-Atmospheres, 104 (D6), 6563-6582.

Stahel, W., 1999: Statistische Datenanalyse. Eine Einführung für Naturwissenschaftler. 2nd Edition. Vieweg Verlag.

Starr, V.P., and J. Peixoto, 1958: On the global balance of water vapor and the hydrology of deserts. Tellus, 10, 189-194.

Stephens, G.L., 1979: Optical properties of eight water cloud types. CSIRO Div. of Atmos. Phy., Tech. Paper No. 36.

Tiedtke, M., 1989: A comprehensive mass flux scheme for cumulus parameterization in large-scale models. Mon. Wea. Rev., 117, 1779-1800.

Trenberth, K.E., 1995: Truncation and use of model coordinate data. Tellus, 47A, 287-303.

Trenberth, K.E., and C.J. Guillemot, 1995: Evaluation of the global atmospheric moisture budget as seen from analyses. J. Climate, 8, 2255-2272.

Trenberth, K.E., J.W. Hurrell, and A. Solomon, 1995: Conservation of mass in three dimensions in global analysis. J. Climate, 8, 692-708.

Trenberth, K.E., 1997: Using atmospheric budgets as a constraint on surface fluxes. J. Climate, 10, 2796-2809.

Venables and Ripley, 1997: Modern applied statistics with S-Plus. 2nd edition. Springer Verlag.

Vidale, P.L., D. Lüthi, C. Frei, S. Seneviratne, and C. Schär, 2003: Predictability and uncertainty in a regional climate model. JGR-Atmospheres, accepted.

Vidale, P.L., and R. Stöckli, 2003: Prognostic canopy air space solutions for SiB2 surface exchanges. Geophys. Res. Lett., in preparation.

Viterbo, P., 1996: The representation of surface processes in general circulation models. PhD thesis, ECMWF, Reading, UK.

Viterbo, P., and Betts, A.K., 1999a: Impact of the ECMWF reanalysis soil water forecasts of the July 1993 Mississippi flood. JGR-Atmospheres, 104 (D16), 19361-19366.

Viterbo, P., and Betts, A.K., 1999b: Impact on ECMWF forecasts of changes to the albedo of the boreal forests in the presence of snow. JGR-Atmospheres, 104 (D22), 27803-27810

Viterbo, P., A.C.M. Beljaars, J-F. Mahfouf, and J. Teixeira, 1999: The representation of soil moisture freezing and its impact on the stable boundary layer. Quart. J. Roy. Meteor. Soc., 125, 2401-2426.

Viterbo, P., and A.C.M. Beljaars, 2003: Impact of land surface on weather. Chapter A3.5, In "Vegetation, Water, Humans and the Climate: A New Perspective on an Interactive System", M. Claussen et al., Eds, Springer-Verlag, New York, to appear.

Vörösmarty, C.J., P. Green, J. Salisbury, and R.B. Lammers, 2000: Global water resources: Vulnerability from climate change and population growth. Science, 289, 284-288.

Wahr, J., M. Molenaar, and F. Bryan, 1998: Time-variability of the Earth's gravity field: Hydrological and oceanic effects and their possible detection using GRACE. J. Geophys. Res., 103(B12), 30,205-30,229.

Wetherald R.T., Manabe S. 1995: The mechanisms of summer dryness induced by greenhouse warming. J. Climate, 8, 3096-3108.

Wetherald R.T., Manabe S., 1999: Detectability of summer dryness caused by greenhouse warming. Clim. Change, 43, 495-511.

Wild, M., A. Ohmura, H. Gilgen, and E. Roeckner, 1995: Regional climate simulation with a high-resolution GCM: Surface-radiative fluxes. Clim. Dyn., 11, 469-486.

Wild, M., L. Dümenil, and J.P. Schulz, 1996: Regional climate simulation with a high resolution GCM: Surface hydrology. Clim. Dyn., 12, 755-774.

Xu, K.-M., and D. Randall, 1996: A semi-empirical cloudiness parameterization for use in climate models. J. Atmos. Sci., 53, 21, 3084-3102.

Yang, Z., and R.W. Arritt, 2002: Tests of a perturbed physics ensemble approach for regional climate modeling. J. Climate, 15, 2881-2896.

Yeh P.J.F., M. Irizarry, E.A.B. Eltahir, 1998: Hydroclimatology of Illinois: A comparison of monthly evaporation estimates based on atmospheric water balance and soil water balance. JGR-Atmospheres, 103 (D16), 19,823-19,837.

Zekster, I.S., and H.A. Loaiciga, 1993: Groundwater fluxes in the global hydrological cycle: past, present and future. J. Hydrology, 144, 405-427.

Acknowledgements

First and foremost, I would like to express my extreme gratitude to Christoph Schär for his constant support back since my first "Semesterarbeit" in his group some 5 years ago (!). He has been a truly wonderful advisor, always open for questions and discussions, and extremely supportive of my initiatives and ideas. I have learned a lot from him and I would like to take this opportunity to thank him sincerely for all the exciting work I could do in his group, as well as for his highly competent guidance throughout this thesis.

It has also been a wonderful experience to work together with Pedro Viterbo, and I would like to thank him here for all the work he contributed to our project, for his great patience with my numerous questions and somewhat chaotic work patterns, and for his invaluable comments on this work. What started as a small side project at the beginning of my thesis became an exciting collaboration I hope we can continue in the future! I would also like to thank Professor Wolfgang Kinzelbach for being my co-examiner and for his useful and sensible comments on my work.

Most sincere thanks as well to Elfatih Eltahir and his group, in particular to Jeremy Pal, Pat Yeh, and Kirsten Findell. I had a wonderful stay in Cambridge where I did my diploma thesis, and it was a great pleasure to have the opportunity to continue some of this work within my PhD thesis. Special thanks to Jeremy who took time to proofread the introduction of this thesis and who helped me with many computing issues.

I am also most grateful to Pier-Luigi Vidale for the many discussions we had together on land surface modelling, ferret, and/or politics, for his great sense of humour, and for his friendship and support in the few weeks preceding my defense. I am very thankful that I could include his paper in the present thesis, and I would also like to acknowledge his pertinent comments on all parts of this thesis, both on form and content.

Work at our institute would certainly be much more difficult without the presence of Dani Lüthi, our computer guru and system administrator. I particularly appreciated his help with the retrieve of ERA-40 data, which he performed despite his many other duties.

I would also like to acknowledge the great work that Martin Hirschi did in his diploma thesis, which provided the groundwork for section 4.2 of this thesis. I very much enjoyed working with him and I am looking forward to his soon beginning PhD thesis!

Many people of this Institute contributed to this thesis directly or indirectly, and I am indebted to all my IAC colleagues for the warm and friendly atmosphere we have here, for the fun and the good time we had together. In particular, I would like to thank Oliver Fuhrer, my office- and flatmate, for his help with Fortran-, Unix-, and many other problems, for his diploma thesis which introduced me into the realms of inverse computations, and for the many discussions and laughs we had all these years; Reto Stöckli, my long-time flatmate and fellow "land surfacer" for many exciting discussions on "SimClimate", complex bucket models, living beings below floor B, and other utopias of the

kind... Thanks to both of you for cheering me up in the last months of my thesis :-) Kindest thanks to Sophie Fukutome for introducing me to Women's history and Aikido, as well as for leading the way in defending her thesis a few weeks before the rest of the "PhD crowd". I am also extremely grateful to Christoph Frei for his advice on the appendix B and many other hydrological and statistical questions. Thanks as well to Achim Gurtz, Hendrik Huwald, Karsten Jaspers, Jan Kleinn, Jürg Schmidli, Andreas Weigel, André Walser, and Massimiliano Zappa, for help with diverse computer, administrative, or hydrological matters. I also have special thoughts for Anne Renaud and Pamela Heck, who lead my first steps in the world of climate research.

Finally, I would like to thank my friends, the 7up WG, and all the people who have been there for me in the last few years. In particular, I feel very much indebted to my parents, John and Anne, my sisters Céline and Alicia, and my grandmother Yvonne, for their love and support during all these years.

Sonia Seneviratne, April 2003

Curriculum Vitae

Sonia Seneviratne, Stampfenbachstr. 151, 8006 Zürich
born on 5 June 1974 in Lausanne, Switzerland
citizen of Switzerland (Lutry, VD) and Sri Lanka

Education and Professional Training

07/99 - 12/02	Research assistant and Ph. D. student (Group of Prof. C. Schär) Institute for Atmospheric and Climate Science, ETH Zurich. (PhD Defense: December 9, 2002)
10/95 - 06/99	Diploma study in Environmental Sciences (equivalent to MSc) Specialization in the field of atmospheric physics Swiss Federal Institute of Technology (ETH) Zurich
10/98 - 04/99	Diploma thesis, Ralph Parsons Laboratory for Hydrodynamics, MIT, Cambridge, USA (Group of Prof. E. Eltahir)
10/96 - 04/97	Internship, PROBONA/IUCN (World Conservation Union), Ecuador Grant from the Swiss Agency for Development and Cooperation
10/92 - 10/95	Undergraduate study of Biology (passed 3rd-year exam) University of Lausanne, Switzerland
10/89 - 06/92	Maturité Fédérale de Type B (Majors: Latin, English) Baccalauréat Vaudois de Type X (Majors: Latin, Mathematics, Physics) Gymnase cantonal de Chamblandes, Pully (VD), Switzerland

International Conferences and Workshops

2nd ICTP Conference on Detection and Modeling of Regional Climate Change 2002; NCCR Summer School 2002; AMS Annual Meeting 2002; ICTP Conference and Workshop on Climate Variability and Land-Surface Processes, 2001; 2nd Swiss Global Change Day (Poster Award) 2001; EGS General Assembly 2001; AGS Annual Meeting 2001; ECMWF training course, module on diabatic processes, 2000